The removal of selected pharmaceuticals from a municipal membrane bioreactor secondary effluent with reverse osmosis membranes

by

Nurah Jacobs

A thesis submitted in fulfilment of the requirements for the degree

Master of Engineering: Chemical Engineering

in the

Faculty of Engineering and the Built Environment

at the

Cape Peninsula University of Technology

Supervisor: **Prof Mujahid Aziz**

September 2022

DECLARATION

I, Nurah Jacobs, declare that the contents of this dissertation/thesis represent my own unaided work, and that the dissertation/thesis has not previously been submitted for academic examination towards any qualification. Furthermore, it represents my own opinions and not necessarily those of the Cape Peninsula University of Technology

Signed: *Nurah Jacobs*   Date: *September 2022*

Abstract

The complexity of water and its need for sustainability is, without a doubt, a global crisis. Water is the precondition for sustainable development, human and animal survival, and healthy ecosystems are critical for socio-economic development. Recycling and reusing municipal secondary wastewater effluent can strengthen the water supply. Membrane technology such as membrane bioreactors (MBR), nanofiltration (NF), and reverse osmosis (RO) have gained a great deal of popularity due to their effectiveness in removing organics, inorganics, emerging micropollutants (EMPs) and contaminants of emerging concerns (CECs).

This research used a bench-scale RO system to investigate the removal of selected inorganics and pharmaceuticals from a municipal membrane bioreactor secondary effluent with reverse osmosis membranes. The study was divided into the RO process, solid-phase extraction (SPE), and gas chromatography-mass spectrometry (GCMS) for quantification analysis.

The effects of operating conditions on the elimination of inorganics by NF and RO membranes were assessed. Experimental runs were performed on the bench-scale RO cell in recycle mode, adjusting the feed pressure. Chemical analysis of various inorganics was conducted to calculate the percentage removal. Results uncovered considerable effects of feed pressure control on eliminating the inorganics of interest and the carbon-oxygen demand (COD). Adjustment of flux due to the feed pressure for the RO membrane was shown to be a factor of consideration for the improvement of inorganic removal in the advanced treatment of domestic secondary MBR effluent. It was shown that water quality obtained with the RO and NF membranes could meet quality requirements for reuse application in cooling systems and irrigation, among others.

Attenuated total reflection, Fourier-transform infrared spectroscopy (ATR-FTIR) was used to identify functional groups on the membrane's surface. The relationship between initial concentration and functional group deposition was monitored. It can be confirmed that the increase in feed pressure resulted in a higher flux and higher rejection of organics and inorganics. However, the feed concentration had negligible changes in the removal efficiencies; it was depicted that there was an increase in fouling with the rise in feed concentration.

Scanning electron microscopy and energy dispersive X-ray (SEM-EDX) were used to analyse the morphology of the membrane's surface. The results showed that NF fouled more than the RO. The foulant deposition onto the polyamide (PA) layer increased for both membranes following the feed pressure increases. A 100-hour-long experimental run was conducted to compare the performance and sustainability of both membranes under the same conditions. The EDX results indicated that the NF had a 13.6% increase in carbon and an 18.8% decrease in oxygen compared to the RO membrane.

The selected pharmaceuticals, namely: aspirin (ASP), carbamazepine (CBZ), ibuprofen (IBU) and diclofenac (DCF), were assessed using solid-phase extraction (SPE) and gas chromatography-mass spectrometry (GCMS). The results indicated that the higher feed pressure resulted in greater removal of target analytes. The lowest rejection of DCF was 87% and >95% for CBZ with the NF membranes at the same feed pressure. The feed concentration did not significantly influence the rejection of CBZ, IBU, DCF and ASP, which was most likely ruled by steric hindrance, electrostatic repulsion (donnon exclusion molecular weight cut-off (MWCO) and hydrophobic/super molecular interactions simultaneously. RO resulted in higher rejections than NF, with average rejections greater than 95% for all CECs.

Consequently, municipal MBR secondary wastewater effluent treated by a bench-scale RO unit with RO and NF membranes is acceptable for effectively removing selected pharmaceuticals (CBZ, DCF, IBU and ASP). The feed concentration does not affect the removal of target analytes by both RO and NF membranes. However, increasing the feed pressure has proven to be more effective in its removal. Ultimately, using a hybrid system could assist in further abatement for reuse applications.

Acknowledgements

I'm most grateful to the Almighty for giving me the strength to persevere and succeed with this project and for blessing me with an indestructible support system, my parents, friends, and family.

Dedication

To my parents, my pillars of support, Gamidah Jacobs and Mogammad Nadeem Jacobs, for their unconditional love and support, their constant involvement, tolerance, motivation and encouragement. None of it would have been possible without you. I love and appreciate you and am forever grateful, Alhamdulillah.

Research outputs

Oral Presentation

Jacobs N & Aziz M; The removal of selected contaminants of emerging concern from a municipal membrane bioreactor secondary effluent with reverse osmosis membranes, CPUT Virtual (online) Annual Post Graduate Conference, SARATEC, Cape Town, South Africa, 12 November 2021

Jacobs N & Aziz M; The reduction of selected Inorganics and anthropogenic micropollutants from MBR secondary effluent with NF/RO membranes, Inter Institutional Post Graduate Symposium, STIAS, Stellenbosch University, Stellenbosch, South Africa, 30 September 2022

Journal Publication

Kasongo, G; Steenberg, C; Morris, B; Kapenda, G; Jacobs, N & Aziz, M; 2019; Surface grafting of polyvinyl alcohol (PVA) cross-linked with glutaraldehyde (GA) to improve resistance to fouling of aromatic polyamide thin-film composite reverse osmosis membranes using municipal membrane bioreactor effluent, IWA: Water Practice, and Technology, 14 (3), 614-626 [ISSN 1751-321X / DOI.org/10.2166/wpt.2019.047].

Jacobs N & Aziz M; 2022. The Exclusion of Selected Pharmaceuticals from Domestic MBR Secondary Effluent using Aromatic Polyamide Thin-film Composite NF/RO Membranes, Suranaree Journal of Science, and Technology. Submitted XX September 2022 [Paper ID.: XX-XX-XX]

Table of Contents

List of Figures

List of Tables

List of Equations

List of Abbreviations

RO	Reverse Osmosis
NF	Nanofiltration
UF	Ultrafiltration
MF	Microfiltration
MBR	Membrane bioreactor
CBZ	Carbamazepine
DCF	Diclofenac
ASP	Aspirin
IBU	Ibuprofen
EMPs	Emerging micropollutants
CECs	Contaminants of emerging concern
COD	Chemical oxygen demand
BOD	Biological oxygen demand
CAS	Conventional activated sludge
OD	Oxidation ditch
TBF	Trickling biologival filters
PCW	Ponds and constructed wetlands
TFC	Thin film composit
DE	Dielectric exclusion
TFC	Thin film composit
NSAIDs	Non-steriodal Anti-inflammatory drugs
STPs	Sewage treatment plants
WWTPs	Wastewater treatment plants
MWCO	Molecular Weight cutoff
SARS	Severe acute respitory syndrome
FRR	Flux recovery ratio
pH	Potential hydrogen
SEM	Scanning electron microscopy
AFM	Atomic force microscopy
GCMS	Gas chromatography mass spectrometry
HPLC	High performance liquid chromatography
LCMS	Liquid chromatography mass spectrometry
SPE	Solid phase extraction
TLC	Thin layer chromatography
SFC	Size exclusion chromatography
DMF	Dimethylformamide

SIM	Selected ion monitoring
IS	Internal stanadard

List of Symbols

D_i	Diffusivity of species
K_{ic}	Hindrance factor
K_{ow}	Octanol-water partition coefficient
pKa	Acid dissociation constant
C_p (µs/cm)	Concentration of permeate
C_f (µs/cm)	Concentration of feed
R (%)	% rejection
J_v (L/m^{2}hr)	Flux
Q	Flow rate
V (m^3)	Volume
A (m^2)	Area
t (s)	Time

Chapter 1

Introduction

1. Introduction

1.1 Background

Conventional wastewater treatment methods have been questioned over the past few years. Endocrine-disrupting chemicals such as pharmaceuticals have been found in several water bodies due to inadequate treatment. Although they are found at low concentrations, they pose a tremendous threat to aquatic and human life (Wang et al., 2018a). The dangers of pharmaceuticals in wastewater stem from their inability to completely metabolize in the human body. They are therefore excreted through urine as mostly active metabolites of compounds that can remain unchanged or be conjugated to polar molecules (Reddersen et al., 2002). In some cases, they are either partially retained in sludge or metabolised to a more hydrophilic but still persistent form, allowing it to pass through the water treatment process (Radjenovic et al., 2007).

Among the several pharmaceuticals that have been found in previous studies, Carbamazepine (CBZ), diclofenac (DCF), ibuprofen (IBU), and aspirin (ASP) be remarkably persistent (Shraim et al., 2017). Membrane technology has been a promising advancement in the water treatment industry due to its high-water quality effluent, small footprint, and shorter treatment time than conventional treatment methods (Aziz & Kasongo, 2021). Membrane technology consists of different types of membrane processes as a practical application, such as microfiltration (MF), ultrafiltration (UF), nanofiltration (NF), and reverse osmosis (RO) and membrane bioreactor (MBR). Previous studies (Chapman et al., 2004) state that the MBR process is already being implemented on an industrial scale in countries like Singapore and Canada.

1.1.1. Municipal wastewater treatment processes

Wastewater treatment stems from domestic, industrial and commercial wastewater that must be transformed into a higher-quality effluent for reuse or disposal in the environment (Ramalho, 2013). The process consists of primary, secondary, and tertiary steps and includes physical, biological, and chemical treatment.

The primary phase in the commercial activated sludge process involves settling the solids in a pre-settling basin or primary clarifier. At the same time, grease and fats float to the top (Sipma et al., 2010). The secondary phase removes dissolved and suspended biological matter and uses a separation process. The tertiary treatment further removes the organic and colloidal matter before discharge.

Conventional activated sludge processes are slowly being phased out and replaced with more modern technology such as membrane technology, but more specifically membrane bioreactors as a means of secondary and reverse osmosis, and tertiary treatment (Cirja et al., 2008)

1.1.2   Problems associated with the discharge of municipal wastewater

Previous studies have made it clear that conventional municipal wastewater treatment processes have not been effective enough in removing micropollutants. Micropollutants such as pharmaceuticals have mimicked endogenous steroid hormones and initiated similar hormonal responses (Susan et al., 1998). Another study (Pomati et al., 2006) suggested that pharmaceuticals at environmental concentrations can inhibit human embryonic cell growth. Experimental evidence indicates that pharmaceuticals may cause harmful effects, such as morphological, metabolic and sex alterations on aquatic species, antibiotic resistance in aquatic pathogenic microorganisms, and disruption of biodegradation activities in sewage treatment plants (Bottoni et al., 2010; Komesli et al., 2015).

1.1.3   Reverse Osmosis Membranes

Several previous researchers have concluded that membrane technology is on the rise to becoming a much more sophisticated treatment process. (Al-rifai et al., 2011) suggests that nanofiltration (NF) and reverse osmosis (RO) are among the most promising technologies and are becoming more popular in wastewater treatment plants. RO can be used to treat secondary municipal wastewater and remove organic, and inorganic constituents producing a higher quality permeate for reuse or disposal into more fragile receiving bodies (Dolar et al., 2012; Aziz & Kasongo, 2021). The advantage of RO membranes is that it produces a high-quality effluent, almost removing all emerging micropollutants (EMPs), contaminants of emerging concerns (CECs) and can perform at low pressures, hence, less energy making it more economically cost-effective.

1.2.   Research problem

The emerging micropollutants (EMPs) in municipal secondary MBR effluent have become a big problem causing immense antagonistic effects on the ecological biota and human health. Existing conventional wastewater treatment plants have demonstrated ineffective removal of MPs, CECs such as pharmaceuticals. Enhanced, innovative and highly sensitive analytical technologies are needed to detect their low concentration in complex matrices such as secondary wastewater. Under these circumstances, reverse osmosis with thin-film composite membranes are a possible solution for pharmaceutical removal.

1.3   Research topic

Researchers say reverse osmosis has shown promising results. They could be a suitable tertiary treatment for secondary municipal wastewater to remove emerging pollutants, specifically pharmaceuticals. It was previously suggested that NF/RO is an ideal treatment process for removing trace organic contaminants; however, the complexity of the separation process and the physiochemical properties play a significant role in the effluent quality. Therefore, parameters such as feed pressure, initial concentration and the type of membrane investigated can be controlled further to investigate the behaviour of the pharmaceuticals and their removal.

1.4   Research questions

o   How effective would the removal of inorganics using an RO bench scale system be, at varying feed pressures and operating time?

o   What effect will the feed pressure and concentration have on the removal of the pharmaceuticals?

1.5   Aim and Objectives

This study investigates the removal of inorganics and pharmaceuticals in secondary municipal MBR effluent with low-pressure and low energy-intensive membranes using a RO bench-scale unit for yielding effluent discharge or recycling application.

Objectives:

o   Evaluate two types of thin-film composite (TFC) polyamide (PA) membranes (NF and RO) based on their different characteristic properties to measure the best quality of effluent with the removal of targeted inorganics and COD.

o   Investigate the removal efficiencies of selected pharmaceuticals: aspirin (ASP), carbamazepine (CBZ), ibuprofen (IBU) and diclofenac (DCF) using solid-phase extraction (SPE) and gas chromatography-mass spectrometry (GCMS) for quantification in the water.

1.6   Delineation

This study focused on removing selected Inorganics, COD and pharmaceuticals, carbamazepine, diclofenac, ibuprofen, and aspirin from secondary municipal membrane bioreactor wastewater effluent using a lab-scale RO system as a tertiary treatment process. A lab-scale RO system was used as a tertiary treatment process and GCMS to analyse and quantify the pharmaceuticals removed. This research focused on the effects of feed pressure and concentration on evaluating the membrane's removal efficiencies and performance. Quantitative analysis investigating membrane surface characteristics with the usage of Scanning Electron Microscopy (SEM), Attenuated Total Reflection-Fourier Transform Infrared Spectroscopy (ATR-FTIR), and Energy Dispersive X-Ray Spectroscopy (EDX) were applied. All other factors were delineated.

1.7   Thesis outline

Chapter 1:
Provides insight and knowledge of the background of the study and focuses on critical points such as research aim and objectives and the significance of the study.

Chapter 2:
Gives a detailed look into the theory and literature of previous studies within a similar context linked to this research.

Chapter 3:
Provides details of the experimental work done, including equipment, apparatus and procedures performed for data acquisition.

Chapter 4:
Discusses results obtained from experimental runs

Chapter 5:
Concludes the research achieved from the experimental work done and gives recommendations and suggestions on improvement

Chapter 2

Literature review

2.   Literature Review

2.1   Water scarcity

The complexity of water and its need for sustainability is, without a doubt, a global crisis. Water is the precondition for sustainable development, human and animal survival, and healthy ecosystems and is critical for socio-economic development. Water is also a primary need for reducing the global burden of diseases and improving health and welfare and the productivity of populations. Water is also at the heart of adaptation to climate change, serving as the crucial link between the climate system, human society and the environment. Without proper water governance and management tactics, competition between sectors would increase and escalate water crises of various kinds. The physical world of water is closely bound to the socio-political world.

Water availability is becoming less predictable in many regions of the world. Increased natural incidences such as floods and droughts have become more popular and put a strain on sanitation facilities and contaminated water sources. Globally, water scarcity already affects every four out of ten people. The lack of clean water and availability increases the risks of water-borne diseases and is the cause of 2.2 million deaths per year (UN, n.d.). It has been predicted that by 2025, 1.8 billion people will live in completely water-scared countries or regions. Two-thirds of the world's population will be under water-stressed conditions, 203 billion people don't have access to basic sanitation, and 31% of schools worldwide don't have clean running water (UNESCO, 2012).

Treating wastewater for reclamation purposes is a great way to save and avoid water shortages for both present and future purposes, especially because South Africa is a semi-arid region with little rainfall and high demands due to increasing population (Adewumi et al., 2010).

2.2 Technologies for the treatment of municipal wastewater

According to (Melvin & Leusch, 2016), five major treatment technologies treat municipal wastewater. The five technologies include conventional activated sludge (CAS), oxidation ditch (OD), membrane bioreactor (MBR), ponds and constructed wetlands (PCW) and trickling biological filters (TBF). However, CAS and MBR have been used globally to treat sewage wastewater.

2.2.1 Conventional activated sludge (CAS)

The activated sludge process has two major units, i.e. aerated reactor and a secondary sedimentation tank (Von sperling, 2007). The biochemical reactions for removing organic and colloidal matter occur in the aeration tank, while biomass solids are settled in the secondary sedimentation tank (Von sperling, 2007). The settled biomass solids in the sedimentation tank are recycled back to the feed tank, producing a higher biomass concentration in the aerated reactor (Von sperling, 2007). The excess sludge from the sedimentation tank is removed and undergoes further treatment.
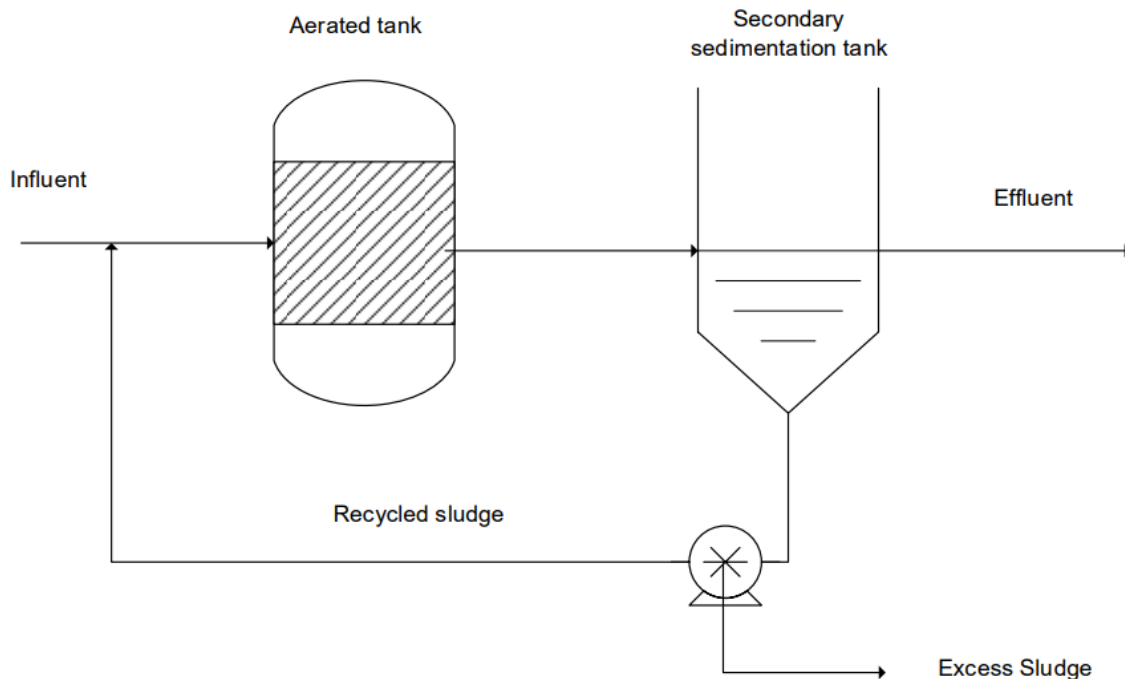
Figure 2-2-1: Representation of the main units in an activated sludge system **(Von sperling, 2007)**

2.2.2 Trickling biological filters (TBF)

Trickling filters consist of a tank packed with a porous medium such as stones, wooden chips, plastics and other materials to create a highly permeable filter (Von sperling, 2007). Above the tank are rotating jets in which the wastewater sprays from the hydraulic head onto the medium for filtration. The water percolates downward over the porous medium, allowing bacterial growth. The wastewater flows through the biofilm media, allowing contact between the wastewater and the biofilm, thus allowing the organic matter to be absorbed by the biofilm and retained long enough for stabilisation to occur (Von sperling, 2007).

2.2.3 Oxidation ditch (OD)

An oxidation ditch is a modified version of an activated sludge system and is typically a complete mix system that utilises long solid retention times for the removal of biodegradable organics; they can, however, be modified to satisfy plug flow conditions (USEPA, 2000). It is preferred due to its high rates of nitrogen and phosphorus removal (Feng et al., 2011).

2.2.4 Ponds and constructed wetlands (PCW)

Ponds and constructed wetlands treat municipal, industrial and grey wastewater and are a completely natural process, utilising vegetation, soil and microbial populations as removal mechanisms (Ynoussa et al., 2017). It was not designed for the removal of pathogens but rather to remove other water constituents such as nutrients, chemical oxygen demand (COD) and biological oxygen demand (BOD) (Ynoussa et al., 2017).

2.2.5 Membrane bioreactor

Membrane bioreactors are generally used to define wastewater treatment processes using a selectively permeable membrane such as microfiltration or ultrafiltration. They are integrated with a biological process (Judd & Judd, 2008). The small pore size of the membrane produces a high-quality effluent and significantly decreased pathogenic concentration. It has become a popular process for treating and reusing municipal wastewater. Mixing characteristics are essential for the MBR systems because they can affect the efficiency of organic removal and the settling of solid sludge (Ladewig & Al-Shaeli, 2017). It has become a more popular solution for clarifiers of conventional activated sludge systems and gravity processes, replacing membrane separation modules (Radjenović et al., 2009). These modules mimic MF and UF processes, have a pore size of 0.05-0.4μm, enable the solid-liquid separation, and act as an advanced treatment unit for specific pollution agents (Ladewig & Al-Shaeli, 2017).

According to Alturki et al. (2010), MBR has been proven to have enhanced the removal of biodegradable and hydrophobic trace contaminants compared to CAS. Table 1 shows a comparison of removal efficiencies between MBR and CAS.

Table 2-1: Comparison of average percentage removal of trace contaminants (pharmaceuticals) from MBR and CAS (Sipma et al., 2010)(Sahar et al., 2011)

Compound	% Average Removal	
Anticonvulsant	CAS	MBR
Carbamazepine	-8	0
Anti-inflammatory		
Diclofenac	21	34
Ibuprofen	93.5	97.3
Pain Killer		
Aspirin	97	99

According to Alturki et al. (2010), some of the advantages of MBR to CAS include the smaller footprint, higher quality effluent, smaller reactor volume required and operating at higher solids retention time. However, despite the high-quality effluents produced, environmental quality standards are still not reached without a tertiary step; thus, MBR is used as a pre-treatment step before the tertiary step is implemented (Hoinkis et al., 2012).

2.2.6 The use of MBR in wastewater treatment

As previously mentioned, membrane bioreactors are slowly phasing out conventional activated sludge systems due to their many advantageous properties. There are two types of membrane configurations, one in which the membrane is connected to an activated sludge system and is known as a side stream configuration (Judd & Judd, 2008). The second configuration is an immersed configuration, in which the membrane is situated inside the tank. This configuration enhanced MBR's performance (Judd & Judd, 2008). The permeate is sucked under pressure through the membrane and removed from the reactor(Galinha et al., 2018). Figure 2-2 below gives a basic representation of the two configurations.
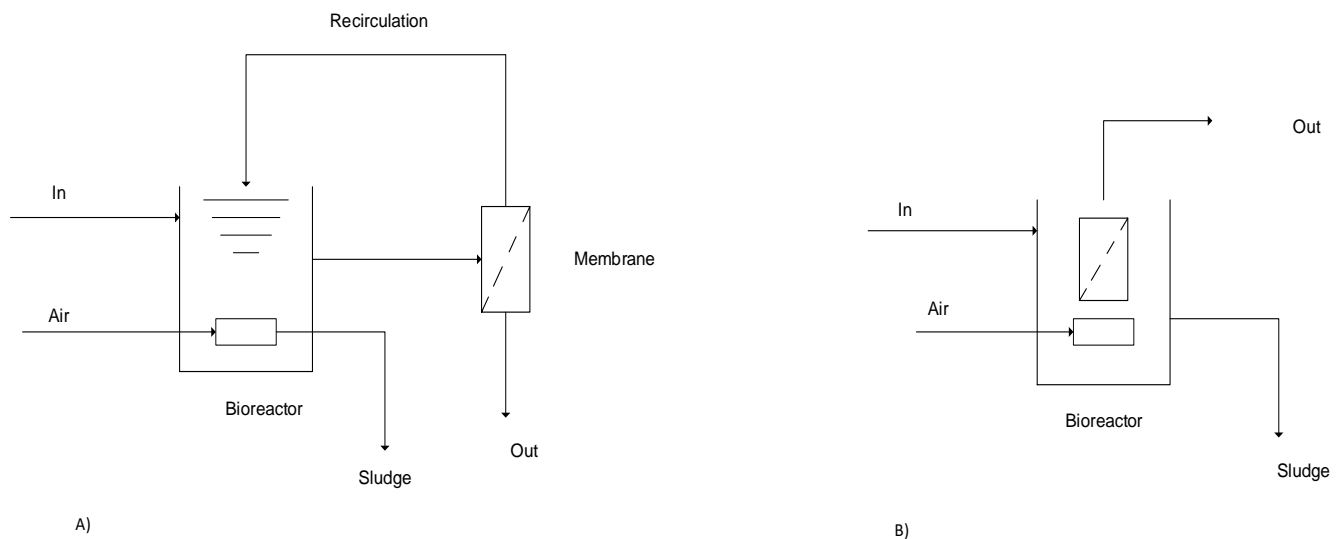
Figure 2-2: A) Sidestream MBR configuration (left), B) Immersed MBR configuration (right) (Judd & Judd, 2008).

2.3   Membrane Technology

Membranes are used for the separation of materials; it is essentially a barrier that can restrict the transportation of various constituents from passing, mainly in a selective manner (Wang et al., 2011)
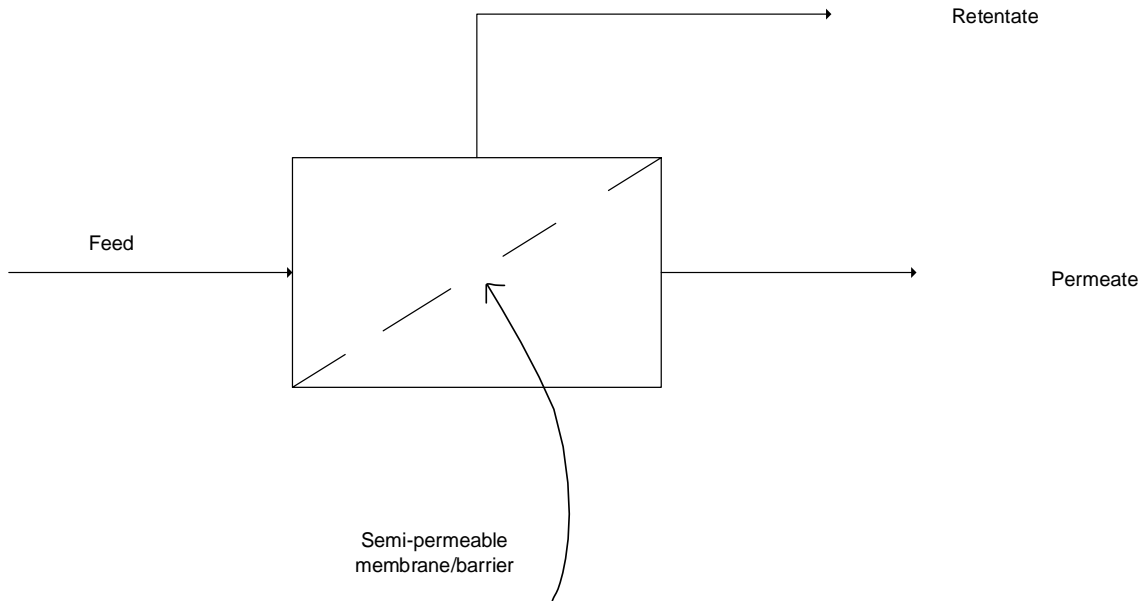
Figure 2-3: Representation of a membrane used for water treatment (Kucera, 2015)

According to (Wang et al., 2011), synthetic membranes can be classified by the properties they hold, i.e. the membrane morphology, charge/zeta potential; geometry as well as separation process; for example, synthetic membranes can be classified as either organic (polymeric) or inorganic (ceramic/metal) (Wang et al., 2011). Membranes produced commercially are either asymmetric or thin-film composite (TFC) membranes. Asymmetric membranes have a dense but very thin top layer supported by a sub-porous layer and characterised by the same chemical composition (Childress & Elimelech, 1996). . Most common TFC RO membranes are typically composed of three layers: a polyamide ultrathin top layer (<0.5 mm), a polysulfone intersupport layer (40-50 μm), and a thicker polyester fabric support (>120 mm) .The dense, thicker support layer is necessary for mechanical strength under high hydraulic pressure (Heo et al., 2019).The polyamide layer is a synthetic layer that makes the membrane less susceptible to biological attack (Scott, 1996). Some advantages of TFC membranes over asymmetric membranes include their ability to operate at a higher flux and lower pressure, making them economically more viable. They have higher salt rejections and a wider pH range between 2-12. They have greater chemical stability, are not biodegradable, and have a broad

temperature spectrum, ranging from 0-40°C (Scott, 1996). Ceramic membranes are often used in ultrafiltration and microfiltration processes when thermal, and solvent resistance are required. (Baker, 2004).

2.4　　　Membrane configurations

There are five basic membrane module designs (Scott, 1996); they include;

- Spiral wound
- Hallow fibre
- Tubular
- Plate and frame
- Capillary

2.4.1　Spiral wound

Spiral wound membranes are the most commonly used membranes for reverse osmosis applications. One of its most significant advantages is its high packing density which ranges from 150-380 ft^2/ft^3 (Kucera, 2015). A spiral wound membrane consists of a flat sheet membrane followed by a mesh spacer and porous permeate flow material wrapped around the permeate collecting tube (Scott, 1996). The sandwich-like assembly is thus wounded spirally, forming a cylindrical module (Berk & Berk, 2009). The feedwater enters the membrane axially and flows through the channels which the spacers create, and exits on the opposite end of the membrane(Kucera, 2015; Scott, 1996; Berk & Berk, 2009)
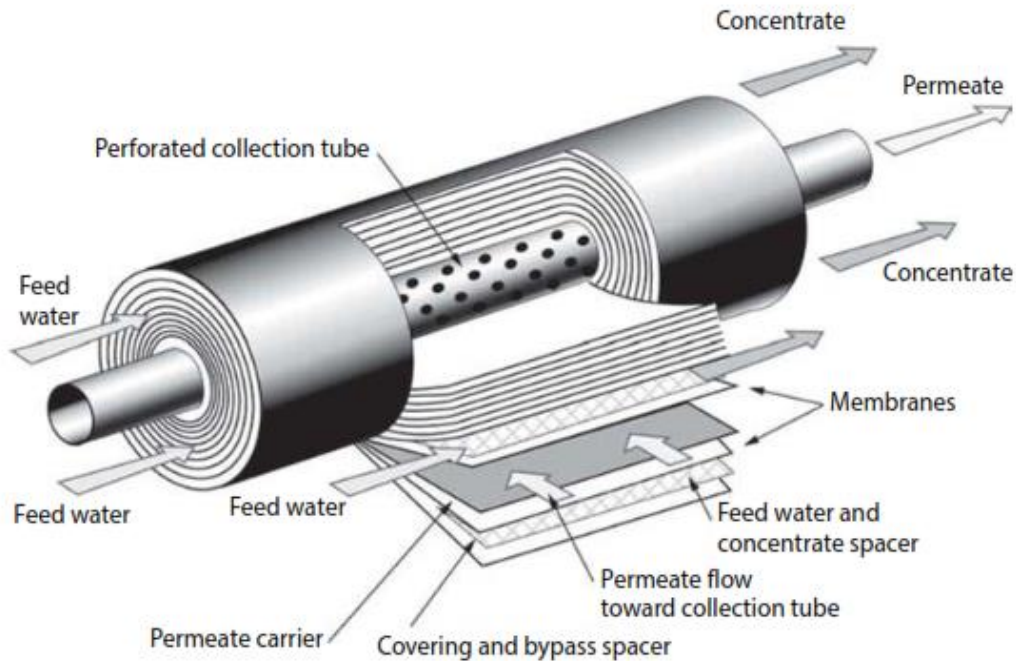
Figure: 2-4: Deconstructed spiral wound RO membrane **(Kucera, 2015)**

2.4.2   Hollow fibre

Hollow fibre membranes are best known for their application in reverse osmosis desalination. The design includes a shell-like structure holding, in which a bundle of membrane fibres are packed. In principle, they are very similar to the tubular module; however, the "tubes" are much thinner in diameter, ranging from 1mm down to capillary size (Berk & Berk, 2009). The diameter of the external membrane fibres is between 80 and 200 microns, while the wall thickness is as low as 20 microns (Scott, 1996).
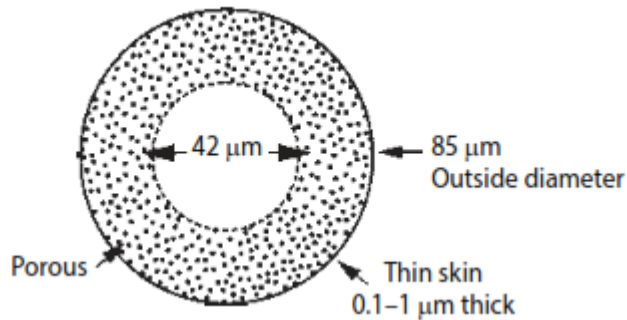
Figure2-5: Cross-sectional view of a hollow fibre membrane **(Kucera, 2015)**

2.4.3 Plate and frame

Plate and frame modules are not typically used in water purification facilities but in exceptional cases where high suspended solids applications are applicable. They consist of flat sheets of the membrane stacked back to back or side by side; these membranes are then stacked within a frame for support (Kucera, 2015). The configuration has spacers between the membranes to avoid sticking and allow the feed and permeate water to pass through (Kucera, 2015). They cannot withstand high pressure and are limited to MF and UF. The surface-to-volume ratio of a plate and frame module is not high (Berk & Berk, 2009)
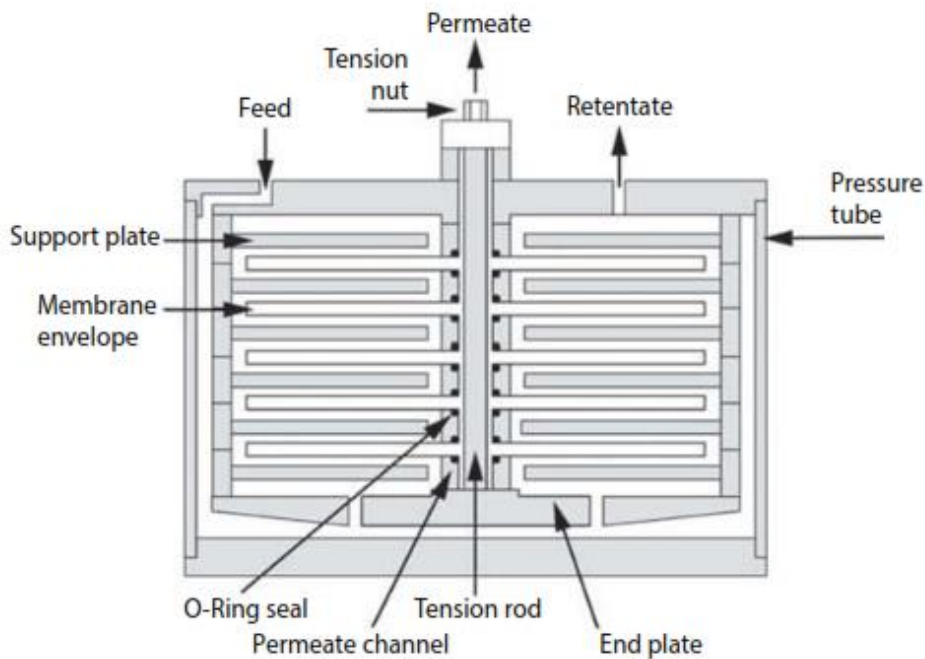
Figure 2-6: Plate and frame membrane configuration **(Kucera, 2015; Baker, 2004; Berk & Berk, 2009)**

2.4.4 Tubular

Tubular modules are commonly used in food and biological processes with high solids applications. The membrane's feed side is on the inside of the tube. The diameters of the tubular modules range from (1.3-to 2.6)cm and have a packing density between (6-and 120) ft^2/ft^3 (Kucera, 2015). The tubular module resembles a shell and tube heat exchanger, having the RO feed on the tube side and the permeate on the shell side (Kucera, 2015). Tubular membrane modules are primarily used in ultrafiltration (UF) and microfiltration (MF) applications as opposed to RO due to their lower packing density (Kucera, 2015).
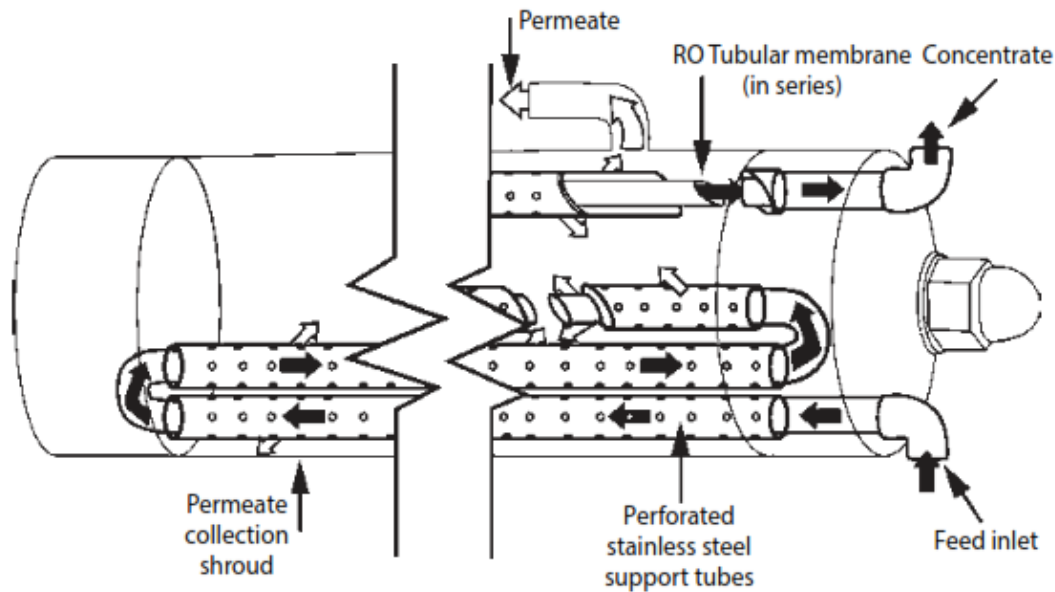
Figure 2-7: Tubular RO module membrane with the membrane tubes in series to the housing (Kucera, 2015).

2.4.5 Membrane processes for wastewater treatment

Membrane processes are based on the application, treatment, and the required quality effluent. Several membranes and applications are available; these include ultrafiltration, microfiltration, nanofiltration, and reverse osmosis (Kucera, 2015).

2.4.5.1 Ultrafiltration (UF)

Ultrafiltration membranes have a finely porous surface layer and can remove particles of size 0.001-0.1µm from fluids (Baker, 2004). It merely separates water and micro solutes from macromolecules and collides. The removal of viruses can be applied to pre-treatment water for Nanofiltration or reverse osmosis (Baker, 2004).

Ultrafiltration is applied to the dairy industry (milk and cheese), food industry (proteins), the metal industry for the separation of oil/water emulsions and paint treatment, as well as the textile industry (Kucera, 2015).

2.4.5.2 Microfiltration (MF)

Microfiltration membranes have a porous membrane often used to remove suspended particles, a pore size of 0.1-10µm. The membrane often falls between ultrafiltration and conventional filters (Baker, 2004).

The membrane removes all bacteria but often serves to remove large organic molecules, large colloidal particles and many micro-organisms. Microfiltration performs as a porous barrier to reduce turbidity and some types of colloidal suspensions. Examples of microfiltration applications include cold sterilisation of beverages and pharmaceuticals, clearing fruit juices, wines and beer, separating wastewater bacteria, effluent treatment, and separating water/oil emulsions (Kucera, 2015; Baker, 2004).

2.4.5.3 Nanofiltration (NF)

Nanofiltration membranes have a pore size of 1-5nm and retain ions and low molecular weight organics. Nanofiltration is the most recent developed pressure-driven membrane process for liquid-phase separations due to lower energy consumption and higher flux rates (Codotte, 1988). The size of pores in nanofiltration membranes is such that even small uncharged solutes are highly rejected. Nanofiltration exhibits properties between those of ultrafiltration and reverses osmosis (Kucera, 2015; Hamingerova et al., 2015).

2.4.5.4 Reverse Osmosis (RO)

Reverse osmosis forces a solvent from a region of high solute concentration through a semi-permeable membrane to an area of low solute concentration by applying pressure above the osmotic pressure (Baker, 2004).

High pressure is exerted on the high concentration side of the membrane. The process is best known for its use in desalination and freshwater purification for medical, industrial, and domestic applications. Reverse osmosis for water purification requires no thermal energy (Kucera, 2015; Mulder, 1998). After secondary treatment, it is recently used as a tertiary process to produce a high-quality effluent for reuse or disposal into more fragile receiving water bodies (Alturki et al., 2010).

2.4.6 MBR-RO hybrid treatment process for the treatment of micropollutants in municipal wastewater.

Several studies have explored different secondary treatment methods that would be viable and sustainable for removing micropollutants. Membrane technology has proven more successful in its economic viability, convenience, and efficiency (Wang et al., 2017). The membrane allows for bacteria and viruses to be partially removed, requiring less chlorine or ozone to be used, which have also been shown to produce toxic by-products (Cartagena et al., 2013).

According to Radjenovic et al. (2007), membrane bioreactors have better removal efficiency of pharmaceuticals, as much as (>80%) as opposed to conventional activated sludge systems. Some of the pharmaceuticals included naproxen (99.3%), ofloxacin (94%), sulfamethoxazole (95.5%) and Carbamazepine (89.5%). The study was performed on a lab-scale MBR system. Another study was done by Kimura et al. (2004) on the effect of reverse osmosis polyamide membrane on the removal efficiencies of different pharmaceuticals. It showed successful results ranging from 51%-91% removal rates. The results produced by both studies and several other studies have shown very promising results. Dolar et al. (2012) decided to combine the two membrane technologies and produce a hybrid system consisting of an MBR-RO pilot-scale plant for the treatment of municipal wastewater but more particularly for the removal of pharmaceuticals of all classes ranging from anti-biotics to psychiatric drugs and produced results that exhibited excellent removal efficiencies, of which some were greater than 99%. The study was conducted using a real wastewater feed from a coastal municipal WWTP (Castell-Platja d'Aro, in Catalonia, NE of Spain). The pilot plant was installed in the WWTP. The plant consisted of a primary wastewater settler, followed by an MBR with an (anaerobic, anoxic and aerobic) configuration with a compartment for biological nutrient removal. The membrane compartment held $8m^2$ of flat sheet membrane, and the temperature inside the reactor was 16±0.5 °C. The MBR system ran at a hydraulic retention time of 8hr and a solid retention time of 45 days. The MBR's effluent served as feed for the RO system, which used a crosslink aromatic polyamide membrane having a negative charge. The transmembrane pressure was 10 bar, and the flow of the RO element was 179.35±1.28 L/hr. Although the removal rates were very high for certain pharmaceuticals in the MBR stage of the process, the physiochemical properties played a big part in the removal efficiencies. Therefore, the RO part of the process showed a >99% removal rate for all compounds, with size exclusion, electrostatic attraction and repulsion being the main removal mechanisms for RO.

2.5   Transport Models

2.5.1 Donnan-Steric-Pore-dielectric Model

The Donnan-Steric-Pore-dielectric model (DSPM&DE) predicts ion rejections of binary and multicomponent systems (Vezzani & Bandini, 2002). The model describes the mass transfer of electrolytes and neutral solutes through a nanofiltration membrane. This model is based on the extended Nernst-Planck equation. The model considers three separation mechanisms, i.e., distribution of species at the membrane/feed solution interface, solute transport through the pores, and distribution of species at the membrane/permeate interface.

The membrane's active layer is considered a charged porous layer characterised by three adjustable parameters, i.e., average pore radius, effective membrane thickness, and volume charge density.

The dielectric exclusion (DE) phenomenon arises when aqueous ionic solutions contact different dielectric media.

By considering the motion of ions unidirectional through the membrane and assuming an ideal solution, the transport equation for a species I can be written as:

Equation 2-1: Transport equation

$$j_i = J_v K_{ic} c_i - D_{ip}\frac{dc_i}{dx} - z_i c_i D_{ip}\frac{F}{RT}\frac{d\psi}{dx}\dots.(2-1)$$

Where $D_{ip} = K_{id} D_{i\infty}$, $D_{i\infty}$ is the diffusivity of the species in water at infinite dilution. Kic and Kid's hindrance factors correct the convection and diffusion terms. K_{ic} is a drag factor accounting for the effects of the walls of the pores on the specie motion (Bandini & Vezzani, 2003). K_{id} represents the effect of the pore to reduce the solute-solvent diffusion coefficient below its value in a free bulk solution, $D_{i\infty}$. Equations 2-1 can be written to obtain a relationship between the concentration and electric potential gradients.

2.6   Pharmaceuticals

2.6.1 NSAID's

Non-Steroidal anti-inflammatory drugs are a class of pharmaceuticals used to treat pain, fever, and blood clotting and are most commonly used to reduce inflammation. The term non-steroidal distinguishes them from the steroid class. NSAIDs work by inhibiting the enzyme cyclooxygenase (COX-1and/or COX-2) (Ardoin & Sundy, 2006). These enzymes are responsible for synthesising biological mediators prostaglandins and thromboxane, responsible for inflammation and blood clotting, respectively (Day & Graham, 2004). There are two classes of NSAIDs available they include non-selective and COX-2 selective. Non-selective NSAIDs inhibit both enzymes COX-1 and COX-2; they are most common and are associated with the risk of gastrointestinal ulcers and bleeds and inhibit platelet aggregation (Day & Graham, 2004). COX-2 selective inhibitors show fewer gastrointestinal side effects but are associated with thrombosis, which leads to an increased risk of heart attacks.

2.6.2 Lipid regulators

Statins (or HMG-CoA reductase inhibitors) are a class of drugs that reduce cholesterol by inhibiting the enzyme HMG-CoA, which has a central role in producing cholesterol in the liver. These drugs share a commonality of the end of their name. This makes recognition of drugs from these drugs easy. The statins (atorvastatin, Fluvastatin, pravastatin, rosuvastatin, and simvastatin) competitively inhibit HMG-CoA reductase. Statins are more effective than other lipid-regulating drugs at lowering LDL-cholesterol concentration but are less effective than fibrates in reducing triglyceride concentration (Tidy. C,2014). Statins are also thought to have non-cholesterol-related effects such as restoring/improving endothelial function and anti-inflammatory properties (Tidy. C,2014).

2.6.3 Anti-convulsants

Anti-convulsant drugs are also known as anti-epileptic drugs and are essentially used to treat seizures without adversely affecting the central nervous system (Beani et al., 1985). This class of pharmaceutical drugs has also been used to treat personality disorders such as bipolar and seems to act as mood stabilisers for treating neuropathic pain. Some common drugs in this class include; Acetazolamide, Carbamazepine/Tegretol, Clobazam, Clonazepam etc. (Rogawski & Löscher, 2004).

2.6.4 Anti-biotics

Anti-biotics are natural compounds that are produced mainly by plant micro-organisms. Their biological activity and behaviour against microorganisms allow them to destroy microbes in-vivo (Korzybski et al., 1967). They treat several bacterial infections, from respiratory to urinary tract infections; however, they do not work to treat viral infections. These classes of antibiotics include (Gualerzi & Brandi 2014):

- Penicillin-based, such as Amoxicillin. They treat various infections such as skin infections, urinary tract infections, and chest infections.
- Cephalosporins such as cephalexin. More effective in treating more severe infections such as meningitis and septicemia.
- Aminoglycosides such as gentamicin and tobramycin. This class of antibiotics are only used in hospitals to treat severe cases of septicemia and is often given via injection.
- Tetracyclines, including doxycycline, treat acne and a skin condition called rosacea.
- Macrolides are often used to treat patients allergic to penicillin-based antibiotics and are more commonly used to treat chest and lung infections.
- Fluoroquinolones such as ciprofloxacin. Not very often used anymore but was used as a wide-spectrum antibiotic for urinary tract and respiratory infections.
- Sulfonamides such as sulfamethoxazole are used to treat ear infections, urinary tract infections, bronchitis and diarrhoea.

2.6.5   β-Blockers

Beta-blockers are a class of medications used to treat several conditions, including high blood pressure, angina, abnormal heart rhythms, heart, anxiety, migraine, glaucoma, and overactive thyroid symptoms. They are often used to prevent the stimulation of the adrenergic receptors responsible for increased cardiac action, control heart rhythm, treat angina, and reduce high blood pressure (Cleophas, 2011; Mottram, 2018).

2.6.6   Stimulants

Stimulants are informally known as "uppers" and fall under a class formally known as psychoactive drugs. They temporarily increase alertness and energy and increase activity in the brain. Stimulants can often be addictive and share commonalities. Drugs that are classed as stimulants include(Juliano & Griffiths, 2004):

- Caffeine
- Nicotine
- Methamphetamine
- Prescription stimulants

2.7   Environmental concerns and commonly found pharmaceuticals

The fundamental concern about pharmaceuticals in several water bodies lies with wastewater treatment before discharge. The increase in population and demand for water puts immense pressure on sewage treatment plants (STPs). Their incompetency to properly treat wastewater, especially for disposal into fragile water bodies, creates a toxic environment for living aquatic life. Most pharmaceuticals are designed to perform their given function and exit the body. However, most pharmaceuticals are not fully metabolised; therefore, when excreted by the body, they leave as active metabolites without degrading, resulting in them entering freshwater systems still pharmacologically active (Klaminder et al., 2014; Radjenovic et al., 2007). The complexity of pharmaceuticals and the different branches makes it challenging to perform specific tests since concentrations of individual pharmaceuticals in the aquatic environments are far lower than effective doses. Therefore, it would seem like they cannot produce acute effects (Bottoni et al., 2010).

2.7.1   Natural removal mechanisms for micropollutants

Micropollutants are present in low concentrations and high diversity. Some micropollutants are only partially removed by wastewater treatment plants (WWTP) by conventional treatment methods through a mechanism known as sorption (including adsorption and absorption) and biodegradation onto activated sludge. This is considered the most important mechanism of removal of emerging contaminants. Adsorption is the physical adherence of molecules or ions of the micropollutant onto the surface of a sorbent. These mechanisms occur with electrostatic interactions characterised by the dissociation constant (pK_a) (Gruchlik et al., 2018). Absorption involves the incorporation of the pollutant into the sorbent. Some examples are algal uptake and hydrophobic interactions characterised by the (octanol-water partition coefficient) K_{ow} value.

Table 2-2: Initial concentration of selected pharmaceuticals from different studies

Compound	Concentration range	Target Analysis	References
Diclofenac	10^4-10^5 ng/l 1 g/l 36.04-87.80 µg/l 0.06-1.9 µg/l 0.17-0.53 µg/l 0.028-6.88 µg/l 6987 ng/l	LC/MS HPLC LC/MS LC-MS HPLC LC-MS HPLC	(Kim et al., 2014) (Radjenovic et al., 2007) (Racar et al., 2020) (Gomez et al., 2006) (Verlicchi et al., 2012) (Sim et al., 2011) (Heo et al., 2019)
Carbamazepine	10000 ng/l 1mg/ll 1g/l 2438.9 ng/l 11.26 µg/l 5mg/l	LC/MS GC/MS HPLC LC-MS LC-MS HPLC	(Kim et al., 2014) (Kimura et al., 2004) (Radjenovic et al., 2007) (Chon et al., 2012) (Kaplan et al., 2020) (Phadunghus et al., 2017)
Ibuprofen	10000 ng/l 1g/l 0.3-63µg/l 1.01-63.87 µg/l 0.069-8.9757 µg/l 2724 ng/l	LC/MS HPLC LC-MS/MS LC-MS/MS LC-MS/MS HPLC	(Kim et al., 2014) (Radjenovic et al., 2007) (Kanama et al., 2018) (Kanama et al., 2018) (Thomas et al., 2007) (Heo et al., 2019)
Aspirin	0.50 mg/l	HPLC-PDA	(Fatima Ayyash, Mustafa Khamis, Samer Khalaf, 2015)

2.7.2   Detection of SARS-CoV-2 in untreated wastewater

The global pandemic caused by the novel Coronavirus in 2019, declared an international public emergency, has reported high fever, coughing, difficulty breathing, diarrhoea, and vomiting. The virus has been detected in symptomatic and asymptomatic patients (Gao et al., 2020; Holshue et al., 2020). The disease was spread through contact with an infectious person through sneezing or coughing droplets. The clinical observations imply that the virus may be detected in wastewater treatment plants in areas affected by SARS-CoV-2. A study conducted by (Ahmed et al., 2020) suggested that the wastewater based-epidemiology be used for surveillance as a public tool for public health monitoring at a community level. Studies conducted in other parts of the world (i.e. Netherlands and USA) detected molecular concentrations of SARS-CoV-2 in wastewater samples (Lodder & de Roda Husman, 2020;

Medema et al., 2020). The increase in the rate of infections means an increase in the viral load on the sewer systems in several cities. Although it has not been confirmed whether or not SARS-CoV-2 can remerge or spread via wastewater, it is essential to collect information and understand the occurrence and fate of the virus and ensure there are no risks to sewage workers. Researchers investigated the presence of such RNA in municipal WWTPs of Spain and detected them in the untreated water (Randazzo et al., 2020). The SARS-CoV-2 RNA was present in 11% of the secondary treated water samples. Studies (Majumder et al., 2021) indicated that the presence of SARS-CoV-2 RNA in wastewater was proportional to the number of people affected.

Furthermore, effective wastewater monitoring can aid in identifying places where people are infected with COVID-19. SARS-CoV-2 was unstable in the presence of disinfectants and at temperatures greater than 20°C (Wang et al., 2005; Race et al., 2020). however, most viruses are highly stable, even in harsh environmental circumstances. On the other hand, these viruses can survive when encased in faeces or suspended solids. Furthermore, the virus entrapped in sewage can produce virus-laden aerosols during wastewater flushing, providing a channel for the virus to spread through the air.

2.7.3 Carbamazepine

Carbamazepine is an anti-epileptic drug used to control seizures and treat trigeminal neuralgia and some psychiatric disorders such as bipolar disorders. It is known to block sodium currents in your brain and body. This helps to reduce abnormal electrical activity between your nerve cells. It often tops the EC list regarding concentration and extent of occurrence (Murray et al., 2010).it has potent physiological effects on non-target organisms. It induces a great deal of oxidative stress on organs, alters the activity of certain enzymes and affects feeding productivity, reproduction and growth of non-target organisms, even when taken up at low concentrations. It is a high risk to humans because it can alter embryonic cells (Pomati et al., 2006). Carbamazepine causes impairments of antioxidant enzymes of Clam Rudi tapes. It is therefore important to mitigate these pharmaceuticals from wastewater before discharge. Carbamazepine is commercially known as Tegretol and is taken orally. The drug's dosage is usually prescribed by a doctor and the patient's response to the medication. Common side effects and allergic reactions include hives, facial or throat swelling, difficulty breathing, nausea and vomiting, dry mouth, dizziness, aplastic anaemia, etc.

A study was done in Germany among 32 drugs found in a wastewater sewage plant; Carbamazepine topped the list with a concentration of 6.3 mg/l. Another study was the second-highest drug found among 73 pharmaceuticals (Urtiaga et al., 2013).
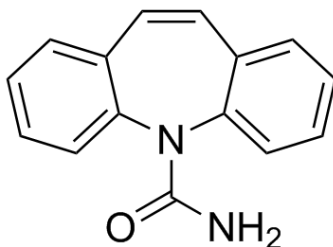
Figure 2-8: Structural formula of carbamazepine (CBZ) **(Grzesiak et al., 2003)**

2.7.4   Diclofenac

Diclofenac is a nonsteroidal anti-inflammatory drug (NSAID) to alleviate degenerative joint diseases. Rheumatoid arthritis, osteoarthritis, non-articular rheumatism and sports injuries (Ensano et al., 2017). It is also used to reduce menstrual pain and as veterinary medicine. It is available in several administration forms, orally, rectally or intramuscularly.

Diclofenac has proved to be less invasive than other NSAIDs like aspirin, naproxen, etc., causing less gastrointestinal damage. According to various sources, diclofenac's anti-inflammatory properties and pharmacological effects are related to the inhibition of the chemical prostaglandin (Radjenovic et al., 2007; Ardoin & Sundy, 2006). Common side effects include abdominal pain, gastrointestinal bleeding, nausea, dizziness, headache, and swelling. Serious side effects may have heart disease, stroke, kidney problems, and stomach ulceration. Use is not recommended in the third trimester of pregnancy.

It has been proven that 1µg/L of DCF changes a rainbow trout's liver's ultrastructure, glycogen, and kidney protein. Higher concentrations can impair a Green shore crab (Triebskorn et al., 2004).
The introduction of activated sludge processes has increased the influent quality by a milestone; however, micropollutants are still emerging, and therefore membrane processes are necessary for adequate removal of these emerging contaminants (Dolar et al., 2012; Luo et al., 2014)
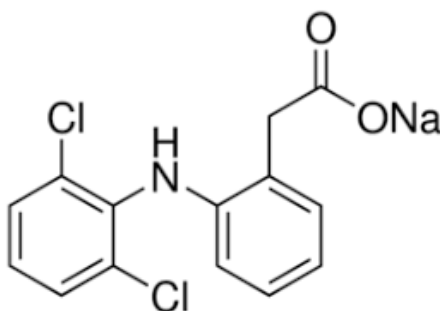
Figure 2-9: Structural formula of diclofenac (DCF) **(Ulubay et al., 2018)**

2.7.5 Sulfamethoxazole

Sulfamethoxazole is a sulfonamide bacteriostatic antibiotic that closely resembles folic acid. It is commonly used in combination with trimethoprim as the drug Bactrim. The anti-biotic is white-yellow and is in a crystal or powder form. It is widely used to treat urinary tract infections, bronchitis and prostatitis and effectively against negative and positive gram bacteria such as E. coli and listeria monocytogenes (Drugbank,2005). Sulfamethoxazole is slightly soluble in water but is soluble in 1 in 50 alcohols and 1 in 3 acetone and alkali hydroxides (Sigma-Aldrich, 2003). Sulfamethoxazole was first developed in the early 1970s as trimethoprim-sulfamethoxazole and was introduced as a wide-spectrum antibiotic used to treat aerobic bacteria (Masters et al., 2003).

Due to the group of antibiotics in which sulfamethoxazole belongs, it was found that they induce a change in microbial diversity by reducing microbial biomass and influencing bacterial and fungal relationships (SSS, 2018).
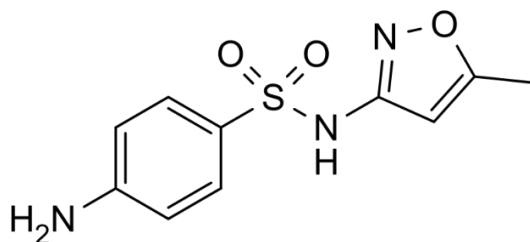
Figure 2-10: Structural formula of sulfamethoxazole (SMX) **(De Amorim et al., 2013)**

2.7.6   Ibuprofen

Ibuprofen belongs to the non-steroidal anti-inflammatory pharmaceutical class. It is often used to treat pain, fever, and inflammation in humans and animals due to its analgesic and antipyretic properties (Ruiz-ordaz & Gal, 2018). The World Health Organisation (WHO) has added Ibuprofen to the essential healthcare list. It is one of the world's most common over-the-counter pain medications (Chopra & Kumar, 2020). It is commonly known as Brufen, Advil, Nurofen and Motrin and appears odourless, with its physical properties as a colourless, crystalline stable solid. It is readily soluble in most organic solvents, very soluble in alcohol and soluble at 21mg/L @ 25°C in water (PubChem 2021). In 1961, Stewart Adams and John Nicholson discovered it to find a safer alternative to Aspirin (Halford et al., 2012).

Ibuprofen is the world's third-highest sold over-the-counter pain medication. Due to its high demand and increased popularity, it is more commonly found in wastewater treatment plants, with a 600-1200mg/day concentration (Chopra & Kumar, 2020). Due to its bioactive nature, it is not completely metabolised in the human body and is excreted as unchanged metabolites like carboxyibuprofen, hydroxyibuprofen and carboxyhydratropic acid (Chopra & Kumar, 2020). The toxicity of ibuprofen to the environment and aquatic life was studied by Chopra & Kumar (2020), and it was found that the estimated actual risk ratio was ≤1, suggesting it poses an environmental risk (Bouissou-Schurtz et al., 2014).
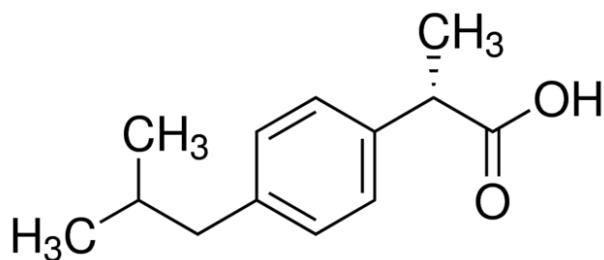
Figure 2-11: Structural formula of Ibuprofen (IBU) **(Togola & Budzinski, 2007)**

2.7.7 Aspirin
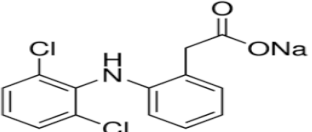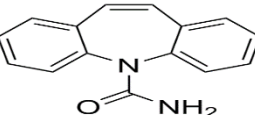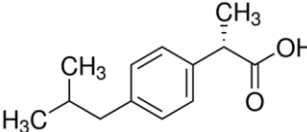
Acetylsalicylic acid, commonly known as aspirin, belongs to pharmaceuticals known as non-steroidal anti-inflammatory drugs. It is widely known for its analgesics and antipyretic properties (Awtry & Loscalzo, 2000). Its commonly used for a variety of inflammatory conditions, mild pain, fever and, in some cases, as a blood thinner for people who are high-risk cardiovascular patients (Brazier, 2020).

It is soluble in water and is a white, odourless crystalline solid at room temperature. It's weakly acidic and has an acid dissociation constant of 3.5 at 25°C (Awtry & Loscalzo, 2000). A well-known Greek physician, better known as hypocrites, wrote that willow leaves and bark relieved pain and fevers. Thousands of years later, a German chemist Felix Hoffmann at Bayer used acetylsalicylic acid to treat his father's rheumatism. Bayer distributed a powder with this ingredient to physicians to give to patients. By 1915 it was bulk produced and sold as an over-the-counter medication. The effects of aspirin on the environment have been studied and have been shown to cause stimulation of growth of cyanobacteria and inhibition of development of the aquatic plant (Pomati et al., 2004).

Figure 2-12: Structural formula of Aspirin (ASP) (Togola & Budzinski, 2007)

Table 2-3: Physio-chemical properties of Diclofenac, Ibuprofen, Aspirin and Carbamazepine (Hu & Wang, 2016; Acero et al., 2016; Comerton et al., 2007; Cartagena et al., 2013; Scheytt et al., 2005; Lobo et al., 2014; Dołowy & Pyka, 2015)

	Diclofenac (DCF)	Carbamazepine (CBZ)	Ibuprofen (IBU)	Aspirin (ASP)
Molecular Formula	$C_{14}H_{10}Cl_2NNaO_2$	$C_{15}H_{12}N_2O$	$C_{13}H_{18}O_2$	$C_9H_8O_4$
Structure				
Classification	Nonsteroidal anti-inflammatory drugs (NSAIDs)	Antiepileptic/ Anticonvulsant	Nonsteroidal anti-inflammatory drugs (NSAIDs)	Nonsteroidal anti-inflammatory drugs (NSAIDs)
Molecular weight (g/mol)	318.3	236.27	206.28	180.16
pKa	4.3	2.3,13.9	4.43±0.03	2.97
Water solubility (g/L at 25°C)	2.37	0.018	0.021	0.03
Log pKa	0.7	2.45	3.97	1.14
Log K_{ow}	4.9	1.51	2.48	1.14
CAS number	135.57-86-5	298-46-4	15687-27-1	50-78-2

2.8 Review of the removal of micropollutants from wastewater done by previous studies.

A previous study done by (Shin et al., 2022) stated that the main mechanisms of removal of trace organic micropollutants are size exclusion, molecular weight cut-off and adsorption. The transport of solutes through RO and Nf membranes are governed by the solute diffusion model. Other interactions on a microscopic level have also rendered as very important. In addition to non-specific interactions (i. e., electrostatic, polar and hydrophobic interactions), specific interactions (i.e., hydrogen bonding and π–π interactions) resulting from the chemical functional groups of the solute and membrane may be involved in adsorption (Schäfer et al., 2011; Fujioka et al., 2020). Another study done by (Racar et al., 2020) evaluated the raw municipal wastewate for reclamation for irrigation purposes and was compared to standards set by the World heath organization. The study was conducted on a MBR-NF-RO hybrid system and found that the reclaimed water satisfied the physico-chemical and microbiological quality requirements only after additional NF/RO treatment (Racar et al., 2020). Other studies conducted looked at surveillance of emerging micropollutants. In Spain several studies were conducted, monitoring the toxicity in rivers and drinking water and found emerging micropollutants in water (Fernández et al., 2010). The Henares-Jarama-Tajo river system makes up the largest drainage basin located in the Province of Madrid, Spain. the research done by (Fernández et al., 2010) aimed to monitor seasonal variations in concentrations of 22 PhACs along specific sites of the river system, and to establish the potential risk of sublethal effects to occur on aquatic organisms.

2.9 Membrane performance characteristics

2.9.1 Recovery

Recovery is also known as a conversion rate and is the permeate flow over the feed flow in which the percentage volume of influent is recovered as permeate. The general RO systems recovery rate ranges between 50%-85%; in most cases, the system is designed to recover 75%. A system with a 75% recovery rate means that for every 100L, 75L will become permeate while the remaining 25L will be retained as a concentrate (Kucera, 2015). Recovery is calculated using the following (Kucera, 2015):

Equation 2-2: Percentage recovery

$$\% \, Recovery = \frac{Permeate \, flow}{feed \, flow} \times 100 \, ... \, [2-2]$$

2.9.2 Salt rejection

Salt rejection is the percentage of feed water retained by the membrane. Rejection is crucial in monitoring the performance of the RO system. For instance, a 98% rejection means that 98% of the material was retained in the influent, and only 2% passed into the permeate (Kucera, 2015). Rejection is dependent on three main factors. These factors include feed constituents, feed characteristics, and RO membrane type in operation. According to (Kucera, 2015), solutes with low polarity, high molecular weight and high dissociation and hydration demonstrate higher rejections. Rejection can be calculated as follows:

Equation 2-3: Percentage of salt rejection

$$R = \frac{C_f - C_p}{C_f} \times 100 \, ... \, [2-3]$$

Where:

C_f: conductivity of the feed (µS/cm)

C_p: conductivity of the permeate (µS/cm)

R: Salt rejection

2.9.3 Fluxs

Flux is expressed as the volumetric flow rate over a given area per unit of time. Regarding reverse osmosis, the volumetric flow rate refers to the water flow, and the area relates to the membrane. It is often expressed in units of litres per square meter of membrane surface area per day (gallons per day per square foot). Water flux through an RO membrane is proportional to the net pressure driving force applied to the water and temperature (Kucera, 2015). It can be calculated as follows:

Equation 2-4: Flux

$$Flux = J_v = \frac{Q}{A} \ldots \quad [2-4]$$

Where:

J_v: Flux

Q: flow rate of the permeate (L/hr)

A: Effective area of the membrane (m^2)

2.9.4 Normalised flux

Flux is affected by the temperature of the water; it is therefore normalised to a standard temperature accounting for any fluctuations in the viscosity of the water. The effect of temperature on flux can be calculated using:

Equation 2-5: Normalised flux

$$J_T = J_{25} \times 1.03^{(T-25)} \ldots \quad [2-5]$$

Where:

J_T: The flux at temperature T

J_{25}: The flux at a temperature of 25°C

2.9.5 Flux Recovery ratio (FRR)

Recovery is a critical aspect of NF and RO, as not all the liquid will pass through the surface of the membrane. In MF and UF, the liquid stream applied will pass. It is required to operate at a higher recovery rate to minimise the waste stream; however, this may affect the fouling rate and increase the cleaning frequencies(Nidal Hilal, Mohamed Khayet, 2012). The flux recovery ratio can be calculated as follows:

Equation 2-6: Flux recovery ratio

$$\%FRR = \left[\frac{Average\ DI\ water\ final\ flux}{Average\ DI\ water\ initial\ flux}\right] \times 100 \ldots \ [2-6]$$

2.9.6 Temperature

Temperature affects both the flux and rejection. If the feed solution is under a temperature of 45°C and runs at constant pressure, the relationship between the permeate flux and the temperature is linear (Kucera, 2015). According to Kucera (2015), for every 1°C change in temperature, there is a 3% change in water flux. However, regarding salt rejection, the increase in temperature causes a decrease in salt rejection due to the diffusion of salt being higher at higher temperatures.
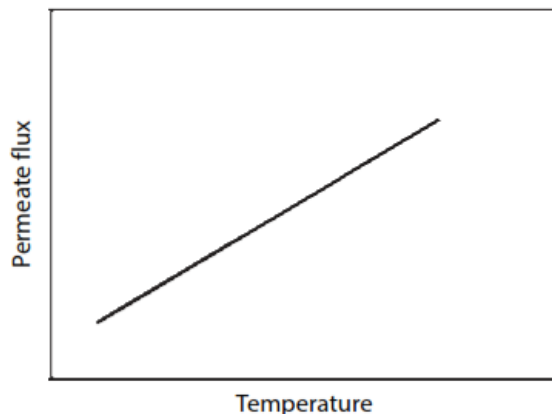
Figure 2-13: Relationship between permeate flux and temperature assuming a feed solution less than 45 degrees Celsius and at constant pressure (Kucera, 2015)*.*
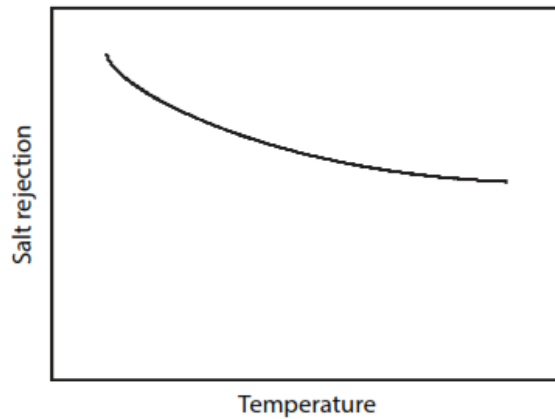
Figure 2-14: The relationship between salt rejection and temperature assuming a feed solution less than 45 deg C and operating at constant pressure (Kucera, 2015)

2.9.7 Pressure

The operating pressure affects the water flux and inversely affects the salt rejection. The driving force directly affects the pressure and, therefore, the flow rate of the water across the membrane, thus producing a higher flux. However, salt rejection is not affected by pressure whatsoever. The amount of salt will pass through the membrane, given that the pressure has increased or decreased (Kucera, 2015). However, since more water passes through the membrane at a higher pressure, it appears as if the salt passage decreases and the salt rejection increases as pressure increases.
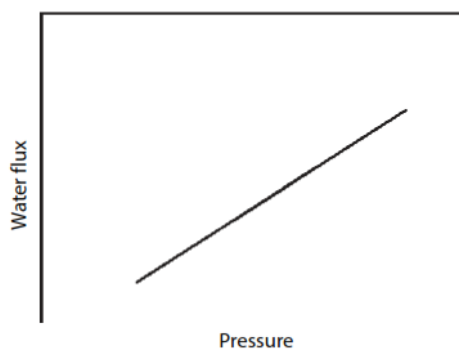
Figure 2-15: Water flux as a function of pressure in an RO system (Kucera, 2015)
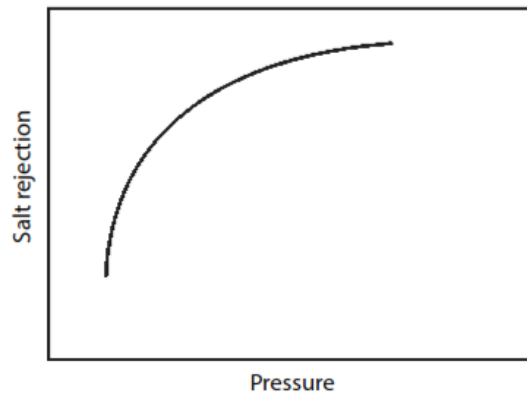
Figure 2-16: Salt rejection as a function of pressure in an RO system **(Kucera, 2015)**

2.9.8   pH

pH affects the stability of polyamide and cellulose acetate membranes; however, the pH range is much broader with polyamide membranes, ranging from as low as 2 to as high as 11 depending on the specific membrane and manufacturer (Kucera, 2015). Operating pH is also a function of temperature. The higher the temperature, the narrower the pH range for operation. pH is also known to affect rejection, with the highest rejection achieved at 7-7.5 pH and a decrease in higher and lower pH levels (Kucera, 2015).
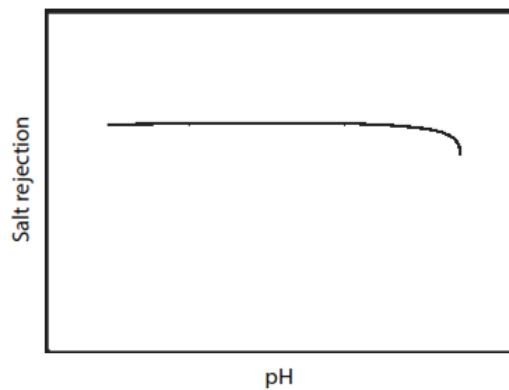
Figure 2-17: Salt rejection of a RO membrane as a function of pH assuming a constant feed pressure **(Kucera, 2015)**
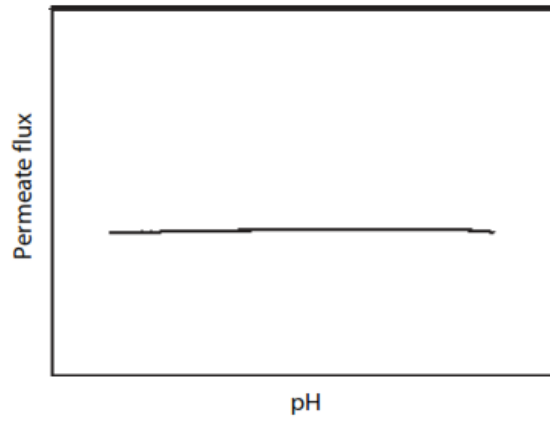
Figure 2-18: RO membrane permeate flux as a function of pH assuming a constant feed pressure **(Kucera, 2015)**

2.10   Membrane surface characteristics

A chemical analysis of a membrane's surface is sometimes necessary for comparative reasons. It is usually done before and after treatment of surface-modified membranes to know what chemical changes occurred and as a fouling test to check foulants adhered to the membrane surface (Xu et al., 2009). Techniques to confirm composition changes include (FTIR, NMR and XPS) while techniques to test morphological structure include (SEM and AFM). (Zhao et al., 2013).

2.10.1 Attenuated total reflectance Fourier transform infrared (ATR-FTIR) spectrometry

FTIR is a technique used to study and identify chemical surfaces and is both quantitative and qualitative. It works with the principle of infrared interactions with a material surface in which molecular vibrations are analysed (Xu et al., 2009). According to Schmitt & Flemming (1996), ATR-FTIR is a fast, reliable and straightforward analytical tool that doesn't need any sample preparation for quantitative analysis. ATR-FTIR spectrometry can identify and monitor fouling of membranes and characterise membranes that have been grafted or modified (Xu et al., 2009).

2.10.2 Nuclei magnetic response (NMR)

NMR works because all nuclei have a spin and carry a charge; once an external magnetic field is introduced, an energy transfer is possible, and energy can be carried over from the base energy level to a higher energy level. Some NMR active nuclei include ^{1}H, ^{13}C, ^{23}Na, etc. The wavelength at which the energy transfer occurs is usually equal to the radio frequency, so energy is emitted at the same frequency when the spin goes back to the base energy level. This yields an NMR spectrum by matching the signal to the transfer and is processed in many ways (Chatham & Blackband, 2001).

NMR was previously used in chemistry to analyse structures and measure electric field gradients and magnetic shielding. Its uses have been extended to further applications such as imaging techniques and observing morphological changes in tissue, protein solutions, single cells and isolated perfused organs (Chatham & Blackband, 2001).

2.10.3 X-ray photoelectron spectrometry (XPS)

X-ray photoelectric effect works under the principle of the photoelectric effect. Photo electrons are emitted with energy values characterised by the elements on the surface, given that they are exposed to X-ray (photon) (Xu et al., 2009). The electron spectrometer analyses the energy of the photoelectrons and presents the data by an intensity vs electron energy curve (Xu et al., 2009). XPS is mainly used to measure the material's chemical and electronic state and the elemental composition (Zhao et al., 2013).

2.10.4 Scanning electron microscopy (SEM) and Atomic force microscopy (AFM)

Scanning electron microscopy (SEM) and atomic force microscopy (AFM) are commonly used in laboratories. They are used for high-resolution surface investigations and resolve surface structure to a nanometer scale (Russell et al., 2001). SEM analysis operates by applying a voltage between a conductive sample and a filament; this results in electron emission from the filament to the sample (Russell et al., 2001). At the same time, AFM works by applying a small force to a cantilever consisting of a sharp tip and scanning it across a sample. These micro-techniques are used to characterise the morphology and structure of modified membranes (Zhao et al., 2013). AFM is preferred over SEM due to its ability to deal with macromolecules and perform at a nano-scale (Xu et al., 2009).

2.11 Analytical tests and screening

2.11.1 Liquid chromatography-mass spectrometry (LC-MS)

Liquid chromatography-mass spectrometry has become a prevalent analytical screening method for detecting trace amounts of target analytes in complex solutions (Dams et al., 2003). The test results can be qualitative, indicating which compounds are present and which are quantitative, presenting the actual concentrations of compounds in a sample (Wellings, 2006). The role of liquid chromatography is to separate mixtures with multiple components, while mass spectrometry identifies individual components with high molecular specificity and detection sensitivity (Jacob et al., 2014; Dass, 2007). This tandem technique can analyse several different complex samples from biochemical, organic and inorganic compounds of environmental and biological origin. Thus, LC-MS may be applied to a broad spectrum of industries, from biotechnology, pharmaceutical, food processing, environmental monitoring, agrochemical and cosmetic industries (Jacob et al., 2014; Dass, 2007). Several other separation techniques are combined with mass spectrometry, such as gas chromatography (GC), high-performance liquid chromatography (HPLC), capillary electrophoresis (CE), and supercritical fluid chromatography (SFC), size-exclusion chromatography, and thin-layer chromatography (TLC) (Dass, 2007).

2.11.2 High-Performance Liquid Chromatography (HPLC)

High-performance liquid chromatography is used extensively in the pharmaceutical industry to detect the drug and composition quantitively and qualitatively (Terrill, 2009). Qualitative tests indicate what compounds are present in a sample, while quantitative tests show the actual concentrations in the sample. Chromatography is a technique used to separate components in a mixture based on the relative amounts of each solute distributed between a moving fluid stream, called the mobile phase, and a contiguous stationary phase. The mobile phase may be a liquid or a gas, while the stationary phase is a solid or a liquid (J.C Giddings, 2019).

Table 2-4: Chromatography types

Type of Chromatography	Mobile phase	Stationary phase
Gas chromatography	Gas	Solid/liquid
Liquid chromatography	Liquid	Solid/Liquid
Supercritical fluid chromatography	Supercritical fluid	Solid/liquid

2.11.3 Gas-Chromatography (GC)

Gas chromatography is a modern analytical technique used to detect and quantify a wide range of compounds and is highly sensitive with a high resolution. It is most commonly used in forensic drug analysis, toxicology, structural characterisation of biomolecules, environmental chemistry, medicinal chemistry and clinical science. It is a method used for the positive identification of target compounds. However, the GC analysis falls short of relatively volatile and thermally stable organic compounds (Dass, 2007). The sample is carried by a mobile phase over a fixed bed of the stationary phase, allowing retardation due to differences in solubility, thus allowing physical separation of compounds. In gas chromatography, the mobile phase consists of inert gas. The stationary phase is a high molecular weight liquid that is either deposited on the surface of finely divided particles or on the walls of the capillary tube.
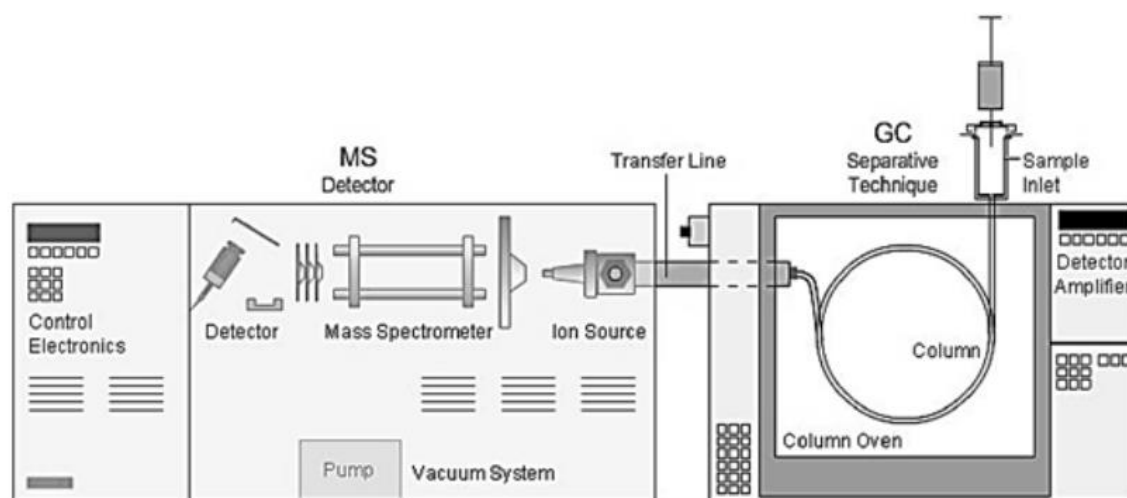
Figure 2-19: Schematic drawing of gas chromatography instrument (Obeidat, 2021).

2.11.4 Agilent 7000C GC/MS triple quad

The 7000C gas chromatography-mass spectrometer is the most sensitive GC/MS/MS system with the lowest, 4fg Octafluoronaphthalene instrument detection level (IDL) specification. The 4fg IDL is demonstrated upon installation, verifying total system performance, the ALS, GC and MS.

Figure 2-20: Agilent GC/MS triple quadropole (Agilent, n.d.)

2.12   Samples preparation

2.12.1 Solid-phase extraction

Solid-phase extraction is an analytical method used to concentrate and purify analytes from solution by sorption onto a disposable solid-phase cartridge, followed by the elution of the analyte with a solvent appropriate for instrumental analysis (E. M. Thurman, 1998). The sample preparation technique enables the extraction, clean-up and concentration of analytes. The retention mechanisms include reversed-phase, normal phase and ion exchange (E. M. Thurman, 1998).

There are four main steps in solid-phase extraction; they consist of the following:

- Conditioning: A solvent is passed through the sorbent (cartridge) to wet the packing material and solvate the sorbent's functional groups.
- Loading step: The analyte is applied to the column. Depending on the sample type, the loading step can be 1ml to 1L.
- The washing step involves eliminating impurities and interferences in the column and retaining the analyte.
- Elution: elute the analyte from the sorbent with an appropriate solvent specifically chosen to disrupt the analyte-sorbent interaction, resulting in elution of the analyte. The eluting solvent should remove the other substances sorbed on the column as little as possible.
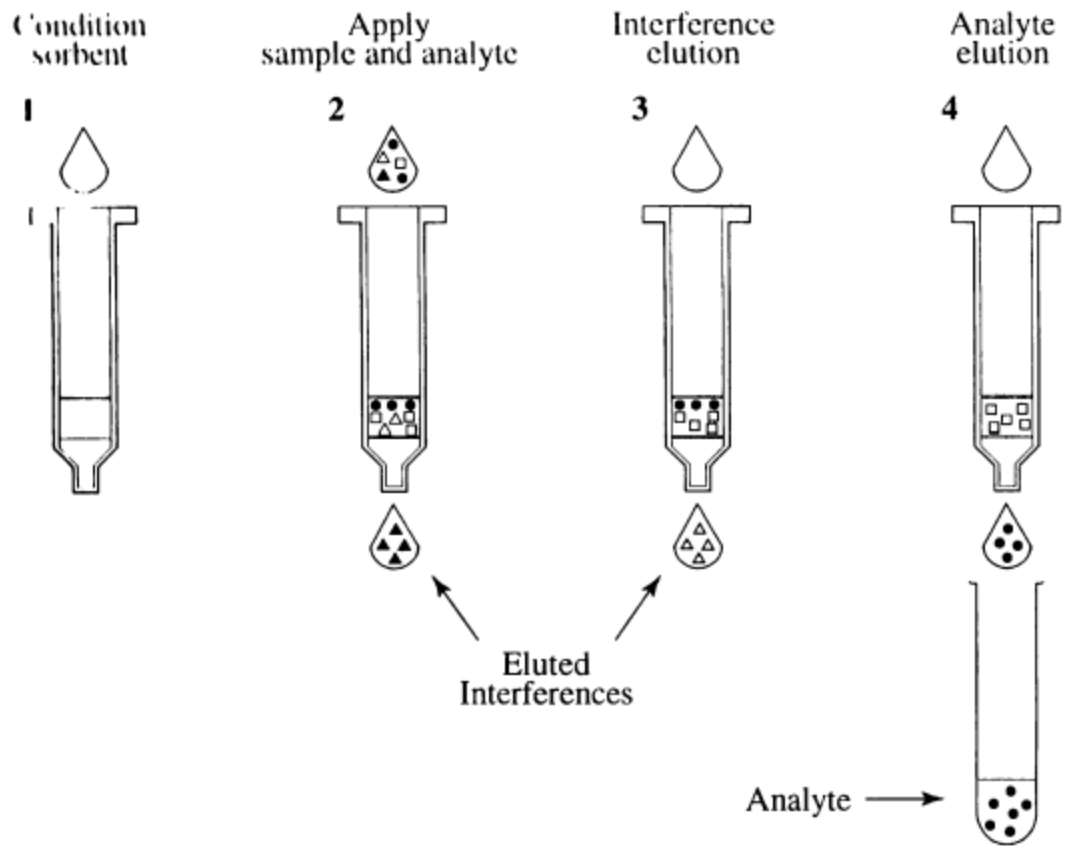
Figure 2-21: The basic process of Solid-phase extraction (E. M. Thurman, 1998)

Chapter 3

Experimental set-up

3   Methodology

3.1   Introduction

This chapter describes the research methodology, experimental laboratory RO bench-scale unit, analytical techniques and experimental procedures, equipment and materials used in this current research work.   A descriptive list of the instruments used has also been included. The experimental procedures were conducted using a quantitative approach.

The project is divided into two sections

1. Bench-scale reverse osmosis process
2. Analytical testing of pharmaceuticals using GC-MS/MS

All the experiments were conducted at the Cape Peninsula University of Technology, Belville, Chemical Engineering and Chemistry Building in the Environmental Research Water Laboratory 1.18.

3.2 RO system design description

The experiments were conducted on a bench-scale RO Cell (SEPA CF Cell) unit. The feed water was a synthetic makeup of MBR secondary effluent of specifically identified organic and inorganics substances. A low-pressure, high flow rate hydra cell pump was used to pump the feed water through the membrane cell. The permeate was collected into a holding tank, and the brine was recycled back into the feed tank. An automated software system controlled the plant. The feed velocity was set manually on the variable speed drive (VSD). Data was captured and recorded accordingly.

Figure 3-1: Bench-scale RO unit in Environmental Engineering Research Water Laboratory 1.18 (August 2021)

Table 3-1: Reverse Osmosis equipment list

1	Feed Tank
2	Hydraulic Pump
3	Data logger & feed pressure controller
4	VSD (Variable speed drive)
5	RO SEPA membrane cell
6	Hydra cell pump
7	Computer with module software

Other equipment used during experiments:

- Bench-scale RO cell
- 15L model secondary MBR municipal wastewater as feed
- Hanna COD multimeter with reagents
- Lasec COD reactor
- Portable EC and pH meter
- Stopwatch
- Measuring cylinder

Figure 3-2: Schematic diagram of RO system

3.3   RO synthetic feed make-up

The MBR secondary municipal synthetic feed makeup was measured in its chemical mass and weighed on an analytical balance. The weighed quantities are transferred to a volumetric flask and diluted with DI water to make up a 1L stock solution. This process is repeated for each induvial chemical. The pharmaceuticals are weighed similarly, transferred to a 1L volumetric flask, and diluted with HPLC grade methanol. The tank is filled with water to make up a 15L synthetic feed.

Table 3-2: Synthetic feed composition and characteristics

Chemical composition	Concentration (mg/l)
Ammonium Phosphate	60
Sodium chloride	7
Potassium chloride	4
Sodium bicarbonate	93
Magnesium sulphate	60
Calcium sulphate	60
Humic Acid	4.2
Aspirin (µg/l)	22, 35.5, 44
Ibuprofen (µg/l)	22, 35.5, 44
Carbamazepine (µg/l)	22, 35.5, 44
Diclofenac (µg/l)	22, 35.5, 44
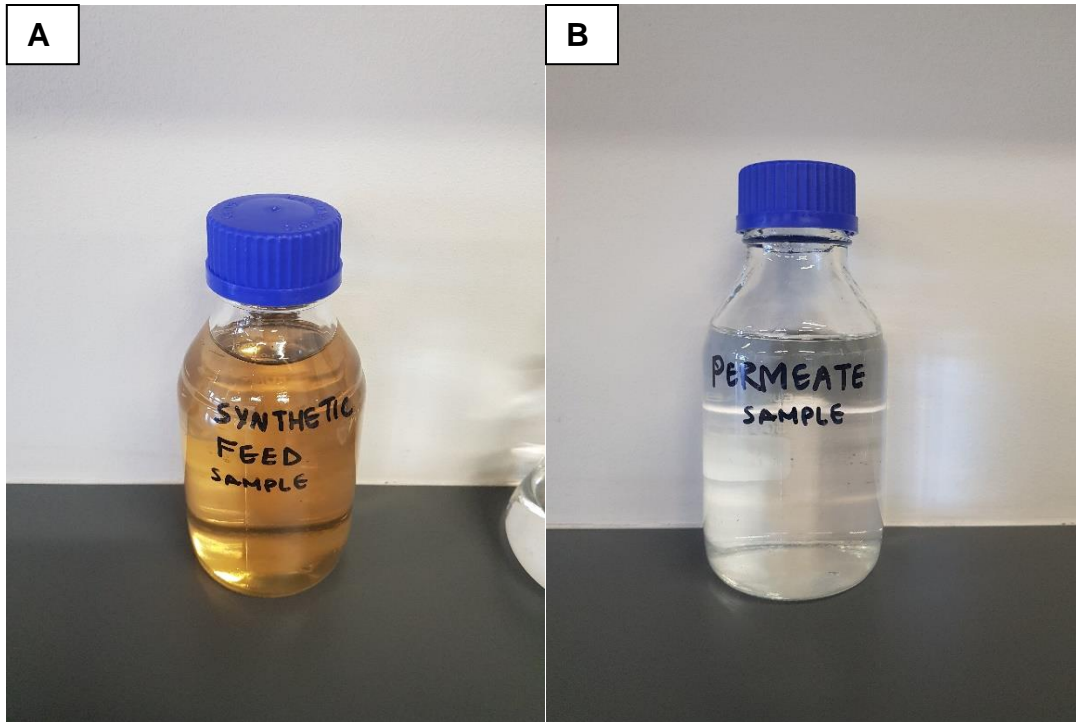
Figure 3-3: A)Synthetic municipal wastewater MBR effluent, B) RO permeate, after treatment.

3.4 RO system operation

The operating conditions were automatically controlled. The conductivity (EC), TDS and temperature of the feed, permeate and brine were recorded at 45min intervals for the 12-hour experimental run.

Treatment/remedial process
Flushing/Cleaning

12hrs
End

Start: 12.05 Hz
Synthetic feed is added
Flow rate: 0.96 L/hr
VSD: 12.05Hz

Duration of the short run

End of run:
Membrane removal and preservation for analysis

System is flushed with DI water
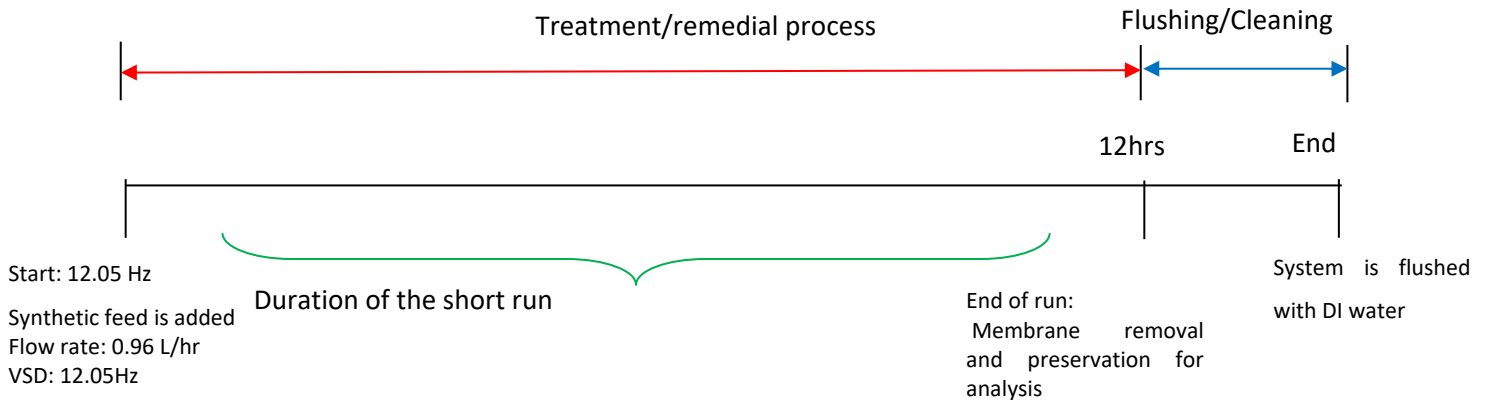
Figure 3-4: Timeline of the Reverse osmosis treatment using the membrane cell

3.4.1 RO cell startup procedure
- The cell is removed from its casing and opened.
- The two spacers are cut into the same shape as the membrane's active surface area. The feed spacer (bigger spacing/holes) is placed on the feed side (higher pressures side), while the permeate carrier (spacer with small holes) is placed on the side with lower pressure, i.e. permeate side.
- Before placing the membrane and spacers in the cell, they are rinsed with de-ionized (DI) water to remove any impurities.
- The membrane is cut from an opened spiral wound DOW FILMTEC membrane (RO and NF-XLE4040 & NF90-4040) in a rectangular shape with dimensions 14.5cm x 9.5 cm, giving an active surface area of 0.014 m^2; it covers the inner O-Ring in the flat cell. The shiny side of the membrane must be faced down on the cell
- The cell is placed back into its casing and pressurized with the hydraulic pump.
- The hydraulic pressure is set to 12-14bar.

- Once the cell is secured, the feed pressure is set with the software, and the data operating box is switched on.
- The experimental run time is set to 12hr for the short run and 100 hours for the long run.
- Feed pressure: 5 bar

    10 bar

    15 bar

- The variable speed drive was set to 12.05 Hz to achieve a feed pressure of 10 bar
- The synthetic feed was added to the tank, and the system was started.
- The conductivity, TDS and temperature of the feed, brine and permeate were recorded every 45 minutes throughout the experimental short run.

3.4.2 Membrane cleaning

- After every run, the system is flushed with deionized water, minimizing cross-contamination between runs.
- Before using the membrane, the membranes were soaked in deionized water for 24 hours.
- The deionized water has an electrical conductivity of 3μs/cm. Each experimental run started with new spacers and a new membrane.
- After experimental runs, the system was shut down, and the membrane was removed from the cell and preserved for analysis.
- 15L of DI water was added to the tank for flushing under the same conditions as the run, ensuring pipes and the membrane cell were cleaned for the next experimental run.

3.4.3   Membrane replacement

Once the membrane was removed, the cell was rinsed with DI water; the spacers were removed and replaced with new ones for each experimental run. Tables 3-3 and 3-4 show the operating limits of the RO and NF membranes, respectively.

Table 3-3: Operating limits of Filmtec XLE4040 polyamide composite membrane (Lenntech, 2017)

Membrane type	Polyamide Thin-Film Composite
Maximum Operating Temperature	45°C
Maximum Operating Pressure	41 Bar
Maximum Feed Flow Rate	3.2 m^3/hr
Maximum Pressure Drop	0.9 Bar
pH Range, Continuous Operation	2-11
pH Range, Short-Term Cleaning (30 min)	1-13
Maximum Feed Silt Density Index (SDI)	5
Free Chlorine Tolerance	<0.1 ppm

Table 3-4: Operating limits of Filmtec NF90-4040 Polyamide composite membrane (Lenntech, 2017)

Membrane type	Polyamide Thin-Film Composite
Maximum Operating Temperature	45°C
Maximum Operating Pressure	41 Bar
Maximum Feed Flow Rate	3.2 m³/hr
Maximum Pressure Drop	0.9 Bar
pH Range, Continuous Operation	2-11
pH Range, Short-Term Cleaning (30 min)	1-12
Maximum Feed Silt Density Index (SDI)	5
Free Chlorine Tolerance	<0.1 ppm

Polyamide thin-film composite membranes have a three-layer configuration. High rejection of unwanted contaminants (such as salts), high filtration rate, and superior mechanical strength are all advantages of the three-layer structure (Alsayed & Ashraf, 2021). The high rejection is due to the polyamide top layer, which was chosen for its water permeability and relative impermeability to various dissolved contaminants such as salt ions and other minutes, unfilterable molecules (Alsayed & Ashraf, 2021).
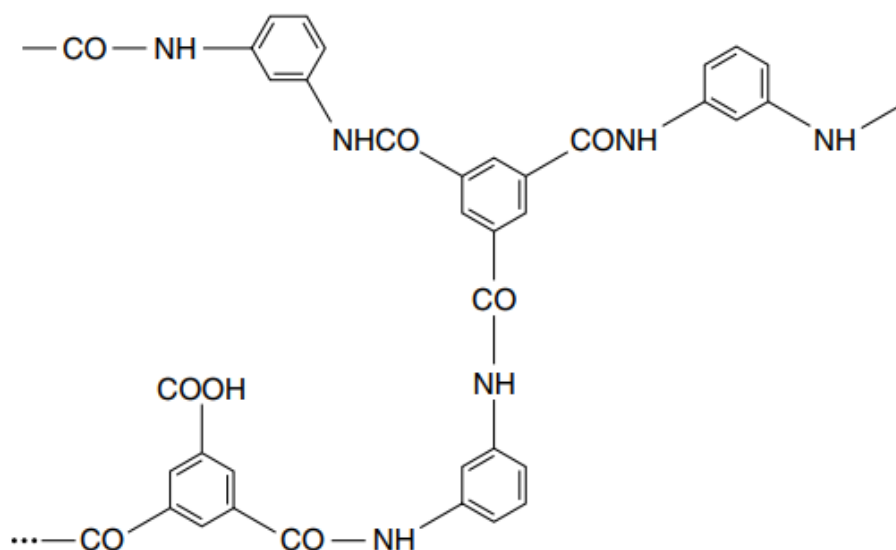
Figure 3-5: Chemical structure of a polyamide composite RO/NF membrane **(Baker, 2004)**

Table 3-5: RO operating conditions

Initial conditions	Feed solution
Flux: 80, 55, 100 L/m²hr	Synthetic MBR secondary municipal wastewater
Pressure: 5, 10, 15 Bar	
Initial concentrations of Pharmaceuticals: 22,35.5,44 µg/l	
Flow rate: 1.104 L/hr	
Temperature: Ambient	
pH: 7± 0.5	

3.4.4 Equipment used during RO experimental runs

The conductivity meter used for experimental runs simultaneously measured conductivity from which the salt rejection (%) was calculated; the salinity (ppt), the total dissolved solids (mg/L) and the temperature (^{o}C).

Figure 3-6: YSI Eco-Sense EC300 conductivity meter model used during experimental runs

A 10ml glass cylindrical flask and the digital stopwatch were used to measure the flow rate of the permeate.

Figure 3-7: Graduated glass cylinder (left), Stopwatch (right)

Using a multiparameter photometer, a COD reactor was used to prepare the MBR secondary wastewater samples for COD analysis. The multiparameter photometer was used to analyse specific ions identified as contaminants in the effluent, such as ammonia, phosphate, nitrate, and nitrite.

Figure 3-8: COD Multiparameter Photometer (left) COD reactor (right)

Table 3-6: Summary of experimental runs

Run:	Membrane type	Feed pressure (bar)	Initial Concentration (μg/L)
1	RO	5	22
2	RO	5	44
3	RO	5	35.5
4	RO	10	44
5	RO	10	22
6	RO	10	35.5
7	RO	15	44
8	RO	15	22
9	RO	15	35.5
10	NF	15	22
11	NF	15	44
12	NF	15	35.5
13	NF	10	22
14	NF	10	35.5
15	NF	10	44
16	NF	5	22
17	NF	5	35.5
18	NF	5	44

3.4.5 Pharmaceuticals of interest

The target compounds selected for this study included carbamazepine, diclofenac, aspirin and ibuprofen. Their physio chemical properties are presented in Table 2-3, chapter 2. The pharmaceuticals exhibit a hydrophilic nature, except for aspirin, which has a log K_{ow} of 1.14.

3.4.6 Addition of pharmaceuticals

The pharmaceuticals were measured in its chemicals mass and weighed on an analytical balance. The weighed quantities were dissolved in 200μl of methanol and diluted with 99.9ml of deionised water to make up a 1L stock solution. The process was done for each pharmaceutical. The stock solutions were added to the feed tank.

Table 3-7: Pharmaceuticals and feed concentrations

Pharmaceutical	Feed concentration (μg/l)
Carbamazepine	22, 35.5, 44
Diclofenac	22, 35.5, 44
Ibuprofen	22, 35.5, 44
Aspirin	22, 35.5, 44

3.5   Sample preparation for pharmaceutical GCMS analysis

Samples are collected every 45min for the reverse osmosis experimental run. The samples are contained in 2L amber glass bottles that have been autoclaved at 121°C. After RO, the samples undergo preparation for quantitative analysis for the removal of pharmaceuticals. Mass spectrometry was performed using an Agilent 700 triple quadrupole mass spectrometer with positive electro-spray modes (ESI+).

3.5.1 Solid phase-Extraction (SPE)

The composite sample collected during the 12hr experimental run was filtered through a Whatman glass fiber filter (pore size 0.7µm) using a Buchner funnel set-up. The temperature of the samples was adjusted in a water bath to an ambient temperature and separated into two 1L beakers, each containing 1L of the sample. The samples were allocated as acidic and the other as neutral.

3.5.2 Derivatization

Derivatization was used to enhance the sensitivity of the analyte after SPE was performed. It was done 30min before GCMS injection by adding N-Methyl-N-(trimethylsilyl)trfluoroacetamide (MSTFA) to the samples and then incubating at 65°C for 35min.

3.5.3 Solid Phase extraction and derivatization method

- Samples are collected in a 2L amber glass bottle and refrigerated for 12 hours before SPE
- The samples are filtered through a 0.7µm Whatman glass fiber filter.
- The samples are split into two 1L beakers as acidic and neutral compounds and placed in a water bath for the samples to reach ambient temperature.
- Once the ambient temperature is achieved, the acidic samples are adjusted to pH 2 using 3.5mol/L H_2SO_4, and the neutral compounds are adjusted to pH 9 using 1mol NaOH.
- 1 µL of 1-hydroxypyrene is added to the acidic and neutral samples after pH adjustment.
- SPE C_{18} cartridges are conditioned successively with 3ml 50:50 ethyl acetate- Acetone.
- 3ml Methanol
- 3ml H_2O adjusted to pH 2 for acidic compounds
- 3ml H_2O adjusted to pH 9 for neutral compounds
- Water samples are loaded under a 12-15 ml/min vacuum flow rate.

- Once samples are completely loaded (1L for acidic compounds and 1L for neutral compounds), cartridges are washed with 3ml 40:60 Methanol-water.
- Cartridges are allowed to dry under vacuum for 1 hour.
- After drying, cartridges are eluted with 9ml 50:50 Ethyl acetate- Acetone and collected in a vial.
- Samples are then centrifuged at 5000 rpm for 10 minutes
- The samples in the vial are then placed in a heating block set to 41°C and dried under a light stream of nitrogen to complete dryness.
- The samples are reconcentrated with 50-100μL of ethyl acetate.
- Acidic samples are derivatized using 30μl of *N*-Methyl-*N*-(trimethylsilyl) trifluoroacetamide (MSTFA) and incubated at 65°C for 35min.
- The samples then undergo GCMS analysis.

3.6   Apparatus for Solid-Phase extraction

Before extraction, the water samples were divided into two parts, each containing 1L. They were adjusted to pH 2 for acidic compounds and pH 9 for neutral compounds—the Hanna instruments HI5522-02 benchtop multimeter was used.

Figure 3-9: Hanna instruments bench-scale pH meter

A polymerically bonded octadecyl (18%C), the end-capped cartridge was used for neutral compounds, and the Oasis HLB 60mg cartridge was used for acidic compounds. The preppy 12 sample holder manifold was used to conduct the SPE analysis.

Figure 3-10: SPE C$_{18}$ cartridge (left) and Supleco SPE manifold (Right)

Figure 3-11: SPE set-up

Table 3-8: List of apparatus for SPE

1	Loading sample
2	SPE Sappy manifold
3	Vacuum Pump
4	SPE Cartridge

3.7 Membrane surface characterisation

A qualitative analysis (SEM-EDS) and semi-quantitative analysis (ATR-FTIR) characterised the membrane before and after modifications. Both analyses were done externally.

3.7.1 ATR-FTIR analysis

ATR-FTIR analysis was conducted to analyse the functional groups on the membrane's surface after RO treatment at different operating conditions and compare the differences between the NF and the RO. The analysis was conducted using a Perkin Elmer spectrum II with the spectrum 10 software. The ATR-FTIR spectra were recorded at a resolution of 2 cm^{-1} during 64 scans at a nominal incident angle of 45° with a wavenumber ranging between 4000 and 400 cm^{-1}.

3.7.2 SEM-EDX Analysis

The membrane morphology was observed using scanning electron microscopy (SEM) analysis. The Mira3 Tescan SEM analysis machine was used to scan the images and was magnified to 50 000x, 10 000x and 1000x and a 5.00 keV landing electron for all samples. The cross-sectional membranes were scanned at 5000x and at a 20.00 KeV landing electron.

Chapter 4

Results and Discussion

4 Results and discussion

The results presented are divided into the following:

- Membrane surface characterisation by SEM and ATR-FTIR
- RO process
- GCMS results

4.1 Statistical analysis

All statistical analysis was performed using Excel 2020. Variation between individual samples was assessed using an unpaired t-test. Significant variance was shown for P-values (below 0.05 to below 0.0001).

4.2 Membrane surface characterisation

The surface interface characterizes membranes to the environment they are in contact with ATR-FTIR, and SEM EDX was used to analyse the membrane surface characteristics.

4.2.1 ATR-FTIR

ATR-FTIR was used to examine the presence of the pharmaceuticals on the RO and NF TFC membranes. The analysis provided a suitable method of identifying selected functional groups on the membrane surface, allowing for differentiation between the virgin membranes and the membranes undergoing remedial treatment. A pharmaceutical feed concentration of 440ng/l was used for the FTIR analysis. The ATR-FTIR spectra were recorded at a resolution of $1cm^{-1}$ during 48 scans at a nominal incident angle of 45°C and a wavelength between 400 and 4000 cm^{-1}. The data were normalised to allow for a more accurate representation and a more straightforward comparison between spectra. The identification of the pharmaceuticals and their different functional groups are represented in the graphs below.
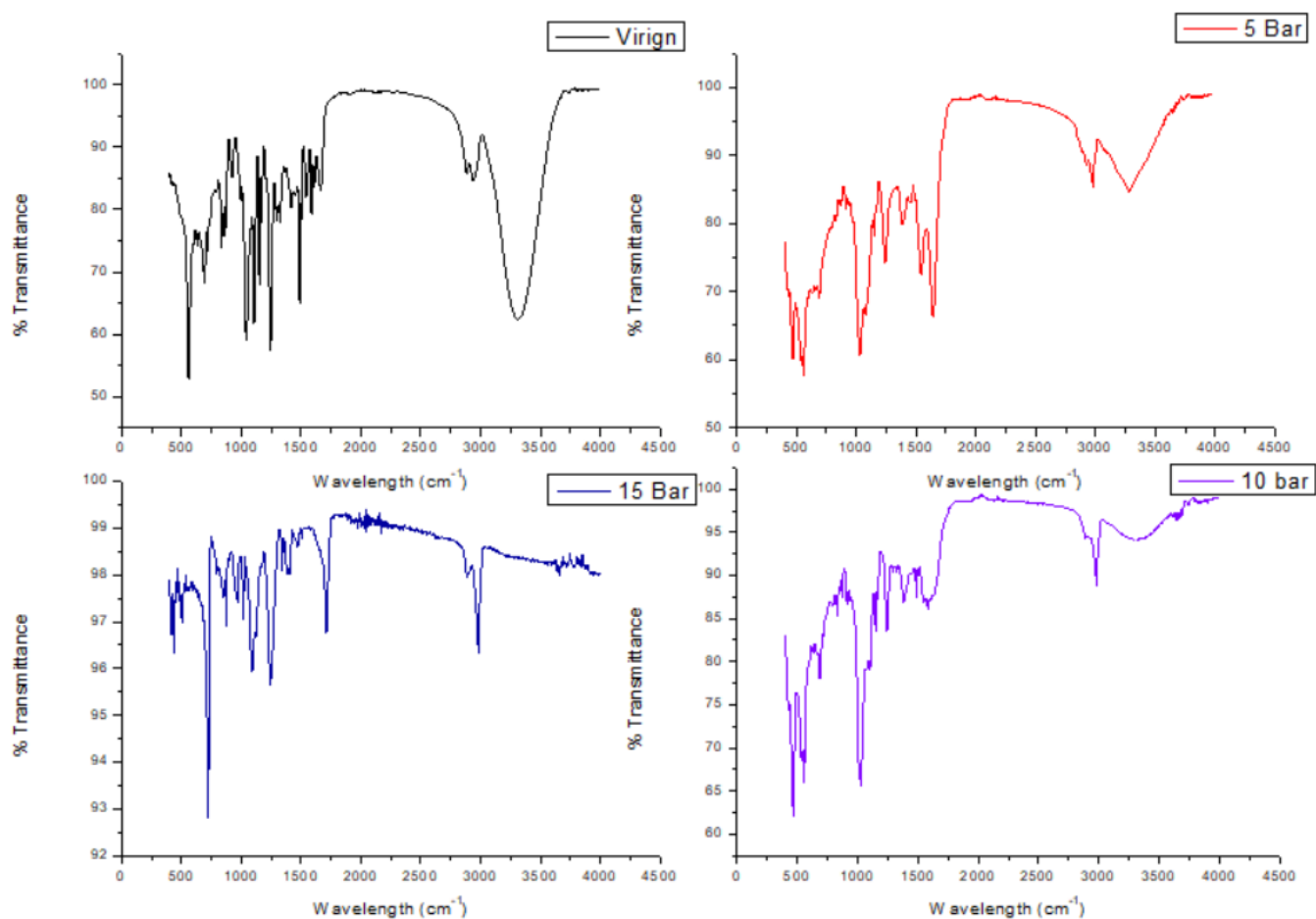
Figure 4-1: FTIR spectra of RO membranes at different feed pressures

Figure 4-1 shows the full spectra of the RO membranes at different feed pressures. The broad peak seen in the virgin membrane, between 3000 cm^{-1} and 3500cm^{-1}, is a complex band stretching from the active polyamide layer consisting of N-H and -COOH functional groups (Tang et al., 2007). Peaks between 1600-1400cm $^{-1}$ are characteristics of a carbonyl functional group (C=O) (Tang et al., 2007). The main differences between the four membranes seem to be in the fingerprint region (400-1500 cm^{-1}) and 3000 cm^{-1}. The prominent peak at 1542 cm^{-1} for the virgin,15 bar and 10 bars is (amide II band) assigned to N-H in-plane bending and C-H stretching. The peak at 1609 cm^{-1} for 5 and 15 bars is assigned to N-H vibration of aromatic amide. The amide I band at 1663 cm^{-1} can be assigned to C=O, C-N and/or C-C-N deformation in the secondary amide group (Dolar et al., 2017).
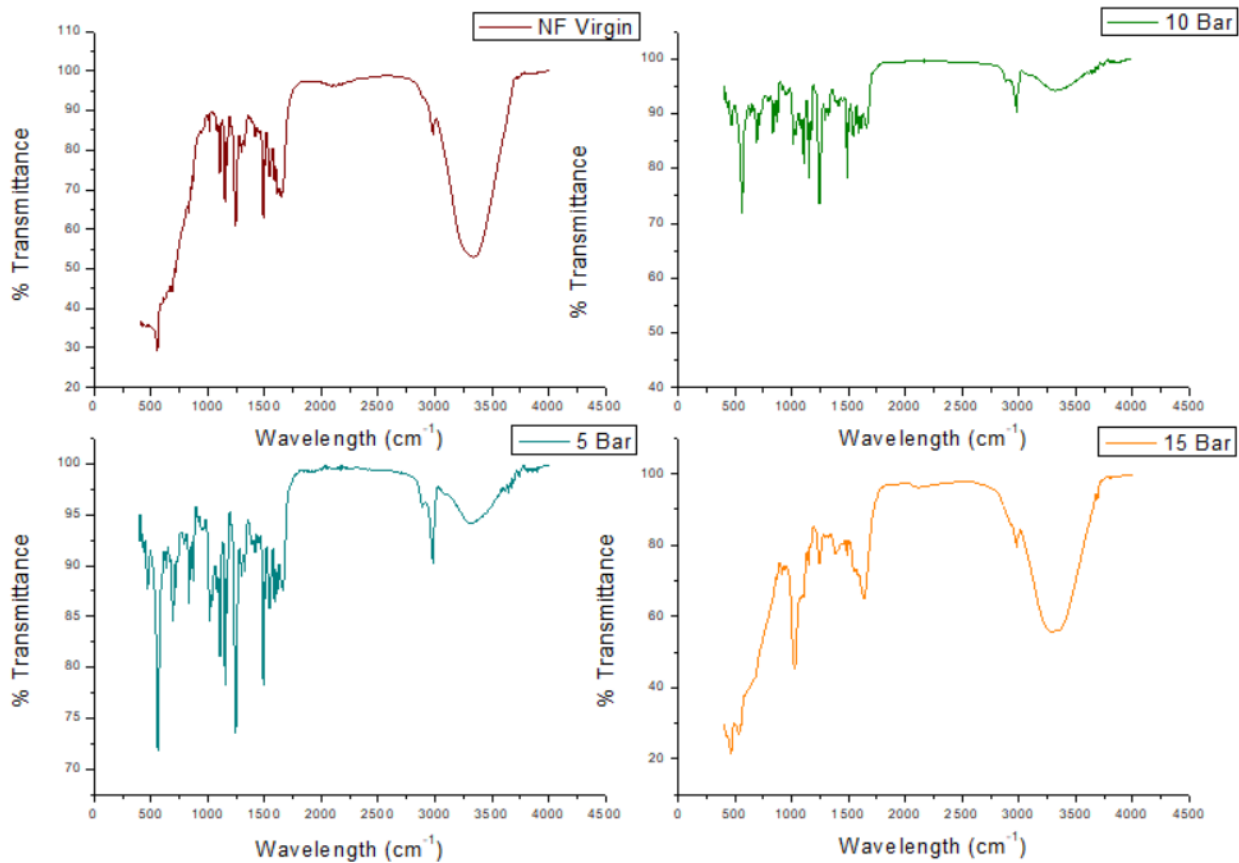
Figure 4-2: FTIR spectra of NF membranes at different feed pressures

Figure 4-2 gives the full spectra from 500cm^{-1} to 4000cm^{-1} of NF membranes at different feed pressures, i.e. 5,10 and 15 Bar. Characteristic peaks observed for the virgin membrane range of 2000–4000 cm^{-1} agree with previous studies (Tang et al., 2007). The prominent peaks were 2800–3000 cm^{-1} and a broad peak centred at 322 cm^{-1}. The peaks in the range of 2800–3000 cm^{-1} may be assigned to aromatic C–H stretching and aliphatic C–H stretching (Silverstein & Webster, 1996). The broad peak centred at 220 cm^{-1} for the virgin NF membrane is due to the overlapping stretching vibration of N–H and carboxylic groups in the polyamide layer (Mondal & Wickramasinghe, 2008). The infrared most likely penetrated through the thin active layer resulting in peaks between 1000cm^{-1} and 1650cm^{-1}, indicative of the microporous support layer. As a result, the two polyamide membranes exhibited almost the same ATR-FTIR spectra with visible peaks at 1650cm^{-1} (amide group), 1492cm^{-1} (methyl group) and 1592 and 1100cm^{-1} (aromatic double-bonded carbon) (Xu & Drewes, 2006). The broad peaks at 220 cm^{-1} (-NH and -OH) were more prominent for the RO than the NF membrane in its virgin state. This suggests that

RO's membranes surface has more (-OH and -NH) groups implying that the presence of hydrophilic compounds can modify them.

The ATR-FTIR spectra of the NF at 15 bar contained peaks at 694, 1151, 1487, 1503, and 1584 cm^{-1} (Xu & Drewes, 2006; Freger et al., 2002), indicating the presence of the polysulphone interlayer. An amide I peak at 1650 cm^{-1} for 5 bars is also present. The presence of an amide II peaks at 1541 cm^{-1}. The NF membranes are made from m-phenylenediamine, a primary amine (Xu et al., 2006).

4.2.2 SEM analysis

SEM was used to qualitatively observe the membrane's surface before and after wastewater treatment. Figure 4-3 shows the virgin RO and NF membrane. The SEM was conducted with a magnification of 50 000, 10 000 and 1000. The SEM images in Figures 4-3 presented a ridge and valley structure for both membranes. However, the NF is more dispersed, representing larger pores than the RO. The composition of the surface of the membrane can be seen in Table 4-1. The weight percent of carbon and sulfur was higher on the surface of the NF membrane than on the RO; however, the percentage of oxygen was higher on the RO membrane than on the NF.
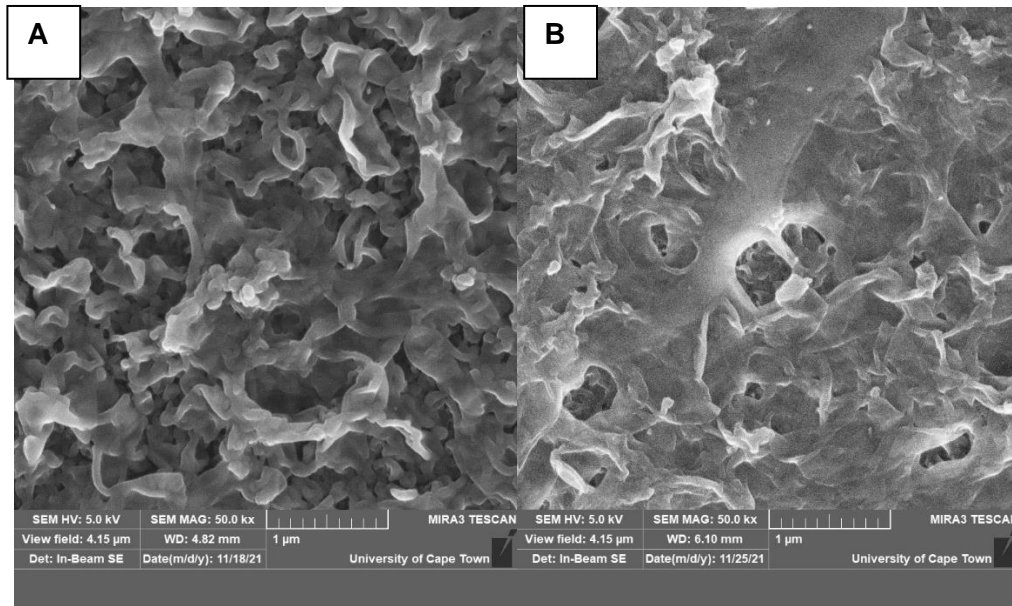
Figure 4-3: SEM image of virgin RO (A) and NF (B)

Table 4-1: SEM EDX of RO and NF virgin membranes

Element	Weight %	
	RO virgin membrane	NF virgin membrane
C	71.82 (1.76)	78.4 (0.78)
O	22.21 (2.15)	15.49 (0.74)
S	5.97 (0.58)	6.1 (0.1)
Total	100	100

n=6, the standard deviation is in parenthesis
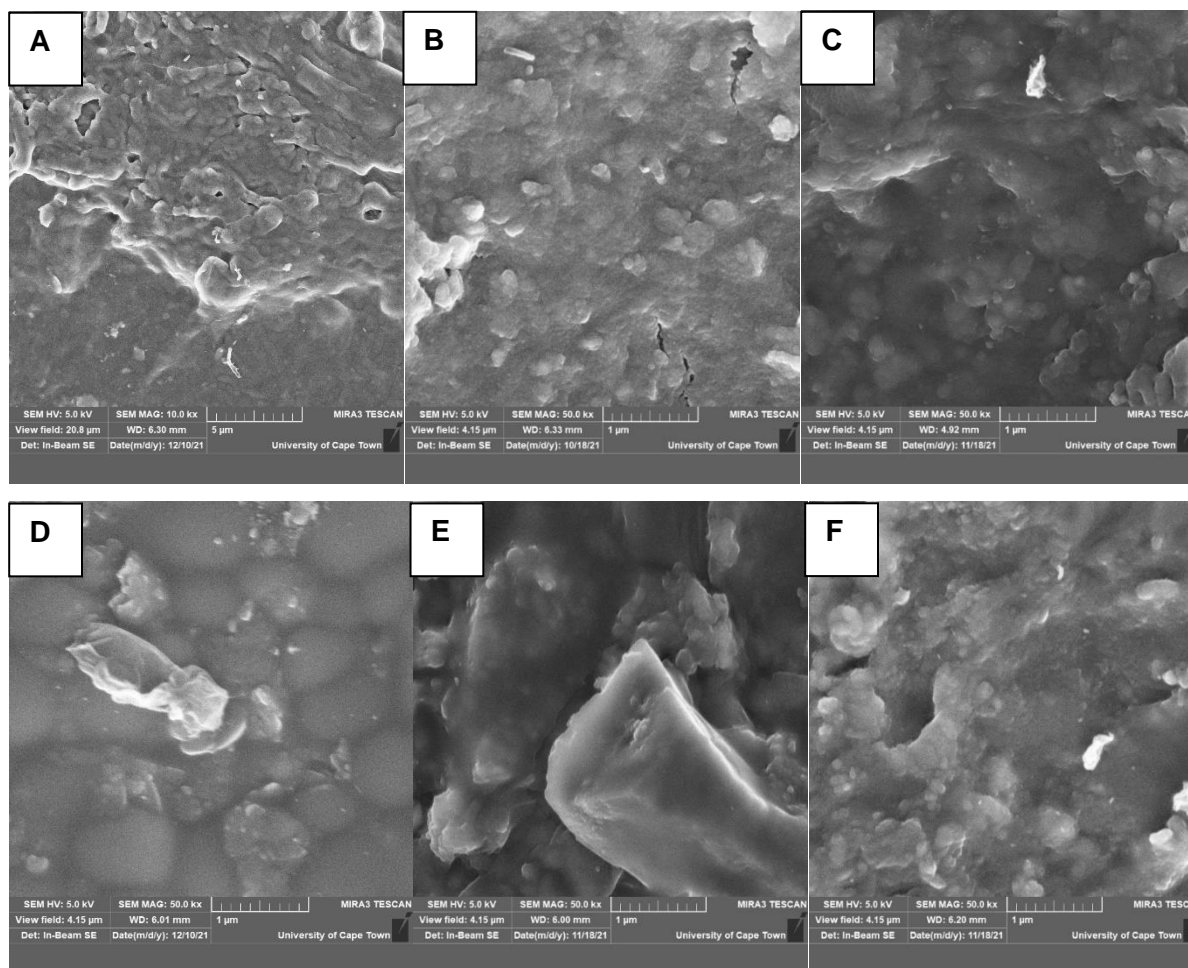
Figure 4-4: SEM image of the top view of RO and NF membranes at different feed pressures A: RO 5 Bar, B: RO at 10 Bar, C: RO at 15 Bar, D: NF at 5 bar, E: NF at 10 bar, F: NF at 15 Bar and constant initial concentration 440ng/l

Figure 4-4 to 4-5 represented the SEM image of RO and NF at 10 bar, 15 bar and 5 bar and 440ng/l, respectively. The experimental time of the run was 12 hours. It can be observed from Figures 4-4 that the NF membrane displayed a more compact top layer compared to the RO membranes under the same conditions. This result revealed that the biofilm layer fouled the membrane, blocking the pores. The larger pore-sized membrane observed a thicker cake layer, NF>RO. The cross-sectional views can confirm this. The NF at 10 bars had a maximum thickness of 13.25µm compared to the RO, with a maximum thickness of 1.68µm. Thus, the increase in feed pressure caused an increase in the thickness of the fouling layer for both membranes.
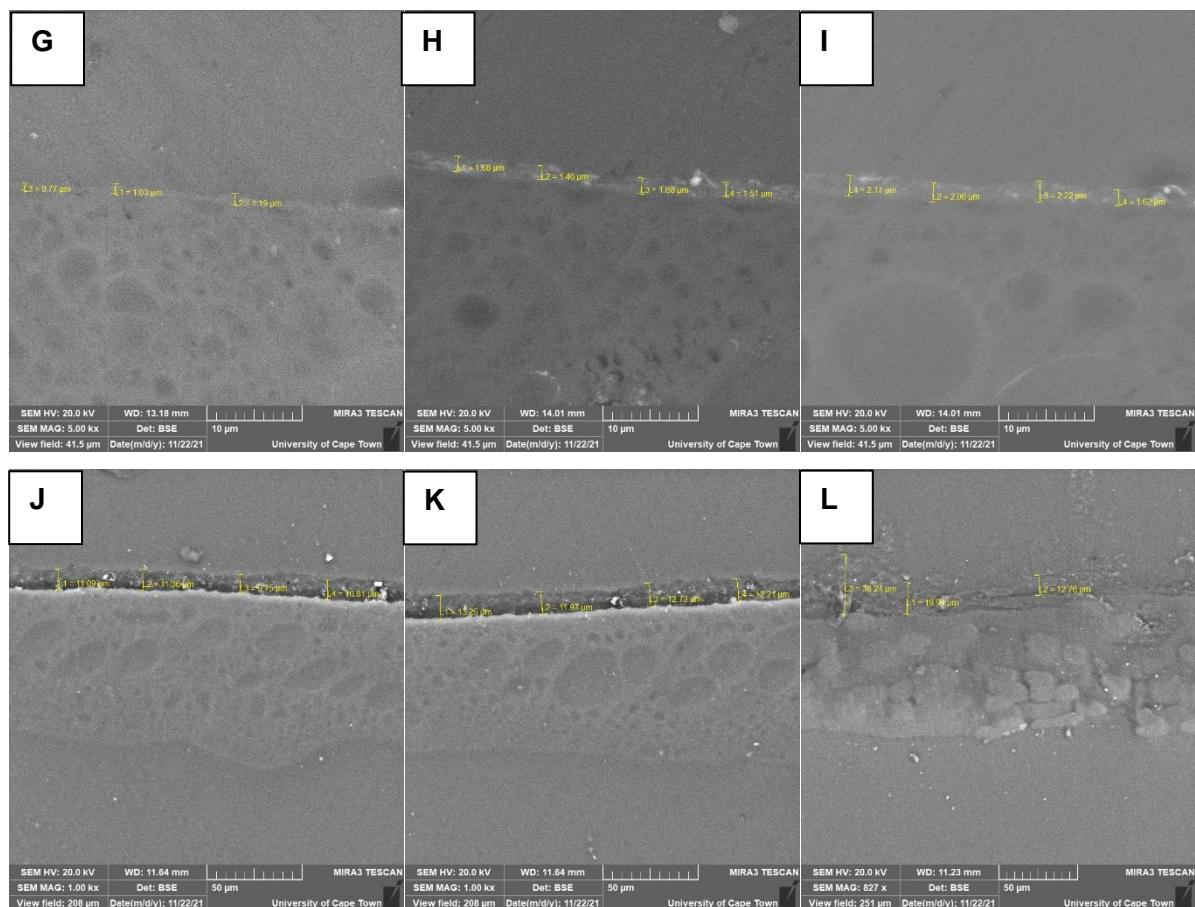
Figure 4-5: SEM image of a cross-sectional view of RO and NF membranes at different feed pressures G: RO at 5 bar, H: RO at 10 bar, I: RO at 15 bar, J: NF at 5 bar, K: NF at 10 bar, L: NF at 15 bar and constant initial concentration, 440ng/l.

The presence of trace inorganics such as Al, F, Ca, and Cl was absent on the NF membrane; however, the NF showed traces of Na, which was not present on the RO membrane. The presence and absence of some aspects of the two different membranes can be attributed to their membrane properties, such as the surface morphology, pore size, zeta potential, MWCO and surface roughness (Lin, 2017; Xu & Drewes, 2006).

The foulant deposition onto the PA layer increased for both membranes following the feed pressure increase of 15 Bar>10 Bar>5 Bar. According to Figure 4-5, the maximum thickness observed for RO at 5, 10, and 15 Bar were 1.19, 1.68 and 2.22µm, while the results for NF under the same conditions were 11.36, 13.25 and 38.24µm, respectively. The high surface roughness of NF and RO could also contribute to the incomplete/complete blocking of membrane pores by trapping foulants in the "valleys" of the membrane surface (Lin, 2017)

Table 4-2: SEM EDX analysis of RO and NF at 10 bar and 44 µg/l

	Weight %		Weight %
Element	**RO**	**Element**	**NF**
C	66,38 (0,77)	C	67,73 (0,8)
O	26,37 (0,46)	O	26,36 (0,87)
F	0,8 (0,49)	-	-
Al	0,33 (0,05)	-	-
Si	0,36 (0,03)	Si	0,37 (0,07)
S	5,42 (0,07)	S	5,41 (0,18)
Cl	0,18 (0,02)	-	-
Ca	0,16 (0,03)	-	-
		Na	0,13 (0,18)
Total	100		100

n=6, Standard deviation in parenthesis

Table 4-3: SEM EDX of NF and RO at 5 Bar, 440ng/l

	Weight %		Weight %
Element	**RO**	**Element**	**NF**
C	71,82 (1,76)	C	70,36 (1,19)
O	22,21 (2,15)	O	23,33 (1,15)
S	5,97 (0,58)	S	6,31 (0,16)
Total	100	Total	100

n=6, Standard deviation in parenthesis

Table 4-4: SEM EDX of RO and NF at 15 Bar, 440ng/l

Element	Weight % RO	Element	Weight % NF
C	60,39 (0,54)	C	81,66 (0,62)
O	32,64 (0,53)	O	15,95 (0,83)
Al	0,54 (0,07)	S	2,39 (0,48)
Si	0,74 (0,14)	-	-
S	5,69 (0,22)	-	-
Total	100	Total	100

n=6, Standard deviation in parenthesis

Carbon, oxygen, and nitrogen are the significant elements for RO and NF membranes, which are important key components of PA. The results in Tables 4-2 to 4-4 show the EDX analysis done on the membrane surface at three different feed pressures. The results indicate that the 10-bar run had a higher elemental deposition percentage than the 5 and 15-bar runs. At 5 bar, minimal elemental deposition was observed when comparing the EDX results to the virgin membrane for both NF and RO membranes. The carbon, oxygen and sulfur content at 5 bars can be observed in Tables 4-3.

It seems likely that the EDX involves the analysis of the virgin membrane material in each condition. Hence for the 5-bar experimental run, there is only a thin layer of foulant on the membrane surface. A similar observation was reported by (Morris, 2020).
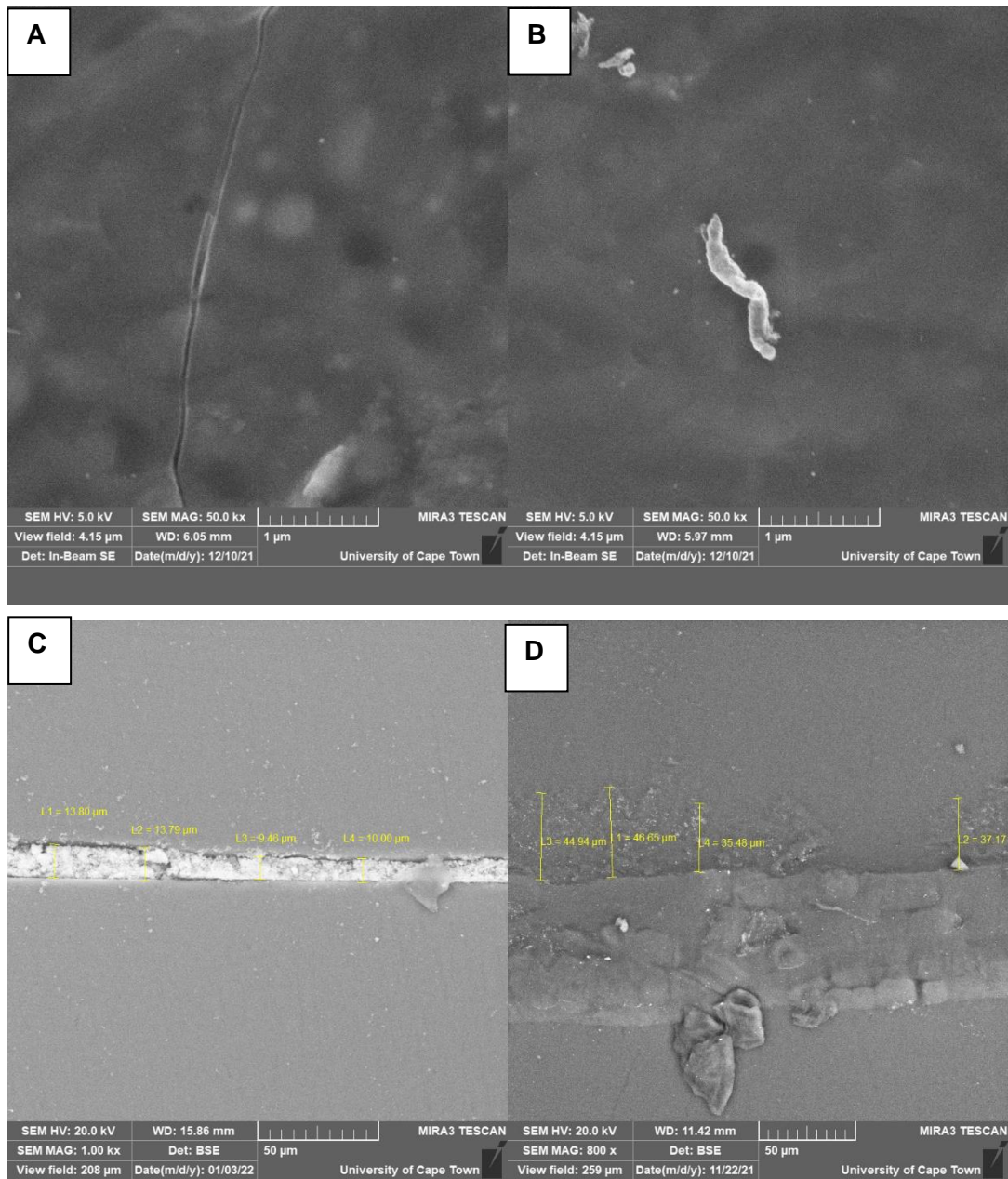
Figure 4-6: SEM Images of RO and NF top view and cross-sectional view after 100 hours, A): RO top view, B): NF top view, C): RO cross-sectional view, D): NF cross-sectional view

Table 4-5: SEM EDX of RO and NF after 100 hr, at 10 Bar

Element	RO	Element	NF
C	49,52 (1,29)	C	57,37 (0,27)
O	49,15 (1,6)	O	39,88 (0,48)
Mg	0,35 (0,18)	S	0.41 (0.08)
P	0,68 (0,18)	P	1,75 (0,15)
Ca	0,3 (0,07)	Ca	0,59 (0,11)
Total	100	Total	100

n=6, the standard deviation in parenthesis

The long experimental run was over 100 hours at a constant pressure of 10 Bar and an initial concentration of 44µg/l. According to the results obtained for the SEM images of the membrane's top view (surface), both membranes experienced severe fouling. Both membranes had smooth surfaces instead of their initial ridge and valley textured surface. The NF had a densely packed fouling layer consisting of organic matter and inorganic salts on the membrane's surface. The fouling layer was 46.65µm and 13.79µm thick for the NF and RO, respectively. The severer fouling of the looser membrane was also observed in previous literature (Nghiem & Hawkes, 2007), which could be attributed to more significant adsorption and pore restriction (Lin, 2017). The removal of these inorganics is discussed further below.

4.3   Performance of the RO system

All experiments were conducted in a crossflow membrane unit with a flat sheet membrane cell (GE Osmonics). The effective membrane area was (0.013775 m^2) with dimensions of (14.5cm X 9.5 cm). After reverse osmosis treatment, synthetic secondary wastewater was analysed to study the treatment efficiency of RO and NF polyamide (PA) thin-film composite (TFC) membrane under different working conditions. Experimental runs were carried out at 5, 10 and 15 bars with three concentrations, i.e. 22 μg/l, 35.5 μg/l and 44 μ/l.

Table 4-10 is a breakdown of all the experimental runs carried out at different feed conditions. Experimental runs 1-9 were performed using the RO membrane, and experiments 10-18 were carried out using the NF membrane. The effluent concentrations of the inorganics are shown in Tables 4-6.

4.3.1   Salt rejection and total dissolve solids (TDS) removal

The salt rejection and TDS were used to measure the system's performance. Figures 4-7 and 4-8 show the effluent salt rejection for RO and NF as a function of time obtained from all three membranes at 5, 10 and 15 bar at a constant initial pharmaceutical concentration of 22μg/l. The highest average salt rejection was 98,7% for the RO at 10 bars, whilst the NF had a 97.3% rejection under the same conditions. The RO performed best at 10 bars, showing membrane and system stability and consistency throughout the 12-hour experimental time. The TDS as a function of time can also be seen in Figures 4-7 and 4-8. The lowest TDS of 3.3mg/l and 7.5mg/l was achieved at 10 bars with the RO and NF membranes, respectively. The rejection for the RO at 5 and 15 bars was 96.8 and 97.4%, while the average TDS was 7.2 and 6.3mg/l, respectively. The main mechanisms of removal were MWCO, charge and electrostatic interactions with the surface of the membrane (Aziz & Ojumu, 2020). The results of the RO were also expected due to its denser skin layer, as opposed to the latter.

Furthermore, a low-pressure RO membrane is a pressure-driven membrane dominated by an increase in permeate flux against increasing transmembrane pressure. It was observed that rejection of several selected inorganics increased with an increase in transmembrane pressure (Ozaki et al., 2002). This may be due to a decrease in the average pore size on the membrane surface and an increase in the favored sorption of pure water at higher pressure: e.g., the solvent permeability increases compared with solute at high pressure, resulting in increased rejection (Heo et al., 2019).
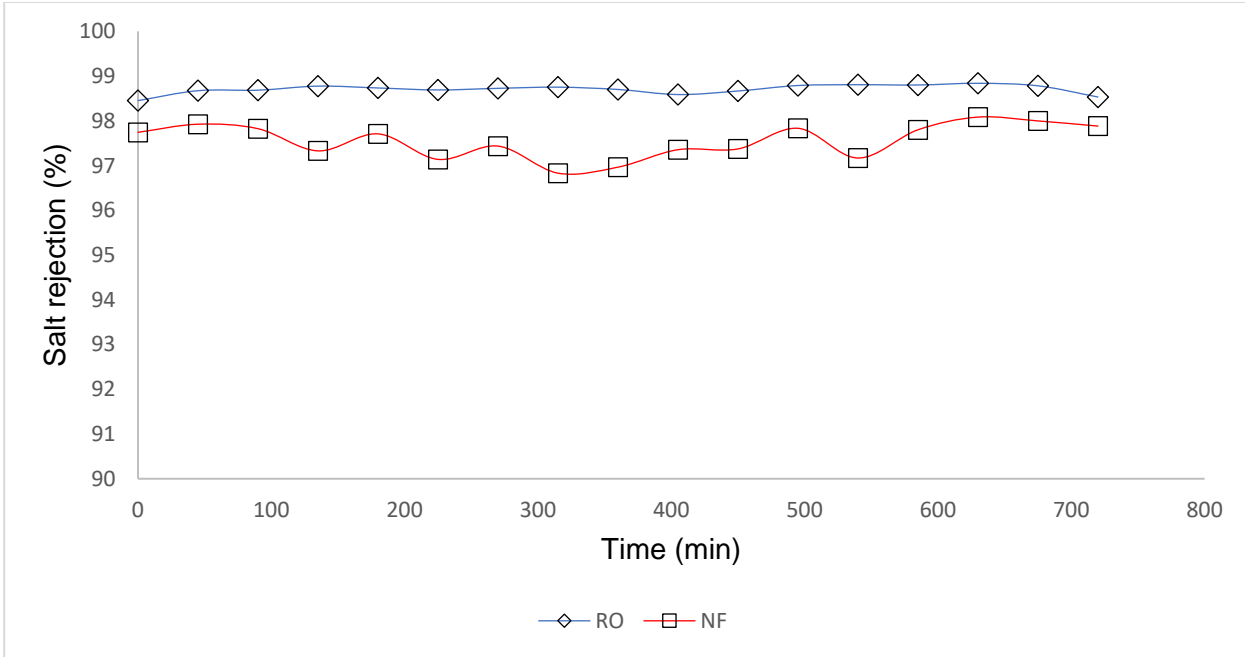
Figure 4-7: Effluent salt rejection (%) vs time of RO and NF membranes at 10 Bar feed pressures and constant initial concentration; 22 μg/l
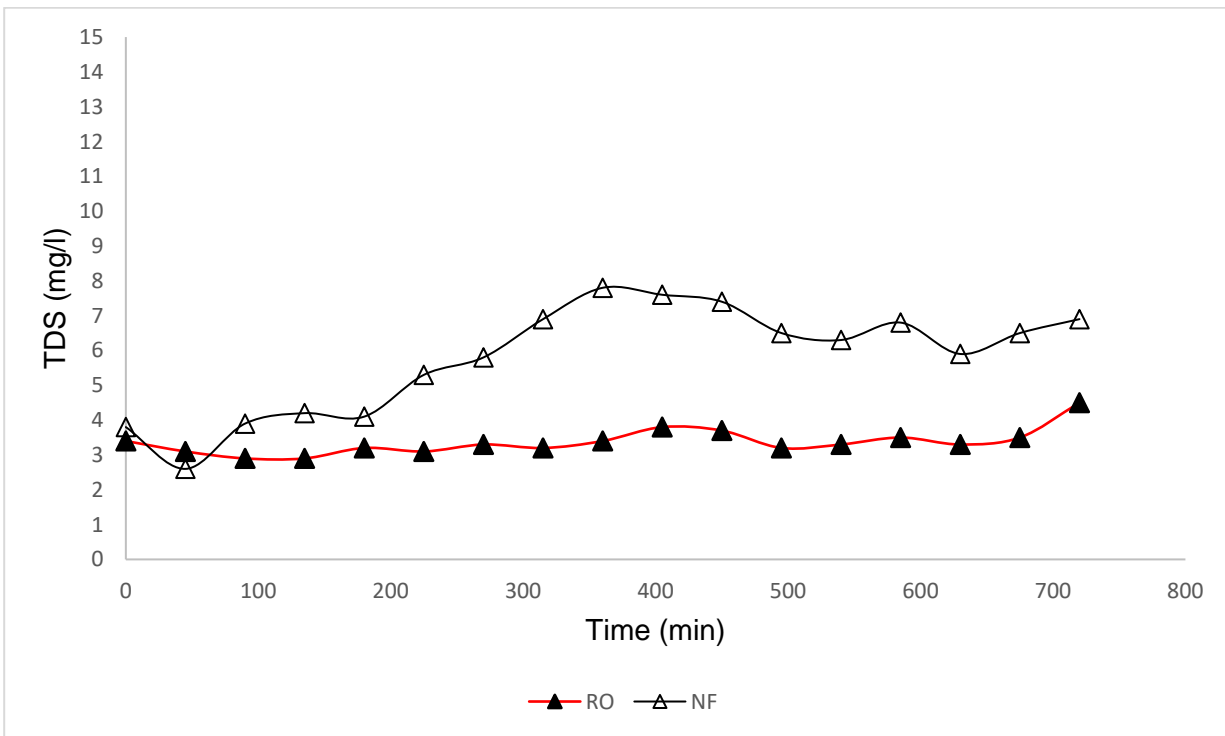
Figure 4-8: Effluent TDS vs time of RO and NF membranes at 10 Bar feed pressures and constant initial concentration; 220ng/l

4.3.2 The removal of inorganics

The permeate quality of RO and NF units of selected inorganics are summarised in Tables 4-6 and 4-7. These tables give a breakdown of the average concentrations and percentage removal of inorganics found in the effluent of the two membranes at three different pressure (5,10,15 bar). It was confirmed by (Shad et al., 2019) that inorganics are found in municipal wastewater originating from industrial and domestic sources in the form of pharmaceutical residues, pesticides, steroid hormones, surfactants, and preservatives and perfluorochemicals, which are all found in excreted human waste.

Table 4-6: Concentration of inorganics in the effluent of NF and RO permeates at different feed pressures (mg/l).

Parameter	RO			NF		
Pressure (bar)	5	10	15	5	10	15
NH_3-N	0,45 (0,592)	0,23 (0,111)	0,243 (0,116)	0,80 (0,57)	0,203 (0,076)	0,597 (0,116)
NH_3	0,537 (0,709)	0,28 (0,137)	0,3 (0,139)	0,97 (0,70)	0,250 (0,087)	0,723 (0,137)
NH_4^+	0,297 (0,143)	0,17 (0,095)	0,32 (0,148)	1,03 (0,74)	0,263 (0,093)	0,763 (0,146)
PO_4^{3-}	0,643 (0,95)	0,07 (0,089)	0,607 (0,990)	0,92 (0,673)	0,217 (0,108)	0,573 (0,569)
P	0,21 (0,312)	0,02 (0,0265)	0,2 (0,32)	0,300 (0,22)	0,073 (0,032)	0,187 (0,185)
P_2O_5	0,483 (0,716)	0,05 (0,06)	0,450 (0,736)	0,683 (0,500)	0,163 (0,076)	0,450 (0,407)
NO_2^- - N (µg/l)	0	0	0,667 (1,15)	2 (1,15)	0,33 (0,57)	2 (1,15)
NO_2^- (µg/l)	0	0	1,67 (2,89)	8 (4,62)	1,67 (2,89)	5,5 (3,21)
$NaNO_2^-$ (µg/l)	0	2 (1,15)	2,67 (4,62)	14 (9,8)	3 (5,19)	8,5 (4,9)
COD (mg/l)	4,4 (0,36)	2,67 (0,15)	3,4 (0,2)	6,3 (0,26)	5,4 (0,25)	6,1 (0,15)

Values are averages from n=3 samples where the standard deviation is in parenthesis

Table 4-6 shows that the phosphorus removal was higher than the phosphate due to the size exclusion and chemical charge on the membrane surface (Aziz & Kasongo, 2021). Phosphate, a multivalent anion, demonstrates a different behaviour to phosphorus, a neutral molecule; thus, electrostatic repulsion to the surface of the membrane may have been the reason for the difference in removal efficiencies (Aziz & Kasongo, 2021). A significant difference in phosphorus removal was observed for RO at 5, 10 and 15 bars (*P=0,000862* at 5 &10 bar, *P=0,000476* at RO 5 & 15 bar and *P=0.00366* at 10&15 bar, α=0.05). The removal of ammonia with RO was 80.2, 85.3 and 92.3%, respectively. This is in order of the increase in pressure from 5 bar to 15 bar the driving force of the water is directly affected by the feed pressure; thus, a higher pressure resulted

Table 4-7: Percentage removal of inorganics from MBR effluent at different pressures

| | | % Recovery | | |
| | | Operating feed pressure | | |
Membrane type	Inorganics	5	10	15
	NH_3-N	85.00	92,33	91,90
	NH_3	85,29	92,33	91,78
	NH_4^+	92,33	95,61	91,73
RO	PO_4^{3-}	72,28	96,98	73,84
	P	74,39	97,56	75,61
	P_2O_5	74,17	97,33	75,94
	NO_2^- - N	87,5	100.0	91,66
	NO_2^-	75.00	100.0	93,04
	$NaNO_2^-$	74,36	94,87	93,15
	NH_3-N	73,33	93,23	80,10
	NH_3	73,42	93,15	80,19
NF	NH_4^+	73,39	93,2	80,28
	PO_4^{3-}	60,34	90,65	75,3
	P	63,41	91,1	77,2
	P_2O_5	63,48	91,28	75,94
	NO_2^- - N	100.0	95,88	93,75
	NO_2^-	91,67	93,04	92,50
	$NaNO_2^-$	82,05	92,31	78,21

in higher flux. On the contrary, according to Kucera (2015), salt transport is unaffected by pressure; thus, the same quantity of salt passes through the membrane whether the pressure is high or low. However, because more water has gone through the membrane at higher pressures, the absolute salt concentration in the permeate is lower. As pressure rises, the salt passage reduces, and the salt rejection increases. The removal of nitrites for RO 5 and 10 bars were 66.7% and 77.1%, respectively. Higher removal rates of nitrites were achieved for NF at 5,10, and 15 bars. Similar results were achieved by (Chon et al., 2012), who reported that significant differences in the removal of nutrients were found for the removal of nitrogen species by the NF membranes, even though the MWCO of RO membranes are lower than <200Da. The removal rates for nitrites of NF at 5,10, and 15 bars were 100, 93 and 93%, respectively. This could be attributed to their differences in zeta potential. RO membranes have an overall negative surface charge and repel negatively charged ions or molecules (Zhao et al., 2005; Amin et al., 2018). As negative ions are repelled, more cations than anions are present near the membrane surface; this phenomenon creates an electric potential known as the Donnan potential, as explained in chapter 2, section 2.5.1 by Vezzani & Bandini, 2002.

 (Zhao et al., 2017) reported that salt rejection increased when water flux increased, and although the two membranes (RO and NF) have similar MWCO properties, the lower rejection could be due to the lower negative charge density of the surface. These results showed that removing negatively charged nutrient ions, such as nitrite and phosphate, can be governed by either membrane characteristics (i.e., MWCO and surface zeta potential) or solute characteristics (numbers of negative charge) (Zhao et al., 2017).

4.4   Chemical Oxygen demand (COD) rejection

The removal of COD with RO and NF membranes at different feed pressures is presented in Figure 4-9. The removal of COD with the RO membrane increased from 5 to 10 bar and decreased at 15 bar. The removal percentages were 91.8, 95 and 93.7%, respectively. This aligns with (Nataraj et al. 2006) research, which reported that COD removal increased with feed pressure. The COD removal for NF was 88, 90 and 88.3% at 5,10 and 15 bar, respectively. Despite the COD rejection being high at 85%, which is desirable, the results indicate the possible penetration of ions through the membrane pores at high pressure (Nataraj et al., 2006).
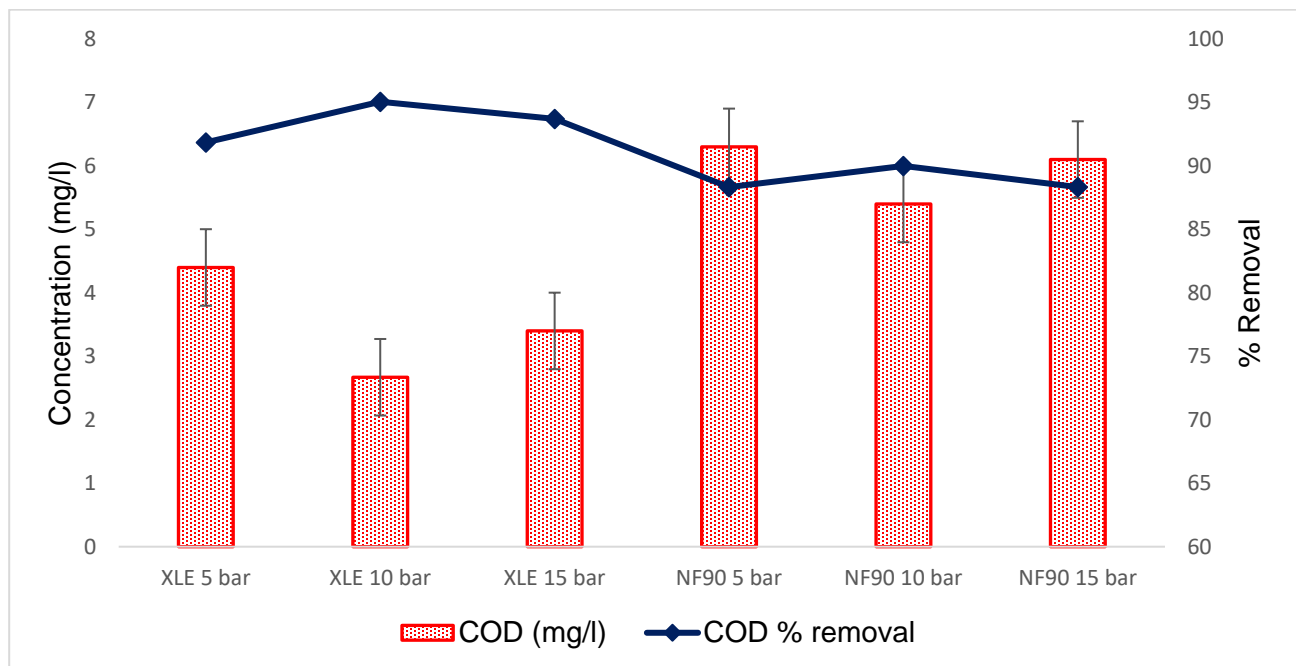
Figure 4-9: The effect of feed pressure on COD removal

The COD removal for the RO was significantly higher than the NF membrane (P=0.000487 RO and NF at 10 bar, α=0.05). This is attributed to the membrane surface properties such as pore size. It may also be noted that at 10 bar, a higher removal of COD was achieved, despite the 15 bar pressure being higher; this is because for higher operating pressures, permeate concentration is more due to an enhanced convective flux through the membrane (because of the higher driving force) and permeate concentration increases with a decrease in retention (Chakraborty et al., 2003).

4.4.1 One-hundred-hour experimental long run

The long experimental runs were conducted at 10 bar and 44µg/l for one hundred hours due to their stability and consistency, as seen in Figures 4-10 to 4-11. Figures 4-12 and 4-13 compare the membranes during the 12-hour short-run and 100-hour long run, showing the flux and percentage rejection simultaneously within the experimental run. Figure 4-10 indicates that the percentage rejection for the long run was slightly lower than in the short run at the same time for the RO membrane. The average % rejection for the RO at 12 and 100 hours was 98.5 and 97.2%, respectively. The increased concentration polarization in the cake layer generated on the membrane's surface may reduce rejection. An increase in rejection is possible when the membrane "pores" is narrowed and the apparent MWCO is lowered. Change of rejection could also result from the variation of membrane surface hydrophobicity and charge caused by the adsorption of membrane foulants (Zhao et al., 2013).

The average % rejection for the NF at 12 and 100 hours was 97.2 and 97.6%, respectively. Both membranes performed as expected and were within the manufacturer's standards. The 12-hour run performed better than the 100-hour run for the NF and RO. The performance of the NF and RO membranes in terms of % rejection was negligible. However, a drop in pH was observed over the 100-hour run for both membranes, from an initial pH of 7.8 to 5.9 for RO and 6.5 for NF, respectively. This explains the removal of ammonia; with the pH drop, there was a shift in the equilibrium of ammonia, resulting in a higher reduction and permeance of cations than the anions due to deprotonated carboxylic groups of the polyamide membrane (Aziz & Kasongo, 2021; Pagès et al., 2017).
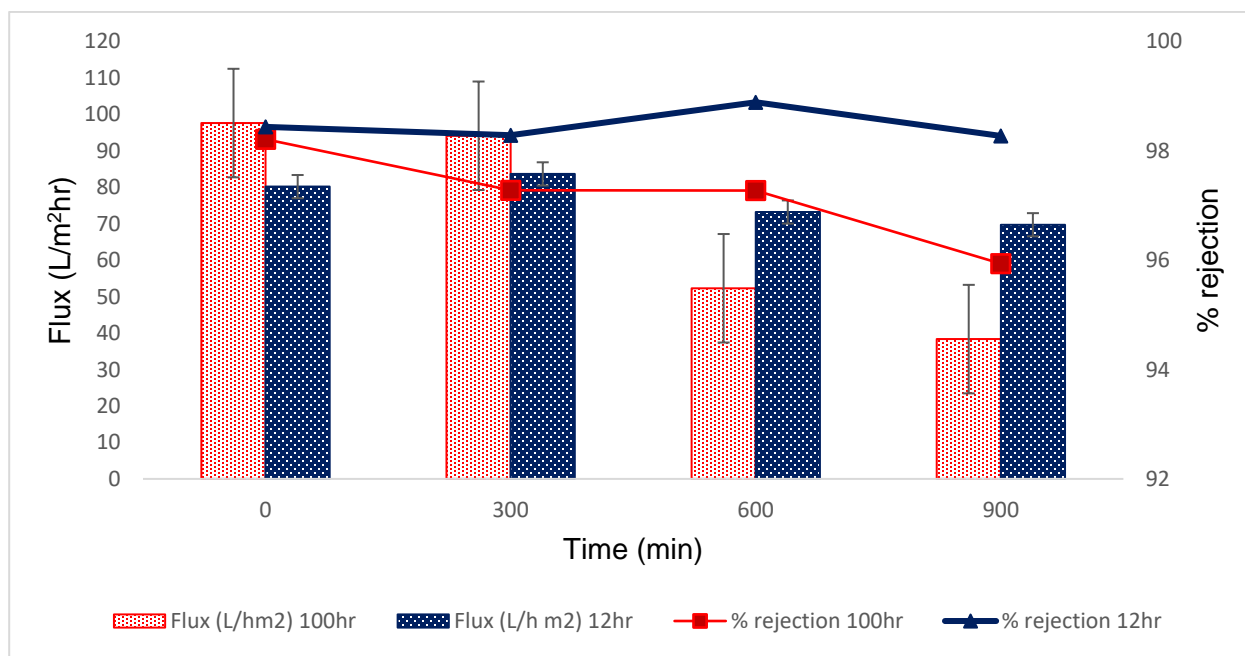
Figure 4-10: Flux and % Rejection of RO at 10 bar and 44ug/l for 100 hr and 12 hr

(Rana et al., 2015) reiterated that RO's higher rejection of these monovalent ions is due to its dense surface layer without pores (Aziz & Kasongo, 2021). A persistent flux decline was observed during both experimental run types. This is attributed to the membrane's pore size and hydrophilicity, which are the two major influences on the water flux performance of the membrane (Sumisha et al., 2015). Furthermore, it can be seen in Figures 4-12 and 4-13 that the rejection of selected inorganics decreased because of time. This could be attributed to the dense cake layer observed in Figures 4-6 (C & D), which consisted primarily of carbon and oxygen; hence organic fouling occurred on the surface of the membrane.
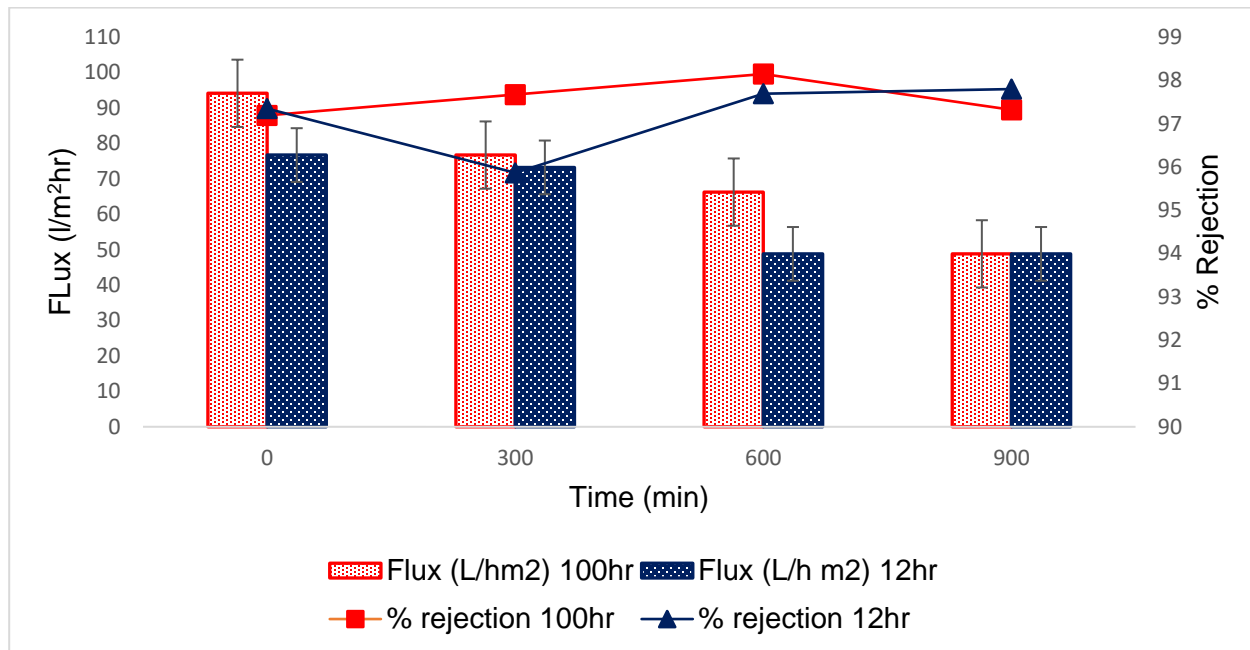
Figure 4-11: % Rejection and flux over time of NF after 100hr vs 12 hrs at 10 bar, 44µg/l
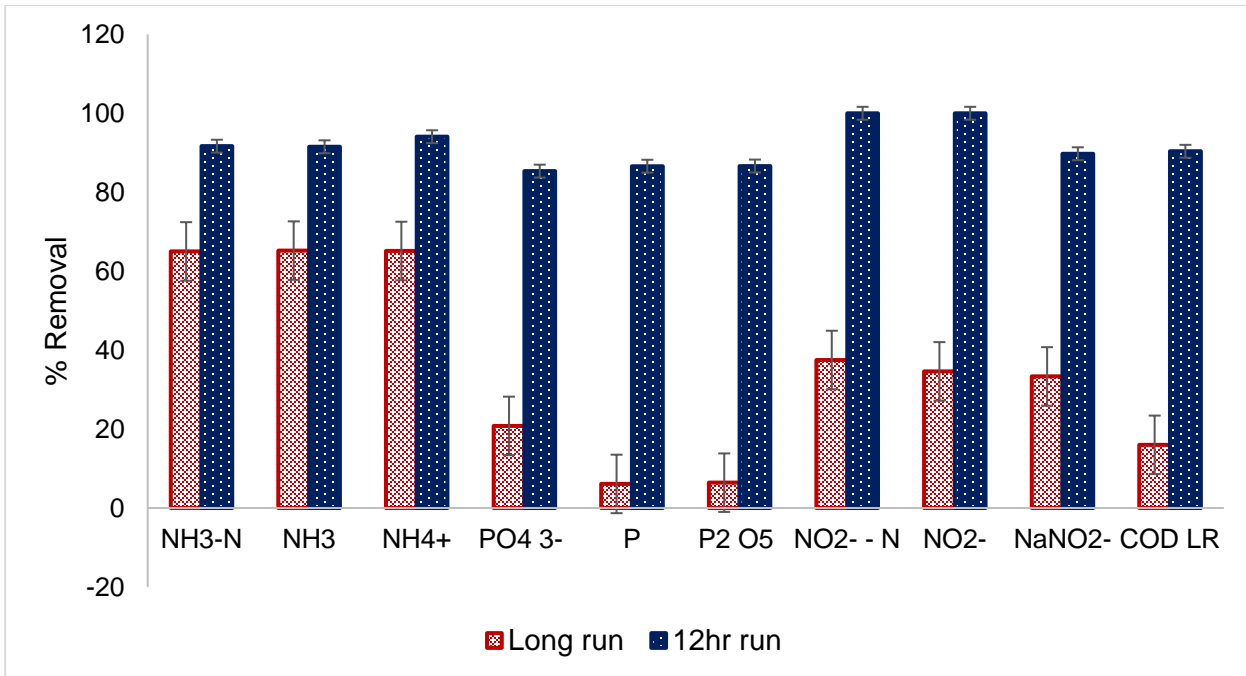
Figure 4-12: Comparison of the %removal of inorganics after short 12hr run vs long 100hr run by NF membrane.
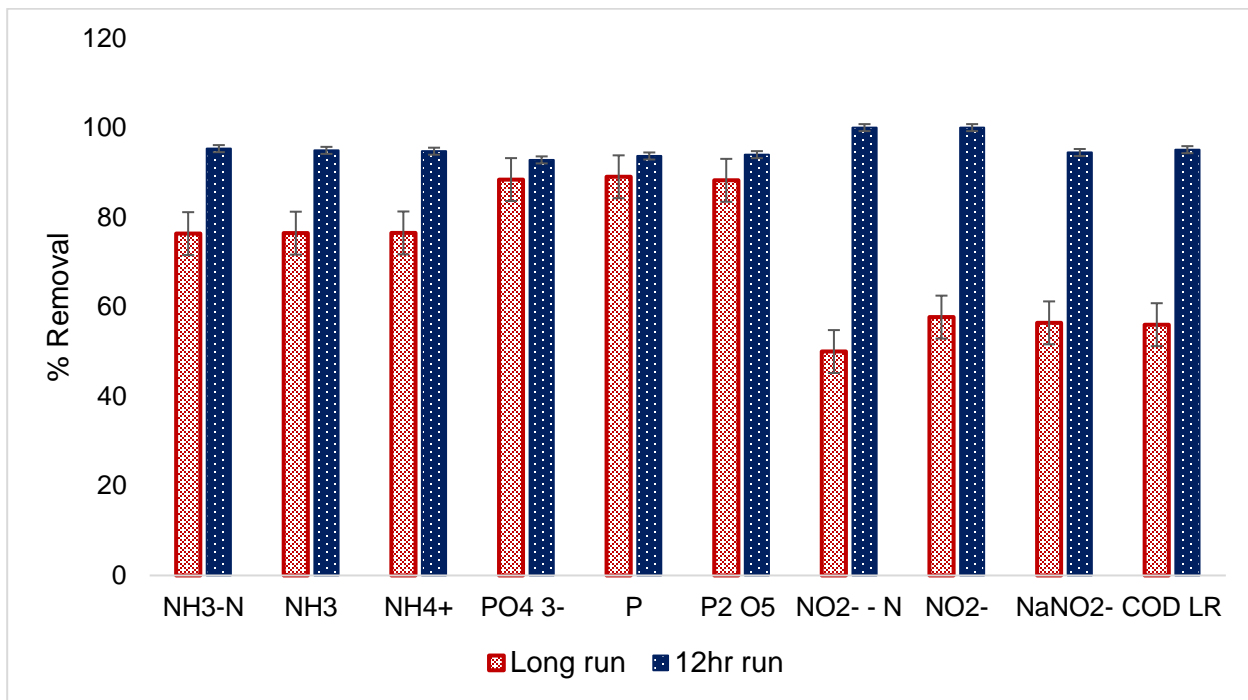
Figure 4-13: Comparison of the %removal of inorganics after short 12hr run vs long 100hr run by RO membrane.

Table 4-8: Characteristics of NF and RO effluent average water quality with reuse criteria for wastewater in different applications (Üstün et al., 2011; Emongor et al., 2005; Hansen et al., 2016; Asano et al., 1988; Aziz & Kasongo, 2021)

Parameter	Irrigation	cooling systems	NF	RO
COD (mg/l)	<50	<30	5,4	2,6
NH_3	<6,08	<1	0,25	0,28
P	<1,5	-	0,073	0,02
PO_4^{3-}	<2	<7	0,22	0,07
TDS (mg/l)	<200	-	7,1	3,4
pH	6,5-8,4	6,8-7,2	6,8	7,2
EC ($\mu s/cm^{-1}$)	<250	<1445	8,1	4,1

The results in Table 4-8 indicate that the removal of ammonia, phosphorus and phosphates by NF and RO are within the range of irrigation and cooling systems specifications and international guidelines for water reuse. The results shown in Table 4-8 by RO and NF membranes make them suitable for irrigation and cooling systems and comply with standard requirements for potable and non-potable water. Low concentrations of pathogens, nutrients, and dissolved solids are common in secondary treatment effluent. There is a risk to sustainable agriculture productivity and aquifer water quality when this effluent is reused for irrigation and/or groundwater recharge over lengthy periods (Üstün et al., 2011). Tertiary treatments are implemented in WWTPs after secondary treatment to improve water quality further. Treated wastewater is an effective alternative for small irrigation areas where clean distribution system water is used (Oron et al., 2008). They might be viable options in areas where the water supply for irrigation is difficult or inaccessible. Cooling towers are among the largest industrial consumers of fresh water and is used as makeup water in the cooling tower. The results obtained in this study make it a promising alternative to fresh water and a great potential for the reuse of effluents in the petrochemical industry. It can significantly reduce the volume of water obtained directly from water sources and wastewater generated in their processes (Hansen et al., 2016).

4.5   Chemical Analysis

In this study, a synthetic MBR secondary effluent model was used as the feed water. The pharmaceuticals of interest include carbamazepine, diclofenac, aspirin, and ibuprofen. Two commercial membranes i.e. RO ad NF were investigated. Composite samples were collected and stored at 4°C before the clean-up and concentrating step, which was done using SPE. The pharmaceutical activity was assessed using GCMS.

4.5.1   Pharmaceuticals in the influent

Target analytes were dosed in the µg/l range into the synthetic secondary municipal wastewater feed solution. Each contaminant was dosed at the same concentration for each experimental run. The attention of contaminants was 22µg, 35.50µg and 44 µg/l. The averages used for this study are within the range of previously reported studies and can be seen in Table 2-2. Standard calibration curves generated using linear regression analysis generally gave good fits to the data ($R^2 > 0.98$) over the established concentration range (0–8 µg/L), excluding where this concentration range fell below the detection limits of a particular compound. A six-point calibration was performed for each pharmaceutical, and possible fluctuations in signal intensity were checked by injection of standard solution at two concentrations after each 4–6 injections. Method detection limits (MDL) were determined from spiked water samples as the minimum detectable amount of analyte with a signal-to-noise ratio of 3.

4.5.2   Pharmaceuticals in the effluent

Selected micropollutants were studied in the permeate streams after RO treatment. Two distinct membranes were used to compare the removal of contaminants of emerging concerns (CEC): diclofenac, Carbamazepine, ibuprofen, and aspirin, under different operating conditions. The breakdown of the experimental runs is shown in Tables 3-6 (Chapter 3). According to the results obtained in Table 4-9 with the RO membrane under 5 bar feed pressure and an initial feed concentration of 44µg/l, all CECs achieved a % rejection <97%. The higher rejections were achieved for the negatively charged CECs, with effluent concentrations below 0.444 and 0.817µg/l for IBU and DCF, respectively. ASP was not detected with eh RO membrane. CBZ had an effluent concentration of 1.198µg/l with a % rejection of 97.2%. Comparing the two membranes, the increase in IBU rejection was not observed for the RO membrane, whereas the increase was evident for the NF membrane as no IBU was detected, indicating steric hindrance was more dominant than the electrostatic repulsion for the RO membrane (Li et al., 2018).

Although high rejections were achieved for all CECs, the negatively charged pharmaceuticals demonstrated better performance than neutral CBZ by negatively charged membranes due to electrostatic repulsion (Li et al., 2018). The NF membrane achieved similar results under the same feed conditions. The concentration of micropollutants for the NF membrane was below the level of detection (LOD) for IBU, 1.194 and 0.297µg/l for CBZ and DCF, respectively.

The initial feed concentration of 35.5µg/l at 5 bars for the RO and NF membranes both achieved % salt rejections of 97%. These experimental conditions indicate that the pharmaceuticals' physio-chemical properties significantly affect the removal efficiencies.

The RO membranes performed better regarding the removal rates of each target analyte. IBU, CBZ, DCF and ASP had effluent concentrations of 0.006, 0.283, 0.003 and 0.763µg/l, respectively. The NF membrane exhibited concentrations of 0,145, 1,761, 2,361µg/l for IBU, CBZ and DCF. Diclofenac's removal rate was lower than the rest of the target analytes in both runs. According to (Cartagena et al., 2013), the low removal rates of DCF and CBZ can be attributed to their recalcitrant nature and physio-chemical properties. The results can be explained by considering the NF and RO membranes and solute-membrane interactions. The three main mechanisms that influence the removal of emerging micropollutants and contaminants of emerging concerns by NF and RO: are steric hindrance (sieving effect), electrostatic interaction (charge effect) and the hydrophobic/adsorptive interactions (Bellona et al., 2004; Cartagena et al., 2013).
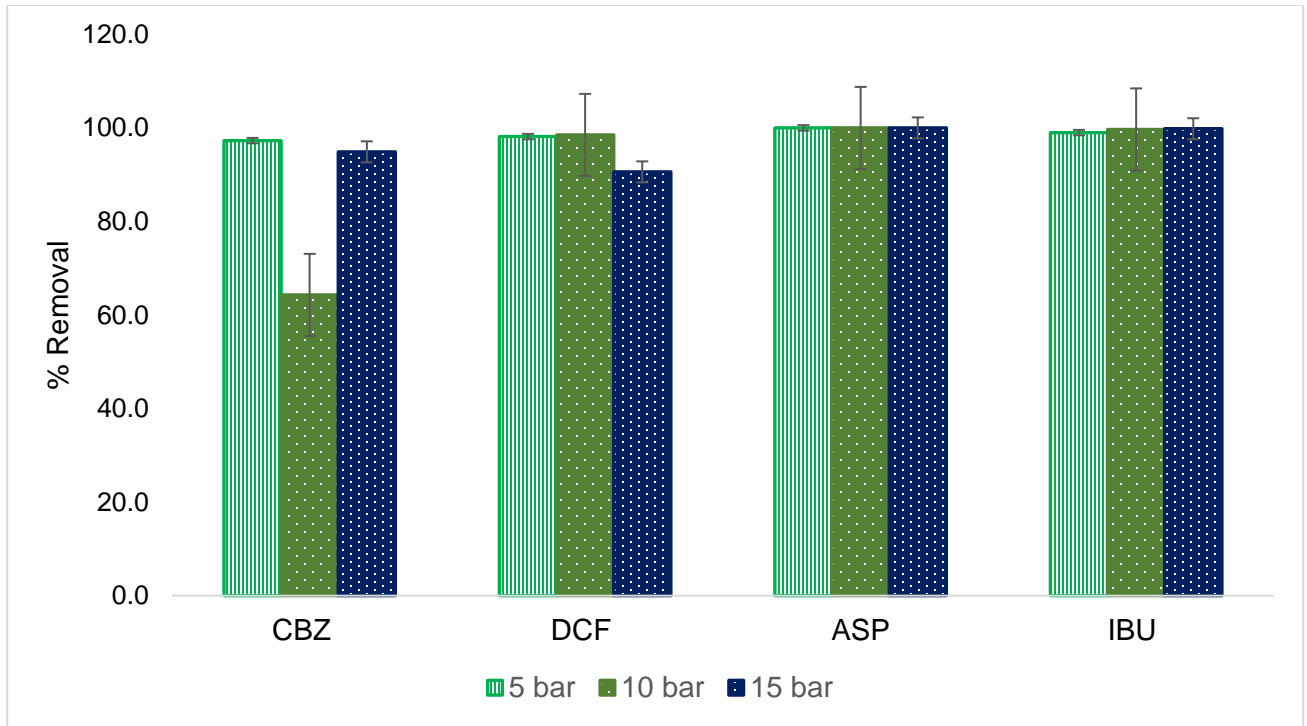
Figure 4-14: % Removal of pharmaceuticals at different feed pressures with RO membrane
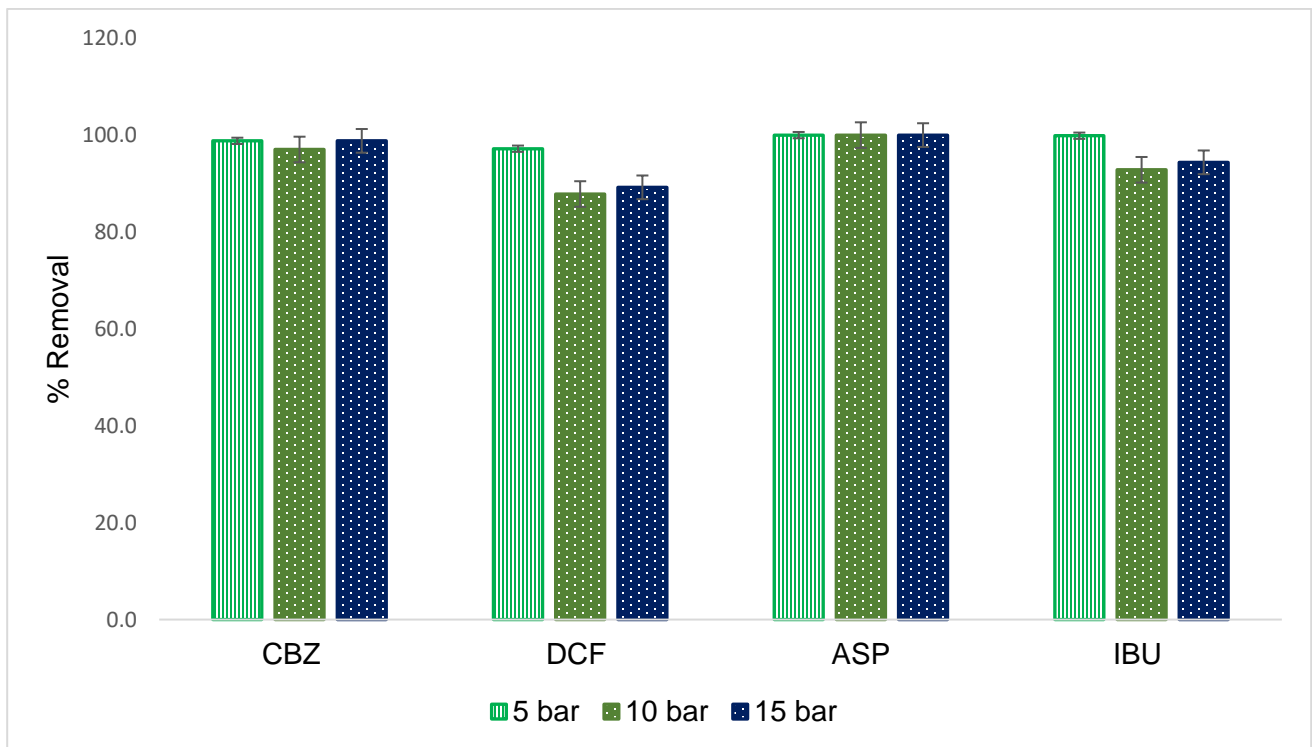
Figure 4-15: % Removal of pharmaceuticals at different feed pressures with NF membrane

Figures 4-14 and 4-15 demonstrate the removal rates of selected CECs at 5,10, and 15 bars by RO and NF membrane with an initial feed concentration of 44µg/l. RO and NF exhibited similar results, with average salt rejections of <98%. At an initial feed concentration of 22µg/l and a feed pressure of 10 bar, the effluent concentrations of CECs for NF were 1.157, 0.653 and 2.676µg/l for IBU, CBZ and DCF, respectively, while ASP was below the level of detection. The effluent concentrations for RO were 0.0258, 1.126 and 0.419µg/l, respectively. RO and NF had average effluent rejections of <94% at 10 bar with an initial feed concentration of 22µg/l. CBZ had a lower concentration with the NF membrane than the latter. The concentration of DCF was relatively high and, according to all the results, was the highest quantity recorded for DCF. As mentioned, DCF shows a similar recalcitrant behavior as CBZ and can be attributed to its hydrophilic nature (log K_{ow} 0.7)(Cartagena et al., 2013).

The effluent concentrations with an initial feed concentration of 44µg/l at 10 bar for the RO membrane were: below LOD, 0.334, 0.009, and 0.260 µg/l for IBU, CBZ, ASP and DCF, respectively; Similarly for the NF membrane: 0.258, 0.542, below LOD and 0.546µg/l for IBU, CBZ, ASP and DCF, respectively. Because operating pressure directly affects the driving force for water across the membrane, a higher pressure will result in higher flux. Salt transport, however, is unaffected by pressure. So, the same amount of salt passes through the membrane at low or high feed water pressure. However, because more water has passed through the membrane at higher pressure, the absolute salt concentration in the permeate is lower. The salt passage appears to decrease, and the salt rejection increases as pressure increases (Kucera, 2015). Thus, it is evident that the increase in pressure contributed to the higher removal rates of selected target analytes.

The % rejections for CBZ at 10 bars, as seen in Figure 4-14, demonstrated an unusually low recovery rate of 64.3%. This goes against literature in terms of performance. The MWCO is frequently used to determine membrane rejection. RO should demonstrate better rejection than NF based on the MWCO assessed in previous work (Kimura et al., 2004). The recalcitrant behavior of CBZ is shown with the RO membrane. The negatively charged pharmaceuticals (i.e., DCF, IBU, ASP) were more effectively removed by the negatively charged NF membrane than non-ionic pharmaceuticals (i.e., carbamazepine). This is due to electrostatic repulsion between the negatively charged pharmaceuticals and the negatively charged membrane surfaces (Nghiem et al., 2005). When dealing with rejecting organic micropollutants by RO membranes, the MWCO should be utilised instead of salt rejection, commonly used to express RO membrane rejection properties. The influence of steric hindrance is related to the molecular size of the compounds and the MWCO/pore size of the membranes.

Conversely, the RO membrane was a physical barrier to the solutes and restricted solute diffusion like traditional RO membranes (Bellona et al., 2004). On the other hand, although all EMPs studied in this work are considered low MW molecules, the sieving effect favoured an increase in the rejection of the compounds by the RO membrane. It was found that CBZ had relatively low removal efficiency compared to the other target compounds. Its moderately hydrophobic nature can partly explain this (log K_{ow} < 3) and chemical stability (Zhou et al., 2011). The recalcitrant nature of CBZ is shown at 10 bars, with a concentration of 8.879 µg/l.

RO and NF at 15 bars with an initial concentration of 44µg/l achieved effluent rejections <98%. The concentrations of IBU, CBZ, ASP and DCF, were 0.256, 0.145, below LOD and 0.298 µg/L for RO and below LOD, 0.027, 0.788, 0.004 and 0.369 µg/l for NF, respectively. The RO membrane performed better in terms of percentage removal of target analytes. The lowest concentration of CBZ was also reported under these conditions. This is because the rejection of uncharged trace organics by NF and RO membranes is predominantly influenced by steric hindrance (size exclusion). In contrast, the rejection of polar trace organics is mainly governed by electrostatic interactions with charged membranes (Radjenovic et al., 2007). In addition, the hydrophobic interactions between the macrolides and the membrane's surface may have contributed to the high removal rate (Cartagena et al., 2013; Radjenovic et al., 2007). RO and NF had average effluent rejections of <95% and <97%, respectively, at a feed pressure of 15 bar and an initial feed concentration of 22µg/l. ASP was below the level of detection for the NF membrane; however, the concentration of DCF was higher with the RO membrane than the NF, with a concentration of 1.709µg/l.

RO and NF membranes at 15 bars with an initial feed concentration of 35.5µg/l achieved salt rejections of <98%. The two membranes had very similar effluent concentrations, and all the pharmaceuticals had rejections < 98%. This also shows that the higher feed pressure (15 bar) demonstrated a higher removal rate of selected target analytes.

Regarding the comparison between both membranes (NF and RO), the differences found in the concentrations (Table 4-9) and the difference in feed pressure on removal efficiencies (Figure 4-14 and 4-15) of the analyzed CECs were not significant in terms of initial concentration since the two membranes have similar physico-chemical characteristics (both are considered hydrophobic and dense membranes with similar rejection characteristics) (Cartagena et al., 2013). Results were consistent with other published works regarding removing CECs by NF and RO membranes (Drewes et al., 2005; Xue et al., 2010).

Table 4-9: Concentration of pharmaceuticals after treatment

Feed pressure (bar)	Effluent Concentration (µg/L)				
	IBU	CBZ	ASP	DCF	
5 bar	0,123 ± 0,0359	0,315 ± 0,133	0,0086 ± 0,00139	0,400 ± 0,207	
	0,444 ± 0,657	1,198 ± 0,403	N.D	0,817 ± 0,856	
	0,00597 ± 0,0302	0,283 ± 0,265	0,00336± 0,0217	0,762 ± 7,817	
10 bar	N.D	0,334 ± 0,335	0,00908±0,0306	0,269 ± 0,0140	
	0,0248 ± 0,0712	1,129 ± 0,357	N.D	0,419 ± 0,299	RO
	0,1197 ± 0,108	8,495 ± 6,499	0,00312±0,0075	0,534 ± 0,262	
15 bar	0,257 ± 0,391	0,145 ± 0,0154	N.D	0,298 ± 0,0959	
	0,0402 ± 0,0931	1,129 ± 1,413	0,000754 ± 0,0191	1,708 ± 2,202	
	0,1233 ± 0,0212	0,233 ± 0,088	0,00250± 0,0199	0,444 ± 0,0235	
15 bar	0,028±0,072	0,420 ± 0,381	N.D	0,617 ± 4,265	
	0,027 ± 0,039	0,808 ± 0,865	0,00414± 0,0231	0,369 ± 0,0672	
	0,227 ± 0,147	0,643 ± 0,0762	0,002441 ± 0,0109	0,472 ± 0,3222	
10 bar	1,574 ± 2,263	0,653 ± 0,374	N.D	2,675 ± 0,302	
	0,084 ± 0,154	0,554 ± 0,212	N.D	0,389 ± 0,259	NF
	0,258 ± 0,400	0,542 ± 1,447	N.D	0,546 ± 0,478	
5 bar	1,236± 1,783	0,261 ± 0,183	N.D	2,372 ± 0,303	
	0,145 ± 0,239	1,735 ± 2,084	N.D	2,361 ± 2,248	
	N.D	1,194 ± 1,503	N.D	0,297± 0,0808	

Concentration ± Standard deviation

Generally, the RO membrane showed greater removal efficiency than the NF membrane. The greater removal efficiency of the four contaminants of emerging concern in wastewater of the RO membrane could be attributable to the positively coupled effects from size exclusion, electrostatic repulsion (Donnan exclusion), and hydrophobic/supramolecular interactions (i.e., hydrogen bonding and pep stacking) to the RO membrane polymer, primarily comprising an aromatic polyamide (Heo et al., 2019).

The removal of CBZ and DCF is due to the direct filtration by the NF/RO membranes (Figures 4-14 and 4-15). This is due to steric hindrance and their adsorption onto the polymeric membrane matrix. Because the feed is continuously filtered through the membrane, the membrane sites will be saturated with hydrophobic MPs; adsorption can only assist with short-term removal. The charged and hydrophilic MPs do not adsorb to the polymeric membrane matrix and can be effectively removed by NF/RO membranes via steric hindrance and electrostatic interaction mechanisms. Steric hindrance occurs because the MW is larger than the RO's membrane pore size (MWCO). Therefore, rejection increased as the MW of the selected MPs increased, thus, explaining the weaker performance demonstrated by the NF membrane (Aziz & Ojumu, 2020; Wang et al., 2018b). .

Chapter 5

Conclusion and Recommendations

5 Conclusion and Recommendations

5.1 Conclusion

The reduction of COD, micropollutants and contaminants of emerging concerns in municipal secondary MBR wastewater by low pressure and extra-low energy PA TFC membranes for effluent discharge or possible recycle application was investigated. Extensive research was done on changing a RO system's physical parameters (feed pressure and concentration) and whether those changes efficiently enhance the elimination of COD, inorganics, and CECs.

Detailed selected quantitative analyses were investigated on membrane surface characteristics using Scanning Electron Microscopy (SEM), Attenuated Total Reflection-Fourier Transform Infrared Spectroscopy (ATR-FTIR), and Energy Dispersive X-Ray Spectroscopy (EDX), before and after RO experimental runs. During the ATR-FTIR analysis, all the characteristic peaks of virgin RO and NF PA TFC membranes can be seen in their clean state. The RO's membranes surface showed more -OH and -NH groups, whereas the NF membranes indicated the presence of the polysulphone interlayers. The weight percent of carbon and sulfur was higher on the surface of the NF membrane; however, the RO membrane had a higher oxygen weight percentage. The effects of feed concentration contributed to the increase in fouling, as seen in the SEM images. The NF membrane also fouled more than the RO, which could be attributed to its larger pore size.

The feed pressure adjustment between 5, 10 and 15 bars had a considerable effect on the rejection of inorganics and COD. As feed pressure increases, the salt passage reduces, and the salt rejection increases. The removal of nitrites for RO at 5 and 10 bars were 66.7% and 77.1%, respectively. Higher removal rates of nitrites were achieved for NF at 5,10, and 15 bar were 100, 93 and 93%, respectively. This could be attributed to their differences in zeta potential. The removal percentage of COD at the various operating conditions for both NF and RO membranes was >90.

RO and NF membrane processes exhibited exceptional removal rates (>95%) for all pharmaceuticals. The lowest concentration of micropollutants recorded was 0.00075µg/l for ASP with the RO membrane at a feed pressure of 15 bar and a feed concentration of 35.5 µg/l, achieving a 99.99% rejection. The RO membrane performed better overall compared to the NF; however, the recalcitrant behaviour of CBZ was shown at 10 bar, with RO having an initial concentration of 35.5µg/l. The negatively charged pharmaceuticals (i.e., DCF, IBU, ASP) were more effectively removed by the negatively charged NF and RO membrane than non-ionic pharmaceuticals (i.e., CBZ). Similar recalcitrant behaviour was demonstrated by DCF and more so with the NF membrane under 5 bar feed pressure. The initial concentration of pharmaceuticals had negligible effects on the removal efficiencies. The main mechanisms of removal were steric hindrance and MWCO.

Finally, COD, Inorganic, and selected pharmaceuticals (CBZ, DCF, IBU and ASP) removal using the RO bench-scale unit with RO and NF membranes at the predetermined process variables were successful for potential future reuse applications.

5.2   Recommendations

Future studies should investigate membrane characteristics such as zeta potential and direct measurement and analysis of the fouling layer formed during the effluent filtration to acquire characteristics of the layer composition using AFM and XPS to assist with remediation action. The effects of SARS-Cov-2 and how it may affect the removal or degradation of pharmaceuticals in the WWTP. Commercial and model municipal secondary MBR wastewater feed should be compared to assist in design solutions for possible scale-up to pilot plant level. Lastly, a cost and feasibility study for possible full-scale implementation.

References

6. References

Acero, J.L., Benitez, F.J., Real, F.J. & Teva, F. 2016. Micropollutants removal from retentates generated in ultrafiltration and nanofiltration treatments of municipal secondary effluents by means of coagulation, oxidation, and adsorption processes. *Chemical Engineering Journal*, 289: 48–58. http://dx.doi.org/10.1016/j.cej.2015.12.082.

Adewumi, J.R., Ilemobade, A.A. & Van Zyl, J.E. 2010. Treated wastewater reuse in South Africa: Overview, potential and challenges. *Resources, Conservation and Recycling*, 55(2): 221–231. http://dx.doi.org/10.1016/j.resconrec.2010.09.012.

Agilent. 7000C Triple Quadrupole GC/MS System. http://www.kprime.net/pdf/products/7000C_GCMS_Data_Sheet.pdf.

Ahmed, W., Angel, N., Edson, J., Bibby, K., Bivins, A., O'Brien, J.W., Choi, P.M., Kitajima, M., Simpson, S.L., Li, J., Tscharke, B., Verhagen, R., Smith, W.J.M., Zaugg, J., Dierens, L., Hugenholtz, P., Thomas, K. V. & Mueller, J.F. 2020. First confirmed detection of SARS-CoV-2 in untreated wastewater in Australia: A proof of concept for the wastewater surveillance of COVID-19 in the community. *Science of the Total Environment*, 728: 138764. https://doi.org/10.1016/j.scitotenv.2020.138764.

Al-rifai, J.H., Khabbaz, H. & Schäfer, A.I. 2011. Removal of pharmaceuticals and endocrine disrupting compounds in a water recycling process using reverse osmosis systems. *Separation and Purification Technology*, 77(1): 60–67. http://dx.doi.org/10.1016/j.seppur.2010.11.020.

Alsayed, A.F.M. & Ashraf, M.A. 2021. Modified nanofiltration membrane treatment of saline water. *Water Engineering Modeling and Mathematic Tools*: 25–44.

Alturki, A.A., Tadkaew, N., McDonald, J.A., Khan, S.J., Price, W.E. & Nghiem, L.D. 2010. Combining MBR and NF/RO membrane filtration for the removal of trace organics in indirect potable water reuse applications. *Journal of Membrane Science*, 365(1–2): 206–215. http://dx.doi.org/10.1016/j.memsci.2010.09.008.

Amin, P.D., Joshi, S. & Bhanushali, V. 2018. Advancements in Technologies for Water Treatment. *International Journal of ChemTech Research*, 11(9): 260–276.

De Amorim, K.P., Romualdo, L.L. & Andrade, L.S. 2013. Electrochemical degradation of sulfamethoxazole and trimethoprim at boron-doped diamond electrode: Performance, kinetics and reaction pathway. *Separation and Purification Technology*, 120: 319–327. http://dx.doi.org/10.1016/j.seppur.2013.10.010.

Ardoin, S.P. & Sundy, J.S. 2006. Update on nonsteriodal anti-inflammatory drugs. *Current*

Opinion in Rheumatology, 18(3): 221–226.

Asano, T., Mujeriego, R. & Dickson Parker, J. 1988. Evaluation of industrial cooling systems using reclaimed municipal wastewater. *Water Science and Technology*, 20(10): 163–174.

Awtry, E.H. & Loscalzo, J. 2000. Aspirin. *Circulation*, 101(10): 1206–1218. https://www.ahajournals.org/doi/abs/10.1161/01.CIR.101.10.1206 17 September 2021.

Aziz, M. & Kasongo, G. 2021. The removal of selected inorganics from municipal membrane bioreactor wastewater using UF/NF/RO membranes for water reuse application: A pilot-scale study. *Membranes*, 11(2): 1–14.

Aziz, M. & Ojumu, T. 2020. Exclusion of estrogenic and androgenic steroid hormones from municipal membrane bioreactor wastewater using UF/NF/RO membranes for water reuse application. *Membranes*, 10(3).

Baker, R.W. 2004. *Membrane Technology and Applications*. http://doi.wiley.com/10.1002/0470020393.

Bandini, S. & Vezzani, D. 2003. Nanofiltration modeling: The role of dielectric exclusion in membrane characterization. *Chemical Engineering Science*, 58(15): 3303–3326.

Beani, L., Bianchi, C., Caccia, S. & B. E. Dwyer. 1985. *Handbook of Experimental Pharmacology: Antiepileptic Drugs*.

Bellona, C., Drewes, J.E., Xu, P. & Amy, G. 2004. Factors affecting the rejection of organic solutes during NF/RO treatment - A literature review. *Water Research*, 38(12): 2795–2809.

Berk, Z. & Berk, Z. 2009. Chapter 10 – Membrane processes. *Food Process Engineering and Technology*: 233–257.

Bottoni, P., Caroli, S. & Caracciolo, A.B. 2010. Pharmaceuticals as priority water contaminants. *Toxicological and Environmental Chemistry*, 92(3): 549–565.

Bouissou-Schurtz, C., Houeto, P., Guerbet, M., Bachelot, M., Casellas, C., Mauclaire, A.C., Panetier, P., Delval, C. & Masset, D. 2014. Ecological risk assessment of the presence of pharmaceutical residues in a French national water survey. *Regulatory Toxicology and Pharmacology*, 69(3): 296–303. http://dx.doi.org/10.1016/j.yrtph.2014.04.006.

Cartagena, P., Kaddouri, M. El, Cases, V., Trapote, A. & Prats, D. 2013. Reduction of emerging micropollutants , organic matter , nutrients and salinity from real wastewater by combined MBR – NF / RO treatment. *Separation and Purification Technology*, 110: 132–143. http://dx.doi.org/10.1016/j.seppur.2013.03.024.

Chapman, S., Leslie, G., Law, I. & Solutions, I.B.L. 2004. Membrane Bioreactors (MBR) for Municipal Wastewater Treatment – An Australian Perspective. *Watertreatmentsinfo*: 1–11. http://www.watertreatments.info/wp-content/uploads/2007/05/mbr-australian-

prespective.pdf.

Chatham, J.C. & Blackband, S.J. 2001. Nuclear magnetic resonance spectroscopy and imaging in animal research. *ILAR Journal*, 42(3): 189–208.

Childress, A.E. & Elimelech, M. 1996. Effect of solution chemistry on the surface charge of polymeric reverse osmosis and nanofiltration membranes. *Journal of Membrane Science*, 119(2): 253–268.

Chon, K., KyongShon, H. & Cho, J. 2012. Membrane bioreactor and nanofiltration hybrid system for reclamation of municipal wastewater: Removal of nutrients, organic matter and micropollutants. *Bioresource Technology*, 122: 181–188. https://www.sciencedirect.com/science/article/pii/S0960852412006530 28 February 2019.

Chopra, S. & Kumar, D. 2020. Heliyon Ibuprofen as an emerging organic contaminant in environment , distribution and remediation. *Heliyon*, 6(February): e04087. https://doi.org/10.1016/j.heliyon.2020.e04087.

Cirja, M., Ivashechkin, P., Schäffer, A. & Corvini, P.F.X. 2008. Factors affecting the removal of organic micropollutants from wastewater in conventional treatment plants (CTP) and membrane bioreactors (MBR). *Reviews in Environmental Science and Biotechnology*, 7(1): 61–78.

Cleophas, T.J.M. 2011. *Beta-Blockers in Hypertension and Angina Pectoris*.

Comerton, A.M., Andrews, R.C., Bagley, D.M. & Yang, P. 2007. Membrane adsorption of endocrine disrupting compounds and pharmaceutically active compounds. *Journal of Membrane Science*, 303(1–2): 267–277.

Dams, R., Huestis, M.A., Lambert, W.E. & Murphy, C.M. 2003. Matrix effect in bio-analysis of illicit drugs with LC-MS/MS: Influence of ionization type, sample preparation, and biofluid. *Journal of the American Society for Mass Spectrometry*, 14(11): 1290–1294.

Dass, C. 2007. Hyphenated Separation Techniques. *Fundamentals of Contemporary Mass Spectrometry*: 151–194.

Day, R.O. & Graham, G.G. 2004. The vascular effects of COX-2 selective inhibitors. *Australian Prescriber*, 27(6): 142–145.

Dolar, D., Drašinac, N., Košutić, K., Škorić, I. & Ašperger, D. 2017. Adsorption of hydrophilic and hydrophobic pharmaceuticals on RO/NF membranes: Identification of interactions using FTIR. *Journal of Applied Polymer Science*, 134(5): 17–21.

Dolar, D., Gros, M., Rodriguez-Mozaz, S., Moreno, J., Comas, J., Rodriguez-Roda, I. & Barceló, D. 2012. Removal of emerging contaminants from municipal wastewater with an integrated membrane system, MBR-RO. *Journal of Hazardous Materials*, 239–240: 64–69.

http://dx.doi.org/10.1016/j.jhazmat.2012.03.029.

Dołowy, M. & Pyka, A. 2015. Lipophilicity study of salicylic and acetylsalicylic acids using both experimental and calculations methods. *Journal of Liquid Chromatography and Related Technologies*, 38(4): 485–491.

Drewes, J.E., Bellona, C., Oedekoven, M., Xu, P., Kim, T.U. & Amy, G. 2005. Rejection of wastewater-derived micropollutants in high-pressure membrane applications leading to indirect potable reuse. *Environmental Progress*, 24(4): 400–409.

E. M. Thurman, M.S.M. 1998. *Solid-Phase Extraction: Principles and Practice*. Wiley-Interscience.

Emongor, V.E., Khonga, E.B., Ramolemana, G.M., Marumo, K., Machacha, S. & Motsamai, T. 2005. Suitability of Treated Secondary Sewage Effluent for Irrigation of Horticultural Crops in Botswana. *Journal of Applied Sciences*, 5(3): 451–454.

Ensano, B.M.B., Borea, L., Naddeo, V., Belgiorno, V., de Luna, M.D.G. & Ballesteros, F.C. 2017. Removal of pharmaceuticals from wastewater by intermittent electrocoagulation. *Water (Switzerland)*, 9(2): 1–15.

Fatima Ayyash, Mustafa Khamis, Samer Khalaf, A.T. and R.K. 2015. Removal of Aspirin, Salicylic Acid, Paracetamol and p-Aminophenol by Advanced Membrane technology Activated Charcoal and Clay Micelles Complex. *International Journal of Case Studies*, 4(2015–05): 74–111. http://www.casestudiesjournal.com.

Feng, L.S., Liu, M.L., Zhang, S., Chai, Y., Wang, B., Zhang, Y. Bin, Lv, K., Guan, Y., Guo, H.Y. & Xiao, C.L. 2011. Synthesis and in vitro antimycobacterial activity of 8-OCH3 ciprofloxacin methylene and ethylene isatin derivatives. *European Journal of Medicinal Chemistry*, 46(1): 341–348.

Fernández, C., González-Doncel, M., Pro, J., Carbonell, G. & Tarazona, J. V. 2010. Occurrence of pharmaceutically active compounds in surface waters of the henares-jarama-tajo river system (madrid, spain) and a potential risk characterization. *Science of the Total Environment*, 408(3): 543–551. http://dx.doi.org/10.1016/j.scitotenv.2009.10.009.

Fujioka, T., Kodamatani, H., Yujue, W., Yu, K.D., Wanjaya, E.R., Yuan, H., Fang, M. & Snyder, S.A. 2020. Assessing the passage of small pesticides through reverse osmosis membranes. *Journal of Membrane Science*, 595: 117577. https://doi.org/10.1016/j.memsci.2019.117577.

Galinha, C.F., Sanches, S. & Crespo, J.G. 2018. *Membrane bioreactors*.

Gao, Q.Y., Chen, Y.X. & Fang, J.Y. 2020. 2019 Novel coronavirus infection and gastrointestinal tract. *Journal of Digestive Diseases*, 21(3): 125–126.

Gomez, M.J., Petrovi, M. & Fern, A.R. 2006. Determination of pharmaceuticals of various therapeutic classes by solid-phase extraction and liquid chromatography – tandem mass

spectrometry analysis in hospital effluent wastewaters &., 1114: 224–233.

Gruchlik, Y., Linge, K. & Joll, C. 2018. Removal of organic micropollutants in waste stabilisation ponds : A review. *Journal of Environmental Management*, 206: 202–214. https://doi.org/10.1016/j.jenvman.2017.10.020.

Grzesiak, A.L., Lang, M., Kim, K. & Matzger, A.J. 2003. Comparison of the Four Anhydrous Polymorphs of Carbamazepine and the Crystal Structure of Form I. *Journal of Pharmaceutical Sciences*, 92(11): 2260–2271.

Gualerzi, C.O. & Brandi, L. 2014. *Targets, Mechanisms and Resistance*.

Halford, G.M., Lordkipanidzé, M. & Watson, S.P. 2012. 50th anniversary of the discovery of ibuprofen: An interview with Dr Stewart Adams. *Platelets*, 23(6): 415–422.

Hamingerova, M., Borunsky, L. & Beckmann, M. 2015. Membrane Technologies for Water and Wastewater Treatment on the European and Indian Market. *Techview membrane*.

Hansen, E., Rodrigues, M.A.S. & Aquim, P.M. de. 2016. Wastewater reuse in a cascade based system of a petrochemical industry for the replacement of losses in cooling towers. *Journal of environmental management*, 181: 157–162. https://pubmed.ncbi.nlm.nih.gov/27343433/ 2 June 2022.

Heo, J., Kim, S., Her, N., Park, C.M., Yu, M. & Yoon, Y. 2019. Removal of contaminants of emerging concern by FO, RO, and UF membranes in water and wastewater. *Contaminants of Emerging Concern in Water and Wastewater: Advanced Treatment Processes*: 139–176.

Hoinkis, J., Deowan, S.A., Panten, V., Figoli, A., Huang, R.R. & Drioli, E. 2012. Membrane bioreactor (MBR) technology - A promising approach for industrial water reuse. *Procedia Engineering*, 33(2009): 234–241.

Holshue, M.L., DeBolt, C., Lindquist, S., Lofy, K.H., Wiesman, J., Bruce, H., Spitters, C., Ericson, K., Wilkerson, S., Tural, A., Diaz, G., Cohn, A., Fox, L.A., Patel, A., Gerber, S.I., Kim, L., Tong, S., Lu, X., Lindstrom, S., Pallansch, M.A., Weldon, W.C., Biggs, H.M., Uyeki, T.M. & Pillai, S.K. 2020. First case of 2019 novel coronavirus in the United States. *New England Journal of Medicine*, 382(10): 929–936.

Hu, D. & Wang, L. 2016. Adsorption of amoxicillin onto quaternized cellulose from flax noil: Kinetic, equilibrium and thermodynamic study. *Journal of the Taiwan Institute of Chemical Engineers*, 64: 227–234. http://dx.doi.org/10.1016/j.jtice.2016.04.028.

Jacob, C., Kirsch, G., Slusarenko, A., Winyard, P.G. & Burkholz, T. 2014. *Recent advances in redox active plant and microbial products: From basic chemistry to widespread applications in medicine and agriculture*.

Judd, S. & Judd, C. 2008. *The MBR book: Principles and Applications of Membrane Bioreactors*

in Water and Wastewater Treatment.
http://medcontent.metapress.com/index/A65RM03P4874243N.pdf.

Juliano, L.M. & Griffiths, R.R. 2004. A critical review of caffeine withdrawal: Empirical validation of symptoms and signs, incidence, severity, and associated features. *Psychopharmacology*, 176(1): 1–29.

Kanama, K.M., Daso, A.P., Mpenyana-Monyatsi, L. & Coetzee, M.A.A. 2018. Assessment of Pharmaceuticals, Personal Care Products, and Hormones in Wastewater Treatment Plants Receiving Inflows from Health Facilities in North West Province, South Africa. *Journal of Toxicology*, 2018(Table 1): 1–15.

Kaplan, A., Mamane, H., Lester, Y. & Avisar, D. 2020. Trace organic compound removal from wastewater reverse-osmosis concentrate by advanced oxidation processes with UV/O3/H2O2. *Materials*, 13(12): 1–13.

Kim, M., Guerra, P., Shah, A., Parsa, M., Alaee, M. & Smyth, S.A. 2014. Removal of pharmaceuticals and personal care products in a membrane bioreactor wastewater treatment plant. : 2221–2229.

Kimura, K., Toshima, S., Amy, G. & Watanabe, Y. 2004. Rejection of neutral endocrine disrupting compounds (EDCs) and pharmaceutical active compounds (PhACs) by RO membranes. *Journal of Membrane Science*, 245(1–2): 71–78.

Klaminder, J., Brodin, T., Piovano, S., Jonsson, M., Fick, J. & Heynen, M. 2014. Ecological effects of pharmaceuticals in aquatic systems--impacts through behavioural alterations. *Philosophical Transactions of the Royal Society B: Biological Sciences*, 369(1656): 20130580–20130580.

Komesli, O.T., Muz, M., Ak, M.S., Bakirdere, S. & Gokcay, C.F. 2015. Occurrence, fate and removal of endocrine disrupting compounds (EDCs) in Turkish wastewater treatment plants. *Chemical Engineering Journal*, 277: 202–208.

Korzybski, T., Kowszky-Gindifer, S. & Kurylowicz, W. 1967. Origin, Nature and Properties.

Kucera, J. 2015. *Reverse Osmosis*.

Ladewig, B. & Al-Shaeli, M.N.Z. 2017. *Fundamentals of Membrane Bioreactors*. http://link.springer.com/10.1007/978-981-10-2014-8.

Lenntech. 2017. Membrane cleaning technologies. http://www.lenntech.com/membrane-cleaning.htm 7 September 2017.

Li, C., Yang, Y., Liu, Y. & Hou, L. 2018. Removal of PhACs and their impacts on membrane fouling in NF / RO membrane fi ltration of various matrices. *Journal of Membrane Science*, 548(November 2017): 439–448. https://doi.org/10.1016/j.memsci.2017.11.032.

Lin, Y. 2017. E ff ects of organic , biological and colloidal fouling on the removal of pharmaceuticals and personal care products by nano fi ltration and reverse osmosis membranes. *Journal of Membrane Science*, 542(August): 342–351. http://dx.doi.org/10.1016/j.memsci.2017.08.023.

Lobo, S., Li, H., Farhan, N. & Yan, G. 2014. Evaluation of Diclofenac Prodrugs for Enhancing Transdermal Delivery. *Drug development and industrial pharmacy*, 40(3): 425. /pmc/articles/PMC4772728/ 19 May 2022.

Lodder, W. & de Roda Husman, A.M. 2020. SARS-CoV-2 in wastewater: potential health risk, but also data source. *The Lancet Gastroenterology and Hepatology*, 5(6): 533–534. http://dx.doi.org/10.1016/S2468-1253(20)30087-X.

Luo, Y., Guo, W., Ngo, H.H., Nghiem, L.D., Hai, F.I., Zhang, J., Liang, S. & Wang, X.C. 2014. A review on the occurrence of micropollutants in the aquatic environment and their fate and removal during wastewater treatment. *Science of the Total Environment*, 473–474: 619–641. http://dx.doi.org/10.1016/j.scitotenv.2013.12.065.

Masters, P.A., Bryan, T.A., Zurlo, J., Miller, D. & Joshi, N. 2003. Trimethoprim-Sulfamethoxazole Revisited. *Trimethoprim-Sulfamethoxazole Revisited Philip*, 163: 402–410.

Medema, G., Heijnen, L., Elsinga, G., Italiaander, R. & Medema, G. 2020. Presence of SARS-Coronavirus-2 in sewage . Methods Sewage samples. *medRxiv*.

Melvin, S.D. & Leusch, F.D.L. 2016. Removal of trace organic contaminants from domestic wastewater: A meta-analysis comparison of sewage treatment technologies. *Environment International*, 92–93: 183–188. http://dx.doi.org/10.1016/j.envint.2016.03.031.

Mondal, S. & Wickramasinghe, S.R. 2008. Produced water treatment by nanofiltration and reverse osmosis membranes. *Journal of Membrane Science*, 322(1): 162–170.

Morris, B.G. 2020. The removal of anionic surfactant from commercial laundry wastewater with reverse osmosis membrane by. , (January).

Mottram, D.R. 2018. Beta blockers. *Drugs in Sport, Seventh Edition*: 307–315.

Mulder, M. 1998. Basic Principles of Membrane Technology. *Zeitschrift für Physikalische Chemie*, 72(3): 564. http://linkinghub.elsevier.com/retrieve/pii/037673889285058Q%5Cnhttp://scholar.google.com/scholar?hl=en&btnG=Search&q=intitle:basic+principles+of+membrane+technology#1%5Cnhttp://scholar.google.com/scholar?hl=en&btnG=Search&q=intitle:Basic+principles+of+me.

Murray, K.E., Thomas, S.M. & Bodour, A.A. 2010. Prioritizing research for trace pollutants and emerging contaminants in the freshwater environment. *Environmental Pollution*, 158(12):

3462–3471. http://dx.doi.org/10.1016/j.envpol.2010.08.009.

Nataraj, S.K., Hosamani, K.M. & Ã, T.M.A. 2006. Distillery wastewater treatment by the membrane-based nanofiltration and reverse osmosis processes $. , 40(92): 2349–2356.

Nghiem, L.D. & Hawkes, S. 2007. Effects of membrane fouling on the nanofiltration of pharmaceutically active compounds (PhACs): Mechanisms and role of membrane pore size. *Separation and Purification Technology*, 57(1): 176–184.

Nidal Hilal , Mohamed Khayet, and C.J.. W. 2012. *Membrane Modification: Technology and Applications.*
10.1201/b12160%5Cnhttp://www.crcnetbase.com/doi/book/10.1201/b12160%5Cn10.1201/b12160%0Ahttp://www.crcnetbase.com/doi/book/10.1201/b12160.

Obeidat, Y. 2021. The Most Common Methods for Breath Acetone Concentration Detection: A Review. *IEEE Sensors Journal*, 21(13): 14540–14558.

Oron, G., Gillerman, L., Bick, A., Manor, Y., Buriakovsky, N. & Hagin, J. 2008. Membrane technology for sustainable treated wastewater reuse: Agricultural, environmental and hydrological considerations. *Water Science and Technology*, 57(9): 1383–1388.

Ozaki, H., Sharma, K. & Saktaywin, W. 2002. Performance of an ultra-low-pressure reverse osmosis membrane (ULPROM) for separating heavy metal: Effects of interference parameters. *Desalination*, 144(1–3): 287–294.

Pagès, N., Reig, M., Gibert, O. & Cortina, J.L. 2017. Trace ions rejection tunning in NF by selecting solution composition: Ion permeances estimation. *Chemical Engineering Journal*, 308: 126–134.

Phadunghus, K., Wongrueng, A., Rakruam, P., Wattanachira, S. & Punyapalakul, P. 2017. Efficiencies of NF and RO membranes on pharmaceutical removal and membrane fouling effects. *Engineering Journal*, 21(3): 101–112.

Pomati, F., Castiglioni, S., Zuccato, E., Fanelli, R., Vigetti, D., Rossetti, C. & Calamari, D. 2006. Effects of a complex mixture of therapeutic drugs at environmental levels on human embryonic cells. *Environmental Science and Technology*, 40(7): 2442–2447.

Racar, M., Dolar, D., Karadakić, K., Čavarović, N., Glumac, N., Ašperger, D. & Košutić, K. 2020. Challenges of municipal wastewater reclamation for irrigation by MBR and NF/RO: Physico-chemical and microbiological parameters, and emerging contaminants. *Science of The Total Environment*: 137959. https://linkinghub.elsevier.com/retrieve/pii/S0048969720314728.

Race, M., Ferraro, A., Galdiero, E., Guida, M., Núñez-Delgado, A., Pirozzi, F., Siciliano, A. & Fabbricino, M. 2020. Current emerging SARS-CoV-2 pandemic: Potential direct/indirect negative impacts of virus persistence and related therapeutic drugs on the aquatic

compartments. *Environmental Research*, 188: 109808.

Radjenovic, J., Petrovic, M. & Barceló, D. 2007. Analysis of pharmaceuticals in wastewater and removal using a membrane bioreactor. *Analytical and Bioanalytical Chemistry*, 387(4): 1365–1377.

Radjenović, J., Petrović, M. & Barceló, D. 2009. Fate and distribution of pharmaceuticals in wastewater and sewage sludge of the conventional activated sludge (CAS) and advanced membrane bioreactor (MBR) treatment. *Water Research*.

Ramalho, R.S. 2013. *Introduction to Wastewater Treatment Processes*.

Rana, H.H., Saha, N.K., Jewrajka, S.K. & Reddy, A.V.R. 2015. Low fouling and improved chlorine resistant thin film composite reverse osmosis membranes by cerium(IV)/polyvinyl alcohol mediated surface modification. *Desalination*, 357: 93–103. http://dx.doi.org/10.1016/j.desal.2014.11.013.

Randazzo, W., Truchado, P., Cuevas-Ferrando, E., Simón, P., Allende, A. & Sánchez, G. 2020. SARS-CoV-2 RNA in wastewater anticipated COVID-19 occurrence in a low prevalence area. *Water Research*, 181.

Reddersen, K., Heberer, T. & Dünnbier, U. 2002. Identification and significance of phenazone drugs and their metabolites in ground- and drinking water. *Chemosphere*, 49(6): 539–544.

Rogawski, M.A. & Löscher, W. 2004. The neurobiology of antiepileptic drugs. *Nature Reviews Neuroscience*, 5(7): 553–564.

Ruiz-ordaz, N. & Gal, J. 2018. Study of the ibuprofen impact on wastewater treatment mini-plants with bioaugmented sludge. *Process Safety and Environmental Protection*. https://doi.org/10.1016/j.psep.2018.08.006.

Russell, P., Batchelor, D., Facility, A.I. & Russell, P.E. 2001. SEM and AFM : Complementary Techniques for Surface Investigations. *Microscopy and Analysis*, (January): 9–12.

Schäfer, A.I., Akanyeti, I. & Semião, A.J.C. 2011. Micropollutant sorption to membrane polymers: A review of mechanisms for estrogens. *Advances in Colloid and Interface Science*, 164(1–2): 100–117. http://dx.doi.org/10.1016/j.cis.2010.09.006.

Scheytt, T., Mersmann, P., Lindstädt, R. & Heberer, T. 2005. 1-Octanol/Water Partition Coefficients of 5 Pharmaceuticals from Human Medical Care: Carbamazepine, Clofibric Acid, Diclofenac, Ibuprofen, and Propyphenazone. *Water, Air, and Soil Pollution 2005 165:1*, 165(1): 3–11. https://link.springer.com/article/10.1007/s11270-005-3539-9 19 May 2022.

Schmitt, J. & Flemming, H. 1996. Microbially Influenced Corrosion of Materials. *Microbially Influenced Corrosion of Materials*, (January).

Scott, K. 1996. *Handbook of industrial membranes.* 1st Editio. Elsevier Advanced Technology.

Shad, M.F., Juby, G.J.G., Delagah, S. & Sharbatmaleki, M. 2019. Evaluating occurrence of contaminants of emerging concerns in MF/RO treatment of primary effluent for water reuse – Pilot study.

Shin, M.G., Choi, W., Park, S.J., Jeon, S., Hong, S. & Lee, J.H. 2022. Critical review and comprehensive analysis of trace organic compound (TOrC) removal with polyamide RO/NF membranes: Mechanisms and materials. *Chemical Engineering Journal*, 427(March 2021).

Shraim, A., Diab, A., Alsuhaimi, A., Niazy, E., Metwally, M., Amad, M., Sioud, S. & Dawoud, A. 2017. Analysis of some pharmaceuticals in municipal wastewater of Almadinah Almunawarah. *Arabian Journal of Chemistry*, 10: S719–S729.

Sigma-Aldrich. 2003. Sigma brand products are sold through Sigma-Aldrich, Inc. Sigma-Aldrich, Inc. warrants that its products conform to the information contained in this and other Sigma-Aldrich publications. Purchaser must determine the suitability of the product(s) for thei. : 7507.

Silverstein, R.M. & Webster, F.X. 1996. Spectrometric Identification Of Organic Compounds 6th Edition. *John Wiley & Sons Ltd*, 6: 1–482.

Sim, W.J., Lee, J.W., Shin, S.K., Song, K.B. & Oh, J.E. 2011. Assessment of fates of estrogens in wastewater and sludge from various types of wastewater treatment plants. *Chemosphere*, 82(10): 1448–1453. http://dx.doi.org/10.1016/j.chemosphere.2010.11.045.

Sipma, J., Osuna, B., Collado, N., Monclús, H., Ferrero, G., Comas, J. & Rodriguez-Roda, I. 2010. Comparison of removal of pharmaceuticals in MBR and activated sludge systems. *Desalination*, 250(2): 653–659. http://dx.doi.org/10.1016/j.desal.2009.06.073.

Von sperling, M. 2007. *Activated sludge and aerobic biofilm reactors*. IWA Publishing, Alliance House, 12 Caxton Street, London SW1H 0QS, UK.

SSS. 2018. Limit of Sulfamethoxazole in wastewater 0. : 0–10.

Sumisha, A., Arthanareeswaran, G., Lukka Thuyavan, Y., Ismail, A.. & Chakraborty, S. 2015. Treatment of laundry wastewater using polyethersulfone/polyvinylpyrollidone ultrafiltration membranes. *Ecotoxicology and Environmental Safety*, 121: 174–179. http://linkinghub.elsevier.com/retrieve/pii/S0147651315001529 7 June 2018.

Susan, J., Monique, N., Charles R, T., Goeff, B. & John P, S. 1998. Widespread Sexual Disruption in. *Environmental Science & Technology*, 32(17): 2498–2506.

Taha, A.H., Joshi, H., Garg, M.C. & Manhee, H.K. 2021. Case Study of Evaluation RO Desalination Systems for Potable Water in Safwan, Iraq. *Journal of Geoscience and Environment Protection*, 09(02): 158–181.

Tang, C.Y., Kwon, Y.N. & Leckie, J.O. 2007. Probing the nano- and micro-scales of reverse

osmosis membranes-A comprehensive characterization of physiochemical properties of uncoated and coated membranes by XPS, TEM, ATR-FTIR, and streaming potential measurements. *Journal of Membrane Science*, 287(1): 146–156.

Terrill, R. 2009. An introduction to HPLC. *San Jose State University*, 44(0): 26.

Thomas, K. V., Dye, C., Schlabach, M. & Langford, K.H. 2007. Source to sink tracking of selected human pharmaceuticals from two Oslo city hospitals and a wastewater treatment works. *Journal of Environmental Monitoring*, 9(12): 1410–1418.

Togola, A. & Budzinski, H. 2007. Analytical development for analysis of pharmaceuticals in water samples by SPE and GC-MS. *Analytical and Bioanalytical Chemistry*, 388(3): 627–635.

Triebskorn, R., Casper, H., Heyd, A., Eikemper, R., Köhler, H. & Schwaiger, J. 2004. Toxic effects of the non-steroidal anti-inflammatory drug diclofenac Part II . Cytological effects in liver , kidney , gills and intestine of rainbow trout (Oncorhynchus mykiss). , 68: 151–166.

Ulubay, M., Yurt, K.K., Kaplan, A.A. & Atilla, M.K. 2018. The use of diclofenac sodium in urological practice: A structural and neurochemical based review. *Journal of Chemical Neuroanatomy*, 87: 32–36.

UN, W. Water Facts | UN-Water. http://www.unwater.org/water-facts/ 1 June 2018.

Urtiaga, A.M., Pérez, G., Ibáñez, R. & Ortiz, I. 2013. Removal of pharmaceuticals from a WWTP secondary effluent by ultrafiltration/reverse osmosis followed by electrochemical oxidation of the RO concentrate. *Desalination*, 331: 26–34. http://dx.doi.org/10.1016/j.desal.2013.10.010.

USEPA. 2000. Wastewater Technology Fact Sheet Dechlorination. *Environmental Protection Agency*: 1–7.

Üstün, G.E., Solmaz, S.K.A., Çiner, F. & Bažkaya, H.S. 2011. Tertiary treatment of a secondary effluent by the coupling of coagulation-flocculation-disinfection for irrigation reuse. *Desalination*, 277(1–3): 207–212.

Verlicchi, P., Al Aukidy, M., Galletti, A., Petrovic, M. & Barceló, D. 2012. Hospital effluent: Investigation of the concentrations and distribution of pharmaceuticals and environmental risk assessment. *Science of the Total Environment*, 430: 109–118. http://dx.doi.org/10.1016/j.scitotenv.2012.04.055.

Vezzani, D. & Bandini, S. 2002. Donnan equilibrium and dielectric exclusion for characterization of nanofiltration membranes. *Desalination*, 149(1–3): 477–483.

Wang, L.K., Chen, J.P., Hung, Y.-T. & Shammas, N.K. 2011. *Membrane and Desalination Technologies.* http://link.springer.com/10.1007/978-1-59745-278-6.

Wang, X.W., Li, J.S., Jin, M., Zhen, B., Kong, Q.X., Song, N., Xiao, W.J., Yin, J., Wei, W., Wang,

G.J., Si, B.Y., Guo, B.Z., Liu, C., Ou, G.R., Wang, M.N., Fang, T.Y., Chao, F.H. & Li, J.W. 2005. Study on the resistance of severe acute respiratory syndrome-associated coronavirus. *Journal of Virological Methods*, 126(1–2): 171–177.

Wang, Y., Wang, X., Li, M., Dong, J., Sun, C. & Chen, G. 2017. Removal of Pharmaceutical and Personal Care Products (PPCPs) from Municipal Waste Water with Integrated Membrane Systems , MBR-RO / NF.

Wang, Y., Wang, X., Li, M., Dong, J., Sun, C. & Chen, G. 2018a. Removal of pharmaceutical and personal care products (PPCPs) from municipalwaste water with integrated membrane systems, MBR-RO/NF. *International Journal of Environmental Research and Public Health*, 15(2).

Wang, Y., Wang, X., Li, M., Dong, J., Sun, C. & Chen, G. 2018b. Removal of pharmaceutical and personal care products (PPCPs) from municipalwaste water with integrated membrane systems, MBR-RO/NF. *International Journal of Environmental Research and Public Health*, 15(2).

Wellings, A.D. 2006. *A practical handbook of preparative HPLC*. Kidlington: Elsevier.

Xu, P. & Drewes, J.E. 2006. Viability of nanofiltration and ultra-low pressure reverse osmosis membranes for multi-beneficial use of methane produced water. *Separation and Purification Technology*, 52(1): 67–76.

Xu, P., Drewes, J.E., Kim, T.U., Bellona, C. & Amy, G. 2006. Effect of membrane fouling on transport of organic contaminants in NF/RO membrane applications. *Journal of Membrane Science*, 279(1–2): 165–175.

Xu, Z., Huang, X. & Wan, L. 2009. *Surface Engineering of\rPolymer Membranes*.

Xue, W., Wu, C., Xiao, K., Huang, X., Zhou, H., Tsuno, H. & Tanaka, H. 2010. Elimination and fate of selected micro-organic pollutants in a full-scale anaerobic/anoxic/aerobic process combined with membrane bioreactor for municipal wastewater reclamation. *Water Research*.

Ynoussa, M., Sperling, M. Von & Mihelcic, J. 2017. Part Four. Management of Risk From Excreta and Wastewater. *Constructed Wetlands*, (September): 1–20.

Zhao, C., Xue, J., Ran, F. & Sun, S. 2013. Modification of polyethersulfone membranes - A review of methods. *Progress in Materials Science*, 58(1): 76–150. http://dx.doi.org/10.1016/j.pmatsci.2012.07.002.

Zhao, Y., Taylor, J. & Hong, S. 2005. Combined influence of membrane surface properties and feed water qualities on RO/NF mass transfer, a pilot study. *Water Research*, 39(7): 1233–1244.

Zhao, Y. ying, Kong, F. xin, Wang, Z., Yang, H. wei, Wang, X. mao, Xie, Y.F. & Waite, T.D. 2017.

Role of membrane and compound properties in affecting the rejection of pharmaceuticals by different RO/NF membranes. *Frontiers of Environmental Science and Engineering*, 11(6): 1–13.

Zhou, X.F., Dai, C.M., Zhang, Y.L., Surampalli, R.Y. & Zhang, T.C. 2011. A preliminary study on the occurrence and behavior of carbamazepine (CBZ) in aquatic environment of Yangtze River Delta, China. *Environmental Monitoring and Assessment*, 173(1–4): 45–53.

Appendices

Appendix A

Data from batch experiments

RO experimental runs at 10 bar and 22, 35.5 and 44µg/l

A. Appendix A

Kinetic data for RO at 10 Bar and 22, 35.5 and 44 µg/l, measuring the operating conditions in the feed, brine and permeate.

Table A-1: Membrane specifications

Membrane Specifications	
Dimensions	14.5 cm x 9.5 cm
Area (m^2)	0,013775
Nomination	XLE4040

Table A-2: Experimental conditions

Initial permeate flux (L/m^2 hr): 80,14	80.145
Feed P_0 (bar): 10	10
Piston P (bar): 13	13
Feed velocity (Hz): 12,05	12.38
Brine p (Kpa): 95	95
Initial Concentration: 44µg/l	44µg/l

Table A-3: Kinetic data for RO 10 bar and 44 µg/l

	Feed			Brine		Permeate							
Time (min)	EC F (µS)	TDS F (mg/L)	Temperature (deg Cel)	EC (µS)	TDS (mg/L)	EC P (µS)	TDS P(mg/L)	Temperature ©	Time (hr)	Volume (L)	Flow Rate (l/h)	Flux (L/h m²)	% Rejection
0	325	152,8	17,1	305	138,2	22,5	18,2	17,2	0,004167	0,0046	1,104	80,15	93,1
45	303	151	17,2	280,3	139,8	5,12	3,5	17,2	0,004167	0,0046	1,104	80,15	98,3
90	318	157	17,3	312	156	8,5	4,25	17,7	0,004167	0,0046	1,104	80,15	97,3
135	317	158	17,5	290	145	3,81	1,91	17,6	0,004167	0,0046	1,104	80,15	98,8
180	310	154	17,8	293,4	148,5	6,67	3,6	17,9	0,004167	0,0045	1,08	78,40	97,8
225	329	162	18,1	310	153	6,51	3,24	17,9	0,004167	0,0045	1,08	78,40	98,0
270	320	162	18,3	304	152	7,07	3,53	18	0,004167	0,0045	1,08	78,40	97,8
315	321	161	17,9	318	159	13,7	6,39	18,5	0,004167	0,0044	1,056	76,45	95,7
360	325	160	17,9	318	153	24,7	12,91	18,5	0,004167	0,0044	1,056	76,45	92,4
405	345	172	18,1	325	162	15,61	8,41	17,9	0,004167	0,0046	1,104	80,15	95,5
450	347	171	18,2	328	164	18,2	11,3	17,9	0,004167	0,0046	1,104	80,15	94,8
495	352	176	18,3	331	166	47,6	23,8	18,2	0,004167	0,0044	1,056	76,45	86,5

540	351	175	18,5	321	162	46,2	33,1	18,9	0,00 4167	0,004 4	1,056	76,45	86,8
585	347	179	17,9	329	164	59,5	30,3	19,1	0,00 4167	0,004 4	1,056	76,45	82,9
630	343	172	19,2	342	173	53,6	34,9	19	0,00 4167	0,004 3	1,032	74,92	84,4
675	345	173	19,1	342	174	67,9	35,2	19,1	0,00 4167	0,004 2	1,008	73,18	80,3
720	347	170	19,2			63,2	32,1	19,1	0,00 4167	0,004	0,95992 3206	69,69	81,8

Table A-4: Duplication of RO at 10 bar and 44 µg/l

Time (min)	Feed			Brine		Permeate							
	EC F (µS)	TDS (mg/L)	Temperature (deg Cel)	EC (µS)	TDS (mg/L)	EC P (µS)	TDS P(mg/L)	Temperature ©	Time (hr)	Volume (L)	Flow Rate (l/h)	Flux (L/h m²)	% Rejection
	327,8	238,2	17,1	317,7	239	3,2	2,5	17,1	0,004167	0,0048	1,152	83,63	99,02
0	315,2	238,2	17,3	320,6	237	6	4,5	17,8	0,004167	0,0048	1,152	83,63	98,10
45	22,3	243,4	19,1	342,5	249,1	8,1	6,1	18,1	0,004167	0,0048	1,152	83,63	97,55
90	343,5	248,9	19,6	362,5	262,8	4,1	3,2	18,4	0,004167	0,0046	1,104	80,15	98,81
135	352,9	256,2	20,5	350,5	250,7	4	3,1	18,6	0,004167	0,0046	1,104	80,15	98,87
180	362	258	20,9	i	255	6,8	5,2	18,6	0,004167	0,0046	1,104	80,15	98,12
225	366,7	256,9	21,2	370,2	260,3	6,3	4,7	18,9	0,004167	0,0046	1,104	80,15	98,28
270	373,2	279	21,5	372,5	278	6,6	4,8	19,1	0,004167	0,0044	1,056	76,45	98,23
315	386	266,6	21,9	395,5	279,2	6	4,4	19,3	0,004167	0,0046	1,104	80,15	98,45
360	392,1	271,1	22	384,6	266,4	11,6	8,5	19,4	0,004167	0,0046	1,104	80,15	97,04
405	394,4	274,3	21,9	393	270,4	7,2	5,3	19,8	0,004167	0,0044	1,056	76,45	98,17
450	398,1	272,5	22,4	401,9	278,3	6,5	4,8	19,6	0,0046	0,0044	1,056	76,45	98,37

| 495 | 416,1 | 284 | 22,7 | 414,8 | 281,4 | 6,4 | 4,6 | 19,7 | 0,0041 67 | 0,0044 | 0,9565 21739 | 69,44 | 98,46 |
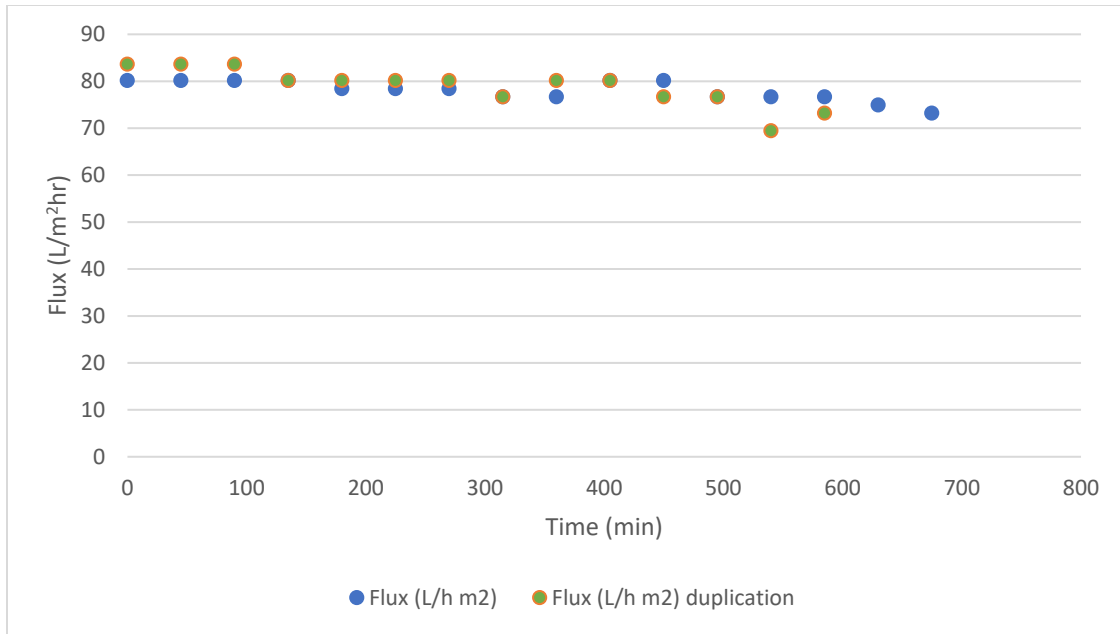
Figure A-1: Permeate flux decline of experimental run and duplication for RO at 10 bar and 44 μg/l.

Table A-5: Experimental conditions

Run	Duplication
Initial permeate flux (L/m² hr): 73.17	Initial permeate flux (L/m² hr): 69.69
Feed P_0 (bar): 10	Feed P_0 (bar): 10
Piston P (bar): 13	Piston P (bar): 13
Feed velocity (Hz): 12,05	Feed velocity (Hz): 12,05
Brine p (Kpa): 95	Brine p (Kpa): 95
Initial Concentration: 22μg/l	Initial Concentration: 22μg/l
Feed pH: 7,32	Feed pH: 7,48

Table A-6: Experimental run of RO at 22ug/l at 10 bar

	Feed			Brine		Permeate								
Time (min)	EC F (µS)	TDS F (mg/L)	Temperature (° C)	EC (µS)	TDS (mg/L)	EC P (µS)	TDS P (mg/L)	Temperature (°C)	Time (s)	Time (hr)	Volume (L)	Flow Rate (l/h)	Flux (L/h m²)	% rejection
0	321,1	232,1	19,5	326,3	236,5	5,1	3,8	18,5	15	0,00416667	0,0042	1,008	73,18	98,41
45	323,4	232,8	19,8	327,7	235,3	2,4	1,8	18,5	15	0,00416667	0,0046	1,104	80,15	99,26
90	340,8	242,5	20,9	345,5	244,2	4,5	3,9	18,5	15	0,00416667	0,0046	1,104	80,15	98,68
135	347,6	243,7	21,1	347,1	248,3	5,8	4,2	19,1	15	0,00416667	0,0046	1,104	80,15	98,33
180	349,9	243,4	21,4	345,4	240,1	11,5	8,3	19,3	15	0,00416667	0,0046	1,104	80,15	96,71
225	375,1	256,9	22,3	375,5	258,6	21,2	16,4	19,9	15	0,00416667	0,0048	1,152	83,63	94,35
270	378,5	259	22,4	379,5	260,3	12,7	9,2	20	15	0,00416667	0,0046	1,104	80,15	96,64
315	385,6	261,5	22,8	422,3	276,5	13,4	9,6	20,1	15	0,00416667	0,0046	1,104	80,15	96,52
360	382,4	262,9	22,9	385,2	260,9	12,2	8,8	20,1	15	0,00416667	0,0048	1,152	83,63	96,81
405	387,5	261,8	23,1	399	268	10,6	7,6	20,6	15	0,00416667	0,0044	1,056	76,66	97,26
450	389,9	270,5	23,8	422,5	277,8	24,2	16,9	21,4	15	0,00416667	0,0044	1,056	76,66	93,79

495	403,1	270,5	23,4	387,1	264,3	8,9	6,5	19,9	15	0,00416666 67	0,0042	1,008	73,18	97,79
540	400,8	272,7	22,8	408,2	276,4	7,4	5,2	19,7	15	0,00416666 67	0,0042	1,008	73,18	98,15
585	404,1	274,5	22,7	402,7	275,6	9,6	6,8	19,2	15	0,00416666 67	0,0042	1,008	73,18	97,62
630	403,5	274,4	22,7	407,9	278,5	8,2	5,9	19,4	15	0,00416666 67	0,004	0,96	69,69	97,97
675	406,4	275,1	22,8	414,6	279,5	8,9	6,5	19,2	15	0,00416666 67	0,004	0,96	69,69	97,81
720	419	281,1	23,4	410,4	276,3	9,6	6,9	19,3	15	0,00416666 67	0,004	0,96	69,69	97,71

Table A-7: Experimental run duplication of RO at 22ug/l at 10 bar

	Feed			Brine		Permeate							
Time (min)	EC F (µS)	TDS (mg/L)	Temperature (°C)	EC (µS)	TDS (mg/L)	EC P (µS)	TDS P (mg/L)	Temperature ©	Time (hr)	Volume (L)	Flow Rate (l/h)	Flux (L/h m²)	% rejection
0	323,5	228,9	19,5	308,8	221,6	8,6	6,5	18,8	0,00416667	0,0046	1,104	80,15	97,34
0	318,6	227,1	20,1	328,3	232,6	6,1	4,4	18,9	0,00416667	0,0048	1,152	83,63	98,09
45	326,4	230,6	21,1	325,4	228,8	12,2	9,1	19	0,00416667	0,0048	1,152	83,63	96,26
90	332,4	234,8	20,9	361,8	252,5	20,1	15	18,3	0,00416667	0,0046	1,104	80,15	93,94
135	329,8	234	20,3	337,3	238,6	22,6	17,3	18,3	0,00416667	0,0044	1,056	76,45	93,15
180	339,9	239,7	20,9	324,8	230,7	22,4	16,8	18,2	0,00416667	0,0042	1,008	73,18	93,41
225	343,6	242	21	346,2	243,2	11,6	8,7	18,4	0,00416667	0,0044	1,056	76,45	96,62
270	345,1	243,2	21,1	355,2	248,6	23,9	17,9	18,3	0,00416667	0,0042	1,008	73,18	93,07
315	359,7	250,7	21,6	359,5	250	23,7	17,7	18,8	0,00416667	0,0044	1,056	76,45	93,41
360	343,6	241,3	20,8	341,2	238,8	25,2	18,8	19,2	0,00416667	0,0046	1,104	80,15	92,67
405	360,4	253,4	21,8	361,2	255,5	25,7	18,9	19,2	0,00416667	0,0042	1,008	73,18	92,87
450	373,3	256,8	22,2	378,1	259,3	24,2	18	19,5	0,00416667	0,0042	1,008	73,18	93,52

495	376,5	258,1	22,4	384,8	262,2	27,2	19,8	19,9	0,0046	0,0044	0,956521739	69,44	92,78
540	382,6	260	22,4	391,8	264,7	22,4	15,7	20,5	0,00416667	0,0044	1,056	76,45	94,15
585	386,2	258,6	23	397	266,4	21,2	14,4	20,6	0,00416667	0,0044	1,056	76,45	94,51
630	389,1	269,6	23,5	400,2	268,4	18,3	13,2	20	0,00416667	0,0042	1,008	73,18	95,30
675	396,8	268,2	23,4	395,6	266,7	17,9	12,4	20,3	0,00416667	0,0042	1,008	73,18	95,49
720	401,2	270,3	23,4	400,8	271,1	16,9	10,7	20,2	0.00416667	0,004	0,959999923	69,69	95,79
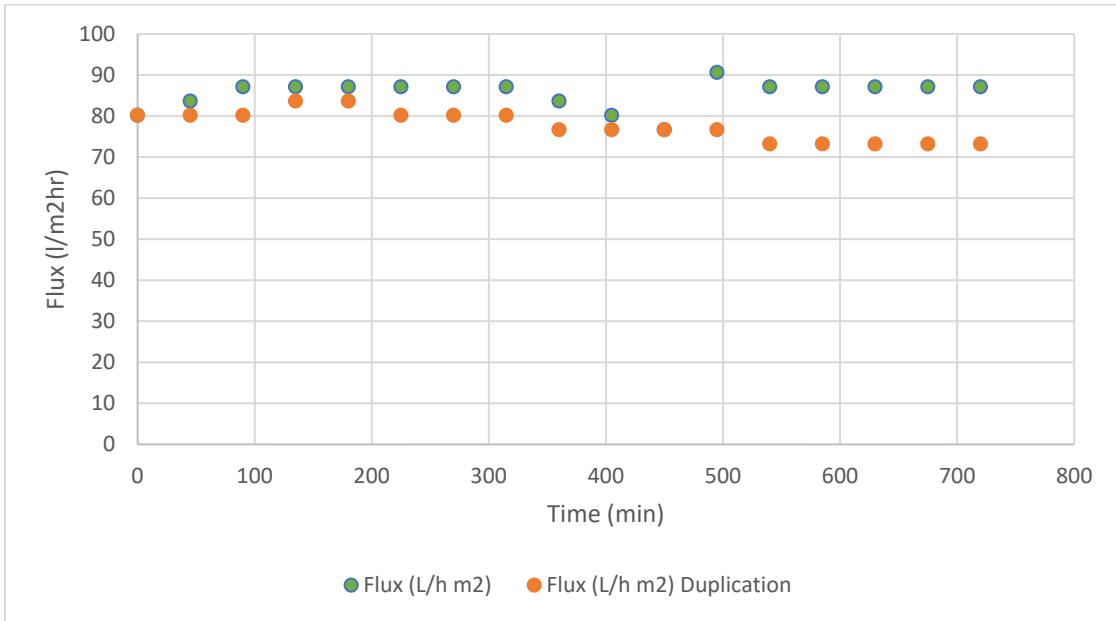
Figure A-2: permeate flux decline of the experimental run (RO at 10 bar and 22µg/l) and duplication

Table A-8: Experimental conditions of run and duplication

Initial permeate flux (L/m^2 hr): 80,145	Initial permeate flux (L/m^2 hr): 80,145
Feed P_0 (bar): 10	Feed P_0 (bar): 10
Piston P (bar): 13	Piston P (bar): 13
Feed velocity (Hz): 12,05	Feed velocity (Hz): 12,05
Brine p (Kpa): 95	Brine p (Kpa): 95
Initial Concentration: 35.5 µg/l	Initial Concentration: 35.5 µg/l
Feed pH: 7,25	Feed pH: 7,38

Table A-9: RO at 10 Bar and 35.5 ug/l

Time (min)	Feed			Brine		Permeate						
	EC F (µS)	TDS F (mg/L)	Tempe rature (deg Cel)	EC (µS)	TDS (mg/L)	EC P (µS)	TDS P (mg/L)	Tempe rature ©	Volum e (L)	Flow Rate (l/h)	Flux (L/h m²)	% Rejecti on
0	323,5	224,2	19,4	311,5	226,2	17	12,6	18,6	0,0046	1,104	80,15	94,74
45	321,1	229,6	20,2	309,6	222,3	5,3	3,9	19	0,0048	1,152	83,63	98,35
90	327,3	230,3	21	329,4	232	4,1	3	19,5	0,005	1,2	87,11	98,75
135	341,2	237,3	21,7	346,7	239,4	10,4	7,5	19,9	0,005	1,2	87,11	96,95
180	336,8	232,5	21,8	348,1	238,4	8	5,8	20,2	0,005	1,2	87,11	97,62
225	341,1	232,6	22,5	355,6	241,6	9	6,5	20,3	0,005	1,2	87,11	97,36
270	350,4	238,9	23	242,2	233,5	10	7	20,6	0,005	1,2	87,11	97,15
315	347	245,8	22,9	357,8	241,5	7,6	5,4	20,7	0,005	1,2	87,11	97,81
360	356,2	239,2	23,1	365,5	264,4	7,8	5,7	20,6	0,0048	1,152	83,63	97,81
405	362,1	242,3	23,1	378,8	251,1	6,9	4,4	20,6	0,0046	1,104	80,15	98,09
450	364,6	244,6	23,2	390,4	269,4	8,2	5,6	20,9	0,0044	1,056	76,45	97,75

495	372,4	248,8	23,8	390,7	258,8	21,3	14,9	21,5	0,0052	1,248	90,60	94,28
540	379,5	253,3	23,7	385,5	256,1	12,6	8,8	21,4	0,005	1,2	87,11	96,68
585	383,2	255,7	23,9	393,8	259,3	8,5	6	21,2	0,005	1,2	87,11	97,78
630	387,7	255,5	24,3	393,9	258,9	7,1	5	21,4	0,005	1,2	87,11	98,17
675	390,8	258,1	24,5	399,9	262,8	6,2	4,4	21,2	0,005	1,2	87,11	98,41
720	393,4	262,1	24,7	402	266,1	6,4	3,9	21,2	0,005	1,2	87,11	98,37

Table A-10: Experimental run duplication RO at 10 Bar and 35.5 ug/l

Time (min)	Feed			Brine		Permeate							
	EC F (µS)	TDS F (mg/L)	Temperature (deg Cel)	EC (µS)	TDS (mg/L)	EC P (µS)	TDS P (mg/L)	Temperature ©	Time (hr)	Volume (L)	Flow Rate (l/h)	Flux (L/h m²)	% Rejection
0	321,3	233,2	19,4	309,8	225,1	6,4	4,8	18,5	0,004167	0,0046	1,104	80,15	98,01
45	319,2	228,4	19,9	329,2	235,1	3,6	2,4	18,5	0,004167	0,0046	1,104	80,15	98,87
90	333,9	229,4	20,5	339,2	237	3,4	2,5	19,3	0,004167	0,0046	1,104	80,15	98,98
135	338,9	237,3	21,5	346,8	240,4	5	3,7	19,1	0,004167	0,0048	1,152	83,63	98,52
180	350,8	240,9	22,2	351,5	241,8	6,8	5	19,9	0,004167	0,0048	1,152	83,63	98,06
225	358,8	243,6	22,8	360,9	244,8	15,2	11	20,2	0,004167	0,0046	1,104	80,15	95,76
270	359,6	243,5	22,9	365,2	246,8	8	5,8	20,1	0,004167	0,0046	1,104	80,15	97,77
315	363,2	245,7	23,5	375,6	251,2	16,6	11,9	20,2	0,004167	0,0046	1,104	80,15	95,43
360	370,8	248,3	23,1	377,2	251,6	10,1	7,1	20,8	0,004167	0,0044	1,056	76,45	97,28
405	366,5	246,1	23,1	375,3	252,8	7,4	5,4	20,8	0,004167	0,0044	1,056	76,45	97,98
450	379,5	253,5	23,3	393	261,5	6,9	4,9	20,8	0,004167	0,0044	1,056	76,45	98,18
495	379,7	260,6	23,8	390,4	261,3	12,3	7,6	20,8	0,004167	0,0044	1,056	76,45	96,76

540	386,1	259,8	23,3	406	268,8	6	4,8	20,7	0,004167	0,0042	1,008	73,18	98,45
585	397,1	264,5	23,8	400,4	265,5	9,1	6,5	20,8	0,004167	0,0042	1,008	73,18	97,71
630	399,5	265,2	23,9	402,4	267,7	6,7	4,7	20,8	0,004167	0,0042	1,008	73,18	98,32
675	403,6	268,6	23,9	406,8	270,1	8,2	5,9	20,7	0,004167	0,0042	1,008	73,18	97,97
720	408,3	270,3	23,9	413,5	273,9	4,8	2,9	20,8	0,004167	**0,0042**	1,008	73,18	98,82
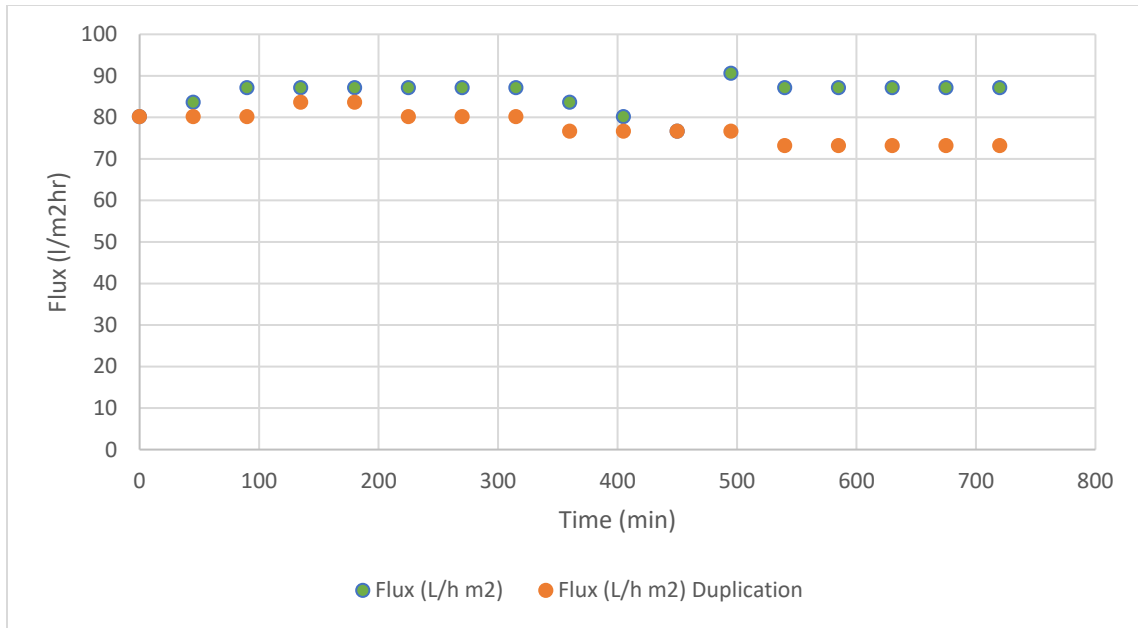
Figure A-3: Permeate flux of experimental run and duplication: RO at 10 Bar and 35.5 ug/l

Appendix B

Data from batch experiments

RO 5 Bar- 22, 35.5 and 44 µg/l

B. Appendix B

Table B-1: Experimental conditions of run and duplication

Run	Duplication
Initial permeate flux (L/m^2 hr): 59,23	Initial permeate flux (L/m^2 hr): 55,75
Feed P_0 (bar): 5	Feed P_0 (bar): 5
Piston P (bar): 13	Piston P (bar): 13
Feed velocity (Hz): 12,98	Feed velocity (Hz): 12,98
Brine p (Kpa): 95	Brine p (Kpa): 95
Initial Concentration: 35.5µg/l	Initial Concentration: 35.5µg/l
Feed pH: 7,2,	Feed pH: 6,98

Table B-2: Kinetic data of RO at 5 bar and 35.5µg/l

Time (min)	Feed			Brine		Permeate							
	EC F (µS)	TDS F (mg/L)	Tempe rature (deg Cel)	EC (µS)	TDS (mg/L)	EC P (µS)	TDS P (mg/L)	Tempe rature ©	Time (hr)	Volum e (L)	Flow Rate (l/h)	Flux (L/h m²)	% Rejecti on
0	316,7	220,4	19,9	323,1	230,8	10	6,7	19,6	0,0041 66667	0,0034	0,816	59,24	96,84
45	318,7	226,2	19,6	321,1	230,9	5,6	4,2	19,5	0,0041 66667	0,0034	0,816	59,24	98,27
90	324,6	230,1	20,4	327,3	231,8	6,6	4,4	19,7	0,0041 66667	0,0034	0,816	59,24	97,97
135	318,6	229,1	20,1	324,8	233,1	5,1	3,7	19,4	0,0041 66667	0,0036	0,864	62,72	98,42
180	322,2	235,1	20,7	338,5	238,4	5,3	3,8	19,8	0,0041 66667	0,0036	0,864	62,72	98,36
225	340,1	239,1	21	349,8	245,2	8,6	6,2	20	0,0041 66667	0,0036	0,864	62,72	97,49
270	342,6	239,6	21,1	344,1	240	7,3	4,8	20	0,0041 66667	0,0036	0,864	62,72	97,87
315	394	258,2	21,2	396,4	259,7	16,8	12,5	20,2	0,0041 66667	0,0038	0,912	66,21	95,74
360	353,5	243,8	21,5	367,9	251,5	45,8	32,2	20,8	0,0041 66667	0,004	0,96	69,69	87,04
405	387,3	253,2	22	399,6	261,7	48,6	36,9	20,8	0,0041 66667	0,004	0,96	69,69	87,45
450	395,4	271,1	22,7	408,9	276,9	51,2	36,4	21,2	0,0041 66667	0,004	0,96	69,69	87,05

495	403,3	275,2	23	413,6	280,9	35,8	25,2	21,6	0,0041 66667	0,0042	1,008	73,18	91,12
540	411,3	276,6	23,3	420,9	282,2	30,1	21,1	21,7	0,0041 66667	0,004	0,96	69,69	92,68
585	419,3	280,2	23,6	428,9	288,1	24,3	16,9	21,6	0,0041 66667	0,004	0,96	69,69	94,20
630	439,8	292,1	23,7	443,5	295,1	22,5	15,7	21,8	0,0041 66667	0,004	0,96	69,69	94,88
675	435,8	290,1	23,9	439,2	291,8	18,3	12,7	21,7	0,0041 66667	0,004	0,96	69,69	95,80
720	426,7	283,1	23,8	440,4	292,6	14,1	12,8	21,9	0,0041 66667	0,004	0,96	69,69	96,70

Table B-3:Duplication of Kinetic data of RO at 5 Bar and 35.5 µg/l

	FEED			Brine		Permeate							
Time (min)	EC F (µS)	TDS F (mg/L)	Tempe rature (deg Cel)	EC (µS)	TDS (mg/L)	EC P (µS)	TDS P (mg/L)	Tempe rature ©	Time (hr)	Volum e (L)	Flow Rate (l/h)	Flux (L/h m²)	% Rejecti on
0	314,8	213,4	19,5	308,6	211,4	11,1	8,3	20,3	0,0041 66667	0,0032	0,768	55,75	96,47
45	318,7	217,8	19,9	321,2	218,5	6,8	4,6	20,3	0,0041 66667	0,0032	0,768	55,75	97,87
90	321,4	218,3	20,2	326,5	221	6,5	5,1	20,5	0,0041 66667	0,0032	0,768	55,75	97,98
135	323,4	219,6	20,1	325,1	220,8	6,1	4,2	20,4	0,0041 66667	0,0034	0,816	59,24	98,11
180	325,9	220,3	20,2	327,5	221,1	5,9	4	20	0,0041 66667	0,0034	0,816	59,24	98,19
225	327,4	221,5	20,1	327,1	221	6,6	4,8	21	0,0041 66667	0,0034	0,816	59,24	97,98
270	22,2	221,6	21,3	332,4	223,4	10,1	8	21,4	0,0041 66667	0,0036	0,864	62,72	96,94
315	334,6	225,1	22,8	337,5	230,1	11,2	8,1	21,5	0,0041 66667	0,0036	0,864	62,72	96,65
360	340,1	232,3	22,8	339,2	232,8	13,2	9,4	22	0,0041 66667	0,0036	0,864	62,72	96,12
405	344,1	236,9	23,2	340,8	236,9	12,4	8,5	22,2	0,0041 66667	0,0038	0,912	66,21	96,40
450	349,1	231,9	23,9	351,6	233,5	12,3	8,7	22,3	0,0041 66667	0,0038	0,912	66,21	96,48
495	349	233,2	23,6	352	235,1	10,4	7,2	22,2	0,0041 66667	0,0038	0,912	66,21	97,02

540	351,9	234,4	23,8	343,5	231,8	9,6	6,9	22	0,0041 66667	0,0038	0,912	66,21	97,27
585	355,4	236,2	23,9	357,3	237,2	9,9	6,9	21,9	0,0041 66667	0,004	0,96	69,69	97,21
630	357,9	240,7	24	363,9	242	10,3	7,1	22,2	0,0041 66667	0,004	0,96	69,69	97,12
675	368,6	243,1	24,2	370,8	244,9	13,7	9,4	22,2	0,0041 66667	0,004	0,96	69,69	96,28
720	365,4	241	24,2	370,6	243,9	9,3	6,4	22,5	0,0041 66667	0,004	0,96	69,69	97,45
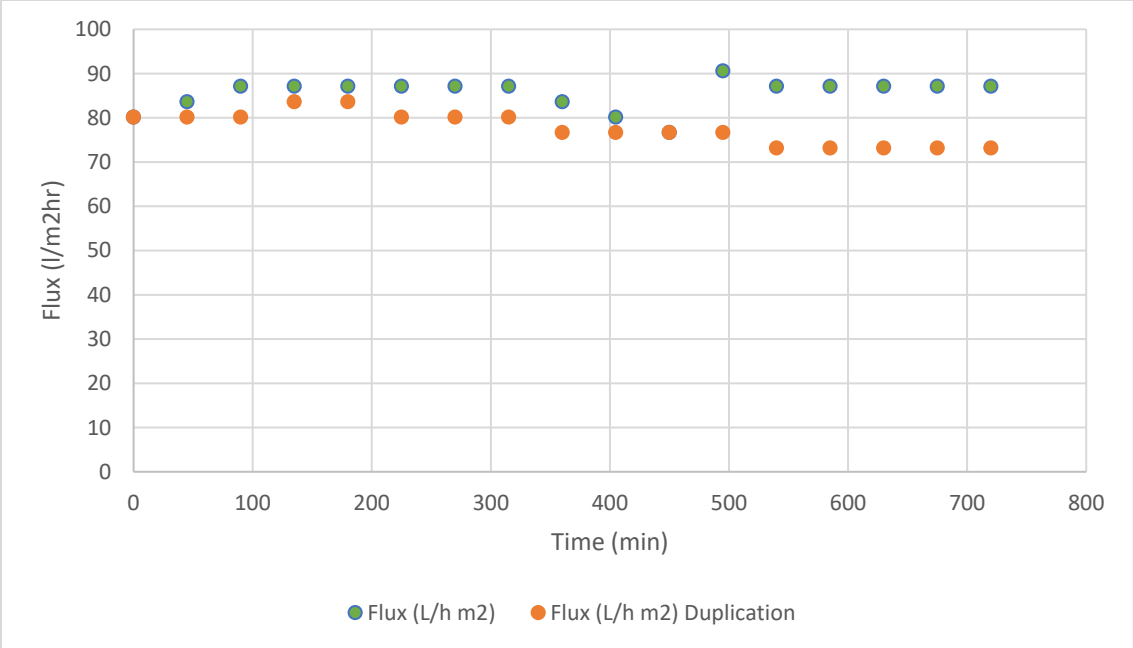
Figure B-1: Permeate flux decline of run and duplication (RO- 5bar, 35.5µg/l)

Table B-4: Experimental conditions

Run	Duplication
Initial permeate flux (L/m^2 hr): 62,72	Initial permeate flux (L/m^2 hr): 55,75
Feed P_0 (bar): 5	Feed P_0 (bar): 5
Piston P (bar): 8	Piston P (bar): 8
Feed velocity (Hz): 12,98	Feed velocity (Hz): 12,98
Brine p (Kpa): 95	Brine p (Kpa): 95
Initial Concentration: 22µg/l	Initial Concentration: 22µg/l
Feed pH: 6,98	Feed pH: 6,74

Table B-5: Kinetic data RO- 5Bar, 22µg/l

Time (min)	Feed			Brine		Permeate							
	EC F (µS)	TDS F (mg/L)	Temperature (deg Cel)	EC (µS)	TDS (mg/L)	EC P (µS)	TDS P (mg/L)	Temperature ©	Time (hr)	Volume (L)	Flow Rate (l/h)	Flux (L/h m²)	% rejection
0	316,7	233,1	18,6	320,6	234,8	8,1	5,6	19,6	0,00416667	0,0036	0,864	62,72	97,44
45	318,7	226,2	19,6	321,1	230,9	6,2	4,7	19,4	0,00416667	0,0036	0,864	62,72	98,09
90	324,6	230,1	20,4	327,3	231,8	6,5	4,7	19,6	0,00416667	0,0036	0,864	62,72	98,00
135	327,4	236,5	19,8	331,9	238,5	6,4	4,2	19,6	0,00416667	0,0036	0,864	62,72	98,13
180	342,4	239,6	21,3	348,4	241,8	9,7	6,9	20,6	0,00416667	0,0036	0,864	62,72	97,17
225	348,5	245,9	22	350,2	247,6	8,6	5,5	21	0,00416667	0,0036	0,864	62,72	97,56
270	351,8	240,4	22,4	354,5	241,4	19,2	13,5	21,6	0,00416667	0,0036	0,864	62,72	94,54
315	357,6	243	23,1	363,1	244,6	16,7	12	22,1	0,00416667	0,0036	0,864	62,72	95,33
360	364,2	242,9	23,6	367,3	244,5	14,1	9,6	22,8	0,00416667	0,0036	0,864	62,72	96,13
405	361,7	239,9	23,9	371,7	247,1	16,1	10,8	23,2	0,00416667	0,0034	0,816	59,24	95,55
450	377,5	244,1	24,5	384,1	251,7	18,9	11,7	23,5	0,00416667	0,0034	0,816	59,24	94,99

495	386,7	249,3	25	392,9	256,3	23,5	15,8	23,6	0,0041 66667	0,0034	0,816	59,24	93,92
540	397,6	255,2	25,6	401,4	259,4	22,5	15,2	24	0,0041 66667	0,0034	0,816	59,24	94,34
585	390,8	250,8	25,7	401,9	257	27,3	18	24	0,0041 66667	0,0032	0,768	55,75	93,01
630	407,3	259,2	26,2	412,2	260,8	22,3	14,2	24,9	0,0041 66667	0,0032	0,768	55,75	94,52
675	412,6	261,8	26,5	420,8	265,8	16,6	10,8	24,8	0,0041 66667	0,003	0,72	52,27	95,98
720	420,9	266,4	26,7	426,8	270,1	17,6	11,9	24,8	0,0041 66667	0,003	0,72	52,27	95,82

Table B-6: Kinetic data RO- 5Bar, 22µg/l Duplication

	FEED			Brine		Permeate							
Time (min)	EC F (µS)	TDS F (mg/L)	Temperature (deg Cel)	EC (µS)	TDS (mg/L)	EC P (µS)	TDS P (mg/L)	Temperature ©	Time (hr)	Volume (L)	Flow Rate (l/h)	Flux (L/h m²)	% Rejection
0	314,8	213,4	20,5	308,6	211,4	9,6	7,1	22,6	0,0041 66667	0,0032	0,768	55,75	96,95
45	320,4	221,3	21,5	325,7	225,6	7	4,5	22,5	0,0041 66667	0,0032	0,768	55,75	97,82
90	326,5	223,4	22,4	331,6	226,2	5,4	3,9	23	0,0041 66667	0,0032	0,768	55,75	98,35
135	339,4	226,8	23,4	434,4	228,9	5,6	3,6	23,4	0,0041 66667	0,0032	0,768	55,75	98,35
180	355,6	234,9	24,3	359,2	237,4	6,3	4,3	23,7	0,0041 66667	0,0034	0,816	59,24	98,23
225	360,4	237,6	24,7	366,3	238,4	10,3	6,7	23,9	0,0041 66667	0,0034	0,816	59,24	97,14
270	362,5	237	25,1	369,1	240,2	22,6	15,1	24	0,0041 66667	0,0034	0,816	59,24	93,77
315	372	238,7	25,4	377,6	242,4	20,5	13,5	24,8	0,0041 66667	0,0034	0,816	59,24	94,49
360	340,1	232,3	22,8	339,2	232,8	24,5	16,7	25	0,0041 66667	0,0036	0,864	62,72	92,80
405	344,1	236,9	23,2	340,8	236,9	22,5	15,2	25,5	0,0041 66667	0,0036	0,864	62,72	93,46
450	349,1	231,9	23,9	351,6	233,5	27,3	18	25,9	0,0041 66667	0,0036	0,864	62,72	92,18

495	349	233,2	23,6	352	235,1	22,3	14,2	26	0,0041 66667	0,0036	0,864	62,72	93,61
540	351,9	234,4	23,8	343,5	231,8	16,9	11	26,3	0,0041 66667	0,0036	0,864	62,72	95,20
585	379,2	242,5	25,8	382,1	244,3	17,3	11,5	27	0,0041 66667	0,004	0,96	69,69	95,23
630	383,5	238,5	26,9	390,6	246,7	23,8	19,2	27,4	0,0041 66667	0,004	0,96	69,69	93,79
675	385,1	241,4	27,1	390,8	244,1	18,6	12,4	25,7	0,0041 66667	0,004	0,96	69,69	95,17
720	394,5	246,8	27,1	397,1	247,5	24	15,7	24,3	0,0041 66667	0,004	0,96	69,69	93,92
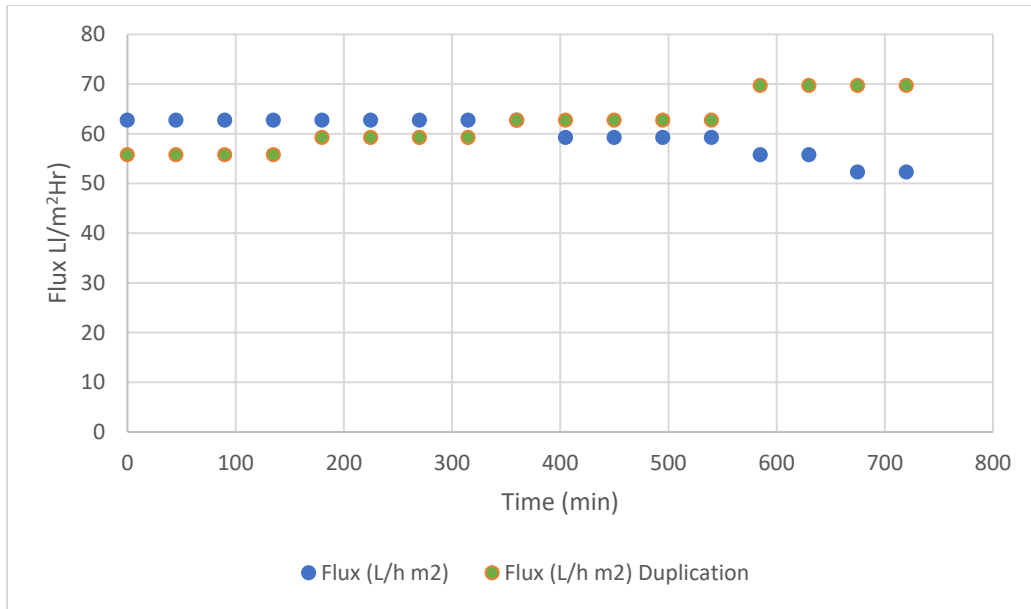
Figure B-2: Permeate flux of run and duplication- RO: 5Bar, 22µg/l

Table B-7: Experimental conditions

Run	Duplication
Initial permeate flux (L/m² hr): 62,72	Initial permeate flux (L/m² hr): 62,72
Feed P_0 (bar): 5	Feed P_0 (bar): 5
Piston P (bar): 13	Piston P (bar): 13
Feed velocity (Hz): 12,98	Feed velocity (Hz): 12,98
Brine p (Kpa): 95	Brine p (Kpa): 95
Initial Concentration: 44 µg/l	Initial Concentration: 44 µg/l
Feed pH: 6,98	Feed pH: 6,74

Table B-8: Kinetic data RO: 5 bar, 44µg/l

	Feed			Brine		Permeate								
Time (min)	EC F (µS)	TDS F (mg/L)	Temperature (deg Cel)	EC (µS)	TDS (mg/L)	EC P (µS)	TDS P (mg/L)	Temperature ©	Time (s)	Time (hr)	Volume (L)	Flow Rate (l/h)	Flux (L/h m²)	% rejection
0	313,4	222,2	20,8	320,6	225,6	8,1	5,9	22	15	0,00416667	0,0036	0,864	62,72	97,42
45	318,7	226,2	19,6	321,1	230,9	6,6	4,9	22,4	15	0,00416667	0,0036	0,864	62,72	98,02
90	333,1	230,4	22,1	340,9	235,1	6,3	4,6	22,5	15	0,00416667	0,0036	0,864	62,72	98,11
135	344,1	233,2	22,3	351,4	237,6	6,5	4,1	22,5	15	0,00416667	0,0036	0,864	62,72	98,14
180	349,9	242,1	22,7	356,6	239,9	5,6	3,9	22,7	15	0,00416667	0,0038	0,912	66,21	98,40
225	354,7	236,9	23,7	360	238,8	6,4	4,4	22,9	15	0,00416667	0,0038	0,912	66,21	98,25
270	364,8	240,9	24,2	373,2	244,9	7,1	4,9	23,1	15	0,00416667	0,0038	0,912	66,21	98,05
315	376,3	246	24,7	380,3	248,1	10,6	7,1	23,5	15	0,00416667	0,0038	0,912	66,21	97,18
360	380,4	249,6	24,9	386,1	250,6	9,4	7,2	23,2	15	0,00416667	0,0038	0,912	66,21	97,53
405	392,9	255,9	24,9	401	259,2	10	6,8	23	15	0,00416667	0,0038	0,912	66,21	97,45
450	398,5	257,4	25,3	401,7	259,4	9,7	6,5	23,6	15	0,00416667	0,0038	0,912	66,21	97,57
495	402	260,3	25,3	409,5	263,2	8,1	5,9	23,7	15	0,00416667	0,0038	0,912	66,21	97,99

540	413,9	265,5	25,7	420,4	269,5	9,8	6,5	23,5	15	0,00416666 67	0,0038	0,912	66,21	97,63
585	421	270	25,7	426,6	274,8	9,4	7,1	23,6	15	0,00416666 67	0,0036	0,864	62,72	97,77
630	425,6	273,5	25,9	430,1	277,7	9,7	7,3	23,7	15	0,00416666 67	0,0036	0,864	62,72	97,72
675	418,5	268,3	25,7	427,4	272,1	14	9,3	24,3	15	0,00416666 67	0,0032	0,768	55,75	96,65
720	434,1	274,9	26,1	440,3	279,7	14,7	9,8	24,3	15	0,00416666 67	0,003	0,72	52,27	96,61

Table B-9: Duplication of kinetic data RO: 5 bar, 44µg/l

	FEED			Brine		Permeate							
Time (min)	EC F (µS)	TDS F (mg/L)	Temperature (deg Cel)	EC (µS)	TDS (mg/L)	EC P (µS)	TDS P (mg/L)	Temperature ©	Time (hr)	Volume (L)	Flow Rate (l/h)	Flux (L/h m2)	% Rejection
0	315,4	208,6	20,4	308,6	211,4	8,7	6,1	22,6	0,00416 6667	0,0036	0,864	62,72	97,24
45	318,5	213,4	21,5	325,7	225,6	7	4,5	22,5	0,00416 6667	0,0036	0,864	62,72	97,80
90	324,2	223,3	22,6	331,5	225,2	5,4	3,9	22,4	0,00416 6667	0,0036	0,864	62,72	98,35
135	326,5	223,4	22,4	331,6	226,2	5,1	3,6	22,6	0,00416 6667	0,0036	0,864	62,72	98,43
180	334,9	223,7	23,5	346,1	230,8	5,7	3,9	22,8	0,00416 6667	0,0036	0,864	62,72	98,30
225	347,1	229,9	23,9	354,9	235,5	5,4	3,9	22,9	0,00416 6667	0,0036	0,864	62,72	98,44
270	351,5	234,3	23,8	356,3	236,4	7,7	5,2	23,7	0,00416 6667	0,0036	0,864	62,72	97,81
315	355,7	233,1	24,6	359,8	235,2	8,1	6,2	23,8	0,00416 6667	0,0036	0,864	62,72	97,72
360	359,5	236,6	24,8	360,5	237,1	6,9	4,8	23,9	0,00416 6667	0,0036	0,864	62,72	98,08
405	375,1	243,3	25,2	379,1	244,9	7,1	4,8	23,9	0,00416 6667	0,0036	0,864	62,72	98,11
450	382,7	246,6	25,6	395,2	254,8	7,2	5,1	23,8	0,00416 6667	0,0036	0,864	62,72	98,12

495	395,8	251,5	26	400,1	254,1	10,3	6,5	24,7	0,0041 66667	0,0036	0,864	62,72	97,40
540	407,1	255,7	26,2	408,6	260	8,4	5,7	24,7	0,0041 66667	0,0038	0,912	66,21	97,94
585	409,8	256,4	26,3	419	264,7	10,5	6,5	25	0,0041 66667	0,0038	0,912	66,21	97,01
630	416,8	259,1	26,5	426,4	269,3	10,8	6,9	25,2	0,0041 66667	0,004	0,96	69,69	97,41
675	424,1	266,1	26,8	431,7	272,9	11,4	7,7	25,3	0,0041 66667	0,004	0,96	69,69	97,31
720	417,9	262,2	26,7	428,8	263,2	8,8	5,7	25	0,0041 66667	0,004	0,96	69,69	97,89
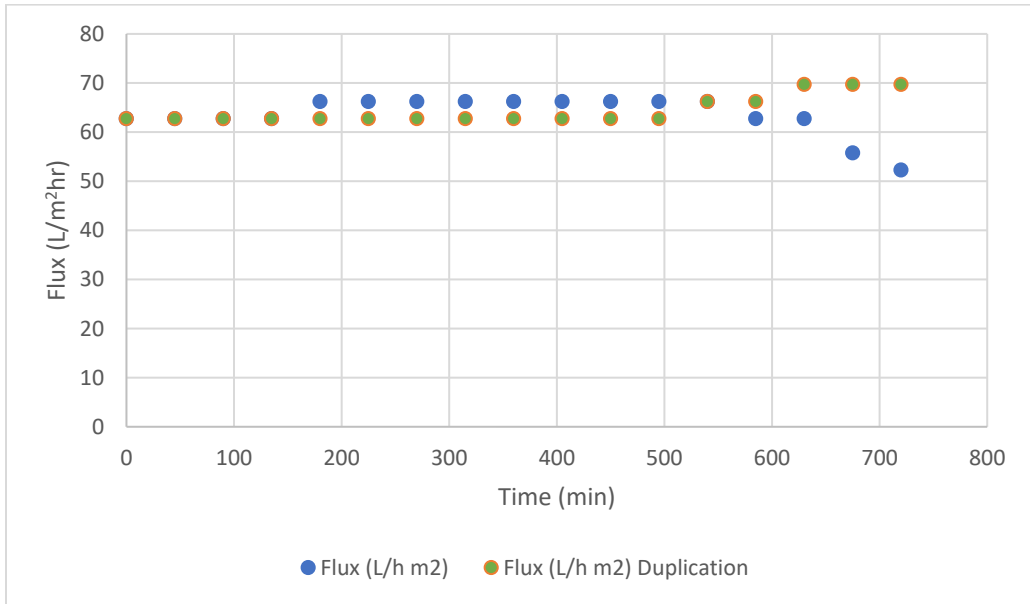
Figure B-3: Permeate flux decline of run (RO 5 bar, 44 ug/l) and duplication

Appendix C

Data from batch experiments

RO 15 bar: 22, 35.5 and 44μg/l

C. Appendix C

Table C-1: Experimental operating conditions

Run	Duplication
Starting time: 7:30	Starting time: 7:15
Initial permeate flux (L/m^2 hr): 101,052	Initial permeate flux (L/m^2 hr): 101,052
Feed P_0 (bar): 15	Feed P_0 (bar): 15
Piston P (bar): 13	Piston P (bar): 13
Feed velocity (Hz): 12,98	Feed velocity (Hz): 12,98
Brine p (Kpa): 95	Brine p (Kpa): 95
Initial Concentration: 44µg/l	Initial Concentration: 44µg/l
Feed pH: 6,74	Feed pH: 6,97

Table C-2: Kinetic data for RO 15 Bar, 44µg/l

	Feed			Brine		Permeate			.				
Time (min)	EC F (µS)	TDS F (mg/L)	Temperature (deg Cel)	EC (µS)	TDS (mg/L)	EC P (µS)	TDS P (mg/L)	Temperature ©	Time (hr)	Volume (L)	Flow Rate (l/h)	Flux (L/h m²)	% Rejection
0	316,5	221,1	21	323,5	225,5	6,9	4,5	22,5	0,004166667	0,0058	1,392	101,05	97,82
45	328,7	228,6	22,4	332,9	234,5	6,2	4,1	22,3	0,004166667	0,0058	1,392	101,05	98,11
90	348,3	232,6	23,4	354,5	236,4	6,4	4,4	22,1	0,004166667	0,0058	1,392	101,05	98,16
135	354,9	235,8	24	363,9	241,2	6,3	4,3	22,1	0,004166667	0,0058	1,392	101,05	98,22
180	369,7	241,3	24,7	374,4	244,4	5,4	3,9	22,2	0,004166667	0,0056	1,344	97,57	98,54
225	375,1	243,9	25,2	380,9	249,6	7,3	5	23,6	0,004166667	0,0056	1,344	97,57	98,05
270	384,3	251,2	25,6	390,2	250,7	7,9	5,6	24	0,004166667	0,0056	1,344	97,57	97,94
315	389,1	250,1	26,1	398,5	256,2	8,4	5,6	23,9	0,004166667	0,0056	1,344	97,57	97,84
360	401,6	253,8	26,5	404,8	255,9	7,4	4,8	24,1	0,004166667	0,0056	1,344	97,57	98,16
405	405,6	256,8	26,9	412,4	259,6	8,9	5,9	24,3	0,004166667	0,0056	1,344	97,57	97,81
450	415,7	260,1	27	417,5	262,2	7,6	5,3	23,6	0,004166667	0,0056	1,344	97,57	98,17

495	421,5	262,5	27,3	423,6	266,3	6,6	4,9	24,4	0,0041 66667	0,0056	1,344	97,57	98,43
540	424,3	265,3	27,3	425,8	264,6	12,4	8,1	24,6	0,0041 66667	0,0055	1,32	95,83	97,08
585	427,3	265,8	27,4	428	265,9	13,3	8,8	24	0,0041 66667	0,0054	1,296	94,08	96,89
630	432,3	268,2	27,5	432,3	269,8	13,8	9,1	23,8	0,0041 66667	0,0054	1,296	94,08	96,81
675	433,2	268,6	27,2	431,8	269,4	15,3	10,2	23,5	0,0041 66667	0,0054	1,296	94,08	96,47
720	435,8	273,3	26,9	437,2	274,8	16,7	11,3	23	0,0041 66667	0,0054	1,296	94,08	96,17

Table C-3: Kinetic data for RO 15 Bar, 44µg/l, duplication

| Time (min) | Feed | | | Brine | | Permeate | | | | | | | |
	EC F (µS)	TDS F (mg/L)	Temperature (deg Cel)	EC (µS)	TDS (mg/L)	EC P (µS)	TDS P (mg/L)	Temperature (°C)	Time (hr)	Volume (L)	Flow Rate (l/h)	Flux (L/h m²)	% Rejection
0	312,6	213,4	22,4	315,4	214,2	6,7	4,7	22,2	0,004166667	0,0058	1,392	101,05	97,86
45	326,9	216,4	23,7	327,1	217,2	4,9	3,2	22,3	0,004166667	0,0058	1,392	101,05	98,50
90	327,5	217	24	328,9	217,8	3,7	2,7	21,8	0,004166667	0,0058	1,392	101,05	98,87
135	337,7	219	25,1	336,7	218,1	4,1	2,7	22,1	0,004166667	0,0058	1,392	101,05	98,79
180	343,3	220,9	26,6	352,2	224	4,7	3,1	22,4	0,004166667	0,0056	1,344	97,57	98,63
225	356,5	224	27,2	360,9	226,9	4,2	2,9	22,6	0,004166667	0,0056	1,344	97,57	98,82
270	361,7	224,8	27,8	366,5	227,1	5,3	3,7	24,7	0,004166667	0,0056	1,344	97,57	98,53
315	376,6	228,9	28,5	384,8	232,8	4,8	3,1	25,4	0,004166667	0,0056	1,344	97,57	98,73
360	377,5	228,3	28,9	389	235,4	6,7	4,5	25,6	0,004166667	0,0056	1,344	97,57	98,23
405	397,5	237,4	29	400,9	241,2	5,8	4,2	26	0,004166667	0,0056	1,344	97,57	98,54
450	403,9	239,7	30	404,5	242,1	7,3	4,8	25,9	0,004166667	0,0054	1,296	94,08	98,19

495	413,2	243,2	29,5	412,8	244,7	6,9	4,9	26	0,0041 66667	0,0054	1,296	94,08	98,22
540	418,9	250,7	30,2	418,4	246,2	7,7	4,9	26,1	0,0041 66667	0,0054	1,296	94,08	98,16
585	424,4	248	31	423,4	250,4	8,4	5,4	26,1	0,0041 66667	0,0052	1,248	90,60	98,02
630	431,4	292	30,9	433,1	253	9,2	5,9	25,9	0,0041 66667	0,0052	1,248	90,60	97,87
675	437,1	259,8	31	444,7	261,4	10,2	6,5	26	0,0041 66667	0,0052	1,248	90,60	97,67
720	454,1	286,1	30,9	453,8	263,4	10,5	6,8	27	0,0041 66667	0,005	1,2	87,11	97,69
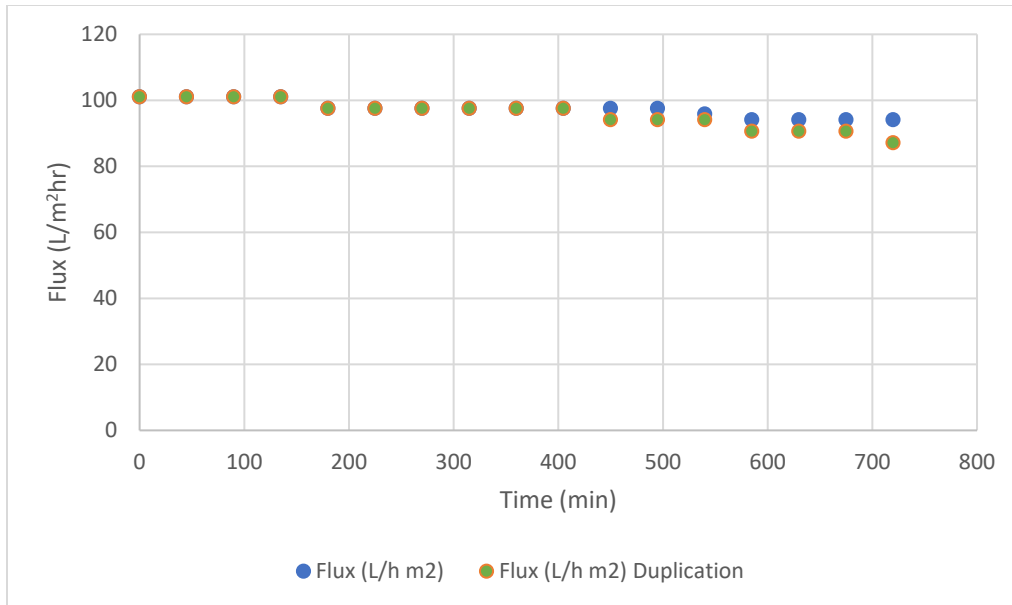
Figure C-1: Permeate flux decline of experimental run and duplicate: RO 15 Bar, 44µg/l

Table C-4: Experimental operating conditions

Run	Duplication
Initial permeate flux (L/m^2 hr): 97,56	Initial permeate flux (L/m^2 hr): 87,114
Feed P$_0$ (bar): 15	Feed P$_0$ (bar): 15
Piston P (bar): 13	Piston P (bar): 13
Feed velocity (Hz): 12,98	Feed velocity (Hz): 12,98
Brine p (Kpa): 95	Brine p (Kpa): 95
Initial Concentration: 22µg/l	Initial Concentration: 22µg/l
Feed pH: 7,14	Feed pH: 6.99

Table C-5: Kinetic data for RO at 15 Bar, 22µg/l

	Feed			Brine		Permeate							
Time (min)	EC F (µS)	TDS F (mg/L)	Temperatur e (deg Cel)	EC (µS)	TDS (mg/L)	EC P (µS)	TDS P (mg/L)	Temperatur e ©	Time (hr)	Volume (L)	Flow Rate (l/h)	Flux (L/h m²)	% Reject ion
0	335,1	263,5	16	339,8	266,4	7,7	6,1	16,2	0,00416667	0,0056	1,344	97,57	97,70
45	343,2	266,1	16,1	346,1	267,4	2,7	1,2	16,3	0,00416667	0,0054	1,296	94,08	99,21
90	349,9	267,8	16,4	358,2	270,5	2,5	1,9	16,1	0,00416667	0,0054	1,296	94,08	99,29
135	355,5	270,6	17,6	367,6	272,3	4,7	3,8	16,2	0,00416667	0,0054	1,296	94,08	98,68
180	374,6	272,9	19,1	377,6	274,7	6,4	4,9	16,8	0,00416667	0,0054	1,296	94,08	98,29
225	377,5	275,3	19,6	385,6	278,6	7,1	5,6	17,1	0,00416667	0,0052	1,248	90,60	98,12
270	385,2	278	20,2	391,9	280,2	8,1	6,2	17,1	0,00416667	0,0052	1,248	90,60	97,90
315	398,4	282,6	20,6	401,9	284,7	9,2	7,6	17,6	0,00416667	0,0054	1,296	94,08	97,69
360	400,5	284,6	20,6	404,2	287	9,8	8,9	18	0,00416667	0,0056	1,344	97,57	97,56
405	412,6	288,8	21,6	415,8	290,2	10,3	7,9	18	0,00416667	0,0056	1,344	97,57	97,50
450	418,1	289,8	21,7	418,3	291,2	10,2	8,3	18	0,00416667	0,0052	1,248	90,60	97,56

495	420,9	292,2	21,7	422,4	293,4	11	8,3	18,1	0,0041 66667	0,005	1,2	87,11	97,39
540	426,3	295,1	21,8	426	296,9	12,5	9,3	18,2	0,0041 66667	0,0048	1,152	83,63	97,07
585	423,6	296,7	21,8	432,3	298,7	11,9	8,7	18,3	0,0041 66667	0,005	1,2	87,11	97,19
630	434,5	299,1	21,9	435,2	301,4	22,8	17,1	18,3	0,0041 66667	0,0048	1,152	83,63	94,75
675	438,4	304,4	22	440,4	304,6	9,3	6,9	18,4	0,0041 66667	0,0048	1,152	83,63	97,88
720	435,6	305,1	21,9	440,7	305,8	13,6	11,2	18,2	0,0041 66667	0,0048	1,152	83,63	96,88

Table C-6: Kinetic data for RO at 15 Bar, 22µg/l duplication

	Feed			Brine		Permeate							
Time (min)	EC F (µS)	TDS F (mg/L)	Temperature (deg Cel)	EC (µS)	TDS (mg/L)	EC P (µS)	TDS P (mg/L)	Temperature ©	Time (hr)	Volume (L)	Flow Rate (l/h)	Flux (L/h m²)	% Rejection
0	326,1	253,4	16,4	323,8	252	4,1	3,4	15,9	0,004166667	0,005	1,2	87,11	98,74
45	343,8	260,6	17,7	345,4	261,2	3,7	2,9	16,2	0,004166667	0,0048	1,152	83,63	98,92
90	348,3	262,9	18,5	353,5	263,5	4,2	3,5	16,3	0,004166667	0,0052	1,248	90,60	98,79
135	359,3	262,7	19,3	379,3	273,2	9,6	7,4	16,7	0,004166667	0,0048	1,152	83,63	97,33
180	370,9	267,2	19,9	372,5	268,2	8,5	7,5	16,9	0,004166667	0,005	1,2	87,11	97,71
225	381,3	271	20,1	382,2	272,2	7,1	5,5	17,7	0,004166667	0,0052	1,248	90,60	98,14
270	386	271,9	21	388,4	274,7	9,9	8,2	17	0,004166667	0,0048	1,152	83,63	97,44
315	394,3	275	21,4	394	276	12,5	9,8	18,1	0,004166667	0,005	1,2	87,11	96,83
360	398,7	277,3	21,7	400	278,6	13,3	9,3	18,3	0,004166667	0,005	1,2	87,11	96,66
405	424,3	290,3	21,9	422,4	292,5	12,5	9,1	18,6	0,004166667	0,005	1,2	87,11	97,05
450	424,4	303,5	21,6	424	296,3	15,4	11	17,4	0,004166667	0,005	1,2	87,11	96,37

495	433,7	302,4	21,4	434,5	304	9,4	7,1	17,8	0,0041 66667	0,0048	1,152	83,63	97,83
540	437,9	304	21,7	438,8	306	12,4	9,5	17,5	0,0041 66667	0,0048	1,152	83,63	97,17
585	441,6	306,6	21,6	441,8	309,1	10,6	8,2	17,8	0,0041 66667	0,0046	1,104	80,15	97,60
630	443,5	312,2	21,6	451,8	315,7	8,5	6,9	18,3	0,0041 66667	0,0048	1,152	83,63	98,08
675	456,4	315,6	21,8	457,8	317,7	9,8	7,2	18,4	0,0041 66667	0,0048	1,152	83,63	97,85
720	463,7	319	22,2	464,5	320,5	10,7	8	17,9	0,0041 66667	0,0048	1,152	83,63	97,69
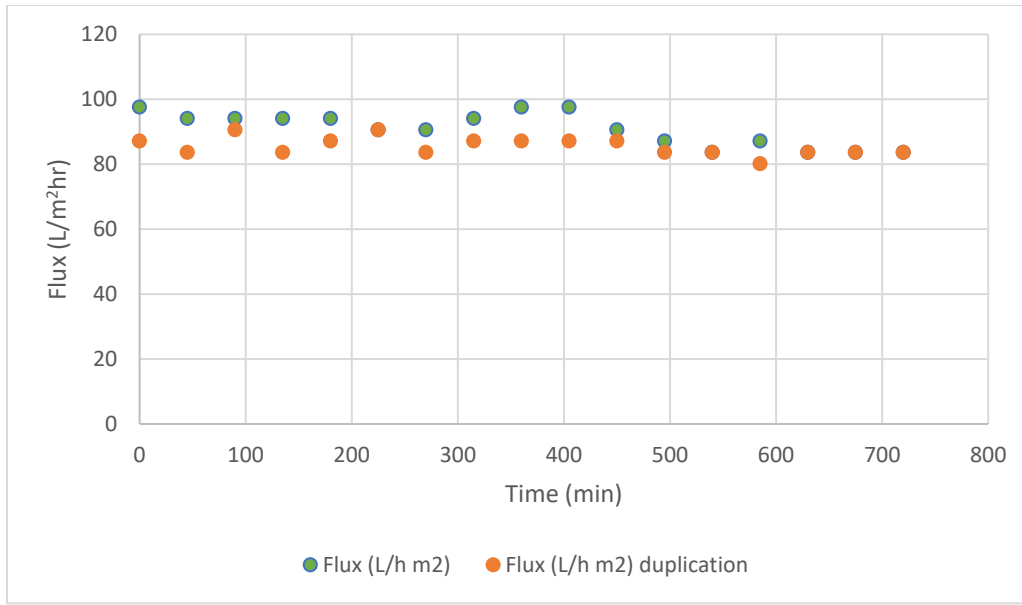
Figure C-2: Permeate flux decline of Run and duplicate RO at 15 Bar, 22µg/l

Table C-7: Experimental operating conditions

Run	Duplicate
Initial permeate flux (L/m² hr):108,02	118.47
Feed P_0 (bar): 15	15
Piston P (bar): 13	13
Feed velocity (Hz): 12,05	12,38
Brine p (Kpa): 95	95
Initial Concentration: 35.5µ/l	35.5µ/l

Table C-8: Sample of kinetic data for RO 15 bar, 35.5ug/l

	Feed			Brine		Permeate							
Time (min)	EC F (µS)	TDS F (mg/L)	Temperature (deg Cel)	EC (µS)	TDS (mg/L)	EC P (µS)	TDS P (mg/L)	Temperature ©	Time (hr)	Volume (L)	Flow Rate (l/h)	Flux (L/h m²)	% rejection
0	293,3	216,1	18,9			6,7	3,3	21,1	0,00416667	0,0062	1,488	108,02	97,72
90	300,4	218,7	19,4			5,4	2,7	20,9	0,00416667	0,0062	1,488	108,02	98,20
180	309,5	222,6	20			5,5	2,8	20,5	0,00416667	0,006	1,44	104,54	98,22
270	317,2	225,9	20,8			5,2	2,6	20,8	0,00416667	0,006	1,44	104,54	98,36
360	22,2	230,1	21,1			5,5	2,8	20,8	0,00416667	0,0058	1,392	101,05	98,33
450	339,1	236,5	21,2			5,4	2,7	21,1	0,00416667	0,0058	1,392	101,05	98,41
540	343,4	238,9	21,4			5,3	2,6	21,2	0,00416667	0,0058	1,392	101,05	98,46

Table C-9: Sample duplicate o kinetic data of RO 15 bar, 35.5 ug/l

Time(min)	Feed			Brine		Permeate							
	EC F (µS)	TDS F (mg/L)	Temperature (deg Cel)	EC (µS)	TDS (mg/L)	EC P (µS)	TDS P (mg/L)	Temperature ©	Time (hr)	Volume (L)	Flow Rate (l/h)	Flux (L/h m²) Duplicate	% Rejection
0	333,2	214,7	25,6			6,7	3,3	26	0,004166667	0,0068	1,632	118,5	97,99
90	339,2	230,1	25,8			7,6	3,8	26,3	0,004166667	0,0068	1,632	118,5	97,76
180	348,5	243,4	25,8			8,1	4	26,5	0,004166667	0,0064	1,536	111,5	97,68
270	360,4	230,6	25,9			8,9	4,2	26,6	0,004166667	0,0064	1,536	111,5	97,36
360	365,5	233,8	25,8			8,6	4,3	26,8	0,004166667	0,0062	1,488	108,0	97,65
450	374,1	238,6	25,9			8,7	4,4	26,8	0,004166667	0,006	1,44	104,5	97,67
540	375,4	239,7	25,9			8,1	4,2	26,8	0,004166667	0,006	1,44	104,5	97,84
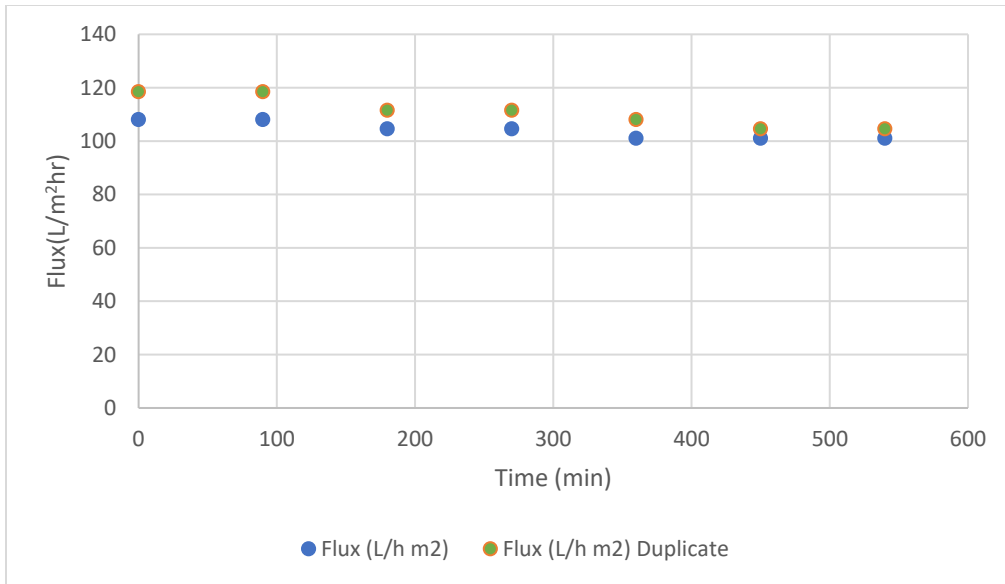
Figure C-3: Permeate flux decline for experimental run and duplicate (RO, 15bar, 35.5µg/l)

Appendix D

Kinetic data from batch experiments

NF: 5 Bar, 22, 35.5 and 44 µg/l

D. Appendix D

Table D-1: Experimental operating conditions

Run	Duplicate
Starting time: 6:30	Starting time: 6:30
Initial permeate flux (L/m^2 hr): 52,26	Initial permeate flux (L/m^2 hr): 52,26
Feed P_0 (bar): 5	Feed P_0 (bar): 5
Piston P (bar): 8	Piston P (bar): 8
Feed velocity (Hz): 12,98	Feed velocity (Hz): 12,98
Brine p (Kpa): 95	Brine p (Kpa): 95
Initial Concentration: 35.5 µg/l	Initial Concentration: 35.5 µg/
Feed pH: 7,2,	Feed pH: 6,98

Table D-2: Kinetic data for NF at 5 bar, 35.5 ug/l

	Feed			Brine		Permeate							
Time (min)	EC F (µS)	TDS F (mg/L)	Temperature (deg Cel)	EC (µS)	TDS (mg/L)	EC P (µS)	TDS P (mg/L)	Temperature ©	Time (hr)	Volume (L)	Flow Rate (l/h)	Flux (L/h m²)	% rejection
0	318,9	228,5	19,9	323,1	230,8	10	7,2	21,6	0,00416667	0,0032	0,768	55,75	96,86
45	324,6	230,1	20,4	327,3	231,8	5,9	3,9	21,2	0,00416667	0,0032	0,768	55,75	98,18
90	337,3	235,6	21,4	340,3	236,4	5,1	3,6	21,6	0,00416667	0,0032	0,768	55,75	98,49
135	344,2	236,2	22,3	350,5	239,2	16	9,1	22	0,00416667	0,003	0,72	52,27	95,35
180	360,4	242,7	22,9	363,3	246	58,8	40,5	21,9	0,00416667	0,003	0,72	52,27	83,68
225	370,4	247,6	23,3	372,5	249,4	67,6	55,7	22	0,00416667	0,003	0,72	52,27	81,75
270	378,4	250,6	24	380,2	251	147,6	101,9	22,7	0,00416667	0,003	0,72	52,27	60,99
315	394	258,2	24,6	396,4	259,7	150,1	101,2	23,2	0,00416667	0,0032	0,768	55,75	61,90
360	397	258,4	24,9	399,8	259,6	151,6	102,7	22,7	0,00416667	0,0032	0,768	55,75	61,81
405	387,3	253,2	24,7	399,6	261,7	183,1	112,6	22,8	0,00416667	0,0032	0,768	55,75	52,72
450	400,3	257,9	25,3	405,1	262,2	183,5	114,9	23,2	0,00416667	0,0032	0,768	55,75	54,16

495	406,6	260,7	25,7	408,8	263,1	184,6	115,9	23	0,00416667	0,003	0,72	52,27	54,60
540	412,5	264	25,8	415,2	266,7	167,9	111,1	24,2	0,00416667	0,003	0,72	52,27	59,30
585	414	264,8	25,8	415,6	266,5	151,7	100,5	23,9	0,00416667	0,0028	0,672	48,78	63,36
630	420,5	268,3	26	423,6	270,1	154,2	102,8	23,7	0,00416667	0,0028	0,672	48,78	63,33
675	421,8	270,5	25,8	429,1	274,8	157,4	105	23,9	0,00416667	0,0027	0,648	47,04	62,68
720	429,9	274,6	25,4	430,2	277,3	159,5	106,5	23,4	0,00416667	0,0027	0,648	47,04	62,90

Table D-3: Duplication of kinetic data of NF, 5bar, 35.5ug/l

| Time (min) | \multicolumn{3}{c}{Feed} | | | \multicolumn{2}{c}{Brine} | | \multicolumn{6}{c}{Permeate} | | | | | |
	EC F (µS)	TDS F (mg/L)	Temperature (deg Cel)	EC (µS)	TDS (mg/L)	EC P (µS)	TDS P (mg/L)	Temperature ©	Time (hr)	Volume (L)	Flow Rate (l/h)	Flux (L/h m²)	% Rejection
0	314,8	213,4	22,8	308,6	211,4	6,1	4,3	21,2	0,004166667	0,003	0,72	52,27	98,06
45	318,7	217,8	22,5	321,2	218,5	5,7	4,1	21,7	0,004166667	0,003	0,72	52,27	98,21
90	322,7	217,2	22,2	324	217,7	5,3	3,7	22,5	0,004166667	0,003	0,72	52,27	98,36
135	324,2	223,3	22,6	331,5	225,2	7	4,8	22,6	0,004166667	0,003	0,72	52,27	97,84
180	321,9	220,7	22,3	323,2	221,9	16,8	11,9	19,8	0,004166667	0,003	0,72	52,27	94,78
225	318,2	218,9	22,2	322,4	325,2	9,1	6,8	20,2	0,004166667	0,0032	0,768	55,75	97,14
270	322,9	225,9	22,2	328	222,4	60,1	42,9	20,2	0,004166667	0,0032	0,768	55,75	81,39
315	323,4	223,5	22,3	22,2	228,4	88,1	63	20,4	0,004166667	0,0032	0,768	55,75	72,76
360	337,8	231	22,6	341,9	237,4	96,3	75,1	22,3	0,004166667	0,0032	0,768	55,75	71,49
405	346,8	232,3	23,4	342,5	238,8	100,1	89,6	22,4	0,004166667	0,0032	0,768	55,75	71,14
450	352,5	234,8	23,8	354,6	235,5	108,9	77,1	21,3	0,004166667	0,0032	0,768	55,75	69,11
495	351,4	234,5	23,6	358,7	240,9	98,5	69,3	21,3	0,004166667	0,0032	0,768	55,75	71,97

540	356,4	236,7	23,8	363,5	241,4	98,2	69,3	21,5	0,00416666 67	0,0032	0,768	55,75	72,45
585	362,7	241,5	23,9	371,5	247,4	103,7	71,4	22,3	0,00416666 67	0,003	0,72	52,27	71,41
630	371,1	241,6	24,4	375,6	246,8	105,6	75,7	22,5	0,00416666 67	0,003	0,72	52,27	71,54
675	372,8	245,6	24,3	375,6	246,8	95,6	70,4	22	0,00416666 67	0,0028	0,672	48,78	74,36
720	372,4	245,8	24,2	375	247,3	98,6	71	22	0,00416666 67	0,0028	0,672	48,78	73,52
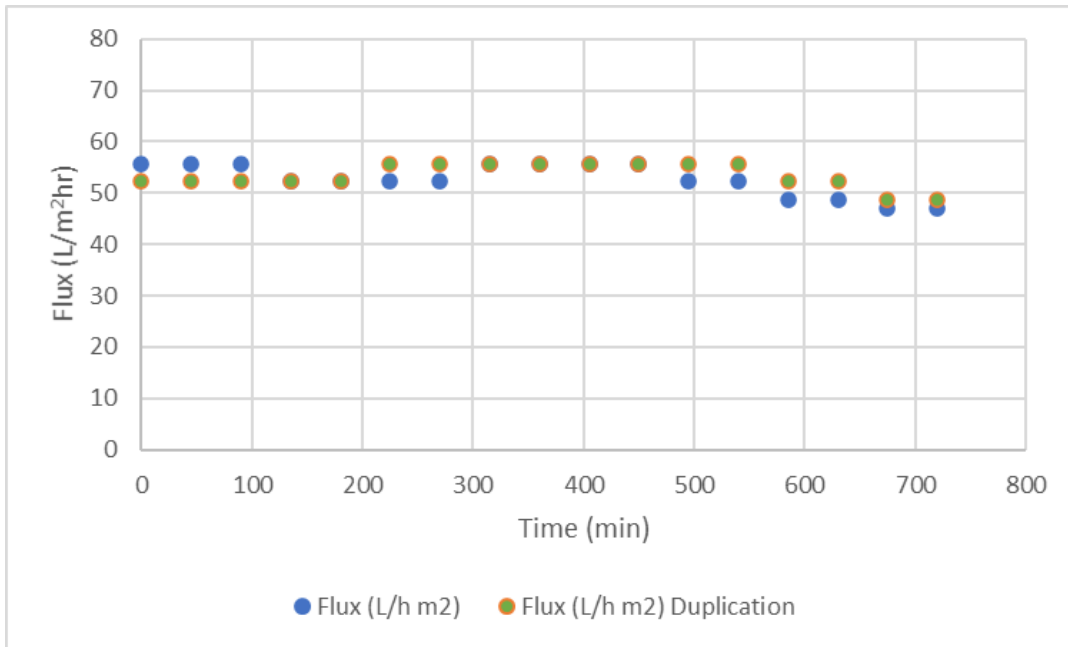
Figure D-1: Permeate flux decline of NF at 5 bar and 35.5 ug/l

Table D-4: Experimental operating conditions

Run	Duplicate
Initial permeate flux (L/m^2 hr): 55,75	Initial permeate flux (L/m^2 hr): 48,8
Feed P_0 (bar): 5	Feed P_0 (bar): 5
Piston P (bar): 8	Piston P (bar): 8
Feed velocity (Hz): 12,98	Feed velocity (Hz): 12,98
Brine p (Kpa): 95	Brine p (Kpa): 95
Initial Concentration: 22µg/l	Initial Concentration: 22µg/l
Feed pH: 6,78	Feed pH: 6,87

Table D-5: Kinetic data for NF at 5bar, 22 ug/l

Time (min)	Feed			Brine		Permeate							
	EC F (µS)	TDS F (mg/L)	Temperature (deg Cel)	EC (µS)	TDS (mg/L)	EC P (µS)	TDS P (mg/L)	Temperature ©	Time (hr)	Volume (L)	Flow Rate (l/h)	Flux (L/h m²)	% rejection
0	347,4	230,8	24	352,1	232,8	8,4	4,5	21,3	0,004166667	0,0032	0,768	55,75	97,58
45	353,1	234,4	23,9	362,4	238,2	7,7	3,4	22,4	0,004166667	0,0032	0,768	55,75	97,82
90	361,4	238,4	23,9	367,6	240,8	7,4	3,3	22,4	0,004166667	0,0026	0,624	45,30	97,95
135	369,8	242,1	24,5	371,8	242,5	11,4	4,5	22,3	0,004166667	0,0026	0,624	45,30	96,92
180	376,2	244,3	25,1	376	243,6	10,2	4,1	23,4	0,004166667	0,0028	0,672	48,78	97,29
225	383,5	247,5	25,2	385,3	248,2	9,1	3,9	24,2	0,004166667	0,003	0,72	52,27	97,63
270	385,4	249,1	25,1	386,6	250,5	9,8	4,1	24,3	0,004166667	0,0028	0,672	48,78	97,46
315	387,6	251,2	25,2	387,2	253,1	9,4	3,9	24,4	0,004166667	0,0028	0,672	48,78	97,57
360	389,9	253,5	25,5	390,1	255,7	10,6	5,7	24,6	0,004166667	0,0028	0,672	48,78	97,28
405	391,3	256,6	25,5	393,8	255,9	11,6	4,9	24,6	0,004166667	0,003	0,72	52,27	97,04
450	392,2	257	25,6	394,1	257,6	12,1	7,4	25	0,004166667	0,003	0,72	52,27	96,91

495	395,1	259,6	25,6	396	259,9	13,5	8,2	25	0,004166667	0,003	0,72	52,27	96,58
540	399,3	260	25,7	401,2	261,1	10,1	6,3	25,1	0,004166667	0,003	0,72	52,27	97,47
585	402,2	263,4	25,6	404,6	266,6	15,8	9,9	25,6	0,004166667	0,0032	0,768	55,75	96,07
630	404,9	265,9	25,5	407,1	268,8	19,1	14,2	25,6	0,004166667	0,0032	0,768	55,75	95,28
675	408,6	267,3	25,5	411,3	270,3	20,3	16,9	25,6	0,004166667	0,0032	0,768	55,75	95,03
720	415,2	277,3	25,6	416,3	279,9	20,1	17,2	26	0,004166667	0,003	0,72	52,27	95,16

Table D-6: Duplicate of kinetic data for NF at 5bar, 22ug/l

	Feed			Brine		Permeate							
Time (min)	EC F (µS)	TDS F (mg/L)	Temperature (deg Cel)	EC (µS)	TDS (mg/L)	EC P (µS)	TDS P (mg/L)	Temperature ©	Time (hr)	Volume (L)	Flow Rate (l/h)	Flux (L/h m²)	% rejection
0	315	203,3	24,6	310,2	208,5	18,02	15,6	22,6	0,00416666 67	0,0028	0,672	48,78	94,28
45	312,5	205,8	24,3	312,8	205,3	6,5	4,8	21,9	0,00416666 67	0,0028	0,672	48,78	97,92
90	325,5	214	24,4	323,3	212,6	9,9	6,6	22,3	0,00416666 67	0,003	0,72	52,27	96,96
135	329,2	215,9	24,5	22,2	216,4	27,7	19	22,4	0,00416666 67	0,0032	0,768	55,75	91,59
180	335,3	219,8	24,8	337,2	220,4	74,7	50,8	23	0,00416666 67	0,0034	0,816	59,24	77,72
225	338,2	225,1	24,5	338,8	221,7	49,7	33,8	23	0,00416666 67	0,0032	0,768	55,75	85,30
270	342,2	224,1	24,7	342,6	224,3	24,8	19,6	23,2	0,00416666 67	0,0032	0,768	55,75	92,75
315	347,4	228,8	24,5	348,5	227,1	19,6	17,2	23,1	0,00416666 67	0,0032	0,768	55,75	94,36
360	353,6	231,2	24,9	354	223,3	18,4	16,3	23,4	0,00416666 67	0,0032	0,768	55,75	94,80
405	358,1	235,6	25,3	359,2	236,7	17,6	15,5	23,2	0,00416666 67	0,0032	0,768	55,75	95,09
450	362,4	239,9	25,6	366,2	241,1	19,4	17,7	23,4	0,00416666 67	0,0032	0,768	55,75	94,65

495	366,5	244,1	25,8	368,3	246,8	20,4	18,9	23,3	0,00416666 67	0,003	0,72	52,27	94,43
540	370	248,6	25,9	371,1	248,9	17,5	14,8	23,6	0,00416666 67	0,003	0,72	52,27	95,27
585	375,9	251,1	26	376,2	253,4	14,9	10,1	23,6	0,00416666 67	0,003	0,72	52,27	96,04
630	380,2	255,6	26,1	382,2	255,9	13,8	9,9	23,7	0,00416666 67	0,0028	0,672	48,78	96,37
675	388,5	263,5	26,2	390,6	265,6	12,1	9,6	23,7	0,00416666 67	0,0028	0,672	48,78	96,89
720	401,1	270,5	26,5	404,2	277,4	13,6	10,2	23,7	0,00416666 67	0,0028	0,672	48,78	96,61
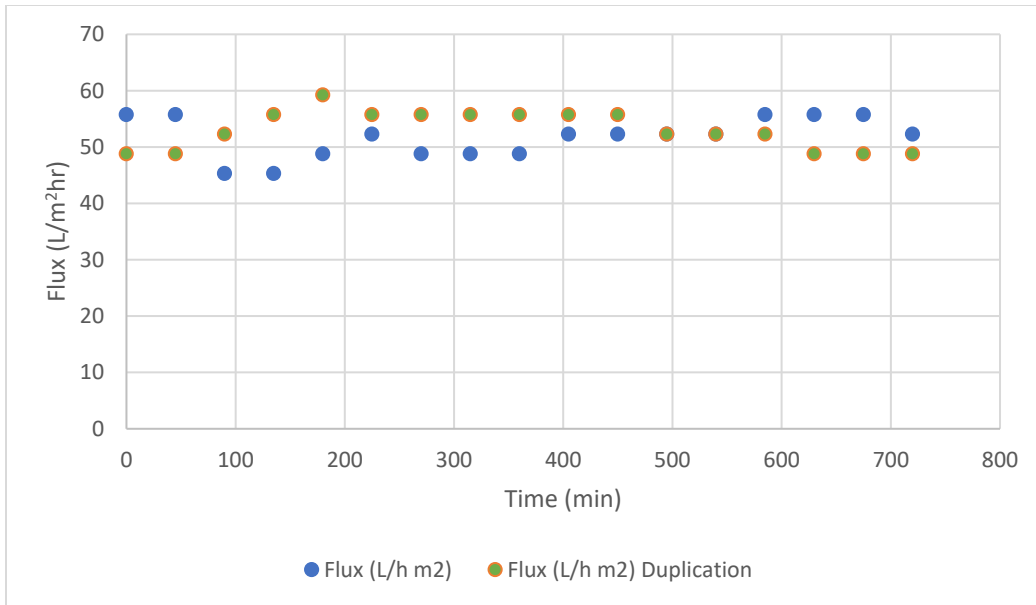
Figure D-2: Permeate flux decline of run (NF, 5bar,22 µg/l) and duplication

Table D-7: Conditions of the experimental run

Run	Duplication
Initial permeate flux (L/m^2 hr): 55.75	55,75
Feed P$_0$ (bar): 5	5
Piston P (bar): 8	8
Feed velocity (Hz): 12,05	12,38
Brine p (Kpa): 95	95
Initial Concentration: 22µg/l	22µg/l

Table D-8: Kinetic data for NF at 5bar, 44ug/l

	Feed			Brine		Permeate								
Time (min)	EC F (µS)	TDS F (mg/L)	Temperature (deg Cel)	EC (µS)	TDS (mg/L)	EC P (µS)	TDS P (mg/L)	Temperature ©	Time (s)	Time (hr)	Volume (L)	Flow Rate (l/h)	Flux (L/h m²)	% rejection
0	314,8	213,4	22,8	308,6	211,4	6,1	4,3	21,2	15	0,00416666 67	0,003	0,72	52,27	98,06
45	318,7	217,8	22,5	321,2	218,5	5,7	4,1	21,7	15	0,00416666 67	0,003	0,72	52,27	98,21
90	322,7	217,2	22,2	324	217,7	5,3	3,7	22,5	15	0,00416666 67	0,003	0,72	52,27	98,36
135	324,2	223,3	22,6	331,5	225,2	7	4,8	22,6	15	0,00416666 67	0,003	0,72	52,27	97,84
180	321,9	220,7	22,3	323,2	221,9	16,8	11,9	19,8	15	0,00416666 67	0,003	0,72	52,27	94,78
225	318,2	218,9	22,2	322,4	325,2	9,1	6,8	20,2	15	0,00416666 67	0,0032	0,768	55,75	97,14
270	322,9	225,9	22,2	328	222,4	60,1	42,9	20,2	15	0,00416666 67	0,0032	0,768	55,75	81,39
315	323,4	223,5	22,3	330,2	228,4	88,1	63	20,4	15	0,00416666 67	0,0032	0,768	55,75	72,76
360	337,8	231	22,6	341,9	237,4	96,3	75,1	22,3	15	0,00416666 67	0,0032	0,768	55,75	71,49
405	346,8	232,3	23,4	342,5	238,8	100,1	89,6	22,4	15	0,00416666 67	0,0032	0,768	55,75	71,14
450	352,5	234,8	23,8	354,6	235,5	108,9	77,1	21,3	15	0,00416666 67	0,0032	0,768	55,75	69,11

495	351,4	234,5	23,6	358,7	240,9	98,5	69,3	21,3	15	0,00416666 67	0,0032	0,768	55,75	71,97
540	356,4	236,7	23,8	363,5	241,4	98,2	69,3	21,5	15	0,00416666 67	0,0032	0,768	55,75	72,45

Table D-9: Duplication of NF 5 bar, 44ug/l kinetic data

| | Feed | | | Brine | | Permeate | | | | | | | |
	EC F (μS)	TDS F (mg/L)	Temperature (deg Cel)	EC (μS)	TDS (mg/L)	EC P (μS)	TDS P (mg/L)	Temperature ©	Time (hr)	Volume (L)	Flow Rate (l/h)	Flux (L/h m²)	% rejection
0	409,2	260,1	26,2			8,9	4,6	22,6	0,004166667	0,0032	0,768	55,75	97,83
90	412,2	261,5	26,3			9	4,5	22,6	0,004166667	0,0032	0,768	55,75	97,82
180	414,8	262,8	26			9,1	4,5	22,6	0,004166667	0,0032	0,768	55,75	97,81
270	418,7	267,3	25,7			8,3	4,1	25,9	0,004166667	0,003	0,72	52,27	98,02
360	426,2	271,3	26			8,3	4,6	26	0,004166667	0,003	0,72	52,27	98,05
450	431,6	276,3	26,3			8,6	4,3	26,1	0,004166667	0,0028	0,672	48,78	98,01
540	433,2	278,6	23,4			8,3	4,1	26,2	0,004166667	0,0028	0,672	48,78	98,08
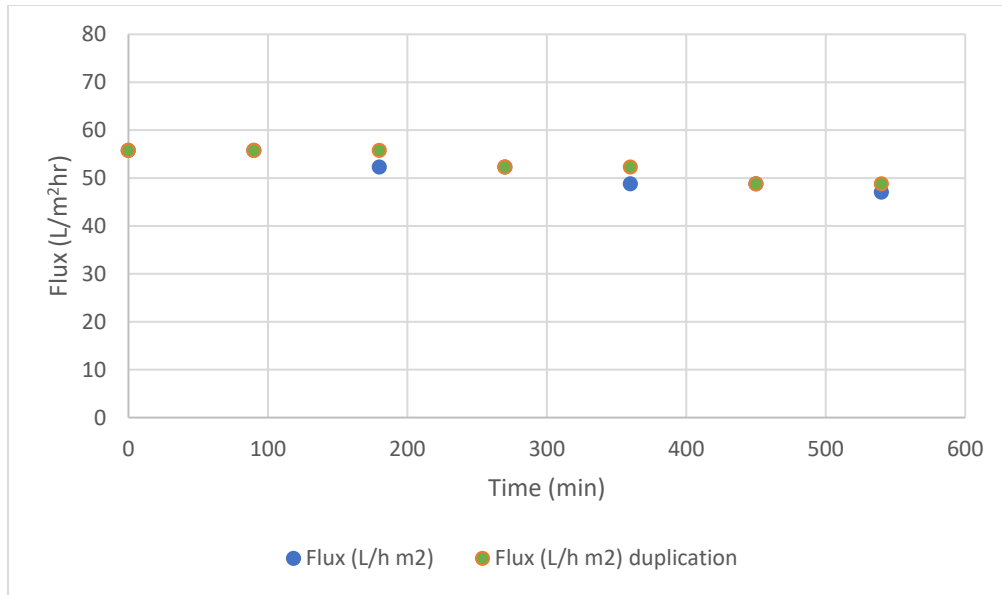
Figure D-3: Permeate flux decline of run and duplication: NF, 5bar, 44 µg/l

Appendix E

Data from batch experiments

NF at 10 Bar, 22, 35.5 and 44 µg/l

E. Appendix E

Table E-1: Experimental operating conditions

Run	Duplication
Initial permeate flux (L/m^2 hr): 76,60	Initial permeate flux (L/m^2 hr): 76,66
Feed P_0 (bar): 10	Feed P_0 (bar): 10
Piston P (bar): 13	Piston P (bar): 13
Feed velocity (Hz): 12,98	Feed velocity (Hz): 12,98
Brine p (Kpa): 95	Brine p (Kpa): 95
Initial Concentration: 22µg/l	Initial Concentration: 22µg/l
Feed pH: 6,78	Feed pH: 6,98

Table E-2: Kinetic data of NF at 10 bar, 22µg/l

	Feed			Brine		Permeate							
Time (min)	EC F (µS)	TDS F (mg/L)	Temperature (deg Cel)	EC (µS)	TDS (mg/L)	EC P (µS)	TDS P (mg/L)	Temperature ©	Time (hr)	Volume (L)	Flow Rate (l/h)	Flux (L/h m²)	% rejection
0	316,4	226,3	20,2	322,7	228,8	5,4	4	20,3	0,004166667	0,0044	1,056	76,45	98,29
45	22,1	232,4	21,1	333,5	233,8	4,9	3,4	20,3	0,004166667	0,0044	1,056	76,45	98,52
90	336,1	233,2	21,6	339,6	234,8	4,3	3,2	21,2	0,004166667	0,0044	1,056	76,45	98,72
135	345,5	235,9	22,1	349,3	237,6	6	4,1	21,7	0,004166667	0,0044	1,056	76,45	98,26
180	353,6	239,2	23	356,5	242,2	7,9	5,5	22,1	0,004166667	0,0044	1,056	76,45	97,77
225	358,4	239,8	23,5	357,6	245,1	8,2	5,4	22,9	0,004166667	0,0044	1,056	76,45	97,71
270	363,6	240,2	23,9	353,9	235,5	10,3	7,8	23,4	0,004166667	0,0042	1,008	73,18	97,17
315	365	238,5	24,7	353,6	232,4	4,6	7,2	23,3	0,004166667	0,004	0,96	69,69	98,74
360	372,8	241,4	25,2	370,8	215,7	36,1	23,9	24,1	0,004166667	0,0038	0,912	66,21	90,32
405	380,4	245,7	25,6	382,5	244,3	27,7	18,6	24,5	0,004166667	0,0038	0,912	66,21	92,72
450	388,6	247,4	25,9	401	253,3	60,7	39,2	25,3	0,004166667	0,004	0,96	69,69	84,38

495	402,6	253,4	26,6	412,8	258,8	61,9	39,8	25,5	0,0041 66667	0,0042	1,008	73,18	84,62
540	405	255,1	26,8	382,8	242,2	48,4	31,6	24,9	0,0041 66667	0,0041	0,984	71,43	88,05
585	423,8	263,7	27,1	423,9	263,3	47,8	30,9	23,7	0,0041 66667	0,0038	0,912	66,21	88,72
630	426,8	267,8	26,8	428,4	267,2	42,4	27,7	24,2	0,0041 66667	0,0036	0,864	62,72	90,07
675	434,3	273,3	26,5	411,7	272,5	42,2	39,4	23,7	0,0041 66667	0,0034	0,816	59,24	90,28
720	445,5	282,6	26,2	436,1	275,5	28,5	19,1	23,5	0,0041 66667	0,0032	0,768	55,75	93,60

Table E-3: Duplication of kinetic data of NF at 10 bar and 22ug/l

Time (min)	Feed			Brine		Permeate							
	EC F (µS)	TDS F (mg/L)	Temperature (deg Cel)	EC (µS)	TDS (mg/L)	EC P (µS)	TDS P (mg/L)	Temperature ©	Time (hr)	Volume (L)	Flow Rate (l/h)	Flux (L/h m²)	% Rejection
0	316,4	220,4	21,2	320,2	221,7	4,9	3,7	21,6	0,0041 66667	0,0044	1,056	76,45	98,45
45	324,1	223,5	22,1	328	225,8	4,3	3,1	21,3	0,0041 66667	0,0044	1,056	76,45	98,67
90	334,5	227,8	22,5	337,6	228,8	4,4	3	21,4	0,0041 66667	0,0044	1,056	76,45	98,68
135	334,8	231,6	23,2	345,8	232,3	4,1	2,9	21,8	0,0041 66667	0,0042	1,008	73,18	98,78
180	355,4	237,2	23,7	349,6	233,8	4,5	3,2	22,3	0,0041 66667	0,0046	1,104	80,15	98,73
225	358,8	238,5	24	362,5	239,2	4,7	3,1	22,6	0,0041 66667	0,0046	1,104	80,15	98,69
270	368,9	243,6	24,2	371,2	244,4	4,7	3,3	22,7	0,0041 66667	0,0044	1,056	76,45	98,73
315	376,6	248,3	24,6	380,8	248,5	4,7	3,2	22,2	0,0041 66667	0,0044	1,056	76,45	98,75
360	384,8	252,6	24,6	388,6	254,6	5	3,4	22,4	0,0041 66667	0,0044	1,056	76,45	98,70
405	389,2	253,9	24,8	389,9	254,5	5,5	3,8	22,3	0,0041 66667	0,0042	1,008	73,18	98,59
450	397,4	257,2	24,9	396,6	257,1	5,3	3,7	22,8	0,0041 66667	0,004	0,96	69,69	98,67
495	404,5	262,3	25,1	405,2	262,6	4,9	3,2	21,9	0,0041 66667	0,004	0,96	69,69	98,79

540	402,3	264,5	24,5	402,6	264,7	4,8	3,3	21,7	0,0041 66667	0,0038	0,912	66,21	98,81
585	408,6	266,8	24,8	410,1	267,8	4,9	3,5	21,8	0,0041 66667	0,0036	0,864	62,72	98,80
630	413,2	275,1	23,7	415,6	275,3	4,8	3,3	21,8	0,0041 66667	0,0034	0,816	59,24	98,84
675	418,9	275,8	24,5	421,2	277,8	5,1	3,5	22	0,0041 66667	0,0032	0,768	55,75	98,78
720	429,2	281,2	24,8	433,8	283,3	6,3	4,5	22,2	0,0041 66667	0,003	0,72	52,27	98,53
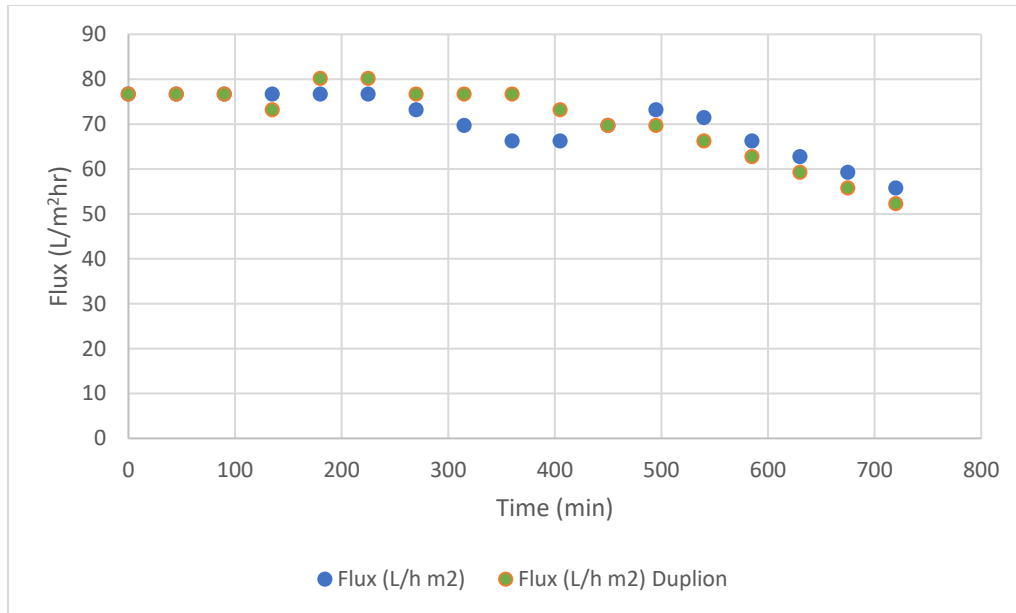
Figure E-1: Permeate flux decline of experimental run and duplication: NF, 10bar, 22µg/l

Table E-4: Experimental operating conditions

Run	Duplicate
Initial permeate flux (L/m² hr): 83,63	Initial permeate flux (L/m² hr): 83,63
Feed P_0 (bar): 10	Feed P_0 (bar): 10
Piston P (bar): 13	Piston P (bar): 13
Feed velocity (Hz): 12,98	Feed velocity (Hz): 12,98
Brine p (Kpa): 95	Brine p (Kpa): 95
Initial Concentration: 35.5 µg/l	Initial Concentration: 35.5 µg/l
Feed pH: 6,74	Feed pH: 6,98

Table E-5: Kinetic data of NF at 10 bar, 35.5µg/l

	Feed			Brine		Permeate							
Time (min)	EC F (µS)	TDS F (mg/L)	Temperature (deg Cel)	EC (µS)	TDS (mg/L)	EC P (µS)	TDS P (mg/L)	Temperature ©	Time (hr)	Volume (L)	Flow Rate (l/h)	Flux (L/h m²)	% rejection
0	313,6	212,4	23,5	317,6	217,6	5,8	4,1	23,9	0,004166667	0,0048	1,152	83,63	98,15
45	318,9	214,6	24,2	321,9	219,8	5,7	3,8	24,2	0,004166667	0,0048	1,152	83,63	98,21
90	327,2	215,4	25	329,8	215,9	6,2	4,3	23,6	0,004166667	0,0048	1,152	83,63	98,11
135	22,5	215,7	24,9	333,5	216,9	6,2	4,1	22,8	0,004166667	0,0048	1,152	83,63	98,12
180	336,1	218	25,1	337,4	220,5	6	4,1	22,7	0,004166667	0,0048	1,152	83,63	98,21
225	344,6	223,2	25,1	345,5	223,7	6,8	4,6	22,8	0,004166667	0,0048	1,152	83,63	98,03
270	347,5	223,7	25,6	347,6	224,9	6,7	4,7	23,6	0,004166667	0,0048	1,152	83,63	98,07
315	353,7	226	25,9	355,1	226,7	6,9	4,6	23,5	0,004166667	0,0046	1,104	80,15	98,05
360	357,6	228,1	26,2	359,9	229,6	7,1	4,5	23,5	0,004166667	0,0046	1,104	80,15	98,01
405	365,2	231,1	26,3	367,5	233,1	6,8	4,6	24	0,004166667	0,0046	1,104	80,15	98,14
450	370,2	231,8	27,1	372,3	231,9	9,2	6	24,6	0,004166667	0,0046	1,104	80,15	97,51

495	371,9	232,3	27,3	373	233,5	9,7	6,2	25	0,0041 66667	0,0044	1,056	76,45	97,39
540	374,5	233,4	27,8	377,4	234,8	8,8	6,3	25,5	0,0041 66667	0,0044	1,056	76,45	97,65
585	380,5	234,4	27,9	380,5	236,3	8,3	5,6	25,8	0,0041 66667	0,0042	1,008	73,18	97,82
630	372,4	227,6	28,3	372,6	228	9,4	5,8	25	0,0041 66667	0,004	0,96	69,69	97,48
675	373,7	229,1	28,3	373,4	231,1	8,9	5,8	24,8	0,0041 66667	0,0038	0,912	66,21	97,62
720	379,1	233,2	28,3	380,6	234,2	9,9	6,5	25	0,0041 66667	0,0034	0,816	59,24	97,39

Table E-6: Duplication of kinetic data of NF, 10 bar, 35.5µg/l

	Feed			Brine		Permeate							
Time (min)	EC F (µS)	TDS F (mg/L)	Temperature (deg Cel)	EC (µS)	TDS (mg/L)	EC P (µS)	TDS P (mg/L)	Temperature (°C)	Time (hr)	Volume (L)	Flow Rate (l/h)	Flux (L/h m²)	% rejection
0	315,3	213,8	21,9	314,6	216,8	6,1	4,3	21,2	0,00416667	0,0048	1,152	83,63	98,07
45	318,7	217,8	22,5	321,2	218,5	5,7	4,1	21,7	0,00416667	0,0048	1,152	83,63	98,21
90	322,7	217,2	22,2	324	217,7	5,1	3,4	21,8	0,00416667	0,0048	1,152	83,63	98,42
135	326,5	218,8	23,5	329,3	221,4	4,5	3,2	21,7	0,00416667	0,0048	1,152	83,63	98,62
180	329,6	219,3	23,8	333,3	221,9	4,9	3,3	22	0,00416667	0,0048	1,152	83,63	98,51
225	339,5	223,8	24,5	341,1	225,1	4,9	3,4	22,7	0,00416667	0,0046	1,104	80,15	98,56
270	346,2	224,1	25,1	348,1	225,8	5	3,3	23,1	0,00416667	0,0046	1,104	80,15	98,56
315	356,4	225,5	25,9	357,3	228,3	5,1	3,3	23,6	0,00416667	0,0046	1,104	80,15	98,57
360	356,8	225,9	26,4	357,4	227,2	4,9	3,4	23,6	0,00416667	0,0046	1,104	80,15	98,63
405	362	227,8	26,8	362,5	227,4	5,7	3,7	23,7	0,00416667	0,0044	1,056	76,45	98,43
450	362,8	226,3	27,1	363,1	226,4	5,6	3,7	24,2	0,00416667	0,0044	1,056	76,45	98,46

495	367,9	226,3	28	367,7	226,8	5,7	3,9	24,5	0,0041 66667	0,004	0,96	69,69	98,45
540	370,5	226,7	28,3	369,8	226,5	6,5	4,2	24,5	0,0041 66667	0,0038	0,912	66,21	98,25
585	381,3	233,6	28,5	382,2	234,4	6,7	4,5	24,5	0,0041 66667	0,0036	0,864	62,72	98,24
630	393,3	238,6	28,6	389,8	239	7	4,6	24,3	0,0041 66667	0,0034	0,816	59,24	98,22
675	395,7	240,4	28,7	393,5	239,8	6,9	4,8	24,5	0,0041 66667	0,0032	0,768	55,75	98,26
720	408,8	248,2	28,7	407,1	247,7	7,2	4,7	23,8	0,0041 66667	0,003	0,72	52,27	98,24
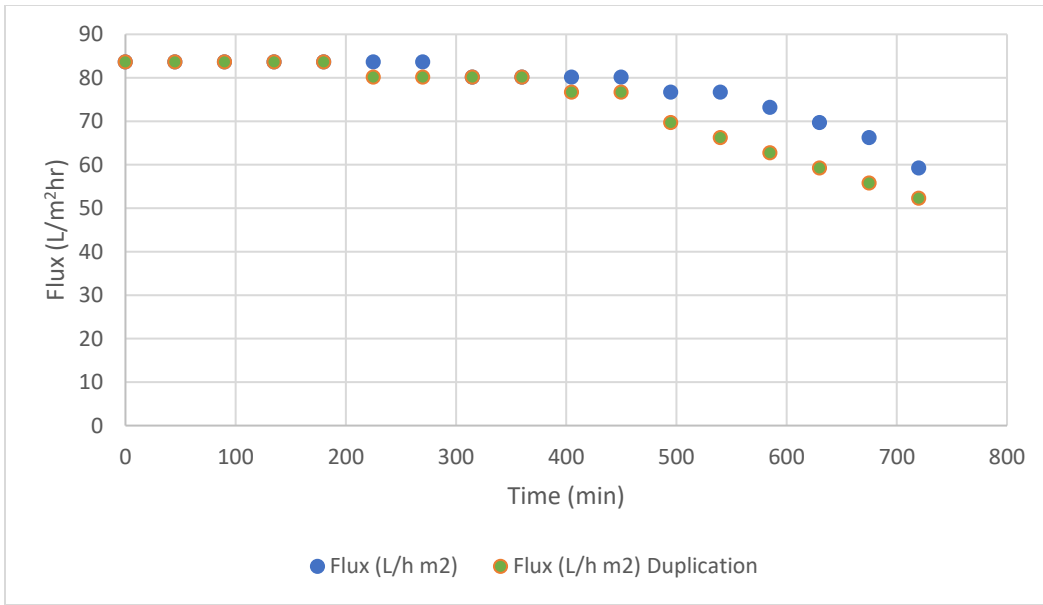
Figure E-2: Permeate flux decline of experimental run and duplication: NF, 10 bar, 35.5µg/l

Table E-7: Experimental conditions

Run	Duplication
Initial permeate flux (L/m² hr): 104,53	108,02
Feed P_0 (bar): 10	10
Piston P (bar): 13	13
Feed velocity (Hz): 12,05	12,05
Brine p (Kpa): 95	95
Initial Concentration: 44µg/l	44µg/l

Table E-8: Kinetic data for NF at 10 bar, 44 μg/l

Time (min)	Feed			Brine		Permeate							
	EC F (μS)	TDS F (mg/L)	Temperature (deg Cel)	EC (μS)	TDS (mg/L)	EC P (μS)	TDS P (mg/L)	Temperature ©	Time (hr)	Volume (L)	Flow Rate (l/h)	Flux (L/h m²)	% rejection
0	328,6	209,7	26,1			7,2	3,5	26,1	0,00416667	0,0055	1,32	95,83	97,81
90	351,7	232,6	26,1			5,7	2,9	26,2	0,00416667	0,0055	1,32	95,83	98,38
180	351,8	225,4	25,8			5,9	2,9	26,3	0,00416667	0,0052	1,32	90,60	98,32
270	359,9	227,8	26,2			5,8	2,9	26,3	0,00416667	0,0052	1,32	90,60	98,39
360	367,7	232,4	26,4			5,8	3	26,3	0,00416667	0,005	1,32	87,11	98,42
450	374,1	236,9	26,7			5,8	2,9	26,3	0,00416667	0,0048	1,32	83,63	98,45
540	380,4	239,1	26,8			5,9	3	26,3	0,00416667	0,0048	1,32	83,63	98,45

Table E-9: Duplication of kinetic data of NF at 10 bar, 44 µg/l

	Feed			Brine		Permeate							
Time (min)	EC F (µS)	TDS F (mg/L)	Temperature (deg Cel)	EC (µS)	TDS (mg/L)	EC P (µS)	TDS P (mg/L)	Temperature ©	Time (hr)	Volume (L)	Flow Rate (l/h)	Flux (L/h m²)	% rejection
0	346,2	223,9	24,9			7,5	3,7	25,7	0,0041 66667	0,0052	1,248	90,60	97,83
90	352,7	226,8	25			7,3	3,2	25,8	0,0041 66667	0,0052	1,248	90,60	97,93
180	359,2	231,4	25,6			7,1	3,5	25,9	0,0041 66667	0,0052	1,248	90,60	98,02
270	366,2	234,5	25,9			7,3	3,5	26	0,0041 66667	0,005	1,248	87,11	98,01
360	376,5	239,8	26,5			7,1	3,3	26,1	0,0041 66667	0,005	1,248	87,11	98,11
450	381,2	241,3	26,4			6,8	3,4	26,1	0,0041 66667	0,0048	1,248	83,63	98,22
540	386,5	244,1	26,5			6,5	3,2	26,2	0,0041 66667	0,0048	1,248	83,63	98,32
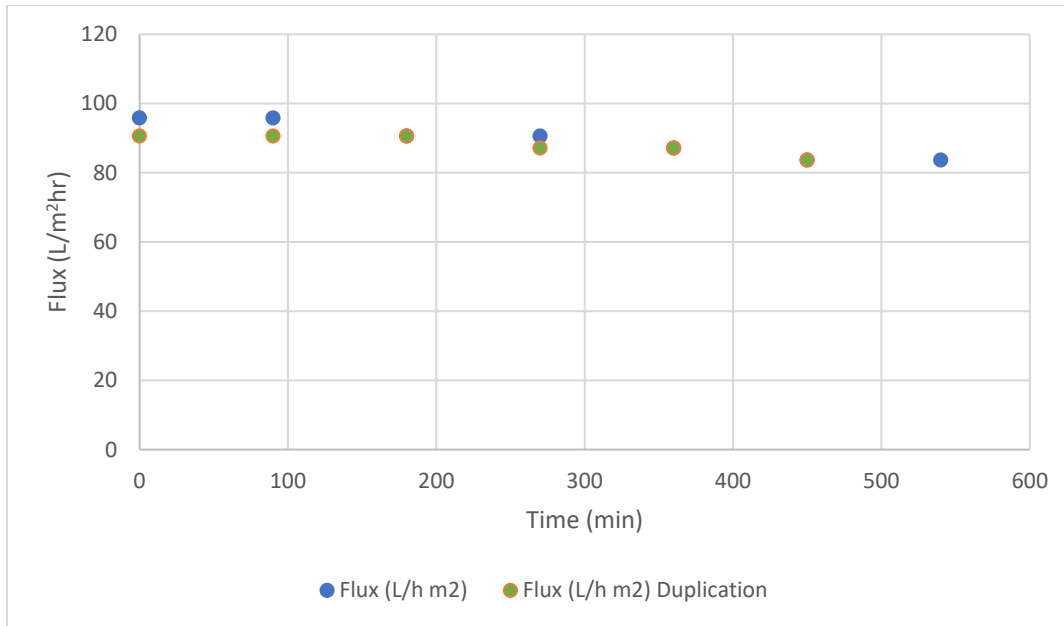
Figure E-3: Permeate flux decline of NF at 10 bar, 44µg/l

Table E-10: Experimental conditions

Initial permeate flux (L/m² hr): 55,75	Initial permeate flux (L/m² hr): 48,8
Feed P_0 (bar): 15	Feed P_0 (bar): 15
Piston P (bar): 13	Piston P (bar): 13
Feed velocity (Hz): 12,98	Feed velocity (Hz): 12,98
Brine p (Kpa): 95	Brine p (Kpa): 95
Initial Concentration: 22µg/l	Initial Concentration: 22µg/l
Feed pH: 6,78	Feed pH: 6,98

Table E-11: Kinetic data of NF at 15bar, 22µg/l

Time (min)	Feed			Brine		Permeate							
	EC F (µS)	TDS F (mg/L)	Temperature (deg Cel)	EC (µS)	TDS (mg/L)	EC P (µS)	TDS P (mg/L)	Temperature ©	Time (hr)	Volume (L)	Flow Rate (l/h)	Flux (L/h m²)	% rejection
0	321,8	230,2	20,6	322,2	227,5	5,3	3,9	20,6	0,004166667	0,0052	1,248	90,60	98,34
45	329,7	231,4	21,3	328,2	228,8	4,4	3,2	20,5	0,004166667	0,0052	1,248	90,60	98,67
90	338,6	233,3	22,1	342,4	235,4	3,8	2,8	20,9	0,004166667	0,0052	1,248	90,60	98,88
135	355,2	242,3	22,6	356,2	243,9	5,1	3,6	20,8	0,004166667	0,005	1,2	87,11	98,56
180	362,4	246,1	22,8	365,4	248,4	12,4	8,7	20,8	0,004166667	0,0052	1,248	90,60	96,58
225	371,1	250,9	23	373,6	251,9	12,6	8,9	20,9	0,004166667	0,0052	1,248	90,60	96,60
270	376,1	253,1	23,2	378,8	255,2	7,2	5,1	20,5	0,004166667	0,005	1,2	87,11	98,09
315	381,9	257,5	23,2	383,5	257,6	8,7	6,2	20,9	0,004166667	0,0048	1,152	83,63	97,72
360	389,8	261,9	23,4	392,7	263,5	10,6	7,5	21	0,004166667	0,0048	1,152	83,63	97,28
405	396,1	266,6	23,5	396,6	270,1	9,6	7,1	21,1	0,004166667	0,0046	1,104	80,15	97,58
450	401	274,3	23,9	402,2	277,2	9,2	6,9	21,1	0,004166667	0,0046	1,104	80,15	97,71

495	409,5	280,6	24	410,5	283,3	8,3	6,3	21	0,0041 66667	0,0044	1,056	76,45	97,97
540	413,1	282,2	24,1	416,6	284,9	8,1	5,9	21,2	0,0041 66667	0,0044	1,056	76,45	98,04
585	420,2	290,3	24,3	422,2	294,6	10,4	7,2	21,3	0,0041 66667	0,004	0,96	69,69	97,52
630	410,5	283,3	24	412,3	290,1	10,6	7,5	21,5	0,0041 66667	0,004	0,96	69,69	97,42
675	419,7	296,4	24,2	423,3	298,7	12	8,9	21,4	0,0041 66667	0,0038	0,912	66,21	97,14
720	422,8	300,6	24,4	429,6	308,5	9,7	7,6	21,2	0,0041 66667	0,0036	0,864	62,72	97,71

Table E-12: Duplication of NF at 15bar and 22µg/l

Time (min)	Feed EC F (µS)	Feed TDS F (mg/L)	Feed Temperature (deg Cel)	Brine EC (µS)	Brine TDS (mg/L)	Permeate EC P (µS)	Permeate TDS P (mg/L)	Permeate Temperature ©	Permeate Time (hr)	Permeate Volume (L)	Permeate Flow Rate (l/h)	Permeate Flux (L/h m²) Duplication	% rejection
0	316,5	222,8	21	318,2	224,8	5,8	4,3	19,7	0,00416667	0,0052	1,248	90,60	98,17
45	324,3	226,4	21,4	325,4	226,3	7,2	5,3	20	0,00416667	0,0052	1,248	90,60	97,78
90	334,8	230,9	22	338,4	233,5	6,7	4,9	20	0,00416667	0,0052	1,248	90,60	98,00
135	342,3	234,5	22,3	345	236,8	12,6	9,1	20,6	0,00416667	0,0052	1,248	90,60	96,32
180	351,4	238,7	22,7	354,8	240,7	8,4	5,9	20,6	0,00416667	0,0052	1,248	90,60	97,61
225	358,4	242,4	23	362,9	244,8	16,1	11,3	20,6	0,00416667	0,0052	1,248	90,60	95,51
270	372,6	249,4	23,6	378,3	252,2	10,9	7,7	21,4	0,00416667	0,0052	1,248	90,60	97,07
315	382,9	252,8	24,3	386,8	254	13,1	9,1	22,3	0,00416667	0,005	1,2	87,11	96,58
360	401,3	261,9	24,9	402,7	262,8	15,2	10,4	22,7	0,00416667	0,0048	1,152	83,63	96,21
405	414,5	267,4	25,4	417,2	269,1	15,8	10,5	23,1	0,00416667	0,0046	1,104	80,15	96,19

450	424,4	271,3	25,9	428,6	273,5	13,8	9,1	23,9	0,0041 66667	0,0046	1,104	80,15	96,75
495	440	277,5	26,6	443,8	279,2	10,9	7,1	24,1	0,0041 66667	0,0046	1,104	80,15	97,52
540	442,3	277,7	26,9	446,3	280,7	10,1	6,6	24,2	0,0041 66667	0,0044	1,056	76,45	97,72
585	450,4	282,1	26,9	452,6	283,4	8,5	5,7	24,5	0,0041 66667	0,0042	1,008	73,18	98,11
630	460,2	286,4	27	462,2	287,1	8,9	5,8	24,4	0,0041 66667	0,004	0,96	69,69	98,04
675	459,1	288,6	26,9	460,5	288,4	7,2	4,8	23,3	0,0041 66667	0,0038	0,912	66,21	98,43
720	461,8	294	26,3	463,9	294,1	6,9	4,5	22,2	0,0041 66667	0,0036	0,864	62,72	98,51
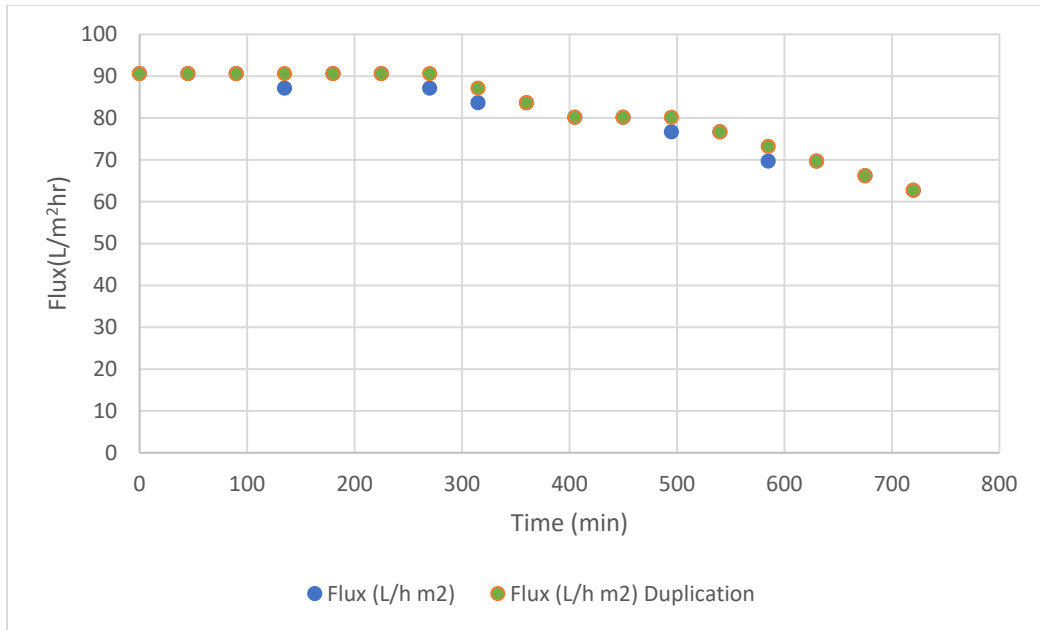
Figure E-4: Permeate flux decline of experimental run and duplication: NF at 15bar, 22µg/l

Table E-13: Experimental operating conditions

Initial permeate flux (L/m² hr): 94,08	Initial permeate flux (L/m² hr): 97,56
Feed P_0 (bar): 15	Feed P_0 (bar): 15
Piston P (bar): 13	Piston P (bar): 13
Feed velocity (Hz): 12,98	Feed velocity (Hz): 12,98
Brine p (Kpa): 95	Brine p (Kpa): 95
Initial Concentration: 44µg/l	Initial Concentration: 44µg/l
Feed pH: 7.22	Feed pH: 7.38

Table E-14: Kinetic data for NF, 15 bar, 44µg/l

	Feed			Brine		Permeate							
Time (min)	EC F (µS)	TDS F (mg/L)	Temperature (deg Cel)	EC (µS)	TDS (mg/L)	EC P (µS)	TDS P (mg/L)	Temperature ©	Time (hr)	Volume (L)	Flow Rate (l/h)	Flux (L/h m²)	% rejection
0	315,2	229,1	19,1	318,5	212,8	6,1	4,7	20,4	0,00416667	0,0054	1,296	94,08	98,06
45	318,5	230,2	19,5	313,2	217,6	5	3,6	20,8	0,00416667	0,0054	1,296	94,08	98,43
90	317,8	216,9	22,5	321	218,3	5	3,4	21,4	0,00416667	0,0054	1,296	94,08	98,43
135	325,6	219,4	23,3	22,5	222,7	4,9	3,6	21,9	0,00416667	0,0054	1,296	94,08	98,50
180	332,4	221,1	24,1	340,2	223,5	5,4	3,7	22,4	0,00416667	0,0054	1,296	94,08	98,38
225	345,1	224,2	25,1	338,9	226,2	5,9	3,8	22,9	0,00416667	0,0052	1,248	90,60	98,29
270	351,9	225,6	26	344,7	226,8	5,8	4,1	22,9	0,00416667	0,0052	1,248	90,60	98,35
315	346,8	224,9	25,8	351,3	228,9	5,4	3,7	23,5	0,00416667	0,0048	1,152	83,63	98,44
360	353,9	223,3	26,6	355,2	224,4	5,9	3,9	24	0,00416667	0,0046	1,104	80,15	98,33
405	357,1	224	26,8	353,3	221,9	6,1	4,2	25	0,00416667	0,004	0,96	69,69	98,29
450	351,8	220,4	27	353,5	220,8	6,7	4,7	24,8	0,00416667	0,0038	0,912	66,21	98,10

495	355,4	219,6	27,2	354,7	219,2	6,5	4,2	25	0,0041 66667	0,0038	0,912	66,21	98,17
540	353,1	215,6	27,9	353,5	217,8	7,5	5,3	25,3	0,0041 66667	0,0038	0,912	66,21	97,88
585	352,4	213,7	28,5	352,1	215,4	8,1	5,6	26	0,0041 66667	0,0036	0,864	62,72	97,70
630	356,4	215,7	28,9	356,7	215,6	8,4	5,3	25,8	0,0041 66667	0,0036	0,864	62,72	97,64
675	359,9	213,3	28,9	360	217,2	7,9	4,8	25,9	0,0041 66667	0,0036	0,864	62,72	97,80
720	362,2	216,6	29	365,1	216,3	8,2	5,5	26	0,0041 66667	0,0036	0,864	62,72	97,74

Table E-15: Duplication of kinetic data of NF at 15 bar, 44µg/l

	Feed			Brine		Permeate							
Time (min)	EC F (µS)	TDS F (mg/L)	Temperature (deg Cel)	EC (µS)	TDS (mg/L)	EC P (µS)	TDS P (mg/L)	Temperature ©	Time (hr)	Volume (L)	Flow Rate (l/h)	Flux (L/h m²) Duplication	% Rejection
0	315,1	214,3	20	316,5	212,6	6,1	4,1	22	0,0041 66667	0,0056	1,344	97,57	98,06
45	319,2	219,3	22,1	319,8	216,5	4,3	3	20,8	0,0041 66667	0,0056	1,344	97,57	98,65
90	321,2	215,1	22,2	321,5	220,2	4,2	2,9	20,7	0,0041 66667	0,0056	1,344	97,57	98,69
135	327,4	220,7	23	332,3	223,8	4,1	2,9	21,6	0,0041 66667	0,0056	1,344	97,57	98,75
180	336,7	223,7	23,9	343	229,4	4,5	3,2	22,3	0,0041 66667	0,0054	1,296	94,08	98,66
225	347,5	229,8	24,6	356,4	232,4	4,9	3,2	22,4	0,0041 66667	0,0054	1,296	94,08	98,59
270	356,3	231,2	25	362,8	236,2	4,9	33	23,7	0,0041 66667	0,0053	1,272	92,34	98,62
315	362,8	234,8	25,2	375,1	245	4,9	34	23,3	0,0041 66667	0,0053	1,272	92,34	98,65
360	381,2	240,4	26,1	385	245,2	5,7	38	23,4	0,0041 66667	0,0052	1,248	90,60	98,50
405	386,3	247,6	25,8	401,1	256,5	6,7	4,8	24	0,0041 66667	0,0052	1,248	90,60	98,27
450	389,3	255,1	25,9	405,6	260,1	5,8	44	24,1	0,0041 66667	0,005	1,2	87,11	98,51

495	394,6	250,5	26,2	407,3	258,1	5,7	24,7	24,2	0,0041 66667	0,0048	1,152	83,63	98,56
540	404,9	256,3	26,7	400,8	258,9	6,4	4,3	24,4	0,0041 66667	0,0048	1,152	83,63	98,42
585	417,8	261,3	27,1	427,8	267	7,3	5,1	24,5	0,0041 66667	0,0046	1,104	80,15	98,25
630	448,9	278,1	27,6	451,9	281,6	9,1	6	24,7	0,0041 66667	0,0046	1,104	80,15	97,97
675	459,2	283,1	27,9	461,9	285,7	7,1	4,7	24,3	0,0041 66667	0,0044	1,056	76,45	98,45
720	471,8	290,9	28	477,5	296,3	6,9	4,6	24,9	0,0041 66667	0,0044	1,056	76,45	98,54
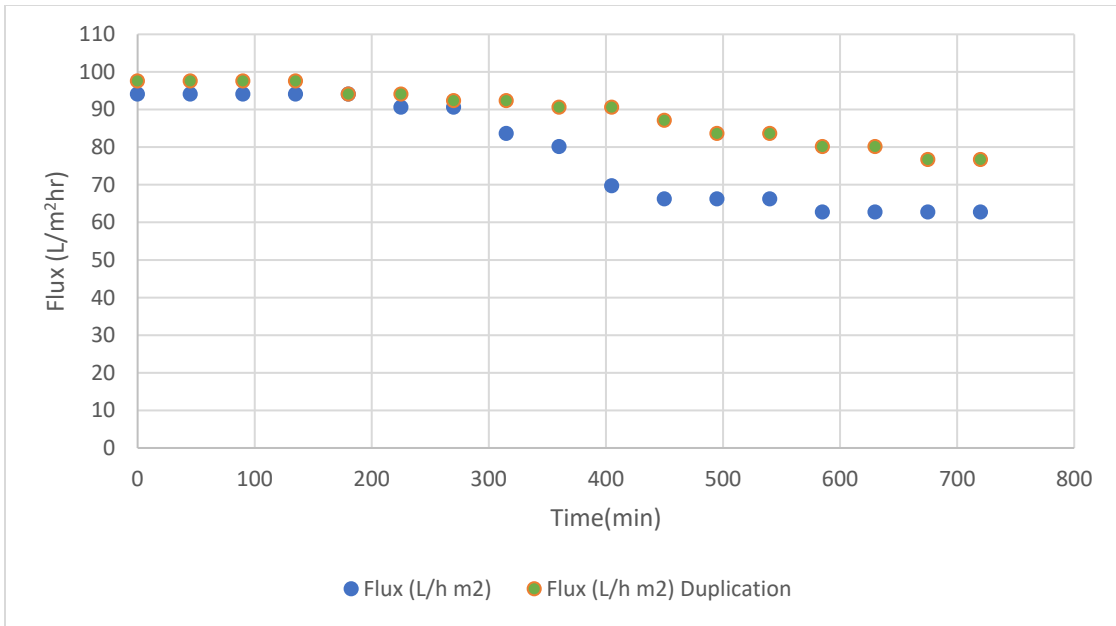
Figure E-5: permeate flux decline of experimental run and duplication: NF at 15 bar, 44µg/l

Table E-16: Kinetic data of NF at 15 bar, 35.5 μg/l

	Feed			Brine		Permeate							
Time (min)	EC F (μS)	TDS F (mg/L)	Temperature (deg Cel)	EC (μS)	TDS (mg/L)	EC P (μS)	TDS P (mg/L)	Temperature ©	Time (hr)	Volume (L)	Flow Rate (l/h)	Flux (L/h m²)	% rejection
0	328,5	214,7	24,5			11,05	5,5	24,2	0,0041 66667	0,0062	1,488	108,02 17786	96,636 2253
90	334,1	218,3	24,9			6,05	3,1	24,2	0,0041 66667	0,0062	1,488	108,02 17786	98,189 1649
180	342,1	221,7	25,1			5,8	2,9	24,4	0,0041 66667	0,0062	1,488	108,02 17786	98,304 5893
270	348,1	224,9	25,4			5,7	2,8	24,4	0,0041 66667	0,006	1,44	104,53 72051	98,362 5395
360	357	227,3	25,6			5,6	2,7	24,5	0,0041 66667	0,006	1,44	104,53 72051	98,431 3725
450	365,4	233,9	25,9			5,6	2,8	24,7	0,0041 66667	0,0058	1,392	101,05 26316	98,467 433
540	377,4	239,6	26,2			5,5	2,8	24,8	0,0041 66667	0,0058	1,392	101,05 26316	98,542 443

Table E-17: Duplication of kinetic data of NF, 15bar, 44 µg/l

Time(min)	Feed			Permeate							
	EC F (µS)	TDS F (mg/L)	Temperature (deg Cel)	EC P (µS)	TDS P (mg/L)	Temperature ©	Time (hr)	Volume (L)	Flow Rate (l/h)	Flux (L/h m²) Duplication	% Rejection
0	293,5	210,6	20,1	7,7	3,8	21,6	0,00416667	0,0062	1,488	108,02	97,38
90	300,2	219,5	20,3	4,1	3,2	21,6	0,00416667	0,0062	1,488	108,02	98,63
180	305,8	217,6	20,5	5,2	2,7	21,5	0,00416667	0,0062	1,488	108,02	98,30
270	318,6	223,1	21,1	4,7	2,4	21,7	0,00416667	0,0062	1,488	108,02	98,52
360	328,3	227,7	21,7	4,9	2,5	22,1	0,00416667	0,0062	1,488	108,02	98,51
450	336,3	231,5	22,1	4,9	2,3	22,1	0,00416667	0,0062	1,488	108,02	98,54
540	347,5	236,4	22,6	4,7	2,3	22,7	0,00416667	0,0062	1,488	108,02	98,65
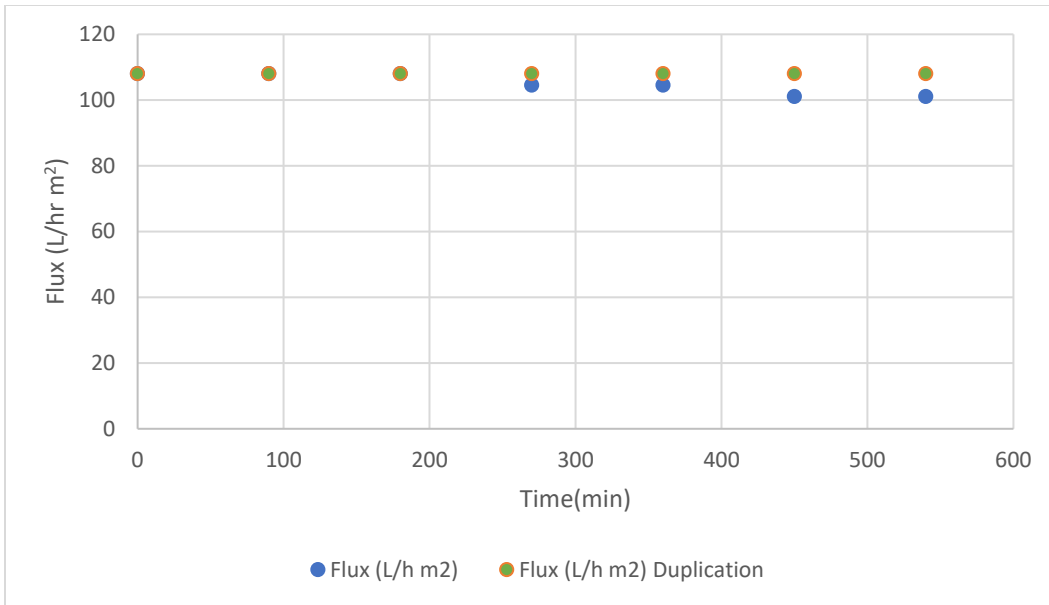
Figure E-6: Permeate flux decline of experimental run and duplication

Appendix F

Data from batch experiments

Experimental long runs: 100 hours

RO: 10 Bar, 44µg/l

NF: 10 Bar, 44µg/l

F. Appendix F

Table F-1: Experimental operating conditions

RO	NF
Initial permeate flux (L/m^2 hr): 97,56	Initial permeate flux (L/m^2 hr): 94,08
Feed P_0 (bar): 10	Feed P_0 (bar): 10
Piston P (bar): 13	Piston P (bar): 13
Feed velocity (Hz): 12,98	Feed velocity (Hz): 12,98
Brine p (Kpa): 95	Brine p (Kpa): 95
Initial Concentration: 44µg/l	Initial Concentration: 100mg/l
Feed pH: 7,2,	Feed pH:
Permeate pH: 5,79	5,96

Table F-2: Kinetic data of 100-hour experimental run with NF at 10 bar, 44µg/l

| Time (min) | Feed | | | Brine | | Permeate | | | | | | | |
	EC F (µS)	TDS F (mg/L)	Temperature (deg Cel)	EC (µS)	TDS (mg/L)	EC P (µS)	TDS P (mg/L)	Temperature ©	Time (hr)	Volume (L)	Flow Rate (l/h)	Flux (L/h m²) NF	% rejection
0	316,5	223,5	18,5	321,2	248,5	8,9	6,2	22,8	0,004166667	0,0054	1,296	94,08	97,19
300	390,4	241,6	27,6	397	245,7	9,1	6	24,6	0,004166667	0,0044	1,056	76,45	97,67
600	366,2	240,3	24,6	367	241,4	6,8	4,8	21,7	0,004166667	0,0038	0,912	66,21	98,14
900	383,9	238,7	27,5	383,3	239,8	10,3	7	24,1	0,004166667	0,0028	0,672	48,78	97,32
1200	384,9	241,8	26,9	386,1	241,7	11,7	7,7	23,2	0,004166667	0,0024	0,576	41,81	96,96
1500	388,9	242	27,4	390	243,5	12,7	8,5	23,8	0,004166667	0,0022	0,528	38,22	96,73
1800	392,9	241,7	28,4	395,6	242,1	15,1	10,2	24,6	0,004166667	0,0018	0,432	31,36	96,16
2100	394,5	242,8	28,1	400,7	245,6	16,3	11,2	24,3	0,004166667	0,0018	0,432	31,36	95,87
2400	402,5	249,4	27,6	403,3	249,8	12,5	8,4	23,4	0,004166667	0,0016	0,384	27,88	96,89
2700	421,2	259,4	27,8	423,6	260,9	18,5	13,8	24,7	0,004166667	0,0016	0,384	27,88	95,61
3000	429,3	462,6	28,3	437,3	267,3	18,2	12,3	24,5	0,004166667	0,0015	0,36	26,13	95,76
220	441,7	272,6	27,9	441,9	273,6	24,9	16,7	23,5	0,004166667	0,0014	0,336	24,39	94,36

3600	444,7	279,9	27,5	448,2	280	23,5	16,2	24	0,0041 66667	0,0013	0,312	22,65	94,72
3900	449,8	286,6	27,1	455,8	284,9	21,4	16	24,5	0,0041 66667	0,0012	0,288	20,91	95,24
4200	469,8	297,4	26,6	469,9	298,1	44,3	30,4	22,7	0,0041 66667	0,0012	0,288	20,91	90,57
4500	508	310	28,5	506,1	309,5	25,7	17,4	23,3	0,0041 66667	0,0012	0,288	20,91	94,94
4800	513,2	314	28,2	512,3	317,6	42,3	28,9	22,4	0,0041 66667	0,001	0,24	17,42	91,76
5100	518	325,1	27,5	528,2	329,6	24,6	16,9	22,2	0,0041 66667	0,001	0,24	17,42	95,25
5400	545	342,3	27,4	551,2	345,9	24,4	16,6	22,5	0,0041 66667	0,0009	0,216	15,68	95,52
5700	582	357	28,1	581,1	257,6	25,8	18	28,2	0,0041 66667	0,0008	0,192	13,94	95,57
6000	60,31	371,4	27,9	600,2	372,1	31,9	22,1	22,1	0,0041 66667	0,0008	0,192	13,94	47,11

Table F-3: Kinetic data of 100-hour experimental run with RO at 10 bar, 44µg/l

| Time (min) | Feed | | | Brine | | Permeate | | | | | | | |
	EC F (µS)	TDS F (mg/L)	Temperature (deg Cel)	EC (µS)	TDS (mg/L)	EC P (µS)	TDS P (mg/L)	Temperature ©	Time (hr)	Volume (L)	Flow Rate (l/h)	Flux (L/h m²)	% rejection
0	312,5	211,7	22	314,3	215,4	5,6	3,5	23,6	0,004166667	0,0056	1,344	97,57	98,21
300	348,8	215,4	27,8	353,1	217,3	9,5	6,1	28	0,004166667	0,0054	1,296	94,08	97,28
600	322,6	196,4	28,5	323,2	197,2	8,8	6,2	25,6	0,004166667	0,003	0,72	52,27	97,27
900	302,6	185,4	28,3	303,5	185,8	12,3	8,3	23,1	0,004166667	0,0022	0,528	38,22	95,94
1200	306,9	190,7	27,3	306	191,1	13,5	9,1	23,2	0,004166667	0,002	0,48	34,85	95,60
1500	308,7	195,2	26,5	310,2	196,2	15,1	10,1	21,6	0,004166667	0,0018	0,432	31,36	95,11
1800	306,2	194,8	26,2	311,5	199,9	16,5	10,9	23,7	0,004166667	0,002	0,48	34,85	94,61
2100	324,1	200,9	27,6	324,6	201,1	13,1	8,6	24,6	0,004166667	0,0018	0,432	31,36	95,96
2400	323,9	203,5	26,7	323,3	204,1	12,6	8,4	23,9	0,004166667	0,0016	0,384	27,88	96,11
2700	335,9	206,8	27,9	336,1	207,5	15,9	10,6	24,1	0,004166667	0,0016	0,384	27,88	95,27
3000	353,7	229,4	25	358,3	231,5	13,4	9,4	24,2	0,004166667	0,0018	0,432	31,36	96,21

220	368,9	228,8	27,6	370,5	230,2	10,3	6,5	25,4	0,0041 66667	0,0018	0,432	31,36	97,21
3600	22,6	204,4	27,4	329,5	207	7,8	5,4	23,1	0,0041 66667	0,0014	0,336	24,39	97,64
3900	332,1	205,8	27	333,3	210,8	8,5	6,6	22	0,0041 66667	0,0012	0,288	20,91	97,44
4200	336,4	210,6	26	339,1	216,6	11,1	7,8	22,1	0,0041 66667	0,001	0,24	17,42	96,70
4500	343,9	218,8	26,5	345,4	220,5	13,5	9	23,6	0,0041 66667	0,0008	0,192	13,94	96,07
4800	354,6	224,3	26,3	360,1	228,9	13,9	9,4	23,5	0,0041 66667	0,0008	0,192	13,94	96,08
5100	384,3	241,5	26,7	384,4	242,7	14,8	9,9	23,6	0,0041 66667	0,0008	0,192	13,94	96,15
5400	405,6	259,4	25,1	411,4	261,3	15,2	10,5	23,4	0,0041 66667	0,0008	0,192	13,94	96,25
5700	431,1	280,7	24,9	431,8	282,4	14,4	10	22,7	0,0041 66667	0,0008	0,192	13,94	96,66
6000	437,7	281,9	25,1	436,9	284,2	14,1	9,7	22,4	0,0041 66667	0,0008	0,192	13,94	96,78
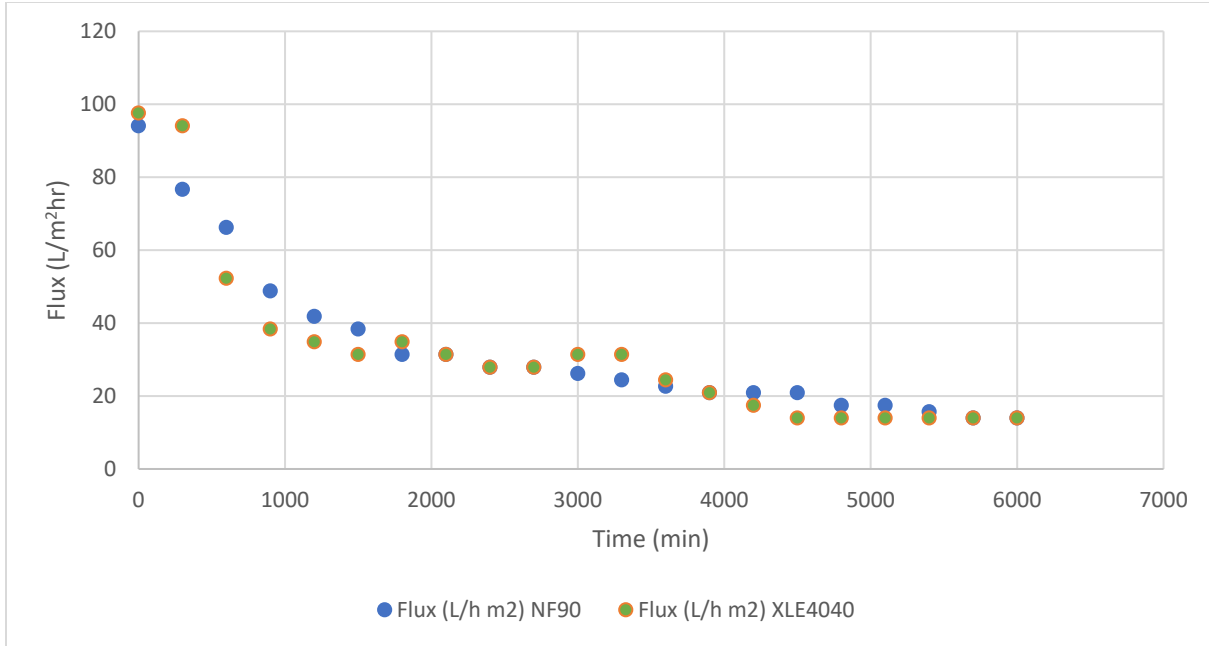
Figure F-1: Permeate flux decline of RO4040 and NF over 100 hours
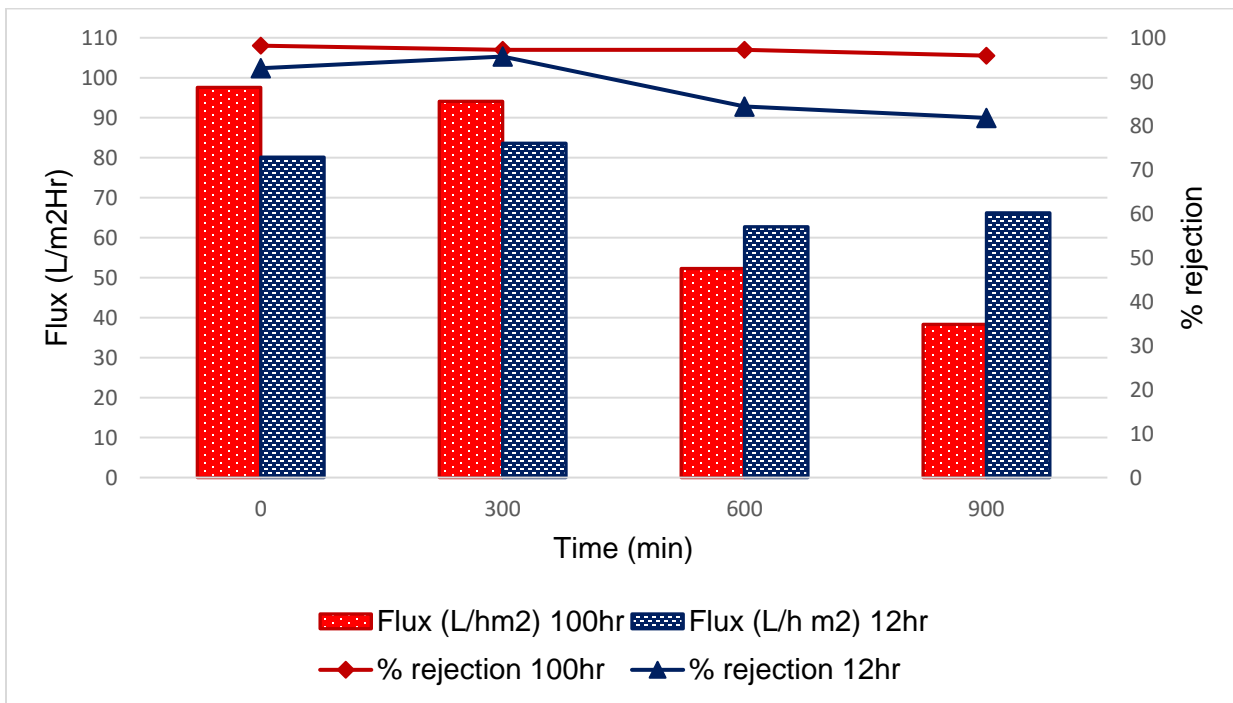
Figure F-2: The comparison of rejection and flux after 100 hr and 12 hr for RO under the same conditions
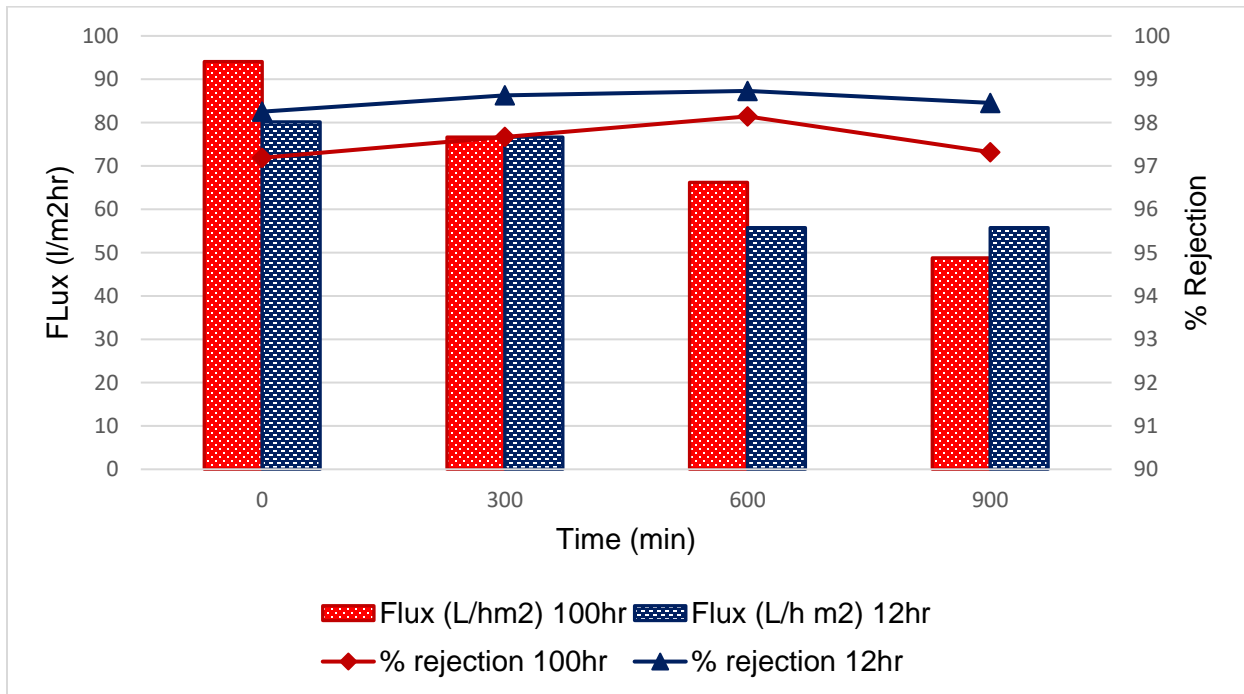
Figure F-3: The comparison of rejection and flux after 100 hr and 12 hr with NF run under the same conditions

Appendix G

Data from Batch experiments

Inorganics

G. Appendix G

The data below is that of inorganic removal with both RO and NF as a comparative analysis against different feed pressures.

Table G-1: Effluent concentration of ammonia (mg/l) after RO treatment

Feed pressure(bar)	NH$_3$-N	NH$_3$	NH$_4^+$
5	1,13	1,35	0,33
	0,17	0,21	0,14
	0,05	0,05	0,42
ave	**0,5**	**0,5**	**0,3**
atd	**0,6**	**0,7**	**0,1**
10	0,15	0,19	0,2
	0,11	0,13	0,22
	0,33	0,4	0,06
ave	**0,20**	**0,24**	**0,16**
std	**0,12**	**0,14**	**0,09**
15	0,3	0,37	0,39
	0,11	0,14	0,15
	0,32	0,39	0,42
ave	**0,24**	**0,30**	**0,32**
std	**0,12**	**0,14**	**0,15**

Table G-2: Effluent concentration of ammonia (mg/l) after NF treatment

Feed pressure (bar)	NH₃-N	NH₃	NH₄⁺
5	1,13	1,38	1,46
	0,14	0,17	0,18
	1,13	1,37	1,46
ave	**0,80**	**0,97**	**1,03**
std	**0,57**	**0,70**	**0,74**
10	0,17	0,21	0,22
	0,29	0,35	0,37
	0,25	0,31	0,23
ave	**0,237**	**0,290**	**0,273**
std	**0,061**	**0,072**	**0,084**
15	0,72	0,87	0,92
	0,58	0,7	0,74
	0,49	0,6	0,63
ave	**0,60**	**0,72**	**0,76**
std	**0,12**	**0,14**	**0,15**

Table G-3: Effluent concentration of phosphates(mg/l) after RO treatment

Feed pressure (bar)	PO_4^{3-}	P	P_2O_5
	0,08	0,03	0,06
5	0,1	0,03	0,08
	1,75	0,57	1,31
ave	**0,643**	**0,210**	**0,483**
std	**0,958**	**0,312**	**0,716**
	0,17	0,05	0,12
10	0,04	0,01	0,03
	0	0	0
ave	**0,070**	**0,020**	**0,050**
std	**0,089**	**0,026**	**0,062**
	0,05	0,02	0,04
15	0,02	0,01	0,01
	1,75	0,57	1,3
ave	**0,61**	**0,20**	**0,45**
std	**0,99**	**0,32**	**0,74**

Table G-4: Effluent concentration of phosphates(mg/l) after NF treatment

Feed pressure (bar)	PO$_4$ $^{3-}$	P	P$_2$O$_5$
	1,68	0,55	1,25
5	0,4	0,13	0,3
	0,68	0,22	0,5
ave	**0,9200**	**0,3000**	**0,6833**
std	**0,6729**	**0,2211**	**0,5008**
	0,17	0,06	0,13
10	0,14	0,05	0,11
	0,34	0,11	0,25
ave	**0,217**	**0,073**	**0,163**
std	**0,108**	**0,032**	**0,076**
	0,23	0,07	0,23
15	1,23	0,4	0,92
	0,26	0,09	0,2
ave	**0,573**	**0,187**	**0,450**
std	**0,569**	**0,185**	**0,407**

Table G-5: Effluent concentration of nitites after NF and RO treatment

Run	Nitrites (µg/L)		
	NO_2^- - N	NO_2^-	$NaNO_2^-$
5	1	6	10
	0	0	2
	0,667	1,67	2,67
ave	**0,56**	**2,56**	**4,89**
std	**0,51**	**3,10**	**4,44**
10	0	N.D	2
	0	0	N.D
	0	N.D	2
ave	**0**	**0**	**2**
std	**0**		**1,15**
15	N.D	5	8
	0	0	0
	N.D	0	0
ave	**0**	**1,67**	**2,67**
std		**2,89**	**4,62**
5	0	2	7
	0	n.d	n.d
	0	n.d	**7**
ave	**0,0**	**2,0**	**4,9**
std	**0,0**	**1,2**	**9,0**
10	0,33	1,67	3
	n.d	0	0
	n.d	0	**4**
ave	**0,33**	**0,56**	**4,58**
std	**0,19**	**0,96**	
15	0,5	1,8	8,5
	0	N.D	N.D
	0	6	9
ave	**0,17**	**3,90**	**8,75**
std	**0,29**	**3,08**	**5,06**

Data analysis of phosphorus at operating conditions with RO and NF membranes

Table G-6: Statistical T-test for RO at different feed pressure

t-Test: Two-Sample
Assuming Unequal Variances
Phosphorus removal by RO

	5 bar	15 bar
Mean	0,4825	0,1975
Variance	0,002492	0,000492
Observations	4	4
Hypothesized Mean Difference	0	
df	4	
t Stat	10,43576	
P(T<=t) one-tail	0,000238	
t Critical one-tail	2,131847	
P(T<=t) two-tail	0,000476	
t Critical two-tail	2,776445	

Table G-7: Statistical T-test of ammonia removal for RO and different feed pressures

t-Test: Two-Sample Assuming
Unequal Variances
Removal of phosphates at
different feed pressures by
RO membrane

	10 bar	15 bar
Mean	0,13	0,1975
Variance	0,0002	0,000492
Observations	4	4
Hypothesized Mean Difference	0	
df	5	
t Stat	-5,13317	
P(T<=t) one-tail	0,001833	
t Critical one-tail	2,015048	
P(T<=t) two-tail	0,003666	
t Critical two-tail	2,570582	

Table G-8: Statistical T-test of RO membrane at 5 & 10 bar

t-Test: Two-Sample Assuming
Unequal Variances
Removal of phosphorus by
RO membrane

	5 bar	10 bar
Mean	0,4825	0,13
Variance	0,002492	0,0002
Observations	4	4
Hypothesized Mean Difference	0	
df	3	
t Stat	13,58872	
P(T<=t) one-tail	0,000431	
t Critical one-tail	2,353363	
P(T<=t) two-tail	0,000862	
t Critical two-tail	3,182446	

Table G-9: Statistical T-test for ammonia at different feed pressures by RO membrane

t-Test: Two-Sample
Assuming Unequal Variances
Removal of ammonia by RO
membrane

	5 bar	*15 bar*
Mean	0,536667	0,3
Variance	0,335022	0,012867
Observations	4	4
Hypothesized Mean Difference	0	
df	3	
t Stat	0,802503	
P(T<=t) one-tail	0,240475	
t Critical one-tail	2,353363	
P(T<=t) two-tail	0,48095	
t Critical two-tail	3,182446	

Data analysis of COD at with RO and NF membranes

Table G-10: Effluent concentrations of COD with RO and NF membrane

Run	COD (mg/l)	Average	STD
5 Bar			
RO (run 1)	4,5		
RO(run 2)	4,7		
RO(run 3)	4	4,4	0,360555
NF (Run 16)	6,6		
NF (Run 17)	6,2		
NF (Run 18)	6,1	6,3	0,264575
10 Bar			
RO (run 4)	2,8		
RO(run 5)	2,5		
RO(run 6)	2,7	2,666666667	0,152753
NF (Run 13)	5,7		
NF (Run 14)	5,5		
NF (Run 15)	5,2	5,466666667	0,251661
15 Bar			
Run 7	3,2		
run8	3,6		
run9	3,4	3,4	0,2
Run 16	5,9		

run 17	6,2		
run 18	6,1	6,066666667	0,152753

Statistical analysis

Table G-11: t-test analysis of COD with RO and NF membrane at constant feed pressure of 10 bar

t-Test: Two-Sample Assuming Unequal Variances		
RO and NF at 10 bar, constant feed concentration		
	RO	NF
Mean	2,666667	5,466667
Variance	0,023333	0,063333
Observations	3	3
Hypothesized Mean Difference	0	
df	3	
t Stat	-16,4738	
P(T<=t) one-tail	0,000243	
t Critical one-tail	2,353363	
P(T<=t) two-tail	0,000487	
t Critical two-tail	3,182446	

Appendix H

Data from batch experiments

(Scanning electron microscopy- Energy Dispersive X-Ray)SEM-EDX data for RO and NF

H. *:* Appendix H

The data below is the analysis of the membrane's surface in which SEM-EDX analysis was performed on RO and NF membranes under different operating conditions.

Table H-1: EDX data for RO at 10 bar, 35.5µg/l

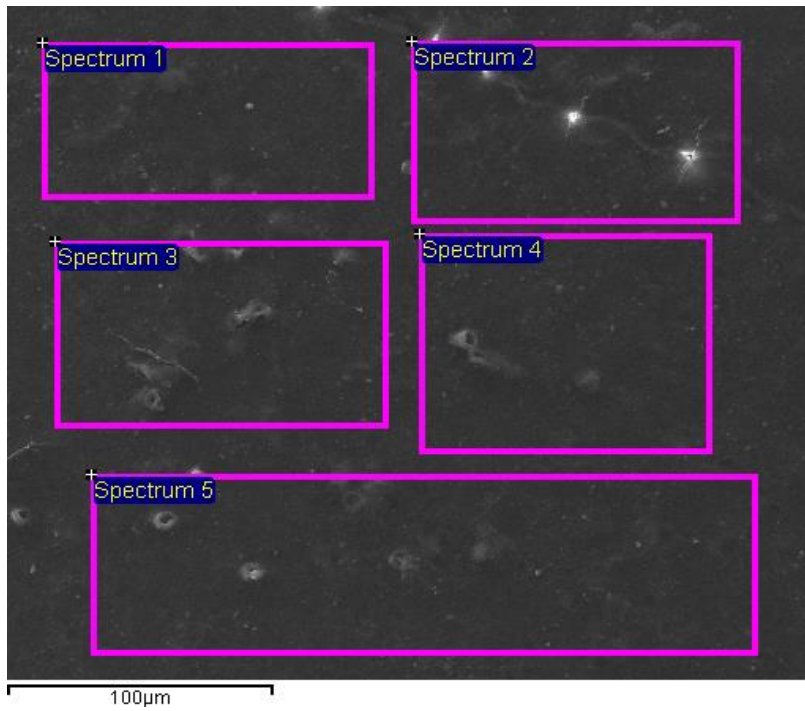| Sample: RO 10 bar 44µg/l								
Processing option: All elements analysed (Normalised)								
All results in weight%								
Spectrum	In stats.	C	O	Al	Si	S	Fe	Total
Spectrum 1	Yes	59,57	31,58	1,51	0,81	6,26	0,26	100
Spectrum 2	Yes	60,43	30,71	1,68	0,87	5,76	0,55	100
Spectrum 3	Yes	59,81	31,16	1,58	0,98	6,12	0,34	100
Spectrum 4	Yes	61,78	29,78	1,29	0,81	6,06	0,29	100
Spectrum 5	Yes	61,02	29,92	1,5	0,88	6,37	0,31	100
Mean		60,52	30,63	1,51	0,87	6,11	0,35	100
Std. deviation		0,9	0,78	0,15	0,07	0,23	0,11	
Max.		61,78	31,58	1,68	0,98	6,37	0,55	
Min.		59,57	29,78	1,29	0,81	5,76	0,26	

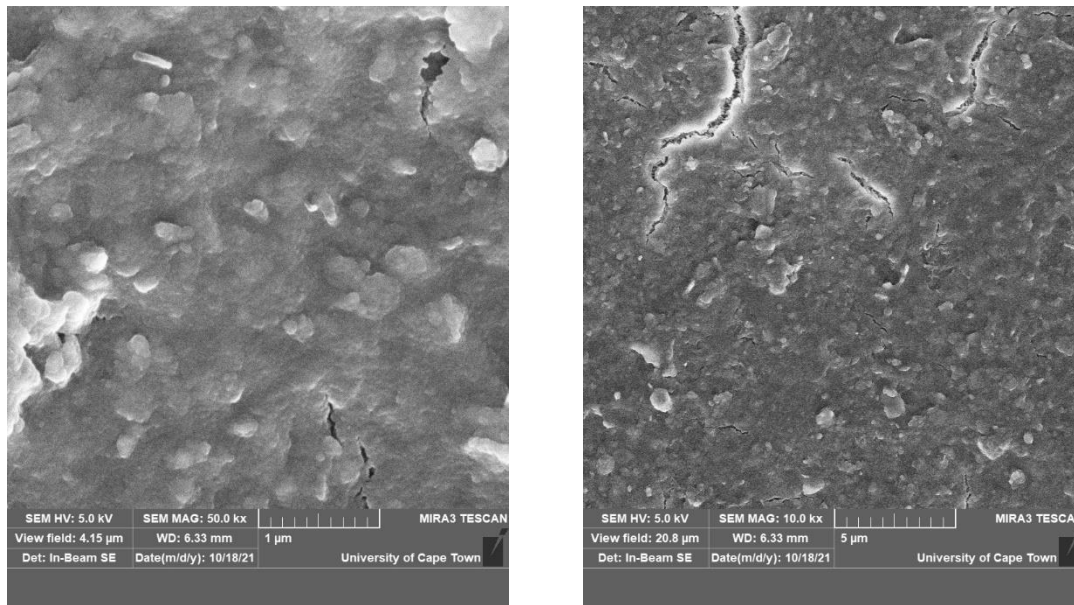**Figure H-1: SEM image of RO at 10 Bar, 35.5μg/l**

Figure H-2: Top view of SEM image of RO, 10 Bar, 35.5 μg/l at 50K (left) and 10K (right) resolution

Table H-2: EDX analysis of RO at 10 Bar, 44 µg/l

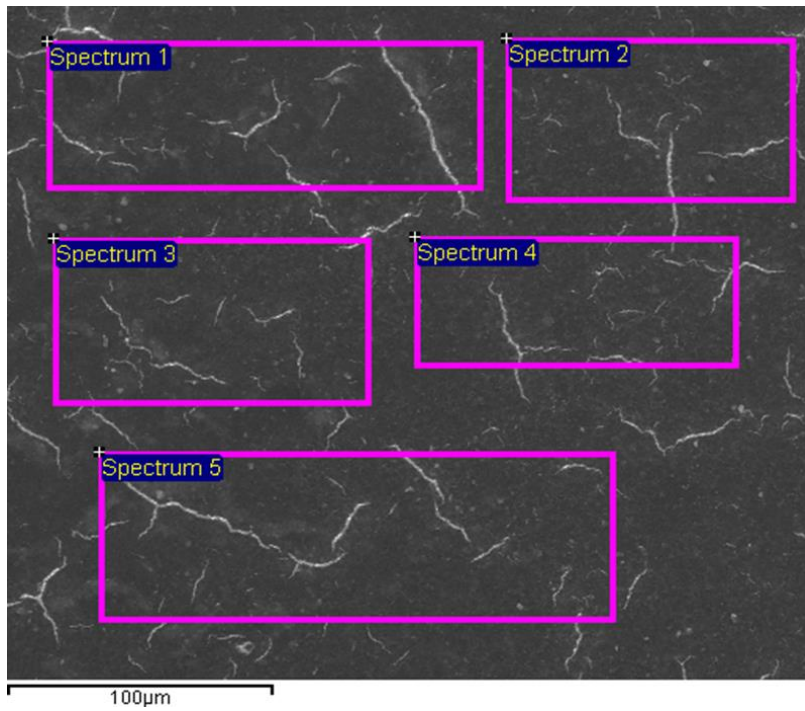| Sample: RO 10 Bar,44µg/l										
Processing option: All elements analysed (Normalised)										
All results in weight%										
Spectrum	In stats.	C	O	F	Al	Si	S	Cl	Ca	Total
Spectrum 1	Yes	66,18	26,75	0,7	0,31	0,36	5,38	0,19	0,14	100
Spectrum 2	Yes	67,55	25,9	0	0,29	0,36	5,54	0,16	0,2	100
Spectrum 3	Yes	65,4	26,95	1,18	0,39	0,36	5,38	0,18	0,16	100
Spectrum 4	Yes	66,52	26	1,14	0,28	0,3	5,39	0,2	0,17	100
Spectrum 5	Yes	66,25	26,23	0,99	0,38	0,39	5,42	0,2	0,14	100
Mean		66,38	26,37	0,8	0,33	0,36	5,42	0,18	0,16	100
Std. deviation		0,77	0,46	0,49	0,05	0,03	0,07	0,02	0,03	
Max.		67,55	26,95	1,18	0,39	0,39	5,54	0,2	0,2	
Min.		65,4	25,9	0	0,28	0,3	5,38	0,16	0,14	

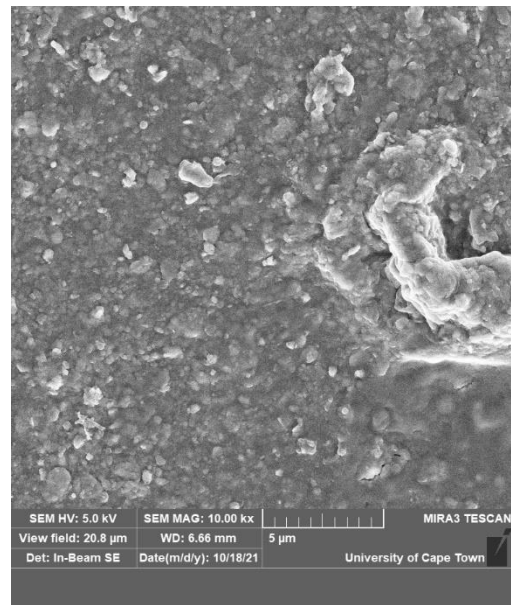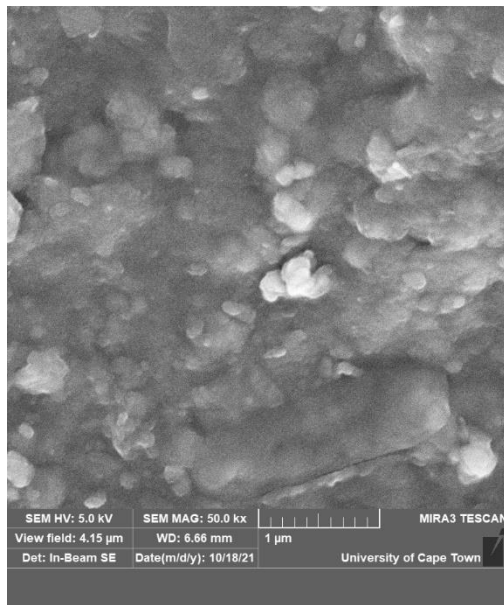*Figure H-3: SEM image of RO at 10 Bar, 44µg/l*

Figure H-4: SEM image top view of memrbanes surface for RO at 10 bar, 44µg/l

Table H-3: EDX analysis of RO at 10 bar, 22µg/l

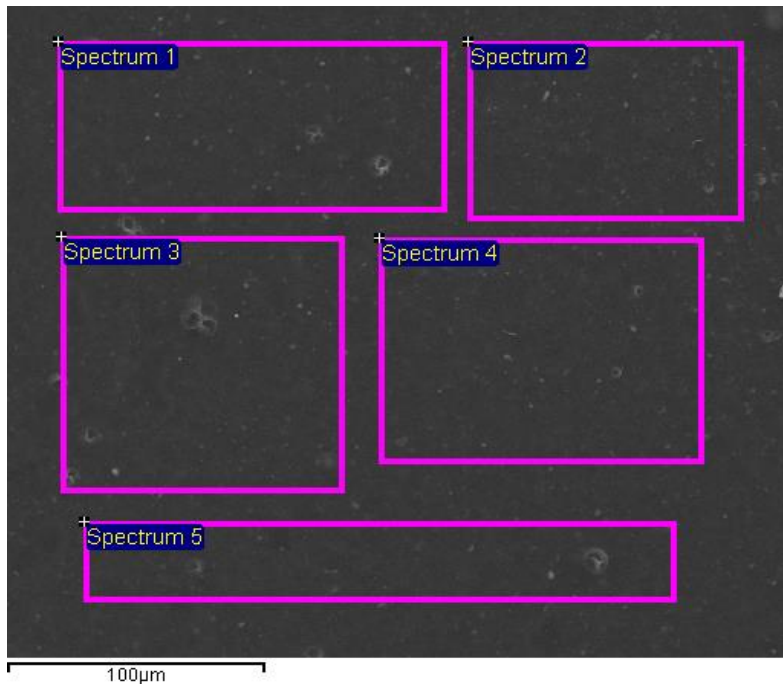| Sample: RO 10 bar, 22µg/l									
Processing option: All elements analysed (Normalised)									
All results in weight%									
Spectrum	In stats.	C	O	Mg	Al	Si	S	Ca	Total
Spectrum 1	Yes	62,63	31,56	0,19	0,39	0,59	4,44	0,2	100
Spectrum 2	Yes	63,92	30,23	0,17	0,37	0,49	4,68	0,13	100
Spectrum 3	Yes	62,14	31,95	0,19	0,44	0,58	4,5	0,21	100
Spectrum 4	Yes	62,65	31,56	0,19	0,41	0,49	4,54	0,17	100
Spectrum 5	Yes	62,11	31,99	0,21	0,44	0,58	4,47	0,2	100
Mean		62,69	31,46	0,19	0,41	0,54	4,53	0,18	100
Std. deviation		0,73	0,71	0,02	0,03	0,05	0,09	0,03	
Max.		63,92	31,99	0,21	0,44	0,59	4,68	0,21	
Min.		62,11	30,23	0,17	0,37	0,49	4,44	0,13	

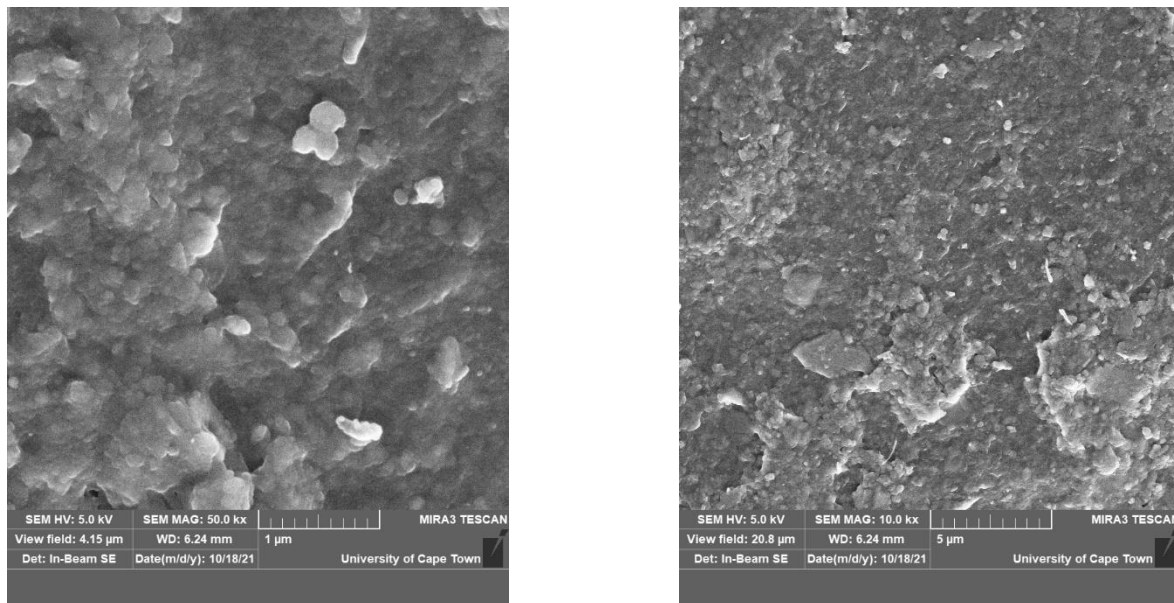**Figure H-5: SEM sample image for EDX analysis of RO, 10 bar, 22µg/**

Figure H-6: SEM image of the top view of RO 10 bar, 22ug/l with a 50K resolution (Left) and a 10K resolution (right)

Table H-4: EDX analysis of RO at 15 Bar, 22 µg/

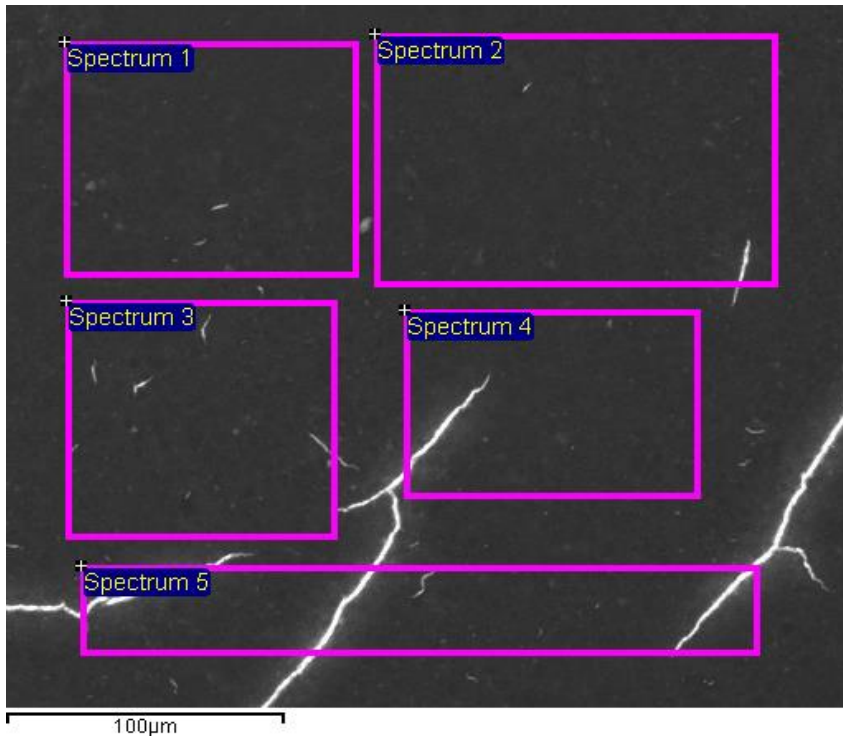| Sample: RO 15 bar 22µg/l								
Processing option: All elements analysed (Normalised)								
All results in weight%								
Spectrum	In stats.	**C**	**O**	**Al**	**Si**	**S**	**Ca**	**Total**
Spectrum 1	Yes	63,84	28,96	0,35	0,35	6,3	0,2	100
Spectrum 2	Yes	62,15	30,51	0,42	0,48	6,2	0,24	100
Spectrum 3	Yes	61,16	31,45	0,39	0,55	6,01	0,43	100
Spectrum 4	Yes	61,44	31,17	0,44	0,59	6,04	0,32	100
Spectrum 5	Yes	61,63	31,29	0,47	0,53	5,77	0,3	100
Mean		62,05	30,68	0,41	0,5	6,06	0,3	100
Std. deviation		1,07	1,02	0,05	0,1	0,2	0,09	
Max.		63,84	31,45	0,47	0,59	6,3	0,43	
Min.		61,16	28,96	0,35	0,35	5,77	0,2	

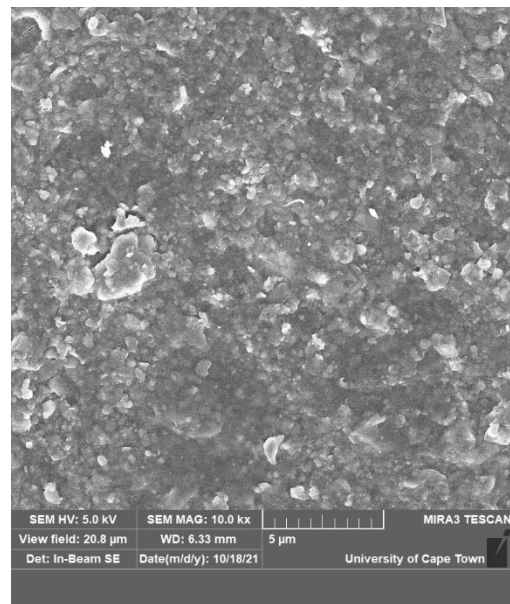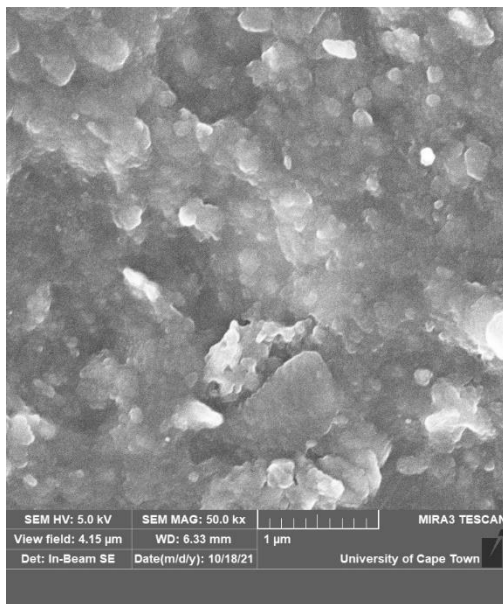*Figure H-7: SEM sample image for EDX analysis of RO, 15 bar, 22µg/l*

Figure H-8: SEM image of the top view of RO 15 bar, 22µg/l with a 50K magnification (Left) and a 10K resolution (right)

Table H-5: EDX analysis of RO at 15 Bar, 44 µg/l

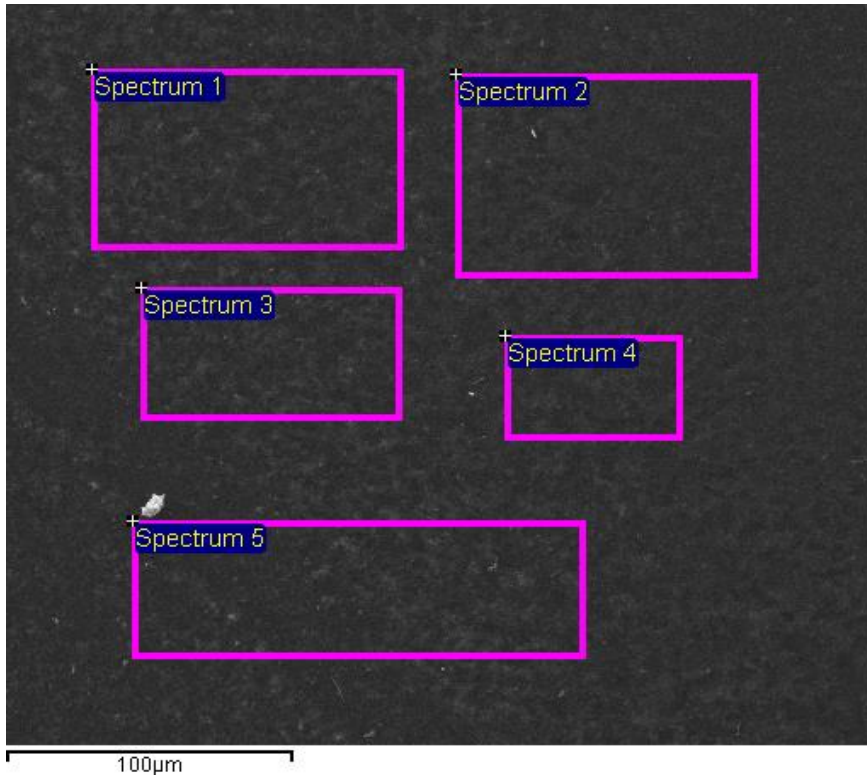| Sample: RO 15bar, 44µg/l							
Processing option: All elements analysed (Normalised)							
All results in weight%							
Spectrum	In stats.	C	O	Al	Si	S	Total
Spectrum 1	Yes	59,71	33,33	0,54	0,93	5,49	100
Spectrum 2	Yes	61,16	31,85	0,51	0,8	5,67	100
Spectrum 3	Yes	60,22	32,82	0,65	0,78	5,53	100
Spectrum 4	Yes	60,23	32,56	0,54	0,61	6,06	100
Spectrum 5	Yes	60,61	32,62	0,48	0,59	5,7	100
Mean		60,39	32,64	0,54	0,74	5,69	100
Std. deviation	0,54		0,53	0,07	0,14	0,22	
Max.		61,16	33,33	0,65	0,93	6,06	
Min.		59,71	31,85	0,48	0,59	5,49	

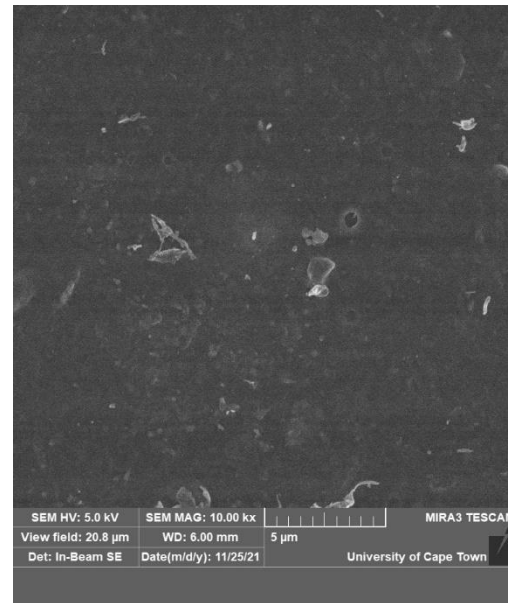**Figure H-9: SEM sample image for EDX analysis of RO, 15 bar, 44μg**
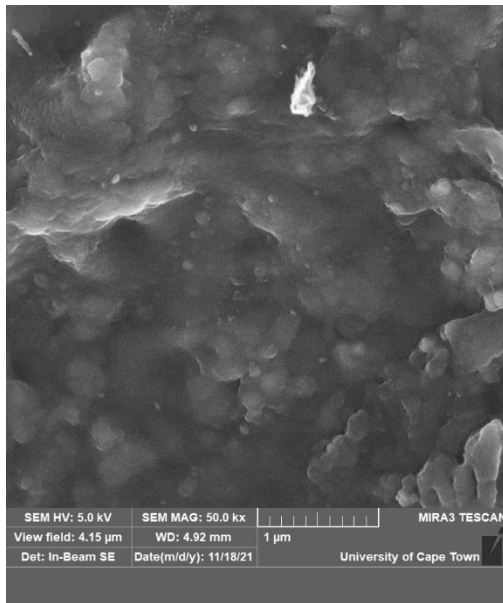

Figure H-10: SEM image of the top view of RO 15 bar, 44μg/l with a 50K magnification (Left) and a 10K magnification (right)

Table H-6: EDX analysis of RO at 15 Bar, 35.5 µg/l

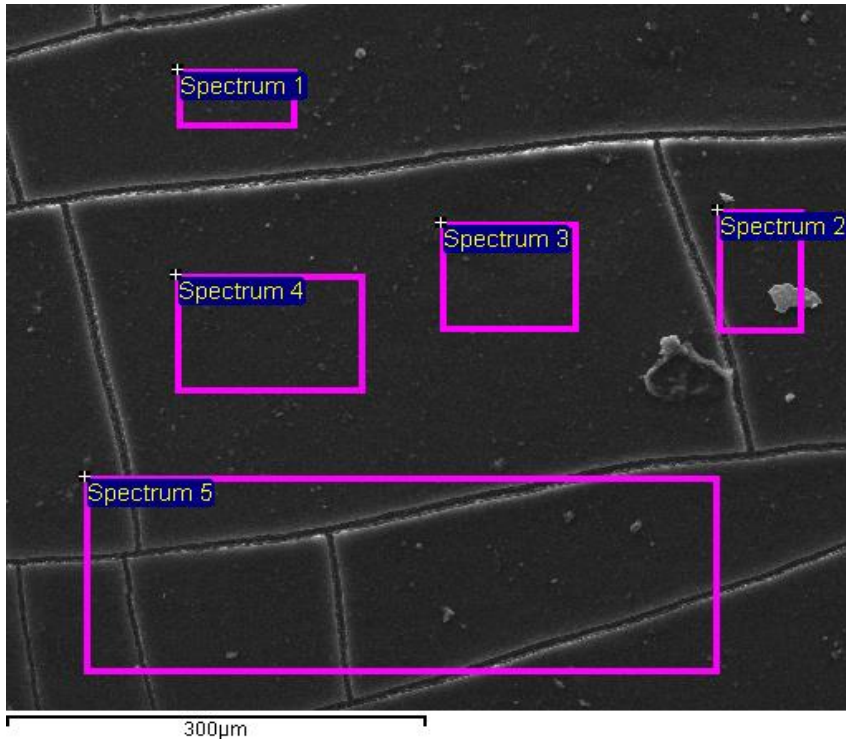| Sample: RO4040 15 Bar, 35.5µg/l										
Processing option : All elements analysed (Normalised)										
All results in weight%										
Spectrum	In stats.	C	O	Mg	Al	Si	P	S	Ca	Total
Spectrum 1	Yes	60,06	32,01	0,7	0,89	1,37	1,39	2,63	0,95	100
Spectrum 2	Yes	56,51	36,22	0,61	0,76	1,63	1,3	2,14	0,83	100
Spectrum 3	Yes	59,55	32,92	0,55	0,88	1,51	1,31	2,52	0,77	100
Spectrum 4	Yes	60,79	31,82	0,58	0,91	1,48	1,28	2,16	0,98	100
Spectrum 5	Yes	60,78	31,05	0,62	0,95	1,43	1,29	2,96	0,92	100
Mean		59,54	32,81	0,61	0,88	1,48	1,32	2,48	0,89	100
Std. deviation		1,77	2,02	0,06	0,07	0,09	0,04	0,34	0,09	
Max.		60,79	36,22	0,7	0,95	1,63	1,39	2,96	0,98	
Min.		56,51	31,05	0,55	0,76	1,37	1,28	2,14	0,77	

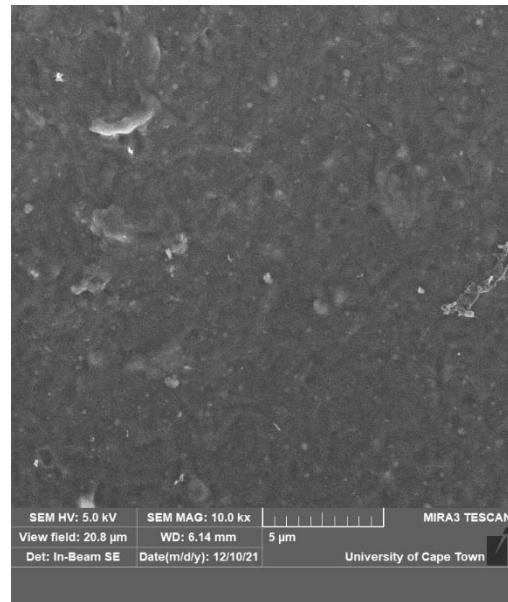*Figure H-11: SEM sample image for EDX analysis of RO, 15 bar, 35.5µg/l*
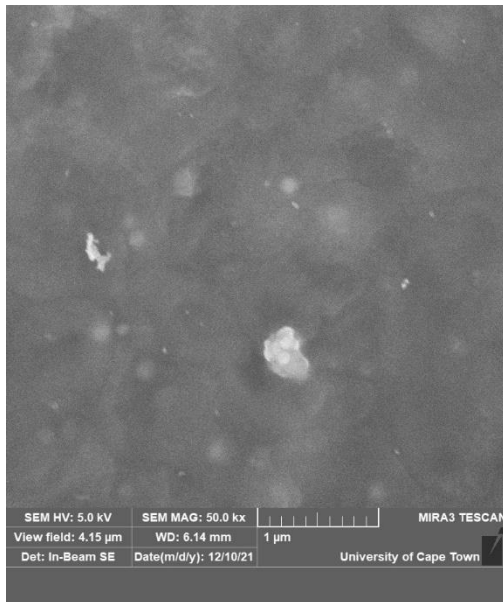

Figure H-12: SEM image of the top view of RO 15 bar, 35.5µg/l with a 50K magnification (Left) and a 10K magnification (right)

Table H-7: EDX analysis of RO at 5 Bar, 22 µg/l

Spectrum	In stats.	C	O	Mg	Al	Si	S	Ca	Total
-9									

Spectrum 1	Yes	56,29	34,76	0,35	0,82	0,92	6,46	0,4	100
Spectrum 2	Yes	58,46	32,96	0,22	0,7	0,82	6,58	0,27	100
Spectrum 3	Yes	57,27	33,79	0,3	0,84	0,93	6,54	0,32	100
Spectrum 4	Yes	59,34	32,09	0,22	0,76	0,68	6,6	0,3	100
Spectrum 5	Yes	59,6	31,91	0,27	0,73	0,75	6,55	0,2	100
Mean		58,19	33,1	0,27	0,77	0,82	6,55	0,3	100
Std. deviation		1,4	1,19	0,06	0,06	0,11	0,05	0,07	
Max.		59,6	34,76	0,35	0,84	0,93	6,6	0,4	
Min.		56,29	31,91	0,22	0,7	0,68	6,46	0,2	

Sample: RO 5 bar 22µg/l

Processing option: All elements analysed (Normalised)
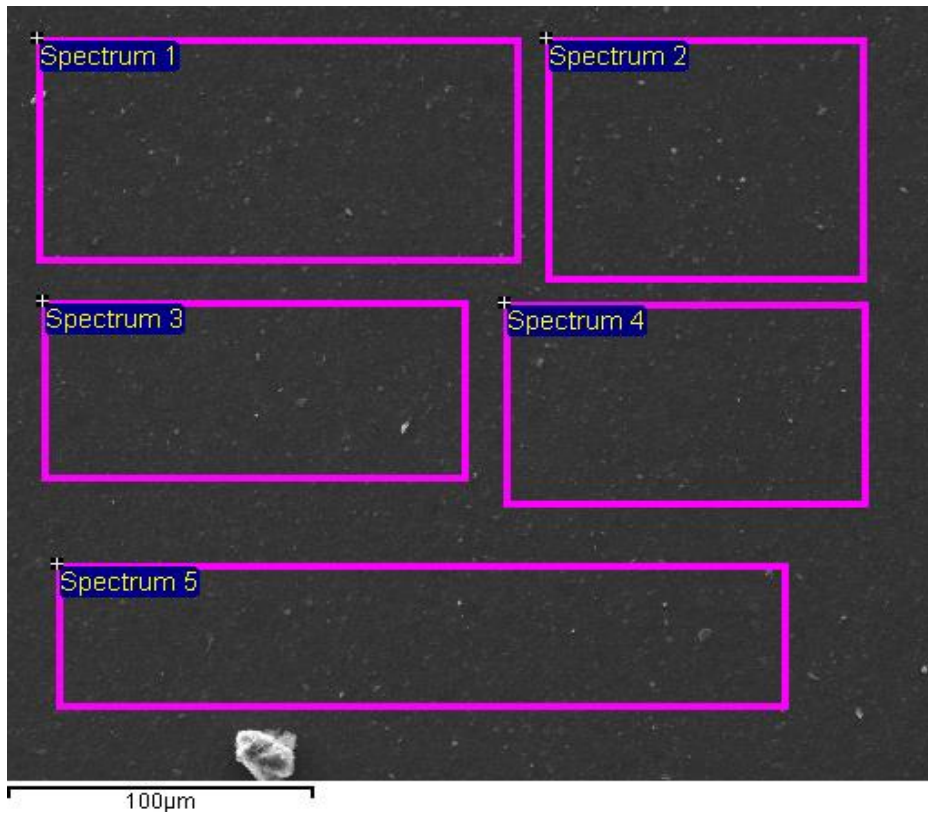
All results in weight%

Figure H-13: SEM sample image for EDX analysis of RO, 5 bar, 22μg/l
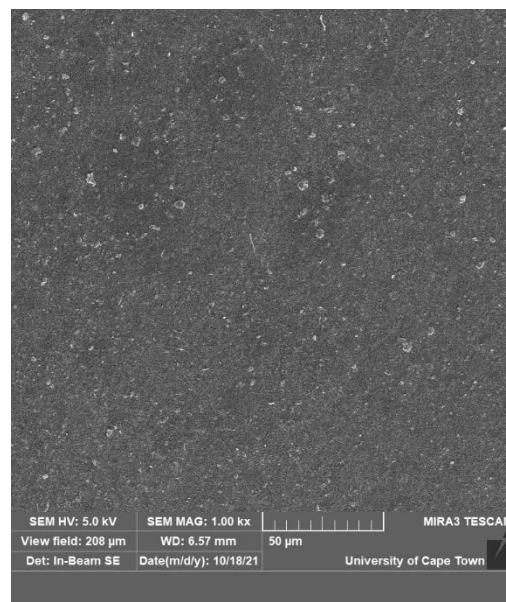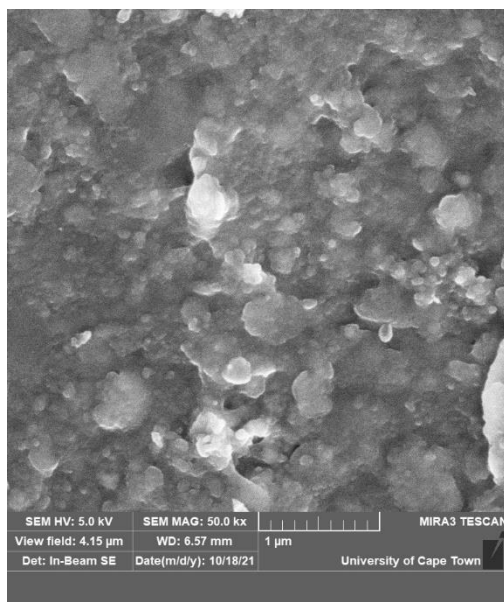

Figure H-14: SEM image of the top view of RO 5 bar, 22μg/l with a 50K magnification (Left) and a 10K magnification (right)

Table H-8: EDX analysis of RO at 5 Bar, 35.5 µg/l

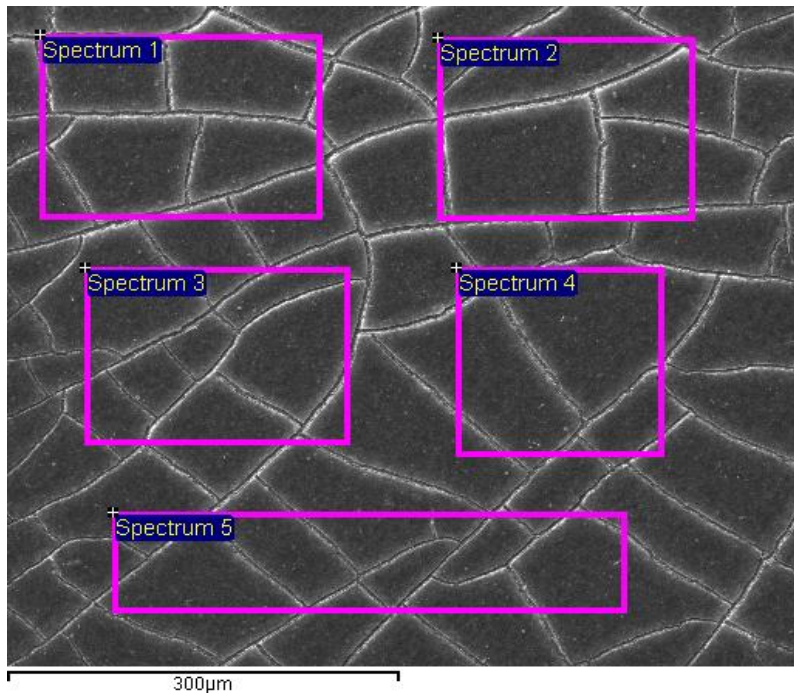| Sample: RO 5 bar 35.5 µg/l									
Processing option : All elements analysed (Normalised)									
All results in weight%									
Spectrum	In stats.	C	O	Mg	Al	Si	P	S	Ca	Total
Spectrum 1	Yes	60,17	31,54	0,56	0,7	1,13	0,83	4,25	0,81	100
Spectrum 2	Yes	58,21	33,66	0,53	1,06	1,18	0,9	3,56	0,9	100
Spectrum 3	Yes	59,51	33,06	0,46	0,59	0,91	0,54	4,31	0,61	100
Spectrum 4	Yes	59,98	32,63	0,49	0,56	0,89	0,97	3,73	0,75	100
Spectrum 5	Yes	60,75	31,57	0,63	0,41	0,99	0,8	4,16	0,68	100
Mean		59,72	32,49	0,53	0,66	1,02	0,81	4	0,75	100
Std. deviation		0,96	0,93	0,07	0,24	0,13	0,16	0,33	0,11	
Max.		60,75	33,66	0,63	1,06	1,18	0,97	4,31	0,9	
Min.		58,21	31,54	0,46	0,41	0,89	0,54	3,56	0,61	

Figure H-15: SEM sample image for EDX analysis of RO, 5 bar, 35.5µg/l
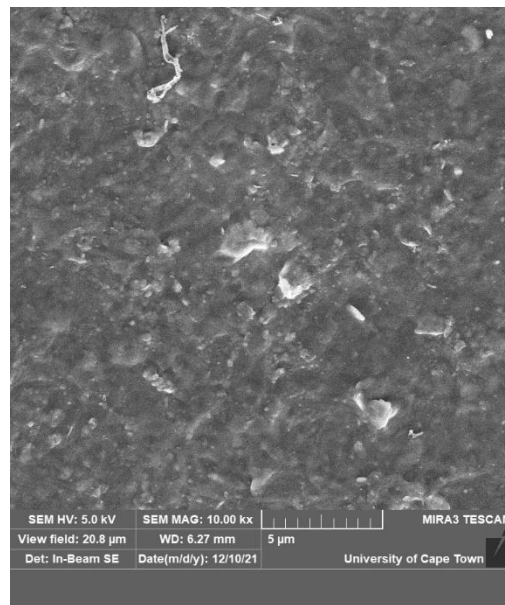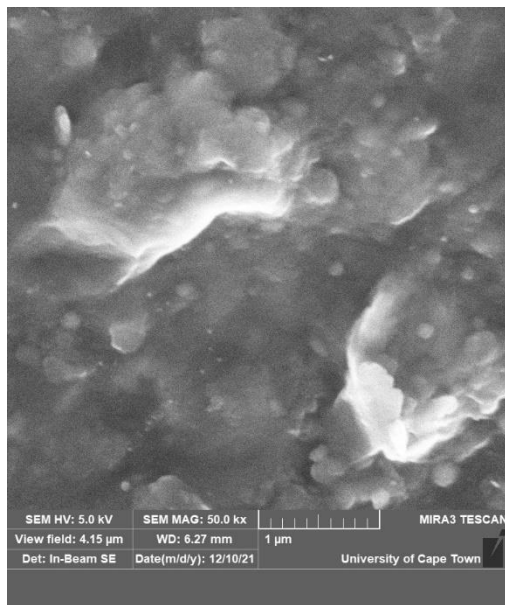

Figure H-16: SEM image of the top view of RO 5 bar, 35.5µg/l with a 50K magnification (Left) and a 10K rmagnification (right)

Table H-9: EDX analysis of RO at 5 Bar, 44 µg/l

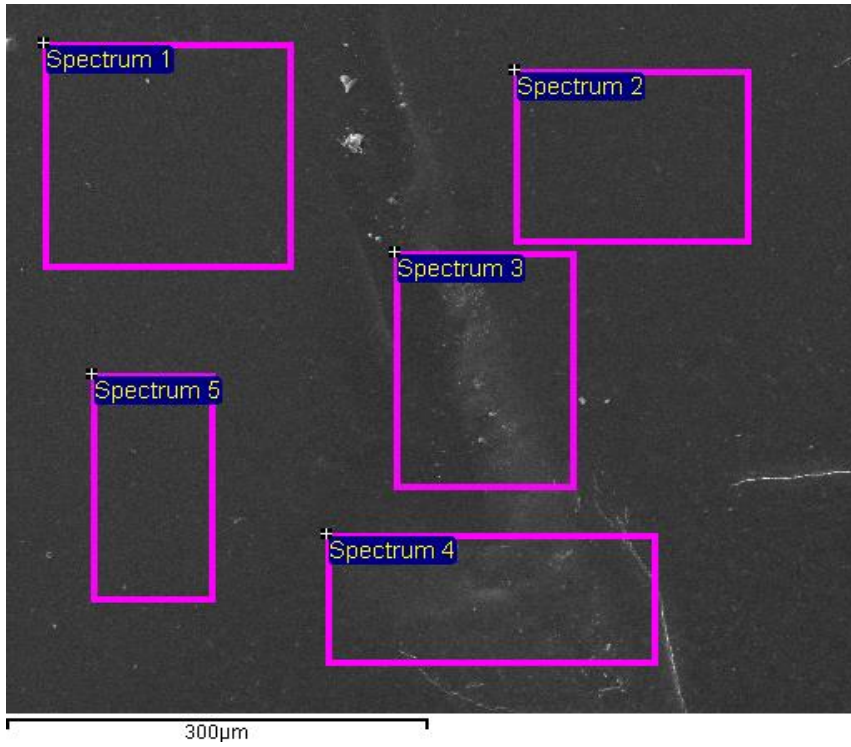| Sample: RO 5 bar 44µg/l					
All results in weight%					
Processing option : All elements analysed (Normalised)					
Spectrum	In stats.	C	O	S	Total
Spectrum 1	Yes	69,85	24,28	5,87	100
Spectrum 2	Yes	72,1	22,12	5,77	100
Spectrum 3	Yes	72,1	21,27	6,63	100
Spectrum 4	Yes	70,63	24,21	5,16	100
Spectrum 5	Yes	74,44	19,16	6,4	100
Mean		71,82	22,21	5,97	100
Std. deviation		1,76	2,15	0,58	
Max.		74,44	24,28	6,63	
Min.		69,85	19,16	5,16	

Figure H-17: : SEM sample image for EDX analysis of RO, 5 bar, 44μg/l
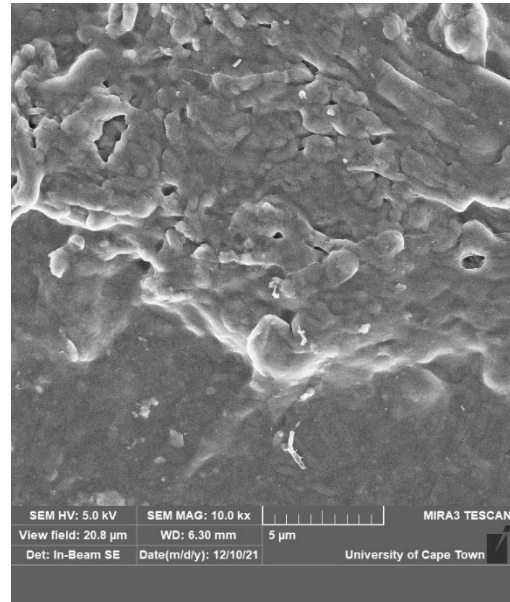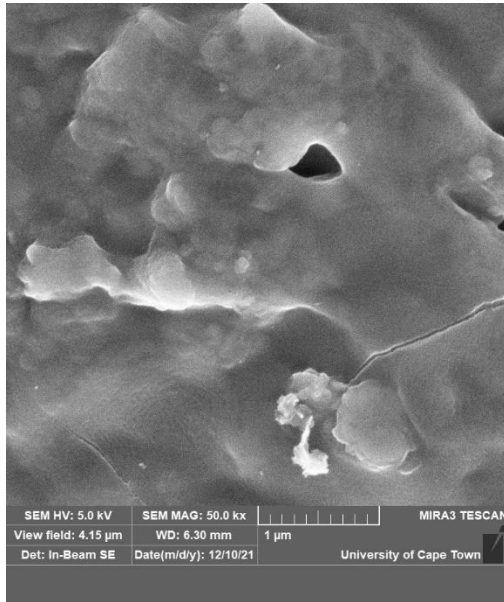
l

Figure H-18: SEM image of the top view of RO 5 bar, 44μg/l with a 50K magnification (Left) and a 10K rmagnification (right)

Table H-10: EDX analysis of NF at 5 Bar, 35.5 µg/l

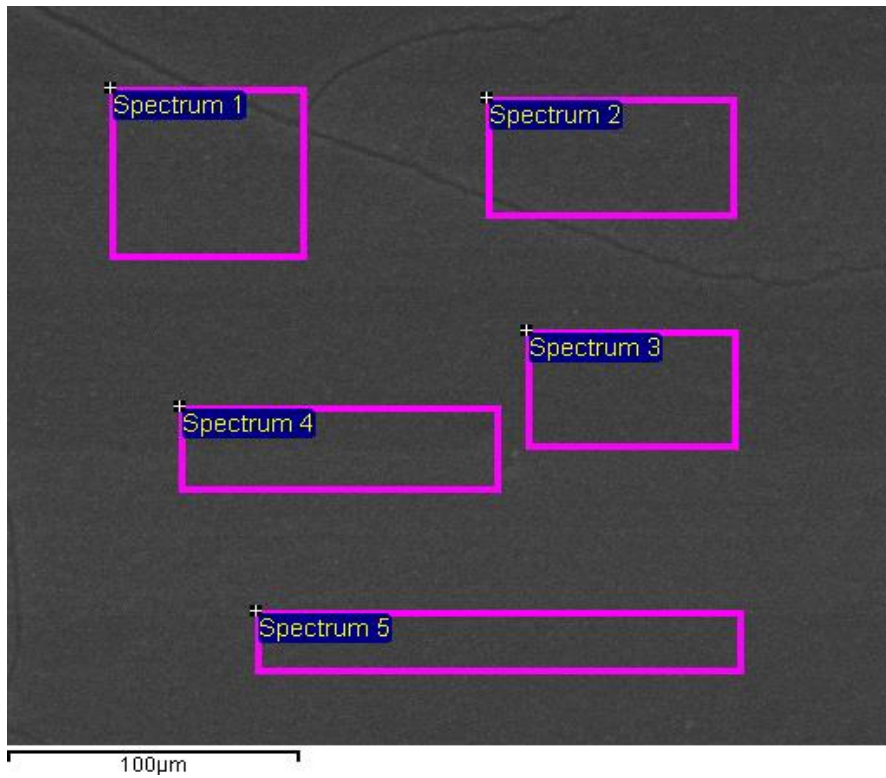| Spectrum	In stats.	C	O	Al	Si	S	Ca	Total
Sample: NF 5bar, 35.5µg/l								
Processing option : All elements analysed (Normalised)								
All results in weight%								
Spectrum 1	Yes	56,3	36,23	1,3	1,5	4,08	0,59	100
Spectrum 2	Yes	57,6	35,05	0,91	1,38	4,71	0,35	100
Spectrum 3	Yes	56,39	36,41	0,89	1,21	4,65	0,45	100
Spectrum 4	Yes	56,16	36,01	1,15	1,43	4,73	0,52	100
Spectrum 5	Yes	58,64	34,19	0,96	1,04	4,8	0,37	100
Mean		57,02	35,58	1,04	1,31	4,6	0,46	100
Std. deviation		1,07	0,93	0,18	0,19	0,29	0,1	
Max.		58,64	36,41	1,3	1,5	4,8	0,59	
Min.		56,16	34,19	0,89	1,04	4,08	0,35	

Figure H-19: SEM sample image for EDX analysis of NF, 5 bar, 35.5µg/l

Figure H-20: SEM image of the top view of NF 5 bar, 35.5µg/l with a 50K magnification (Left) and a 10K rmagnification (right)

Table H-11: EDX analysis of NF at 5 Bar, 22 µg/l

Sample: NF 5 bar, 22µg/l					
Processing option : All elements analysed (Normalised)					
All results in weight%					
Spectrum	In stats.	**C**	**O**	**S**	**Total**
Spectrum 1	Yes	76,06	17,25	6,69	100
Spectrum 2	Yes	75,54	17,92	6,54	100
Spectrum 3	Yes	74,86	18,82	6,32	100
Spectrum 4	Yes	75,65	17,79	6,56	100
Spectrum 5	Yes	75,8	17,98	6,22	100
Mean		75,58	17,95	6,47	100
Std. deviation		0,45	0,57	0,19	
Max.		76,06	18,82	6,69	
Min.		74,86	17,25	6,22	

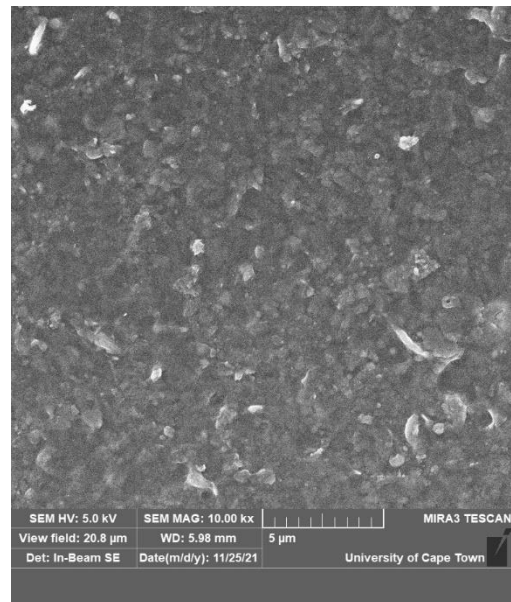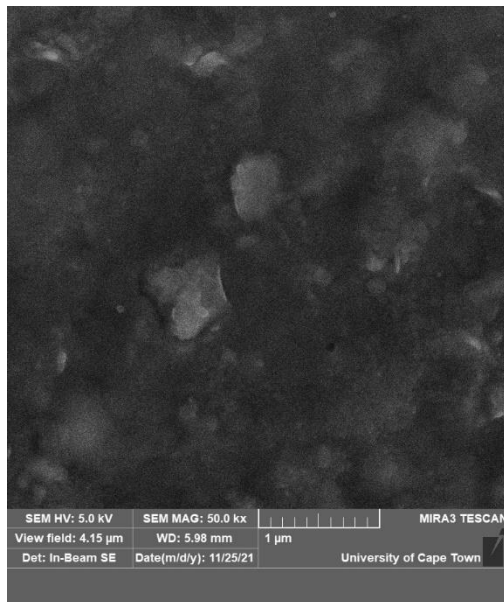*Figure H-21: SEM sample image for EDX analysis of NF, 5 bar, 22µg/l*

Figure H-22: SEM image of the top view of NF 5 bar, 22µg/l with a 50K magnification (Left) and a 10K rmagnification (right)

Table H-12: EDX analysis of NF at 5 Bar, 44 µg/l

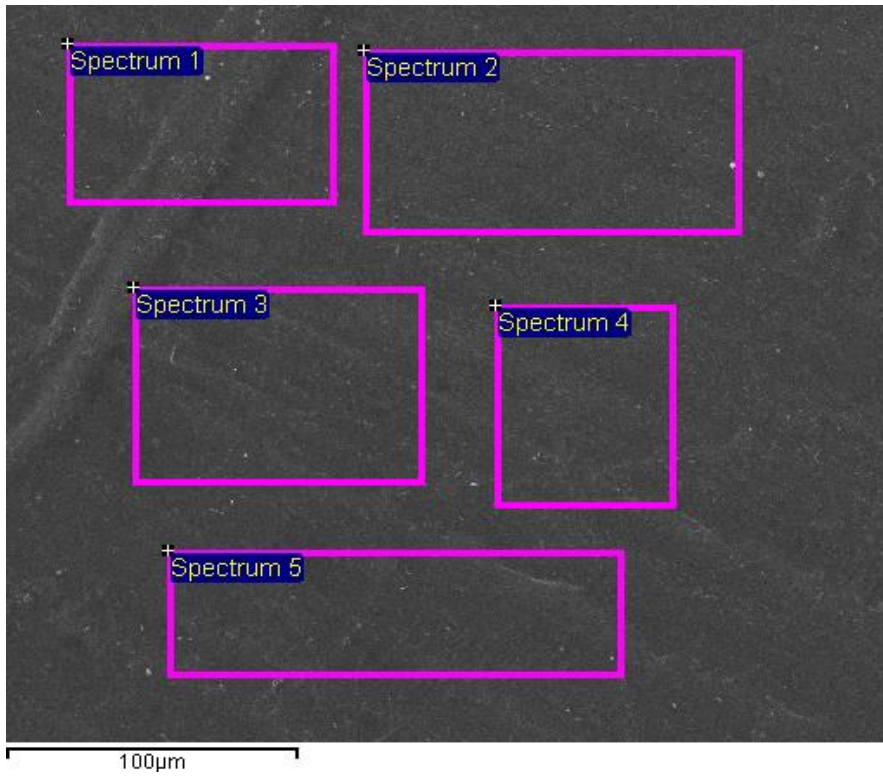| Sample: NF 5 bar 44µg/l					
Processing option : All elements analysed (Normalised)					
All results in weight%					
Spectrum	In stats.	**C**	**O**	**S**	**Total**
Spectrum 1	Yes	70,29	23,63	6,08	100
Spectrum 2	Yes	68,8	24,73	6,47	100
Spectrum 3	Yes	70,01	23,58	6,41	100
Spectrum 4	Yes	70,6	23,18	6,22	100
Spectrum 5	Yes	72,1	21,55	6,35	100
Mean		70,36	23,33	6,31	100
Std. deviation		1,19	1,15	0,16	
Max.		72,1	24,73	6,47	
Min.		68,8	21,55	6,08	

Figure H-23: SEM sample image for EDX analysis of NF, 5 bar, 44µg/l
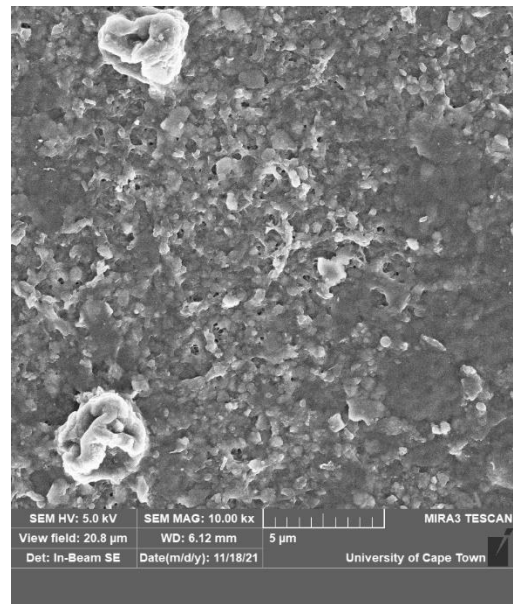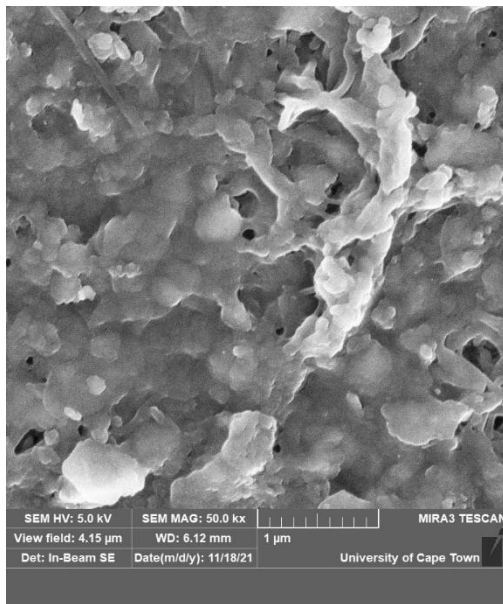

Figure H-24: SEM image of the top view of NF 5 bar, 44µg/l with a 50K magnification (Left) and a 10K rmagnification (right)

Table H-13: EDX analysis of NF at 10 Bar, 44 µg/l

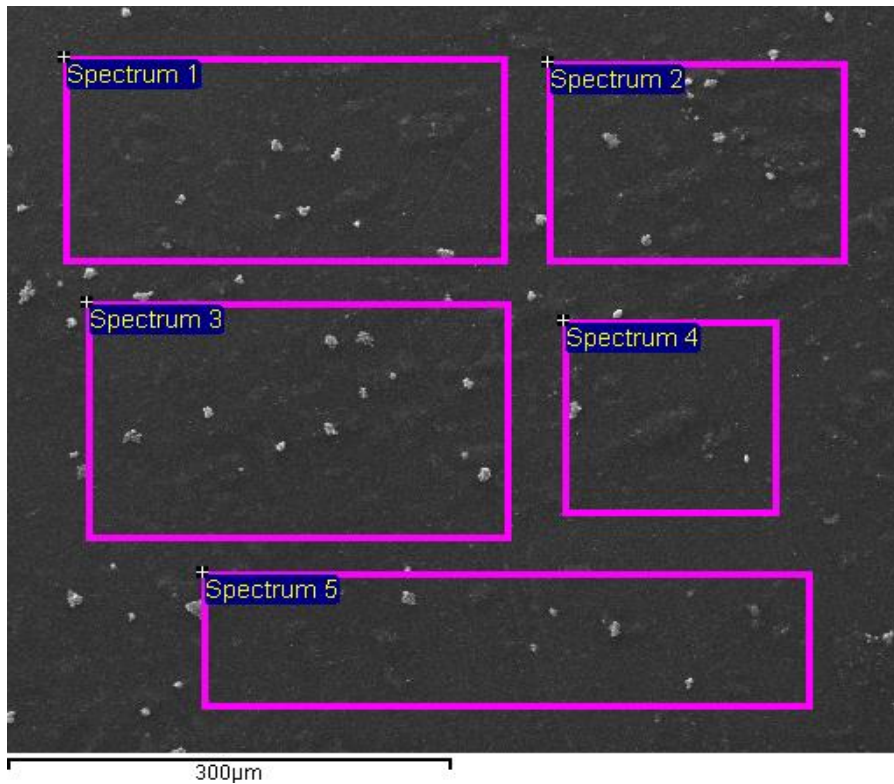| Spectrum	In stats.	C	O	Na	Si	S	Total
Sample: NF 10bar, 44 µg/l							
Processing option : All elements analysed (Normalised)							
All results in weight%							
Spectrum 1	Yes	68,63	25,49	0,38	0,28	5,22	100
Spectrum 2	Yes	66,73	27,41	0	0,33	5,53	100
Spectrum 3	Yes	67,05	27,16	0	0,47	5,32	100
Spectrum 4	Yes	67,98	26	0,26	0,42	5,33	100
Spectrum 5	Yes	68,23	25,74	0	0,35	5,68	100
Mean		67,73	26,36	0,13	0,37	5,41	100
Std. deviation		0,8	0,87	0,18	0,07	0,18	
Max.		68,63	27,41	0,38	0,47	5,68	
Min.		66,73	25,49	0	0,28	5,22	

Figure H-25: SEM sample image for EDX analysis of NF, 10 bar, 44µg/l
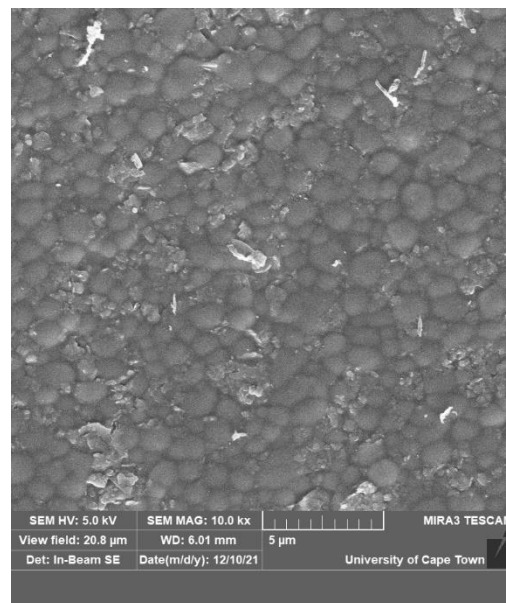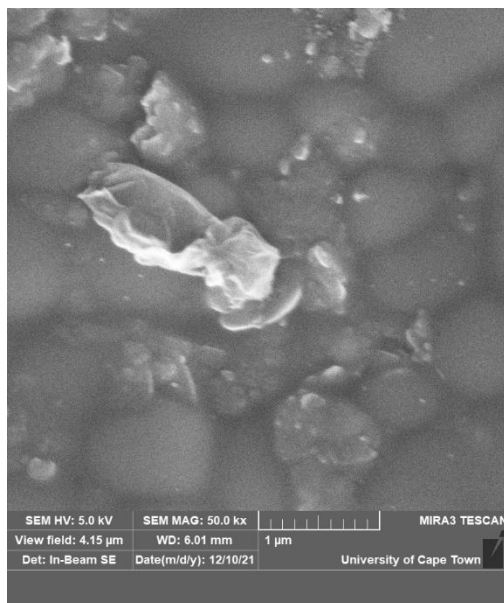

Figure H-26: SEM image of the top view of NF 10 bar, 44µg/l with a 50K magnification (Left) and a 10K rmagnification (right)

Table H-14: EDX analysis of NF at 10 Bar, 35.5 µg/l

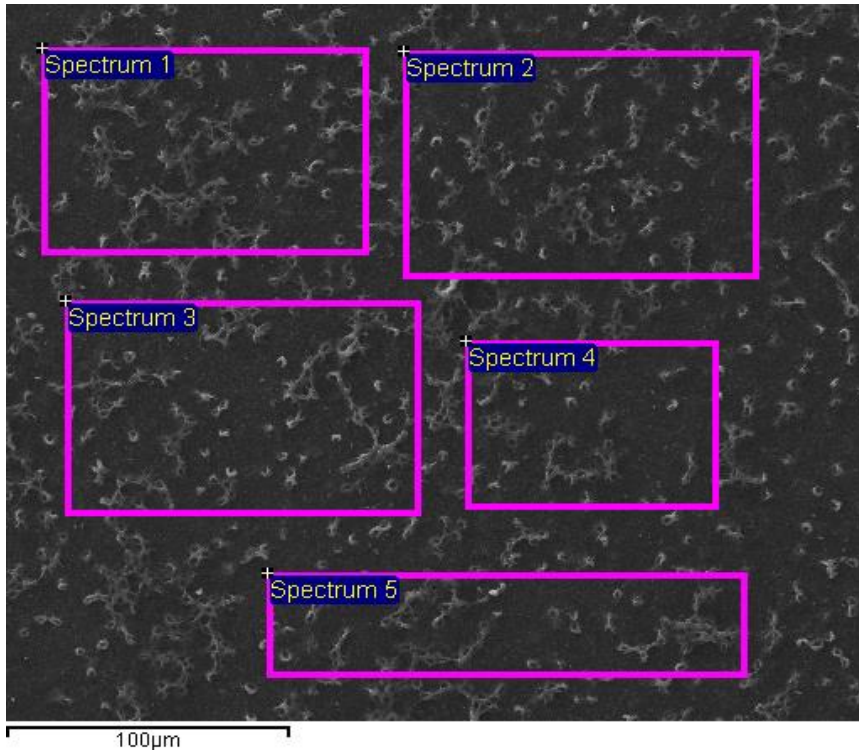| Spectrum	In stats.	C	O	Mg	Al	Si	P	S	Ca	Total
Sample: NF 10bar, 35.5µg/l										
Processing option : All elements analysed (Normalised)										
All results in weight%										
Spectrum 1	Yes	59,43	32,43	0,6	0,76	1,18	1,14	3,58	0,87	100
Spectrum 2	Yes	58,31	33,89	0,72	0,63	1,11	1,24	3,13	0,97	100
Spectrum 3	Yes	59,82	32,69	0,74	0,69	1,09	1,26	2,91	0,79	100
Spectrum 4	Yes	59,52	32,2	0,73	0,8	1,18	1,21	3,3	1,05	100
Spectrum 5	Yes	59,54	31,81	0,77	0,83	1,45	1,24	3,52	0,85	100
Mean		59,32	32,6	0,71	0,74	1,2	1,22	3,29	0,91	100
Std. deviation		0,59	0,79	0,06	0,08	0,14	0,05	0,28	0,11	
Max.		59,82	33,89	0,77	0,83	1,45	1,26	3,58	1,05	
Min.		58,31	31,81	0,6	0,63	1,09	1,14	2,91	0,79	

Figure H-27: SEM sample image for EDX analysis of NF, 10 bar, 35.5µg/l
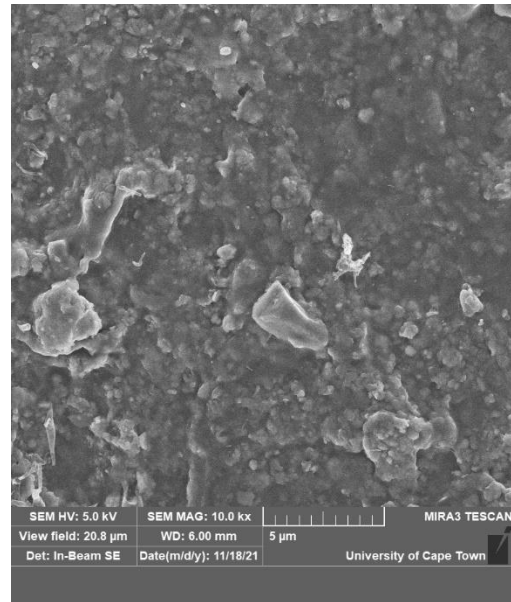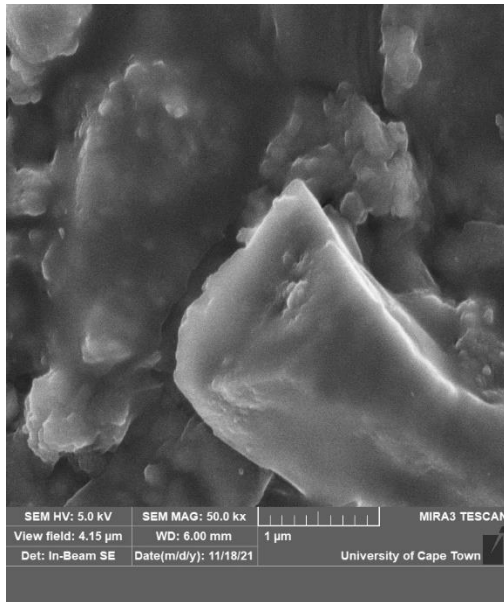

Figure H-28: SEM image of the top view of NF 10 bar, 35.5µg/l with a 50K magnification (Left) and a 10K rmagnification (right)

Table H-15: EDX analysis of NF at 10 Bar, 22 µg/l

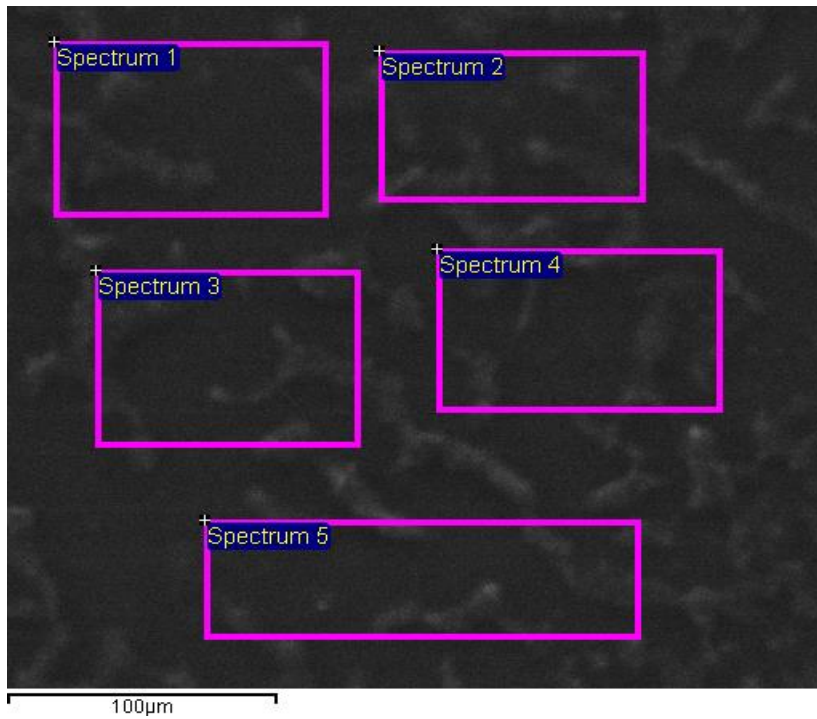| Spectrum	In stats.	C	O	S	Total
Sample: NF 10bar, 22µg/l					
All results in weight%					
Processing option : All elements analysed (Normalised)					
Spectrum 1	Yes	75,05	18,85	6,1	100
Spectrum 2	Yes	73,48	20,74	5,78	100
Spectrum 3	Yes	73,47	20,59	5,94	100
Spectrum 4	Yes	72,48	22,26	5,26	100
Spectrum 5	Yes	75,15	19,16	5,69	100
Mean		73,93	20,32	5,75	100
Std. deviation		1,15	1,37	0,32	
Max.		75,15	22,26	6,1	
Min.		72,48	18,85	5,26	

Figure H-29: SEM sample image for EDX analysis of NF, 10 bar, 22µg/l

Figure H-30: : SEM image of the top view of NF 10 bar, 22µg/l with a 50K magnification (Left) and a 10K rmagnification (right)

Table H-16: EDX analysis of NF at 15 Bar, 22 µg/l

Sample: NF 15bar, 22µg/l								
Processing option : All elements analysed (Normalised)								
All results in weight%								
Processing option : All elements analysed (Normalised)								
Spectrum	In stats.	**C**	**O**	**Al**	**Si**	**S**	**Ca**	**Total**
Spectrum 1	Yes	64,6	29,13	0,4	0,44	4,99	0,45	100
Spectrum 2	Yes	62,17	30,74	0,67	0,68	5,18	0,57	100
Spectrum 3	Yes	60,79	31,84	0,88	1,29	4,62	0,58	100
Spectrum 4	Yes	62,22	31,44	0,47	0,52	4,85	0,5	100
Spectrum 5	Yes	61,16	32,18	0,63	0,76	4,79	0,48	100
Mean		62,19	31,07	0,61	0,74	4,89	0,51	100
Std. deviation		1,49	1,21	0,19	0,33	0,21	0,06	
Max.		64,6	32,18	0,88	1,29	5,18	0,58	
Min.		60,79	29,13	0,4	0,44	4,62	0,45	

Figure H-31: SEM sample image for EDX analysis of NF, 15 bar, 22µg/l
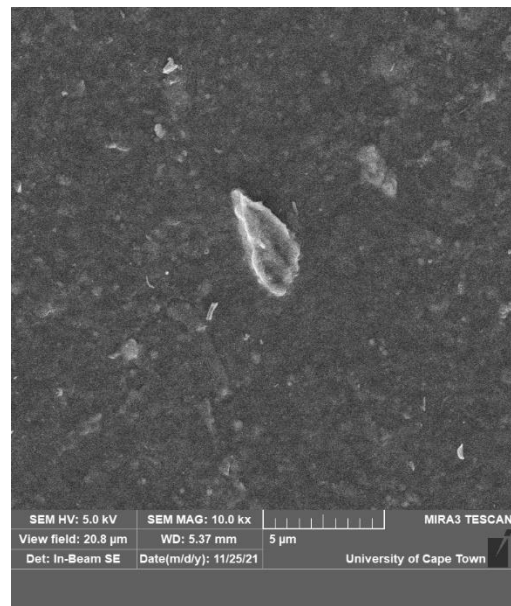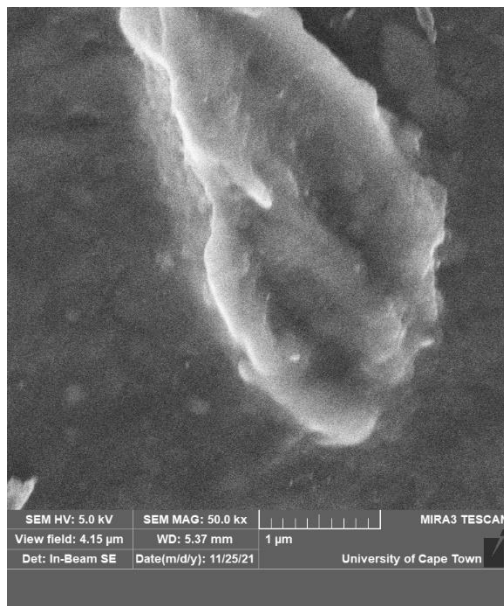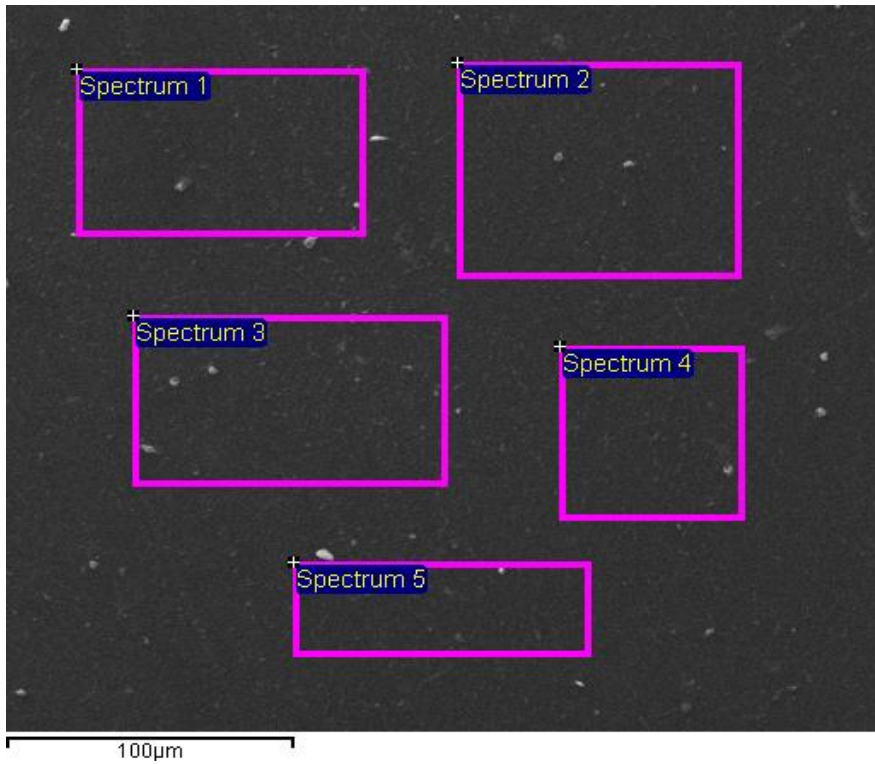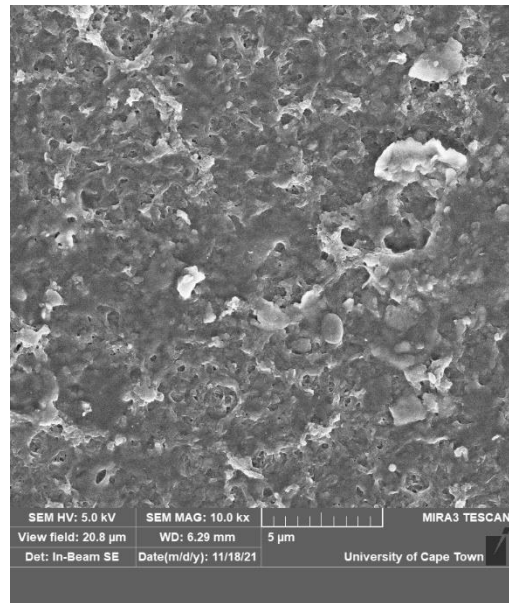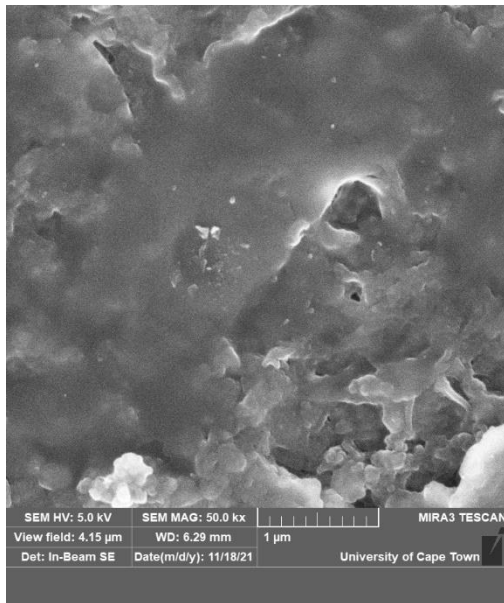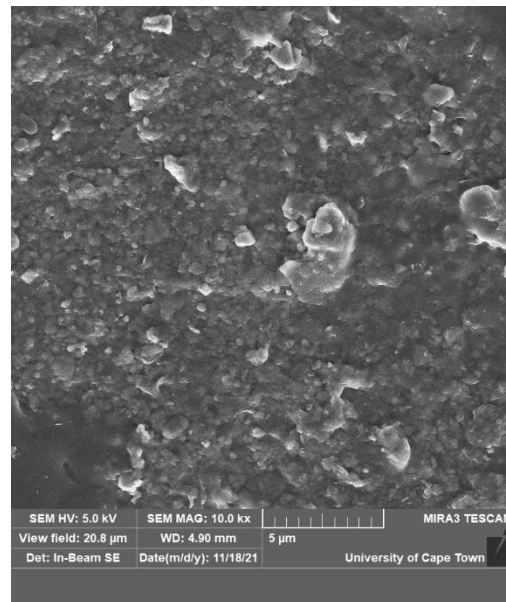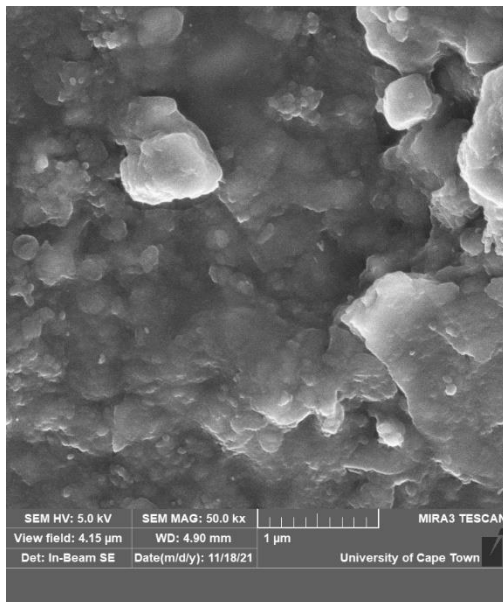

Figure H-32: SEM image of the top view of NF 15 bar, 22µg/l with a 50K magnification (Left) and a 10K rmagnification (right)

Table H-17: EDX analysis of NF at 15 Bar, 35.5 µg/l

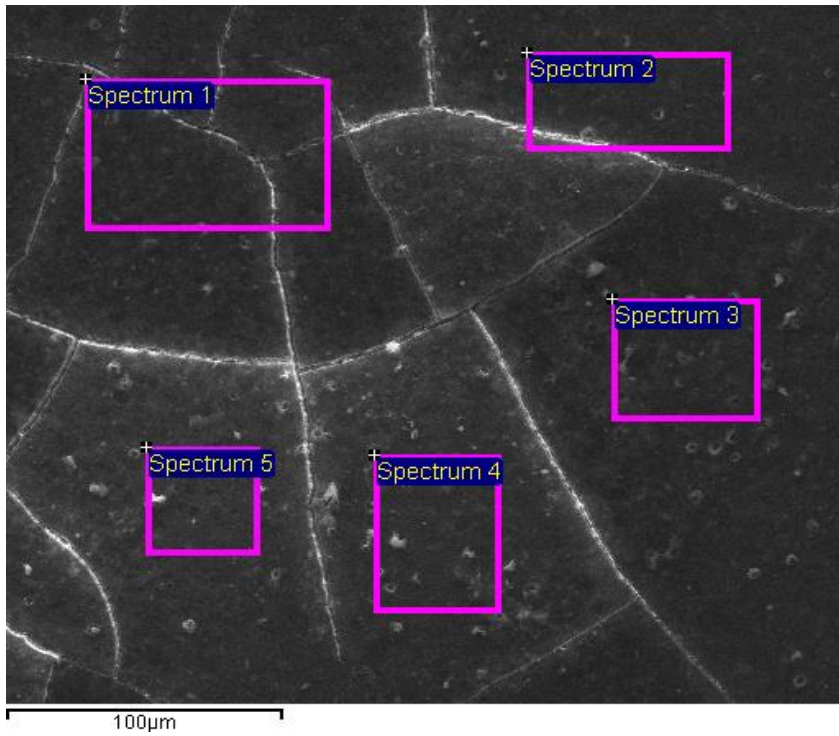| Sample: NF 15Bar, 35.5µg/l										
Processing option : All elements analysed (Normalised)										
All results in weight%										
Spectrum	In stats.	**C**	**O**	**Mg**	**Al**	**Si**	**P**	**S**	**Ca**	**Total**
Spectrum 1	Yes	57,45	34,47	0,94	0,89	2,1	0,99	1,96	1,18	100
Spectrum 2	Yes	60,37	31,79	0,45	0,68	0,88	0,56	4,59	0,67	100
Spectrum 3	Yes	60,26	32,23	0,35	0,58	0,81	0,46	4,76	0,56	100
Spectrum 4	Yes	60,09	32,03	0,76	0,84	1,37	1,05	2,78	1,07	100
Spectrum 5	Yes	59,58	32,21	0,5	0,81	1,42	0,72	4,02	0,73	100
Mean		59,55	32,55	0,6	0,76	1,32	0,76	3,62	0,84	100
Std. deviation		1,21	1,09	0,24	0,13	0,52	0,26	1,21	0,27	
Max.		60,37	34,47	0,94	0,89	2,1	1,05	4,76	1,18	
Min.		57,45	31,79	0,35	0,58	0,81	0,46	1,96	0,56	
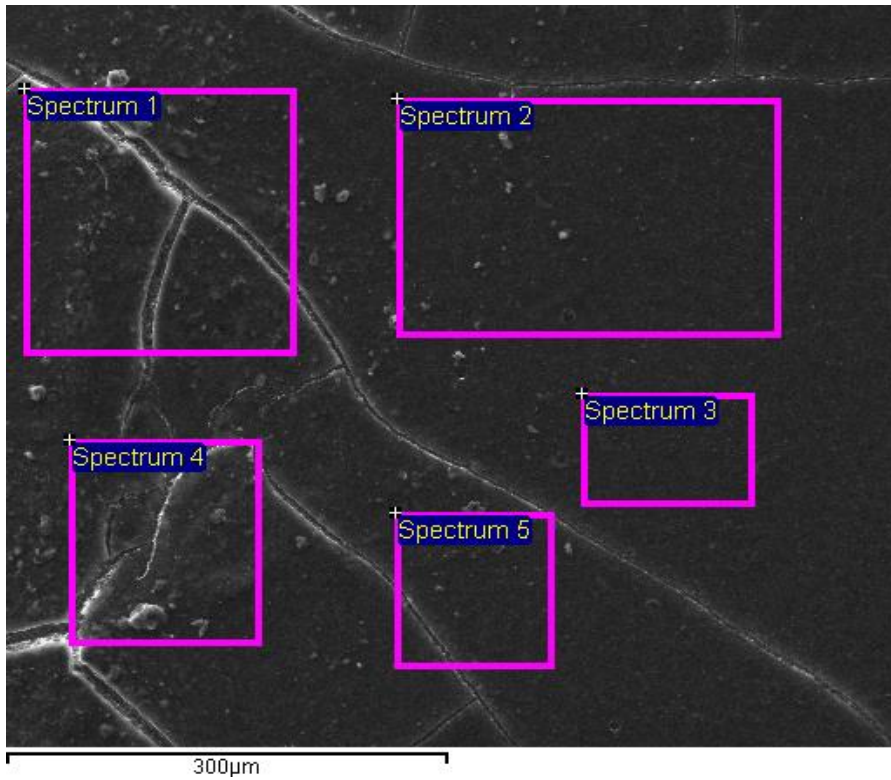
Figure H-33: SEM sample image for EDX analysis of NF, 15 bar, 35.5µg/l

Figure H-34: SEM image of the top view of NF 15 bar, 35.5µg/l with a 50K magnification (Left) and a 10K rmagnification (right)

100-Hour experimental long runs

Table H-18: EDX analysis of RO after 100 hours at 10 bar, 44 µg/l

Spectrum	In stats.	C	O	Mg	P	Ca	Total
Sample: RO 100hr 10 bar, 44µg/l							
Processing option: All elements analysed (Normalised)							
All results in weight%							
Spectrum 1	Yes	50,71	47,34	0,67	0,95	0,33	100
Spectrum 2	Yes	50,11	48,64	0,3	0,65	0,3	100
Spectrum 3	Yes	49,49	49,43	0,23	0,6	0,25	100
Spectrum 4	Yes	49,94	48,66	0,26	0,74	0,39	100
Spectrum 5	Yes	47,35	51,66	0,31	0,47	0,2	100
Mean		49,52	49,15	0,35	0,68	0,3	100
Std. deviation		1,29	1,6	0,18	0,18	0,07	
Max.		50,71	51,66	0,67	0,95	0,39	
Min.		47,35	47,34	0,23	0,47	0,2	
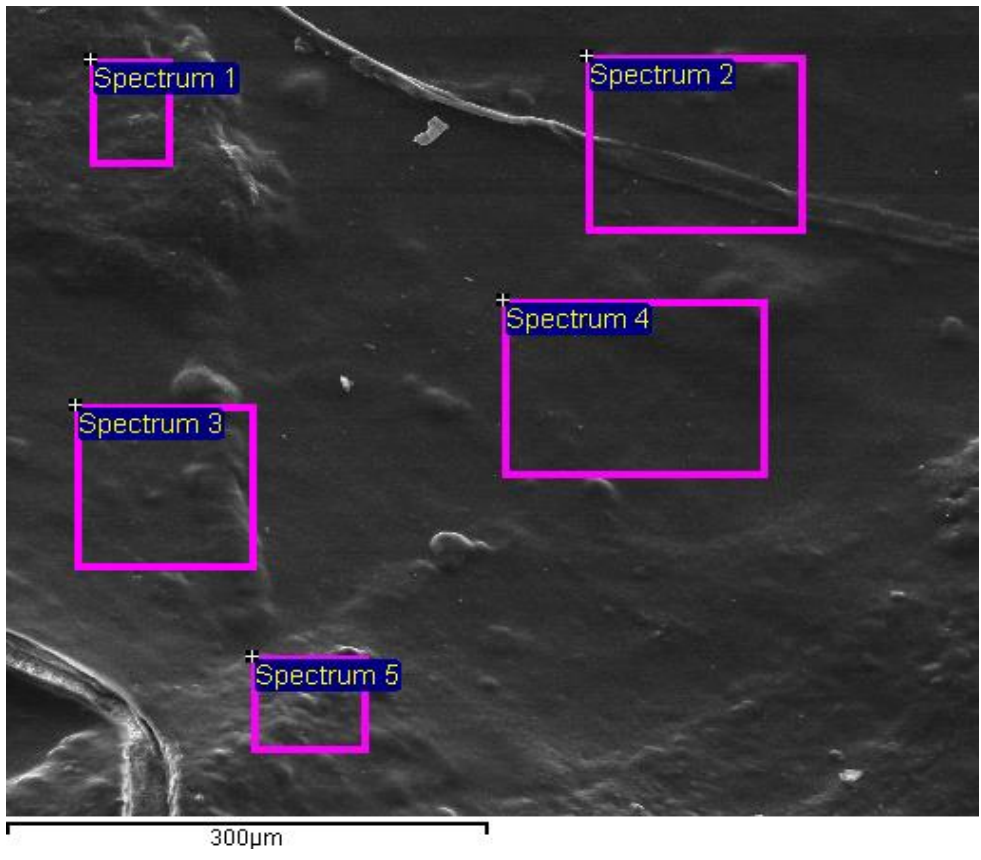
*Figure H-35: SEM sample image for EDX analysis of RO4040, 10 bar, 44µg/l after 100-hours*

....
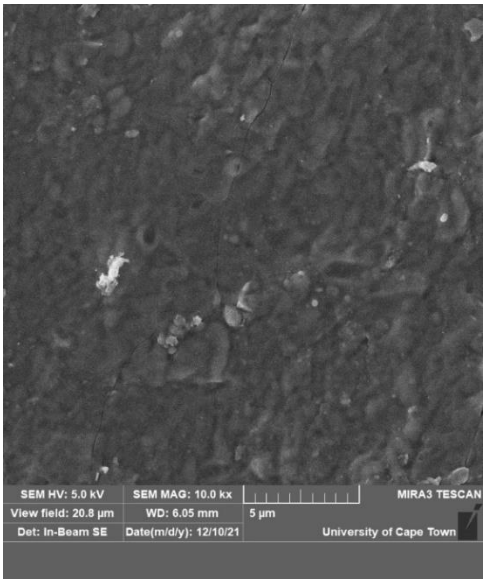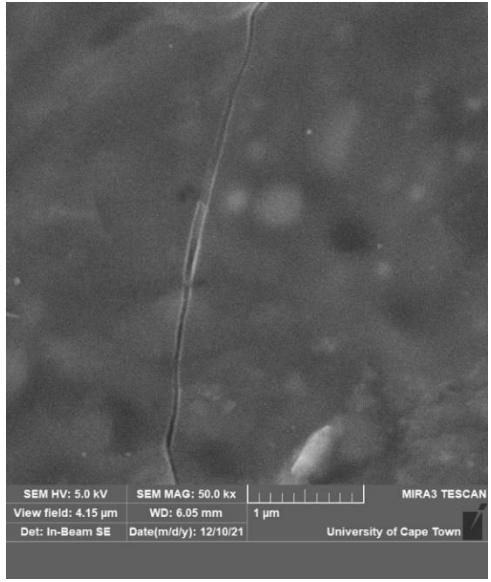
Figure H-36: SEM image of the top view of RO4040 10 bar, 44µg/l with a 50K magnification (Left) and a 10K rmagnification (right) after 100 hours.

Table H-19: EDX analysis of NF after 100 hours at 10 Bar, 44 µg/l

Sample: NF 100hr 44µg/l							
Processing option: All elements analysed (Normalised)							
All results in weight%							
Spectrum	In stats.	**C**	**O**	**P**	**S**	**Ca**	**Total**
Spectrum 1	Yes	57,2	40,27	1,71	0,28	0,53	100
Spectrum 2	Yes	57,72	39,3	1,95	0,43	0,61	100
Spectrum 3	Yes	57,15	40,02	1,68	0,4	0,76	100
Spectrum 4	Yes	57,6	39,46	1,84	0,49	0,6	100
Spectrum 5	Yes	57,18	40,36	1,57	0,43	0,46	100
Mean		57,37	39,88	1,75	0,41	0,59	100
Std. deviation		0,27	0,48	0,15	0,08	0,11	
Max.		57,72	40,36	1,95	0,49	0,76	
Min.		57,15	39,3	1,57	0,28	0,46	

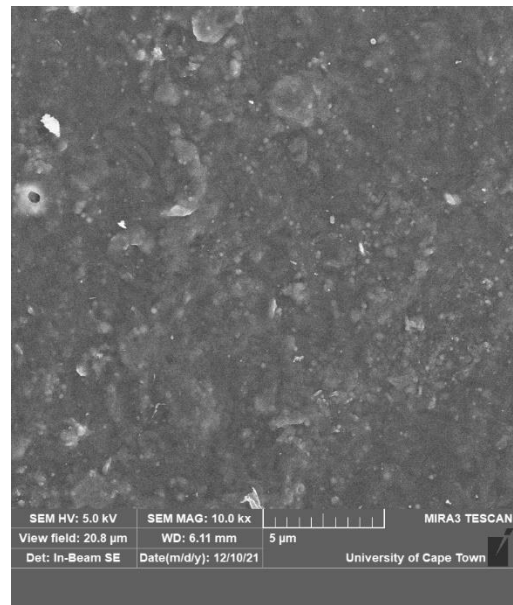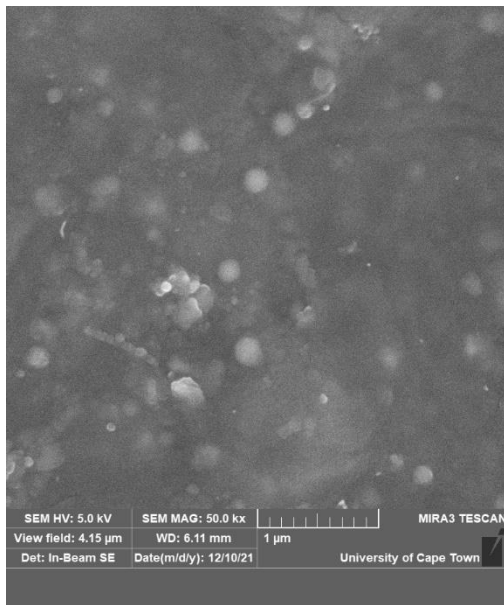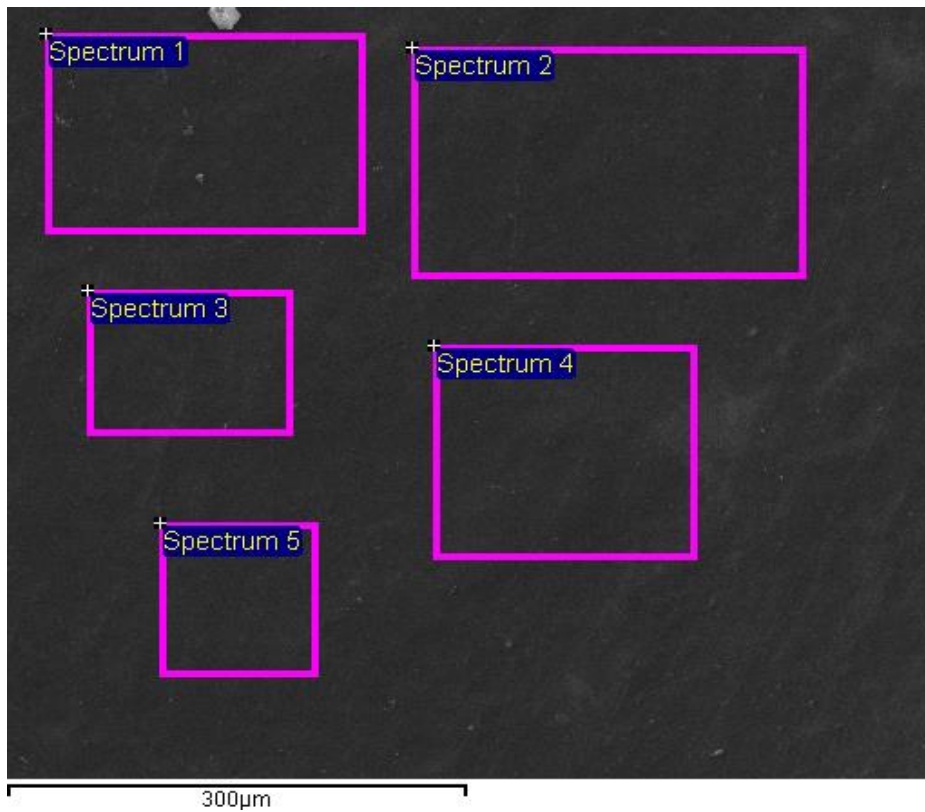*Figure H-37: SEM sample image for EDX analysis of NF, 10 bar, 44µg/l after 100-hours*
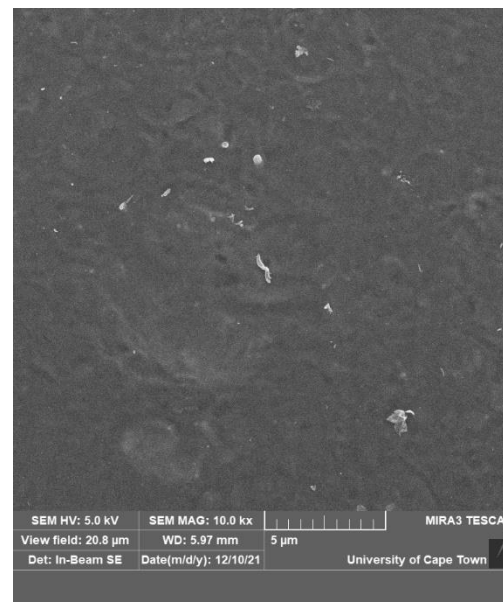
Figure H-38: SEM image of the top view of NF 10 bar, 44µg/l with a 50K magnification (Left) and a 10K magnification (right) after 100 hours.

Appendix I

Data from batch experiments

Attenuated total reflection - Fourier-transform infrared spectroscopy (ATR-FTIR) analysis for RO and NF

Data of FTIR analysis presented below are 10 points obtained for each experimental run. The ATR-FTIR spectra were recorded at a resolution of $1cm^{-1}$ during 48 scans at a nominal incident angle of 45°C and a wavelength between 400 and 4000 cm^{-1} To capture certain functionalities in both the clean and fouled membrane samples, spectra were zoomed into a region of 2000-400 cm^{-1}.

I. Appendix I

Table I-1: FTIR data for NF at different operating conditions

NF Virgin membranes		NF 10 Bar, 22µg/l		NF 10 Bar, 44µg/l		NF 10 Bar, 35.5 µg/l	
Wavelength	Transmittance	Wavelength	Transmittance	Wavelength	Transmittance	Wavelength	Transmittance
cm^{-1}	%T	cm^{-1}	%T	cm^{-1}	%T	cm^{-1}	%T
400	36,16	400	71,33	400	91,01	400	34,51
401	36	401	72,1	401	91,61	401	34,46
402	35,92	402	72,59	402	92,07	402	34,22
403	36,06	403	72,66	403	92,34	403	34,08
404	36,21	404	72,42	404	92,35	404	34,18
405	36,11	405	72,15	405	92,35	405	34,32
406	35,87	406	72,14	406	92,39	406	34,33
407	35,87	407	72,43	407	92,62	407	34,29
408	36,21	408	72,57	408	92,88	408	34,27

409	36,52	409	72,44	409	93	409	34,17
410	36,48	410	72,09	410	92,93	410	33,93
411	36,21	411	71,68	411	92,67	411	33,64
412	35,95	412	71,29	412	92,29	412	33,32
413	35,77	413	70,93	413	91,94	413	32,84
414	35,64	414	70,58	414	91,69	414	32,29
415	35,59	415	70,25	415	91,53	415	31,98

Table I-2: FTIR data for NF at different operating conditions

NF Virgin membranes		NF 5 Bar, 22µg/		NF 5 Bar, 35.5µg/l	
Wavelength	Transmittance	Wavelength	Transmittance	Wavelength	Transmittance
cm^{-1}	%T	cm^{-1}	%T	cm^{-1}	%T
400	36,16	400	92,41	400	87,49
401	36	401	93,41	401	88,2
402	35,92	402	94,37	402	88,79
403	36,06	403	95,01	403	88,99
404	36,21	404	95,09	404	88,67
405	36,11	405	94,79	405	88,14
406	35,87	406	94,45	406	87,86
407	35,87	407	94,21	407	87,97
408	36,21	408	94,1	408	88,32
409	36,52	409	94	409	88,53
410	36,48	410	94,01	410	88,56

411	36,21	411	94,05	411	88,31
412	35,95	412	93,98	412	87,8
413	35,77	413	93,76	413	87,24
414	35,64	414	93,43	414	86,9
415	35,59	415	93	415	86,79

Table I-3: : FTIR data for NF at 15 Bar and different initial feed concentrations

NF Virgin membranes		NF 15 Bar, 44µg/		NF 15 Bar, 22µg/l	
Wavelength	Transmittance	Wavelength	Transmittance	Wavelength	Transmittance
cm^{-1}	%T	cm^{-1}	%T	cm^{-1}	%T
400	36,16	400	29,76	400	29,74
401	36	401	29,83	401	29,93
402	35,92	402	29,42	402	29,77
403	36,06	403	28,97	403	29,4
404	36,21	404	28,72	404	29,08
405	36,11	405	28,52	405	28,85
406	35,87	406	28,2	406	28,7
407	35,87	407	27,88	407	28,67
408	36,21	408	27,63	408	28,73
409	36,52	409	27,35	409	28,7
410	36,48	410	26,96	410	28,5

411	36,21	411	26,59	411	28,3
412	35,95	412	26,39	412	28,22
413	35,77	413	26,31	413	28,1
414	35,64	414	26,25	414	27,82
415	35,59	415	26,23	415	27,5
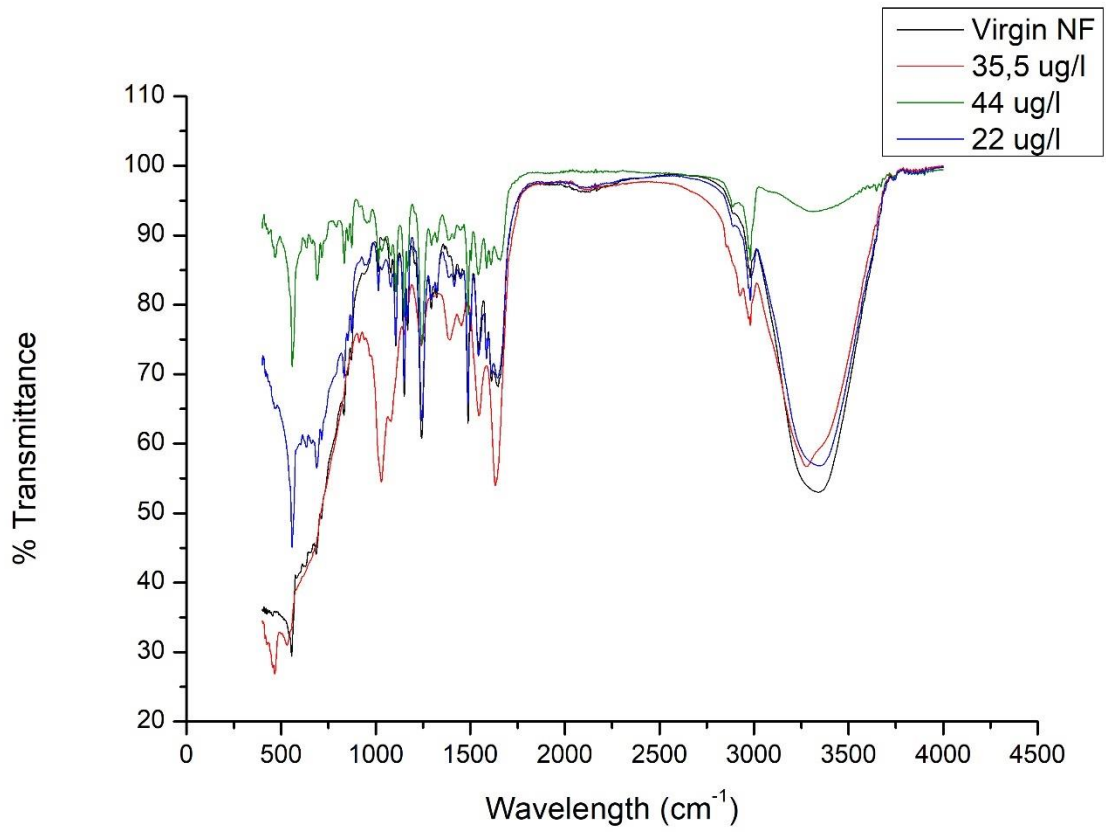
Figure I-1: ATR-FTIR spectra for NF at 10 Bar at different initial feed concentrations
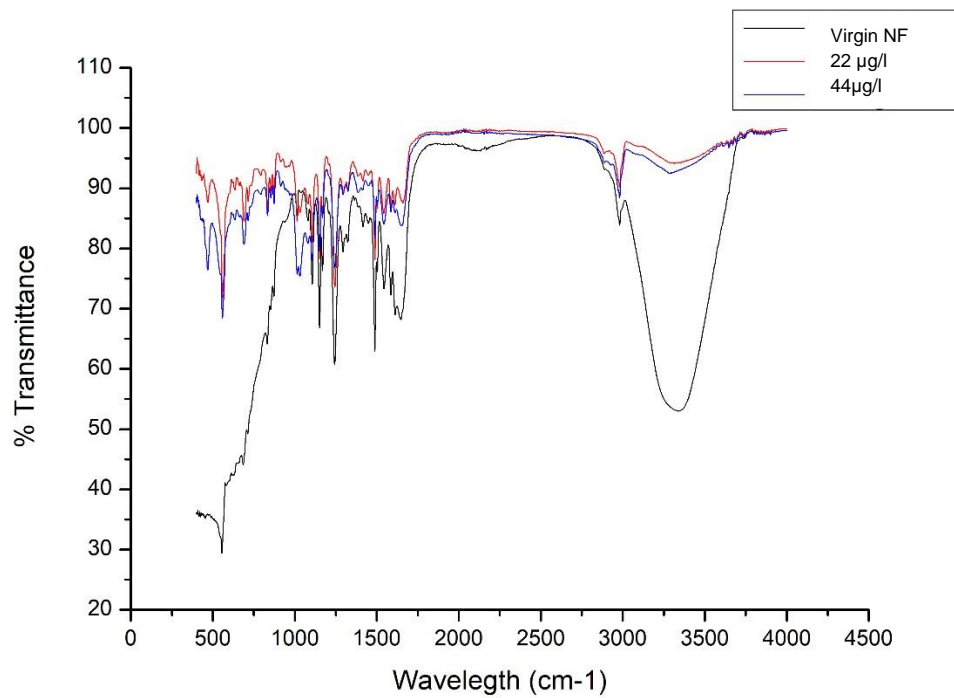
Figure I-2: ATR-FTIR spectra for NF at 5 bar and different feed initial concentrations
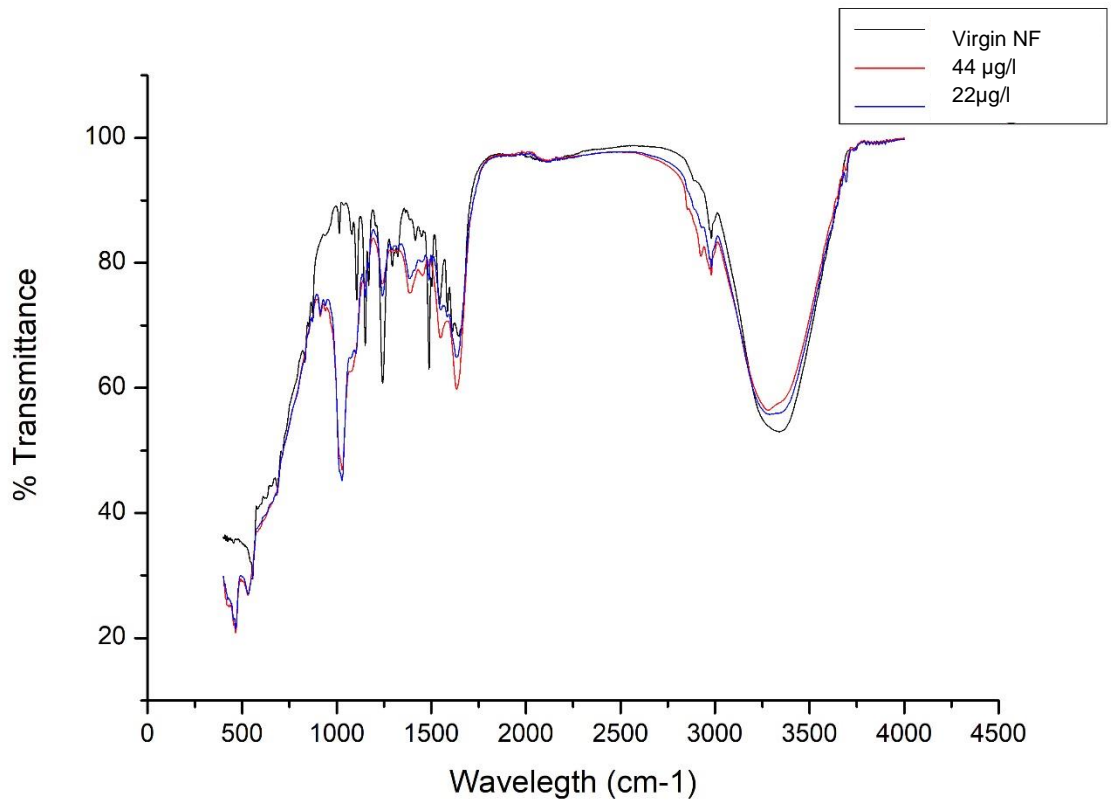
Figure I-3: ATR-FTIR spectra for NF at 15 bar and different feed initial concentrations

Table I-4: FTIR data for RO at 10 Bar

RO Virgin membranes		RO 10 Bar, 22µg/		RO 10 Bar, 44µg/l		RO 10 Bar, 35.5µg/l	
Wavelength	Transmittance	Wavelength	Transmittance	Wavelength	Transmittance	Wavelength	Transmittance
cm^{-1}	%T	cm^{-1}	%T	cm^{-1}	%T	cm^{-1}	%T
400	85,98	400	81,89	400	82,95	400	86,41
401	85,78	401	81,74	401	82,97	401	85,87
402	85,4	402	81,46	402	82,73	402	85,23
403	84,98	403	81,23	403	82,36	403	84,87
404	84,62	404	81,07	404	81,87	404	84,74
405	84,28	405	80,75	405	81,38	405	84,51
406	84,07	406	80,21	406	81,05	406	84,05
407	84,2	407	79,77	407	80,9	407	83,6
408	84,69	408	79,64	408	80,82	408	83,39
409	85,23	409	79,62	409	80,69	409	83,27
410	85,45	410	79,43	410	80,46	410	83,03
411	85,31	411	79,1	411	80,07	411	82,74

412	85,05	412	78,73	412	79,56	412	82,5
413	84,84	413	78,25	413	79,07	413	82,27
414	84,69	414	77,63	414	78,73	414	81,98
415	84,52	415	77	415	78,46	415	81,71

Table I-5: FTIR data for RO at 5 Bar

RO4040 Virgin membranes		RO 5 Bar, 22µg/		RO4040 5 Bar, 35.5µg/l		RO4040 5 Bar, 44µg/l	
Wavelength	Transmittance	Wavelength	Transmittance	Wavelength	Transmittance	Wavelength	Transmittance
cm^{-1}	%T	cm^{-1}	%T	cm^{-1}	%T	cm^{-1}	%T
400	92,64	400	46,18	400	56,8	400	77,23
401	92,72	401	46,02	401	57,02	401	76,73
402	92,44	402	46,23	402	56,85	402	76,25
403	92	403	45,98	403	56,37	403	75,89
404	91,65	404	45,89	404	55,7	404	75,58
405	91,43	405	45,78	405	55,08	405	75,24
406	91,31	406	45,62	406	54,76	406	74,91
407	91,31	407	45,5	407	54,78	407	74,64
408	91,46	408	45,48	408	54,93	408	74,4
409	91,65	409	45,39	409	54,94	409	74,13
410	91,68	410	45,11	410	54,72	410	73,81

411	91,5	411	44,71	411	54,36	411	73,42
412	91,27	412	44,38	412	54,02	412	73,04
413	91,19	413	44,21	413	53,78	413	72,76
414	91,28	414	44,13	414	53,6	414	72,58
415	91,4	415	44,04	415	53,37	415	72,41

Table I-6: FTIR data for RO at 15 Bar

RO Virgin membranes		RO 5 Bar, 22µg/		RO 5 Bar, 35.5µg/l	
Wavelength	Transmittance	Wavelength	Transmittance	Wavelength	Transmittance
cm^{-1}	%T	cm^{-1}	%T	cm^{-1}	%T
400	92,64	400	69,5	400	84,78
401	92,72	401	69,82	401	85,04
402	92,44	402	69,79	402	84,95
403	92	403	69,47	403	84,7
404	91,65	404	68,97	404	84,46
405	91,43	405	68,39	405	84,21
406	91,31	406	67,86	406	83,96
407	91,31	407	67,5	407	83,81
408	91,46	408	67,25	408	83,82
409	91,65	409	66,91	409	83,85
410	91,68	410	66,45	410	83,8

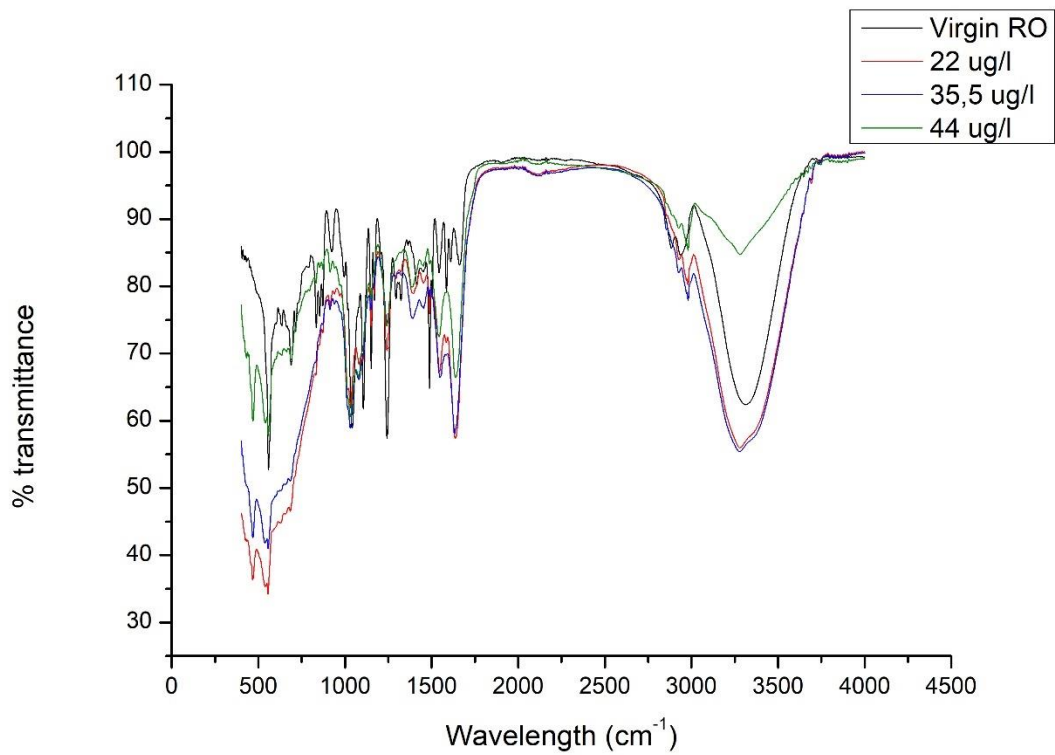|					
411	91,5	411	66,03	411	83,72
412	91,27	412	65,75	412	83,65
413	91,19	413	65,47	413	83,56
414	91,28	414	65,1	414	83,37
415	91,4	415	64,74	415	83,15

Figure I-4: ATR-FTIR spectra of RO at 5 Bar with different initial feed concentrations
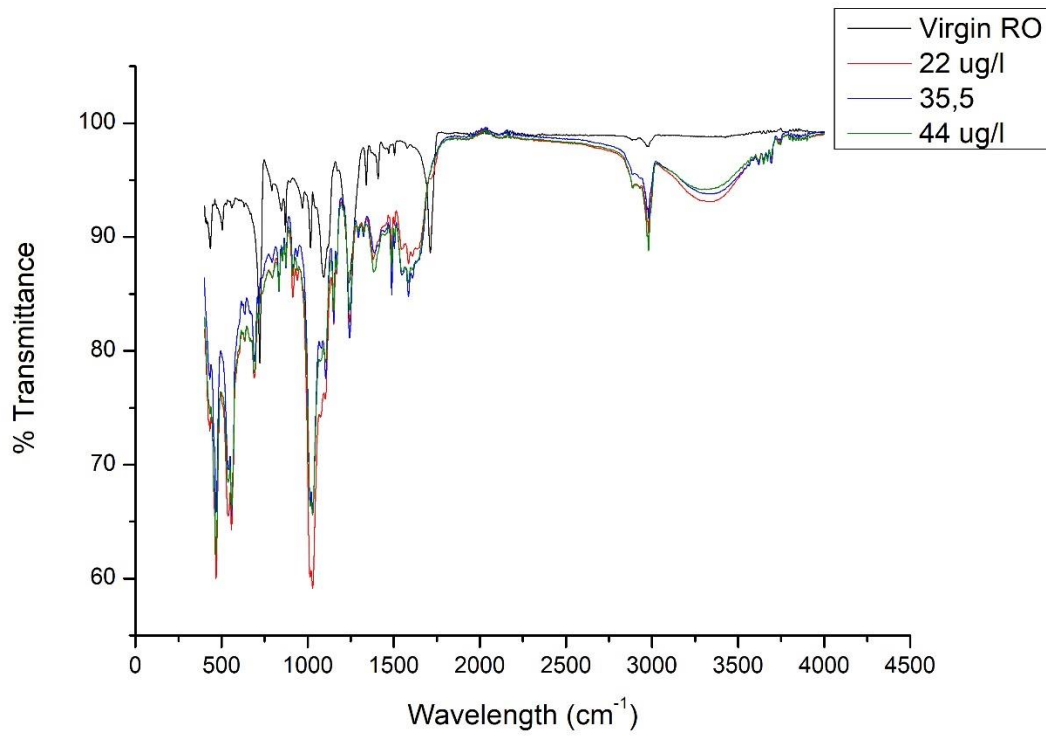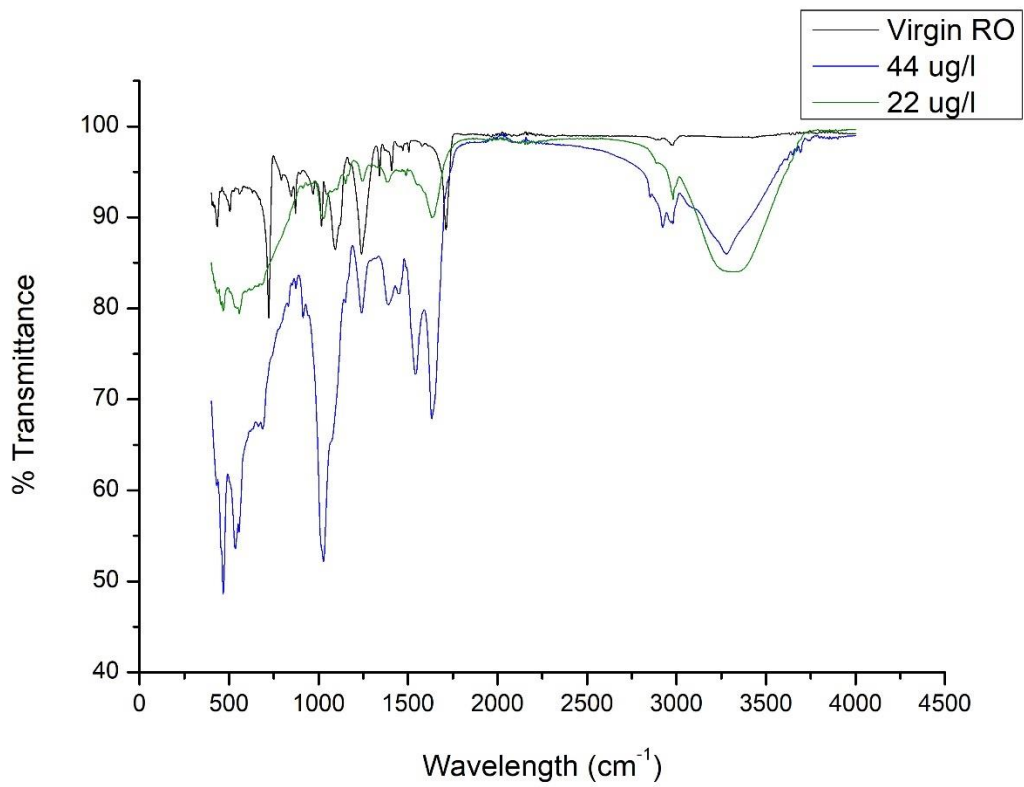
Figure I-5: ATR-FTIR data for RO at 10 Bar

Figure I-6: ATR-FTIR data for RO at 15 Bar

Table I-7: FTIR data of pharmaceuticals

Aspirin (ASP)		Carbamazepine (CBZ)		Diclofenac (DCF)		Ibuprofen (IBU)	
Wavelength	Transmittance	Wavelength	Transmittance	Wavelength	Transmittance	Wavelength	Transmittance
cm^{-1}	%T	cm^{-1}	%T	cm^{-1}	%T	cm^{-1}	%T
400	99,04	400	78,73	400	91,57	400	93,23
401	99,02	401	77,5	401	91,45	401	93,04
402	98,78	402	76,41	402	91,32	402	93,12
403	98,49	403	75,81	403	91,28	403	93,49
404	98,19	404	75,67	404	91,33	404	93,74
405	97,88	405	75,57	405	91,28	405	93,6
406	97,61	406	75,34	406	91,02	406	93,18
407	97,46	407	75,19	407	90,68	407	92,87
408	97,46	408	75,42	408	90,5	408	92,91
409	97,52	409	75,94	409	90,57	409	93,08
410	97,48	410	76,43	410	90,65	410	92,95
411	97,22	411	76,67	411	90,47	411	92,38

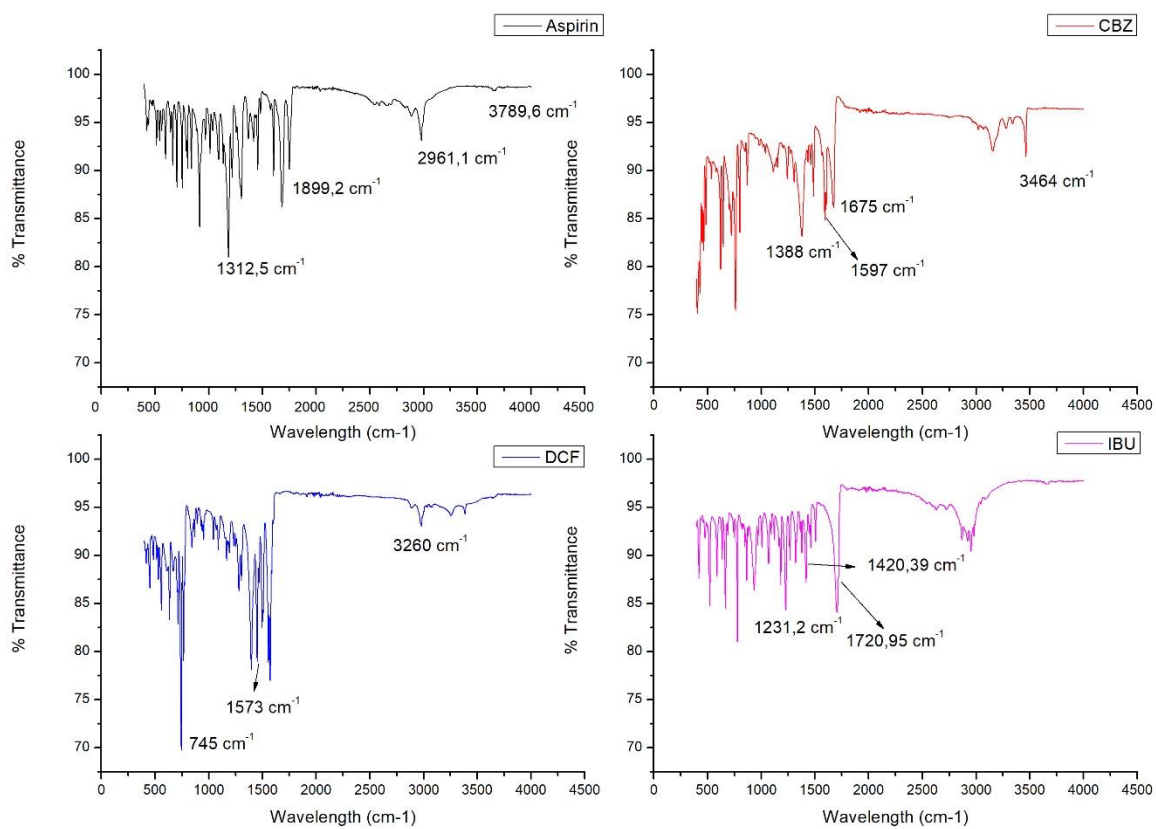|							
412	96,82	412	76,68	412	90,04	412	91,66
413	96,51	413	76,68	413	89,64	413	91,2
414	96,45	414	76,93	414	89,49	414	91,1
415	96,57	415	77,47	415	89,56	415	91,12
416	96,66	416	78,17	416	89,6	416	90,89
417	96,44	417	78,9	417	89,45	417	90,19
418	95,83	418	79,63	418	89,19	418	89,05
419	95,12	419	80,28	419	89,17	419	87,97
420	94,71	420	80,61	420	89,46	420	87,59

Figure I-7: ATR-FTIR spectra of pharmaceuticals

Appendix J

Data from batch experiments

Gas chromatography mass spectrometry of pharmaceuticals

GCMS Method

Methods:

Derivitization

Compounds (aspirin, ibuprofen, diclofenac and carbamazepine) were derivatized. They all have 1TMS added.

Resuspend the dried standards and samples in 80 μL of ethyl acetate, mix well and add 35 μL of MSTFA to the tubes, transfer to screw lids Eppendorfs: derivatize at 65°C for 35 minutes

GC method

GC–MS analysis was performed with an HP 6890 gas chromatograph (Agilent Technologies, Palo Alto, CA, USA) equipped with a 30 m×0.25 mm i.d. capillary column coated with a 0.25 μm film of 5/MS (5% diphenyl, 95% dimethylpolysiloxane) from Bios Analytique (L'Union, France). Samples (1 μL) were injected in (split: 1:4) mode at (240°C) using an HP 6890 series injector (autosampler). The carrier gas was ultrapure helium (99.99990%, Linde Gas, Bassens, France) in constant-flow mode (1 mL/min). The oven temperature was held at 70 °C for 2 min, then programmed at 10°C min^{-1} to 250°C which was held isothermally for 5 min. The gas chromatograph was coupled to an HP 5973N mass-selective detector (LMSD; Agilent Technologies) operated in electron-impact (EI) mode at 70 eV using single ion monitoring (Table 1) at 0.92 scan s^{-1} (dwell time 70 ms for each ion SIM). The electron multiplier potential was set to 1976 V (will set according to autotune result). The transfer line, source, and quadrupole temperatures were 280, 230, and 150 °C, respectively.

GC info and program:

- MS1 SIM mode
- Agilent 7890A GC system
- Agilent 7000C GC/MS triple quad
- Column: J&W 122-5532G DB-5ms+DG
- Temp setting: inlet: 240°C; transfer line: 280°C; ion source: 230°C
- Electron-impact (EI) mode at 70 eV
- Injection volume: 1 μL (autosampler)
- Oven temp gradient:
- 120°C hold 1 min

- 120-250°C: 12°C/min, hold 6 min

250-320°C: 20°C/min

Split ratio: 4:1 (5 times dilution)

Constant ultrapure helium flow rate (column): 1 mL/min

Injector pressure: 15.6 psi

Gain factor: 5

Table I-8: SIM method used for GCMS at 2.9 cycles/s

	MS1 mass	MS1 resolution	Dwell (ms)	R.T.
1-hydroxypyrene	290	Unit	60	18.481
Diclofenac	214	Unit	100	15.328
Pyrene	202	Unit	30	13.733
Aspirin	195	Unit	40	8.002
Carbamazepine	193	Unit	40	14.990
Ibuprofen	160	Unit	70	8.884

Table I-9: Concentrations used for each target analyte for the calibration curve

Compound Method		Standard curve (µg)-dilute with methanol					
Name	RT	Level 1	Level 2	Level 3	Level 4	Level 5	Level 6
Aspirin, TMS derivative	8.002	0.01 (1µl of 0.01 µg/µl)	0.1 (1µl of 0.1 µg/µl)	0.2 (1µl of 0.25 µg/µl)	0.5 (1µl of 0.5 µg/µl)	1.0 (1µl of 1 µg/µl)	2.0 (1µl of 2 µg/µl)
Ibuprofen, TMS derivative	8.884	0.1 (1µl of 0.1 µg/µl)	0.2 (1µl of 0.2 µg/µl)	0.5 (1µl of 0.5 µg/µl)	1.0 (1µl of 1 µg/µl)	2.0 (1µl of 2 µg/µl)	4.0 (2µl of 2 µg/µl)
Pyrene (IS)-Toluene	13.729	4.0 (1µl of 4 µg/µl)	4.0 (1µl of 4 µg/µl)	4.0 (1µl of 4 µg/µl)	4.0 (1µl of 4 µg/µl)	4.0 (1µl of 4 µg/µl)	4.0 (1µl of 4 µg/µl)
Carbamazepine, TMS derivative 193	14.990	0.1 (1µl of 0.1 µg/µl)	0.2 (1µl of 0.2 µg/µl)	0.5 (1µl of 0.5 µg/µl)	1.0 (1µl of 1 µg/µl)	2.5 (1µl of 2 µg/µl)	5.0 (2.5 µl of 2 µg/µl)
Diclofenac, TMS derivative	15.301	0.1 (1µl of 0.1 µg/µl)	0.5 (1µl of 0.5 µg/µl)	1.0 (1µl of 1 µg/µl)	2.0 (1µl of 2 µg/µl)	4.0 (2µl of 2 µg/µl)	8.0 (4µl of 2 µg/µl)
1-Hydroxypyrene, TMS derivative (IS)-DMF (LC grade)	18.481	2.0 (1µl each of 2 µg/ µl)	2.0 (1µl each of 2 µg/ µl)	2.0 (1µl each of 2 µg/ µl)	2.0 (1µl each of 2 µg/ µl)	2.0 (1µl each of 2 µg/ µl)	2.0 (1µl of 2 µg/µl)

J. Appendix J

Table J-1: Raw GCMS spectra data for all pharmaceuticals and internal standards

Samples		Aspirin			Ibuprofen			Carbamazepine			Diclofenac			1-hydroxypyrene		
Name	Type	RT	Area	S/N	RT	Area	S/N	RT	Area	S/N	RT	Area	S/N	RT	Area	S/N
Blank 1	Blank	8,003	5835	39	8,884	4013	34	15,002	10435	29	15,308	37408	422	18,476	7768145	4334
L1	Cal	8,003	34377	115	8,884	164247	2525	14,996	400248	476	15,302	162767	602	18,476	9064104	4978
L2	Cal	8,003	686117	1868	8,884	636899	4843	14,996	1188362	737	15,308	1452301	3252	18,482	14943667	224939
L3	Cal	8,003	870277	Infinity	8,884	705009	9685	14,996	1456867	3603	15,302	1112058	3413	18,476	8282985	62939
L4	Cal	7,997	1425043	Infinity	8,884	1222874	9880	14,996	3243752	3556	15,302	2237070	Infinity	18,476	8430291	8670
L5	Cal	8,003	2603315	Infinity	8,884	2560360	12993	14,994	6364780	15499	15,308	4164462	12269	18,474	7557588	4572
L6	Cal	8,003	4431823	19160	8,884	3973182	39755	15,002	14042429	5611	15,313	8697368	42502	18,474	6238158	2781
9N	Sample	8,001	2967	41	8,889	7466	36	15,007	27678	33	15,312	12520	87	18,492	284735	2905
5A	Sample	8,001	148083	197	8,883	273941	1078	14,995	5636841	9661	15,306	1239259	4894	18,486	16941649	Infinity
2N	Sample	8,065	4586	11	8,883	13869	108	14,995	8585208	6350	15,306	12377	85	18,486	14304256	Infinity
7N	Sample	7,996	894	5	8,883	1556	10	14,995	40258	60	15,306	6576	57	18,475	1424090	3232
5N	Sample	8,059	2492	7	8,883	2545	15	14,995	10494689	10641	15,306	8573	65	18,486	18894400	9704

17N	Sample	8,059	3376	3	8,883	1444	31	14,995	3902924	Infinity	15,301	1840372	6459	18,469	2869130	3788
2A	Sample	8,001	127675	73	8,883	2929632	12799	14,995	6857485	1695	15,306	4105898	16680	18,492	19668545	Infinity
8A	Sample	8,001	44315	68	8,883	97460	1027	14,995	4090457	4558	15,306	2370222	1329	18,475	4623913	3364
8N	Sample	8,059	2252	3	8,883	1884	20	15,018	46112	40	15,312	9189798	7500	18,481	15686643	146376
3A	Sample	8,001	2805	4	8,883	12476	120	14,995	58309	152	15,306	72709	343	18,475	7103547	7063
1A	Sample	8,001	3417	8	8,883	16138	188	14,995	35674	118	15,306	48087	352	18,475	818375	1
1N	Sample	8,059	2861	10	8,883	7186	10	14,995	32697	45	15,306	2200	19	18,475	258560	454
4A	Sample	8,001	1023	3	8,883	6336	45	14,995	37548	55	15,306	38430	223	18,475	4821618	4263
7A	Sample	8,001	10344	Infinity	8,883	425186	23359	15,001	180832	201	15,301	133253	897	18,475	4773614	7
6A	Sample	8,001	123734	107	8,883	594142	Infinity	15,064	120756698	Infinity	15,318	1480873	8093	18,486	19869514	5087
6N	Sample	8,053	2277	7	8,883	2887	50	14,989	408495	280	15,306	4155	48	18,475	797017	2653
4N	Sample	8,059	3838	11	8,883	487	4	14,995	54232	91	15,306	2845	15	18,481	250149	8
3N	Sample	8,059	2793	10	8,883	2140	17	14,995	43446	72	15,301	477793	2833	18,481	250362	689
Blank 2	Blank	8,007	3731	5	8,889	5636	44	15,001	21925	33	15,312	10688	67	18,481	9933579	Infinity
6Ar	Sample	8,007	233938	Infinity	8,883	1061798	Infinity	15,070	131367437	Infinity	15,324	2621828	6830	18,498	29267990	Infinity
9A	Sample	8,001	9583	Infinity	8,883	391303	8321	14,995	776914	1423	15,306	698529	2527	18,486	18252164	9844

|																
12N	Sample	8,059	2151	3	8,883	6295	118	14,989	69923	82	15,306	1797	17	18,475	263524	96
14A	Sample	8,001	11933	5	8,883	518946	7654	14,989	2057496	879	15,301	941180	7003	18,475	1488217	9583
13A	Sample	8,001	15915	71	8,883	735997	5298	14,989	2144289	Infinity	15,301	1219081	4544	18,481	1444101	47291
15N	Sample	8,065	2980	Infinity	8,889	4186	24	15,007	16586633	Infinity	15,312	6529	37	18,492	16694803	12065
12A	Sample	8,001	77080	658	8,883	1598545	17638	14,989	6115771	8263	15,301	2388293	7781	18,492	28081481	12624
18N	Sample	8,059	3013	Infinity	8,883	1973	22	14,995	1252056	7663	15,301	342887	2147	18,481	1329824	89523
16A	Sample	8,002	16975	6	8,883	604306	6034	14,990	366389	954	15,295	1113558	3080	18,481	1504447	6951
18A	Sample	8,002	4350	36	8,883	14108	114	14,990	89971	126	15,301	152061	3754	18,487	24637960	Infinity
13N	Sample	8,053	2271	5	8,883	2072	40	14,990	6450788	3687	15,301	3720	28	18,481	17792469	11945
Blank Neu	Blank	8,053	2739	7	8,883	1354	18	14,990	96960	238	15,295	1729	8	18,475	12756582	52671
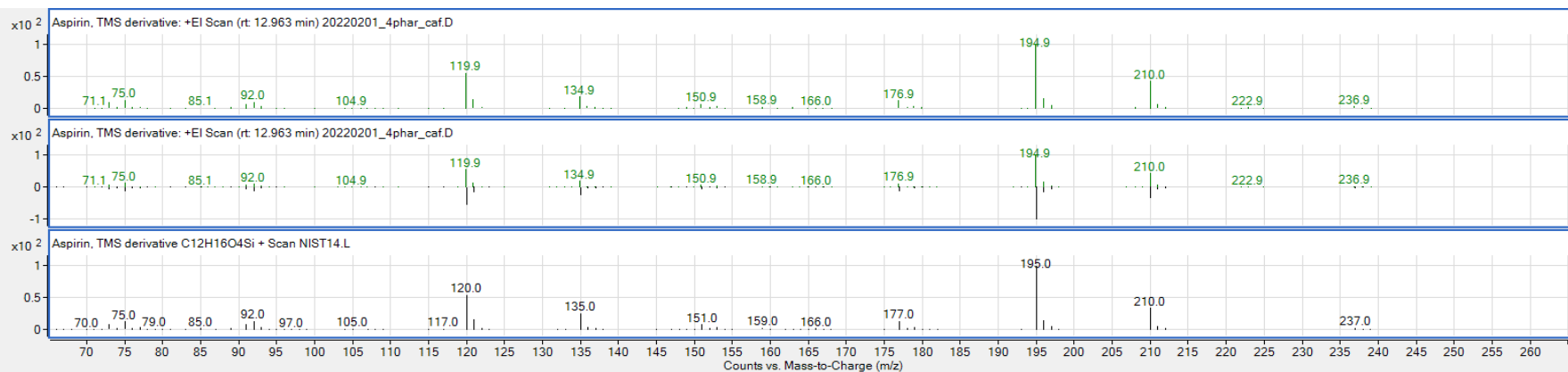
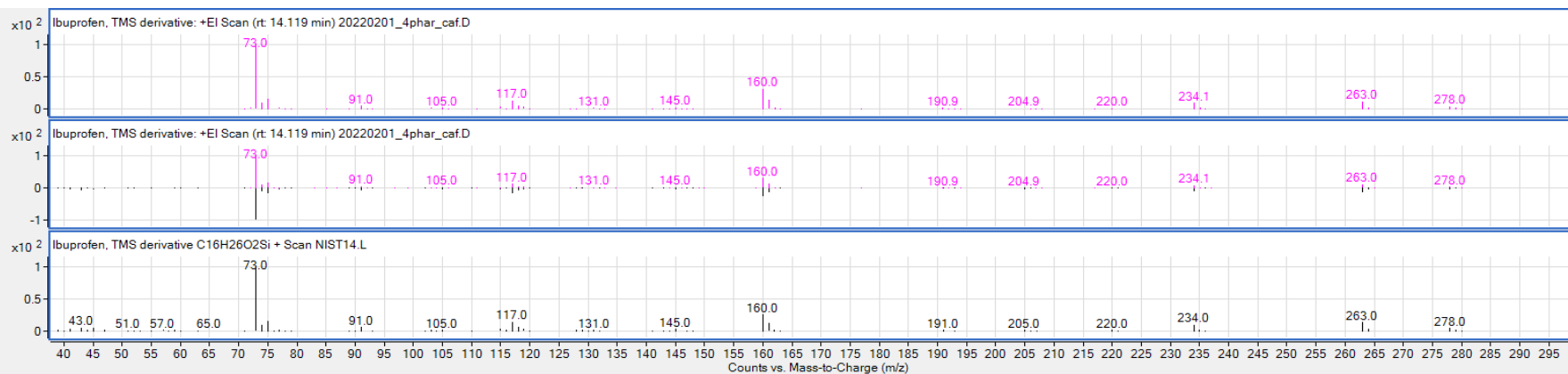*Figure J-1: GCMS spectra for Aspirin*

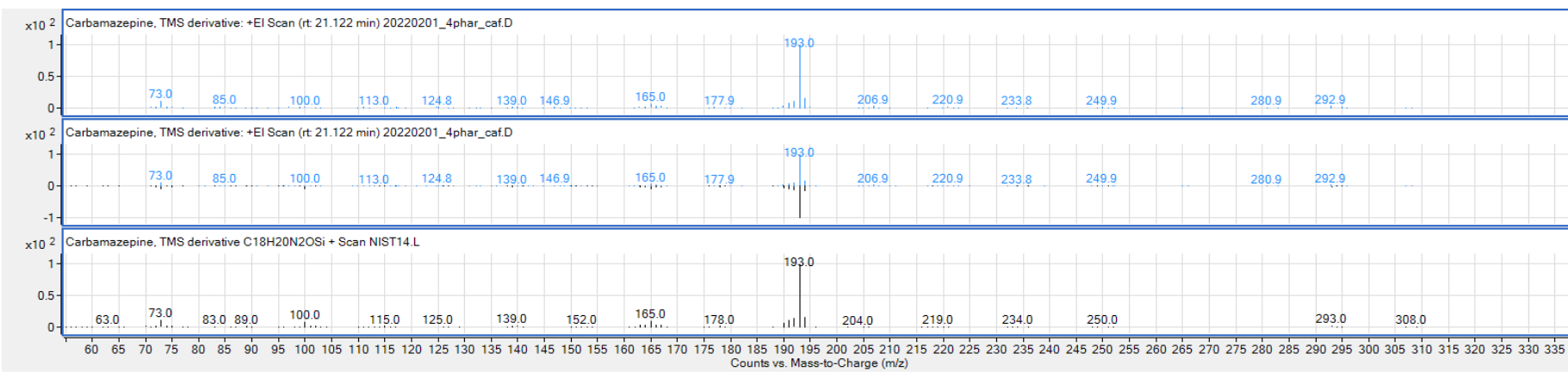*Figure J-2: GCMS spectra for Ibuprofen*

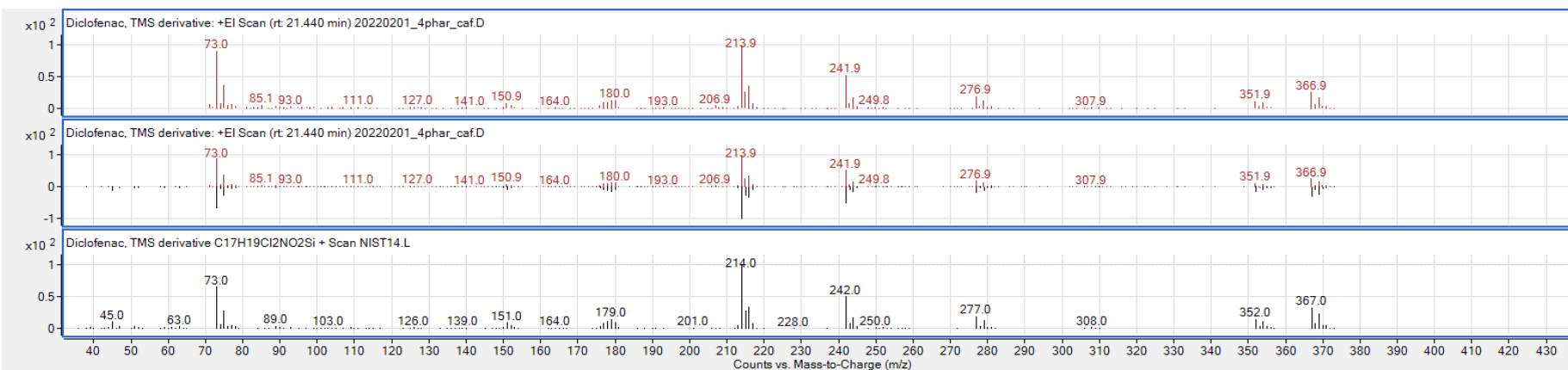*Figure J-3: GCMS spectra for Carbamazepine*

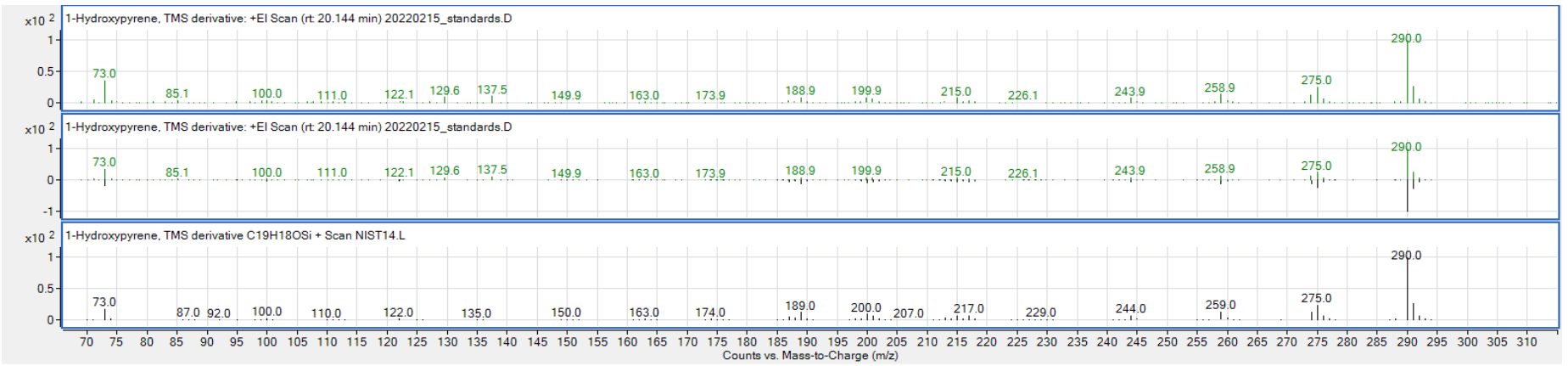*Figure J-4: GCMS spectra for Diclofenac*

Figure J-5: GCMS spectra for 1-hydroxypyrene
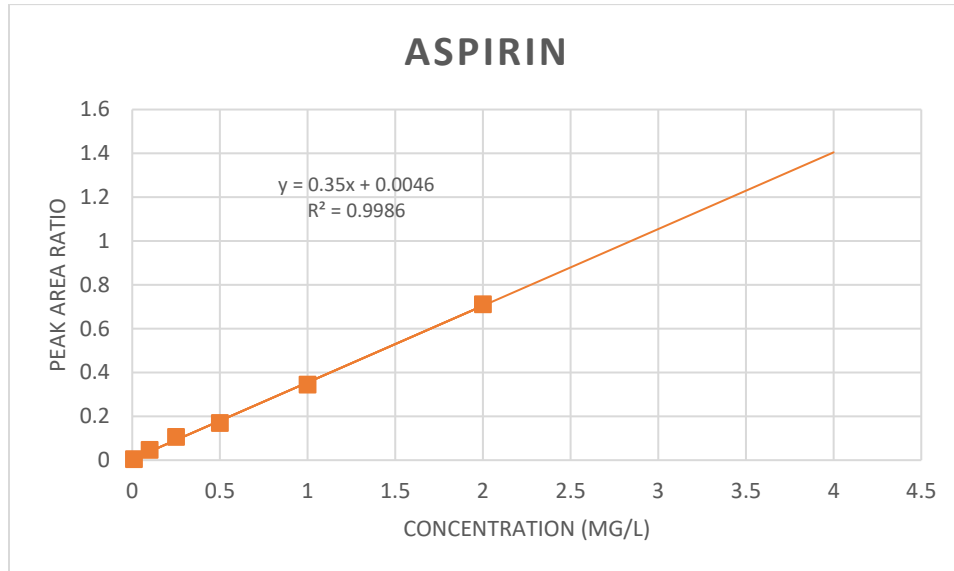
Calibration curves of pharmaceuticals
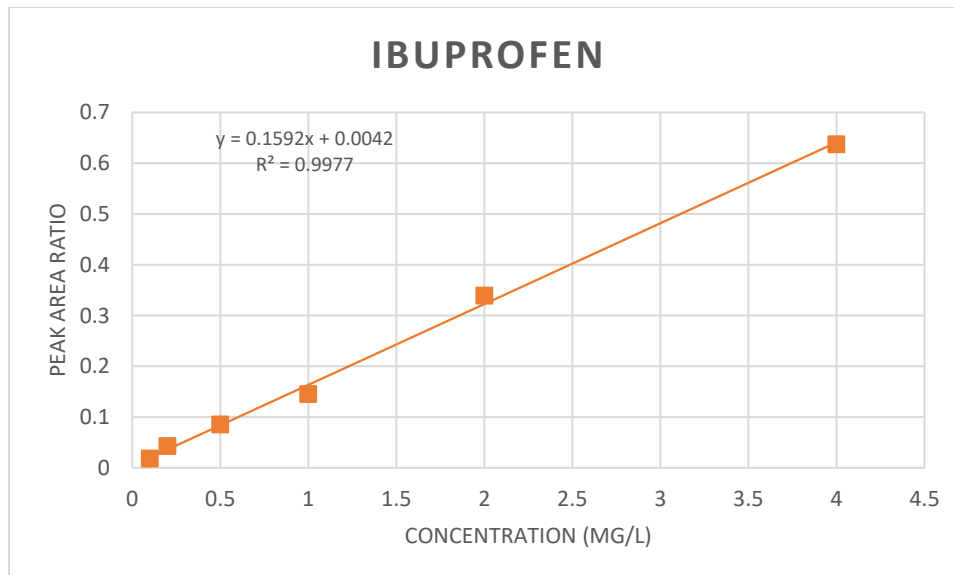

Figure J-6: Calibration curve of aspirin
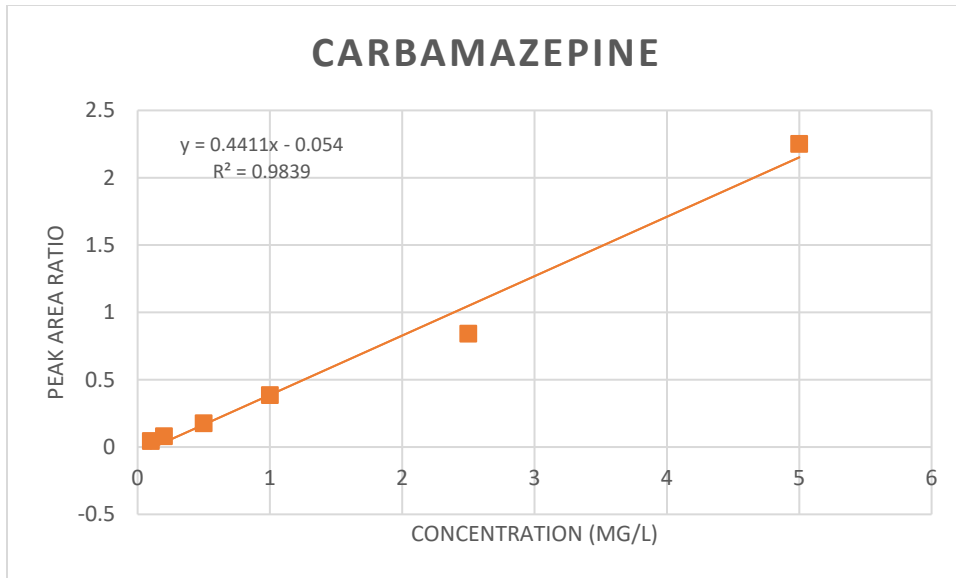

Figure J-7: Calibration curve of ibuprofen

Figure J-8:Calibration curve of carbamazepine

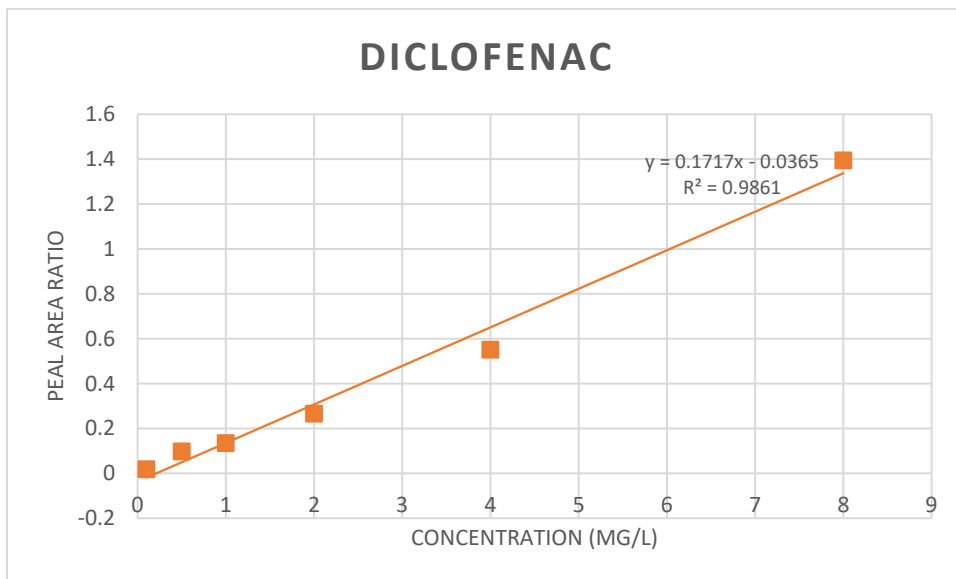**Figure J-9: Calibration curve of diclofena**

% Removal									
RO	*Compound*				*NF*	*Compound*			
Run :	*CBZ % removal*	*DCF % removal*	*ASP % removal*	*IBU % removal*	*Run:*	*CBZ % removal*	*DCF % removal*	*ASP % removal*	*IBU % removal*
1	98,78	98,18	99,92	99,4417	*10*	98,82	97,19	100,00	99,87
2	*97,28*	98,14	100,00	98,9898	*11*	98,21	99,16	99,99	99,94
3	99,20	97,85	99,91	99,9832	*12*	98,19	98,67	99,99	99,36
4	99,24	99,41	99,93	100,0367	*13*	97,03	87,84	100,00	92,84
5	94,88	98,09	99,95	99,8872	*14*	97,48	98,90	100,00	99,76
6	64,30	98,50	99,99	99,6626	*15*	96,91	98,76	100,00	99,41
7	99,67	99,32	100,00	99,4164	*16*	98,81	89,22	100,00	94,38
8	94,88	92,23	100,00	99,8173	*17*	95,04	93,35	100,00	99,59
9	99,34	98,75	99,99	99,6527	*18*	97,29	99,32	100,00	100,05

Appendix K

Sample calculations for RO parameters

K. Appendix k

Sample calcualtions

Flux:

The permeate flux was calculated using the following formula (Hu & Wang, 2016):

$$J = \frac{V}{A \times \Delta t} = \frac{0.0042}{0.013775 \times 0.00416} = 73.17 \; L/m^2 hr$$

The flux was normalized to account for temperature fluctuations using the following formula (Taha et al., 2021):

$$Normalised \; flux = \frac{Actual \; flux}{1.03^{(T-25)}} = \frac{88.67}{1.03^{(18.5-25)}} = 88.75 \; L/m^2 hr$$

Salt rejection:

The observed salt rejection was calculated for the conductivity of the feed (E_c) and permeate (E_p) (Kucera, 2015):

$$Salt \; rejection = \left(1 - \frac{E_p}{E_c}\right) \times 100 = \left(1 - \frac{5.1}{321.1}\right) \times 100 = 98.4\%$$

Appendix L

Sample calculations for pharmaceuticals

L. Appendix L

Concentration of pharmaceuticals:

The concentration of the pharmaceuticals were calculated using the following formula:

$$Normalisation = \frac{Peak\ area\ of\ aspirin}{peak\ area\ of\ internal\ standard}$$

$$= \frac{123734}{19869514} = 0.0062$$

The concentration is calculated using the equation of the calibration curve:

$$y = 0.35x + 0.0046$$

Where Y is the normalized peak area ratio and x is the concentration of the pharmaceutical.

$$x = \frac{y - 0.0046}{0.35} = \frac{0.0062 - 0.0046}{0.35} = 4.6\ ng/l$$